CATALYTIC CONVERSION OF VEGETABLE OILS TO BIOFUELS OVER TRANSITION METAL CATALYSTS

A THESIS

SUBMITTED TO THE

UNIVERSITY OF PUNE

FOR THE DEGREE OF

DOCTOR OF PHILOSOPHY

IN

CHEMISTRY

BY

JITENDRA KUMAR SATYARTHI

UNDER THE GUIDANCE OF

DR. D. SRINIVAS

CATALYSIS DIVISION

NATIONAL CHEMICAL LABORATORY

PUNE - 411 008, INDIA

FEBRUARY 2011

CERTIFICATE

This is to certify that the work incorporated in the thesis entitled **"Catalytic Conversion of Vegetable Oils to Biofuels over Transition Metal Catalysts"** submitted by **Mr. Jitendra Kumar Satyarthi**, to the University of Pune, for the degree of Doctor of Philosophy in Chemistry, was carried out by the candidate under my supervision at Catalysis Division, National Chemical Laboratory, Pune − 411 008, India. Such material as has been obtained from other sources has been duly acknowledged in the thesis. To the best of my knowledge, the present work or any part thereof has not been submitted to any other university for the award of any other degree or diploma.

Date: **Dr. D. Srinivas**

Place: Pune   Research Guide

DECLARATION

I hereby declare that the work described in the thesis entitled "**Catalytic Conversion of Vegetable Oils to Biofuels over Transition Metal Catalysts**" submitted for the **Degree of Doctor of Philosophy** in **Chemistry** to the University of Pune, has been carried out by me at the Catalysis Division, National Chemical Laboratory, Pune – 411 008, India, under the supervision of **Dr. D. Srinivas**. Such material as has been obtained from other sources has been duly acknowledged in this thesis. The work is original and has not been submitted in part or full by me for any other degree or diploma to this or any other University.

Date: **Jitendra Kumar Satyarthi**

Place: Pune   Research Scholar

.... dedicated to my
beloved parents

Acknowledgments

Table of Contents

Chapter 6 : Hydrodeoxygenation of Vegetable Oils into Hydrocarbon-based Biofuels — 162

Chapter 7 : Summary and Overall Conclusions — 179

List of Publications

List of Patents

List of Figures

List of Schemes

List of Tables

Chapter 1
General Introduction

1.1. Introduction

Today we are living in a world which is facing an acute energy crisis. This is because of the fact that at present not only most of the energy demand but also feedstock requirement for chemical industries is fulfilled by the fossil fuels i.e. coal, petroleum and natural gas. These are non-renewable sources of energy which are getting consumed by us at an unprecedented rate and our energy demand is increasing even at a higher rate than ever. To meet this demand and supply deficit we have to switch from non-renewable energy sources to alternative and renewable energy resources. Therefore, the demand for renewable fuels and chemicals has increased many folds in the last few decades and expected to continue in the near future also [1]. The advantages of the biomass-derived fuels (biofuels) are their renewability, biodegradability, non-toxicity and low emissions. Use of biochemicals helps to complement chemicals from non-renewable sources. However, the food vs. fuel issues should be kept in mind while dealing with the production, processing, and applications of biofuels and biochemicals [2]. Due to this, synthesis of biofuels and biochemicals from non-food crops and non-edible oils is getting more attention especially in the developing countries.

1.2. Alternative Energy and Renewable Resources

Use of alternative and renewable energy is must for a continuous and sustainable development. These energy sources have always been existing but the depleting fossil fuel resources, their escalating prices and environmental concerns have revived the interest in these energy sources enormously [3]. The main sources of these energy include solar energy, wind energy, hydro-power, geothermal energy, tidal energy and biomass (Fig. 1.1). Except biomass, other energy sources contain energy in the form of heat energy, radiation energy, kinetic energy or potential energy and have to be trapped and converted into electricity.
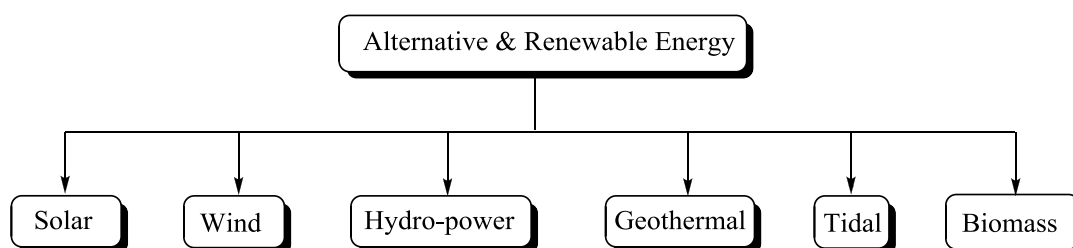
Fig. 1.1. *Sources of alternative and renewable energy*

But biomass is the only renewable energy source which contains energy in the chemical form like fossil fuels. Besides using for energy requirements, Biomass can also be converted into a variety of useful chemicals.

1.3.Biomass

Biomass is the dried mass of living plants and animals. It includes wood, leaves, fruits, flower, grains, vegetable oils, animal waste and meat, milk, oils & fats from animals. It is one of the oldest sources of energy of mankind. Main sources of biomass are forest, agriculture plants, human and animal waste, municipal solid waste and industrial waste [4]. Chemically biomass from plants can be broadly classified into cellulose, hemicellulose, lignin, starch, sugar, protein and triglyceride (Fig. 1.2). It is one of the most important renewable sources as it contains energy in chemical form stored in plants, produced from carbon dioxide and water in the presence of solar light. It is similar to fossil fuels i.e. petroleum and coal, as they also contain energy in chemical form. That's why; it is the most suitable renewable alternative which can be used to replace fossil fuel not only for fuels but also for a variety of useful chemicals.
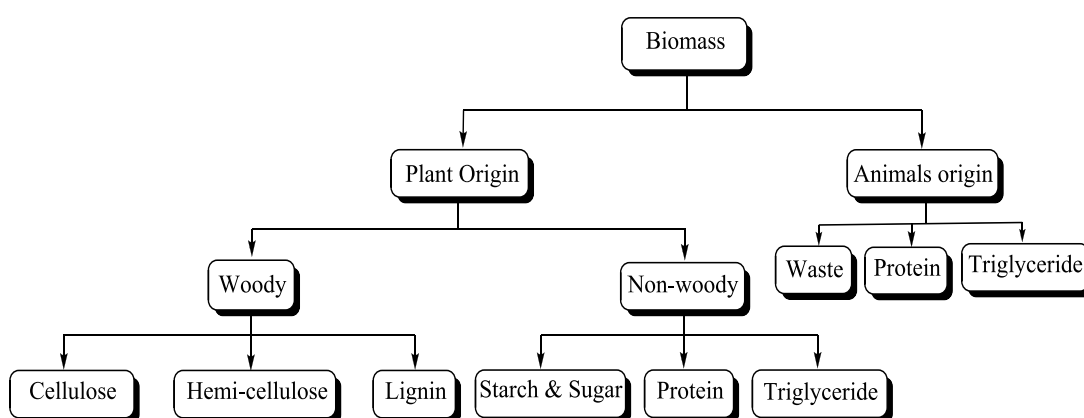
Fig. 1.2. Classification of biomass

1.4. Vegetable Oils and Fats

Alternate fuel should be technically feasible, environmentally acceptable, readily available and economically viable to be for any practical application. From these criteria vegetable oils (triglycerides) prove to be a good renewable alternative fuel source. Oils and fats are high-energy density liquid molecules, which can be used to make liquid fuels. Oils and fats are found in the plant and animal kingdom and are water insoluble and hydrophobic substances. Oils, fats and fatty acids are also called lipids. The annual global production of major vegetable oils amounted to 128 million

tons (Mt) in 2007-08, and 132 Mt in 2008-09. It was expected to be 137 Mt in 2009-10. In addition, about 31 Mt of minor plant oils and animal fats were produced and consumed [5]. Fats and oils are used mainly for cooking and food purposes, as well as for lubricants and raw materials for soap, detergents, cosmetics, and chemicals. For long, it has been considered that oil and fat consumption was shared between food, feed, and industrial use in the ratio 80 : 6 : 14, but with increasing production of biodiesel this is probably now closer to 74 : 6 : 20. In 2008, biodiesel production and capacity amounted globally to 11.1 and 32.6 Mt, respectively [5]. This is most remarkable because biodiesel as fatty acid methyl ester (Scheme. 1.1) can also be used as chemical feedstock.
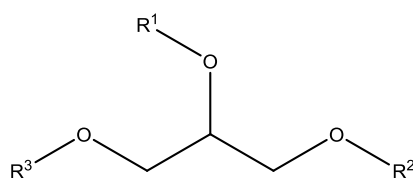
Triglyceride (oils & fats)

R^1, R^2 & R^3 are Fatty acids chains of Fatty acids :

Lauric acid

Myristic acid

Palmitic acid

Stearic acid

Oleic acid

Linoleic acid

Linolenic acid

Ricinolic acid

Erucic acid
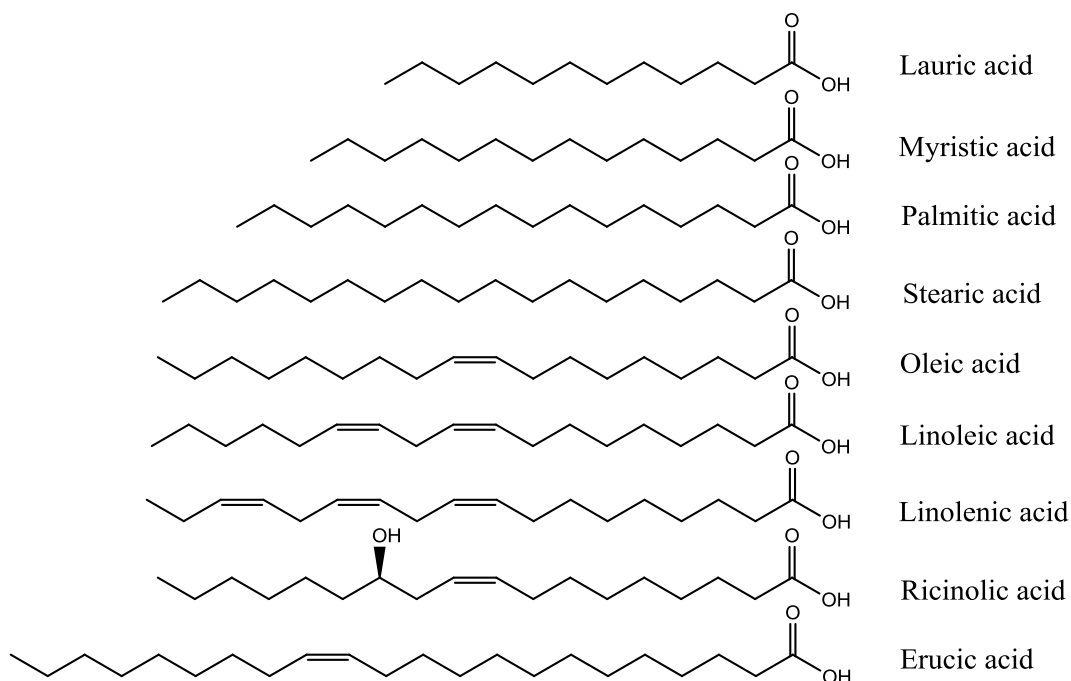
Scheme. 1.1. Structure of oils & fats and common fatty acids

Table 1.1. Fatty acid profile of some common vegetable oils and animal fats [1, 7, 11]

Vegetable oil	Iodine value	C_{12}	C_{14}	C_{16}	C_{18}	$C_{18:1}$	$C_{18:2}$	$C_{18:3}$	other
									Fatty acid composition (wt %)
Edible oils									
Soybean oil	128-143	-	-	12	3	27	52	6	-
Sunflower oil	125-140	-	-	7	5	19	68	1	-
Rapeseed oil (Mustard oil)	98-110	-	-	4	1	65	22	8	-
Palm oil	48-58	-	1	45	4	40	10	-	-
Cotton seed oil	103-115	-	1	22	3	19	54	1	-
Coconut oil	7-11	51	18	9	3	6	2	-	Capric acid (6) caprylic acid (5)
Rice bran oil	90-108	-	-	15	2	43	39	1	-
Corn (Maize) oil	103-128	-	-	2	11	28	58	1	-
Peanut / Ground nut/ Arachis oil	84-100	-	-	11	2	48	30	2	-
Non-Edible oils									
Karanja oil	81-90	-	-	6	7	62	17	-	Eicosanoic acid (3), Dosocasnoic acid (4)
Jatropha oil	82-98	-	1	15	6	55	23	-	
Rubber seed oil	132-148	-	-	10	9	25	40	16	-
Mahua oil	58-70	-	-	28	23	50	9	-	-
Tung oil	160-175	-	-	4	1	8	4	3	Eleostearic acid (80)
Neem oil	65-80	-	-	16	10	50	16	8	-
Animal Fats									
Chicken fat (poultry fat)	75	-	1	23	6	42	17	1	$C_{16:1}$ (8), $C_{20:1}$ (2)
Fish oil (Menhaden)	167	-	11	20	3	15	2	1	$C_{16:1}$ (15), $C_{20:1}$ (1), $C_{18:4}$ (4), $C_{20:5}$ (5), $C_{20:6}$ (12)
Beef tallow	35-48	1	3	27	17	42	3	1	$C_{16:1}$ (4), $C_{17:0}$ (2)

Eleostearic acid – conjugated Linolenic acid

Chemically oils and fats are known as triacylglycerol or triglycerides (TG) i.e. triester of fatty acids with glycerol (Scheme 1.1). Chemical and physical properties of oils and fats depend on composition of their fatty acids. The composition of oils is reported in terms of the fatty acid profile of the oil or fat [6]. For example, fatty acid profile of a representative soybean oil is palmitic acid (12 wt %), stearic acid (3 wt %), oleic acid (27 wt %), linoleic acid (52 wt %) and linolenic acid (6 wt %). The transesterification reaction of an oil or fat with alcohol leads to biodiesel which is a mixture of fatty esters with each ester component contributing to the properties of the fuel. Therefore, it is very important and crucial to have the knowledge of fatty acid profile of oil and fat and their properties. Table 1.1 shows the fatty acid profile of some oils [7]. Table 1.2 lists the physical properties of common fatty acids occurring in natural oils and fats [8]. Fatty acids are classified into the following three categories on the basis of number of double bonds they contain.

1. Saturated fatty acids : stearic acid [$C_{18:0}$], palmitic acid [$C_{16:0}$], myristic acid [$C_{14:0}$], lauric acid [$C_{12:0}$]

2. Mono-unsaturated fatty acids : oleic acid [$C_{18:1}$], palmitoleic acid [$C_{16:1}$]

3. Poly-unsaturated fatty acids : linoleic acid [$C_{18:2}$], linolenic acid [$C_{18:3}$]

While the suitability of any material as fuel, including biodiesel, can be influenced by contaminants arising from production or other sources. The nature of the fuel components ultimately determines the fuel properties. Some of the properties included as specifications in standards can be traced to the structure of the fatty esters (biodiesel) formed from the fatty acids of the parent oil or fat [6]. Originally, the term "fatty acids" was applied only to carboxylic acids separated from animal and vegetable fats. Today, it includes all saturated and unsaturated aliphatic carboxylic acids with carbon chain lengths in the range of C_6-C_{24}. Fatty acids obtained by splitting natural fats and oils are quantitatively far more important than synthetic fatty acids. Different processes for modification of natural fatty acids have been developed and are used to achieve special properties in the different fields of application. The principle production flow-sheet in the oleochemistry chain is shown in Fig. 1.3 [9]. A large number of oleochemicals can be derived from natural fats and oils. These oleochemicals find increasing use in various applications.

Table 1.2. Physical properties of common fatty acids [8]

Systematic name (trivial name)	Formula	Molecular weight (g)	Acid value (mg KOH/g)	Iodine value	M.P. (K)	B.P(K) (P, KPa)	Density kg/m^3 (T, K)
Saturated Fatty Acids							
Octanoic (caprylic)	$C_8H_{16}O_2$	144.22	389	0	289.5	512.7 (10.13)	861.2 (353)
Decanoic (capric)	$C_{10}H_{20}O_2$	172.27	325	0	304.6	468.9 (10.13)	851.8 (353)
Dodecanoic (lauric)	$C_{12}H_{24}O_2$	200.32	280	0	316.8	491.9 (10.13)	845.4 (353)
Tetradecanoic (myristic)	$C_{14}H_{28}O_2$	228.38	245	0	327.2	514.5 (10.13)	844.0 (353)
Hexadecanoic (palmitic)	$C_{16}H_{32}O_2$	256.43	218	0	335.8	534.7 (10.13)	839.7 (353)
Octadecanoic (stearic)	$C_{18}H_{36}O_2$	284.49	197	0	342.6	555.4 (10.13)	837.4 (80)
Eicosanoic (arachidic)	$C_{20}H_{40}O_2$	312.54	179	0	348.3	573.1 (10.13)	836.7 (373)
Docosanoic (behenic)	$C_{22}H_{44}O_2$	340.60	164	0	353.0	536.0 (1.33)	822.1 (373)
Monosaturated Fatty Acids							
cis-9-Hexadecenoic (palmitoleic)	$C_{16}H_{30}O_2$	254.42	221	100	301-303	491–493 (2.0)	900.3 (288)
cis-9-Octadecenoic (oleic)	$C_{18}H_{34}O_2$	282.47	199	90	286.4 (α) 289.3 (β)	496 (1.33)	890.5 (293)
trans-9-Octadecenoic (elaidic)	$C_{18}H_{34}O_2$	282.47	199	90	318.0	498 (1.33)	873.4 (318)
cis-9-Eicosenoic (gadoleic)	$C_{20}H_{38}O_2$	310.53	181	82	297.5	-	888.2 (298)
cis-13-Docosenoic (erucic)	$C_{22}H_{42}O_2$	338.58	166	75	307.7	527.5 (1.33)	869.9 (328)
Polysaturated Fatty Acids							
9Z,12Z-Octadecadienoic (linoleic)	$C_{18}H_{32}O_2$	280.45	200	181	267.8	497 (1.33)	902.5 (293)
9Z,12Z,15Z-Octadecatrienoic (linolenic)	$C_{18}H_{30}O_2$	278.44	202	274	262	497.5 (1.33)	915.7 (293)
9E,12E,15E-Octadecatrienoic	$C_{18}H_{30}O_2$	278.44	202	274	303	358.9 (101.3)	915.9 (293)
9Z,11E,13E-Octadecatrienoic (α-eleostearic)	$C_{18}H_{30}O_2$	278.44	202	274	322	508.0 (1.6)	898.0 (329)
5, 8, 11, 14 -Eicosatetraenoic (arachidonic)	$C_{20}H_{32}O_2$	304.48	184	334	223.5	442-445 (0.02)	922 (293)
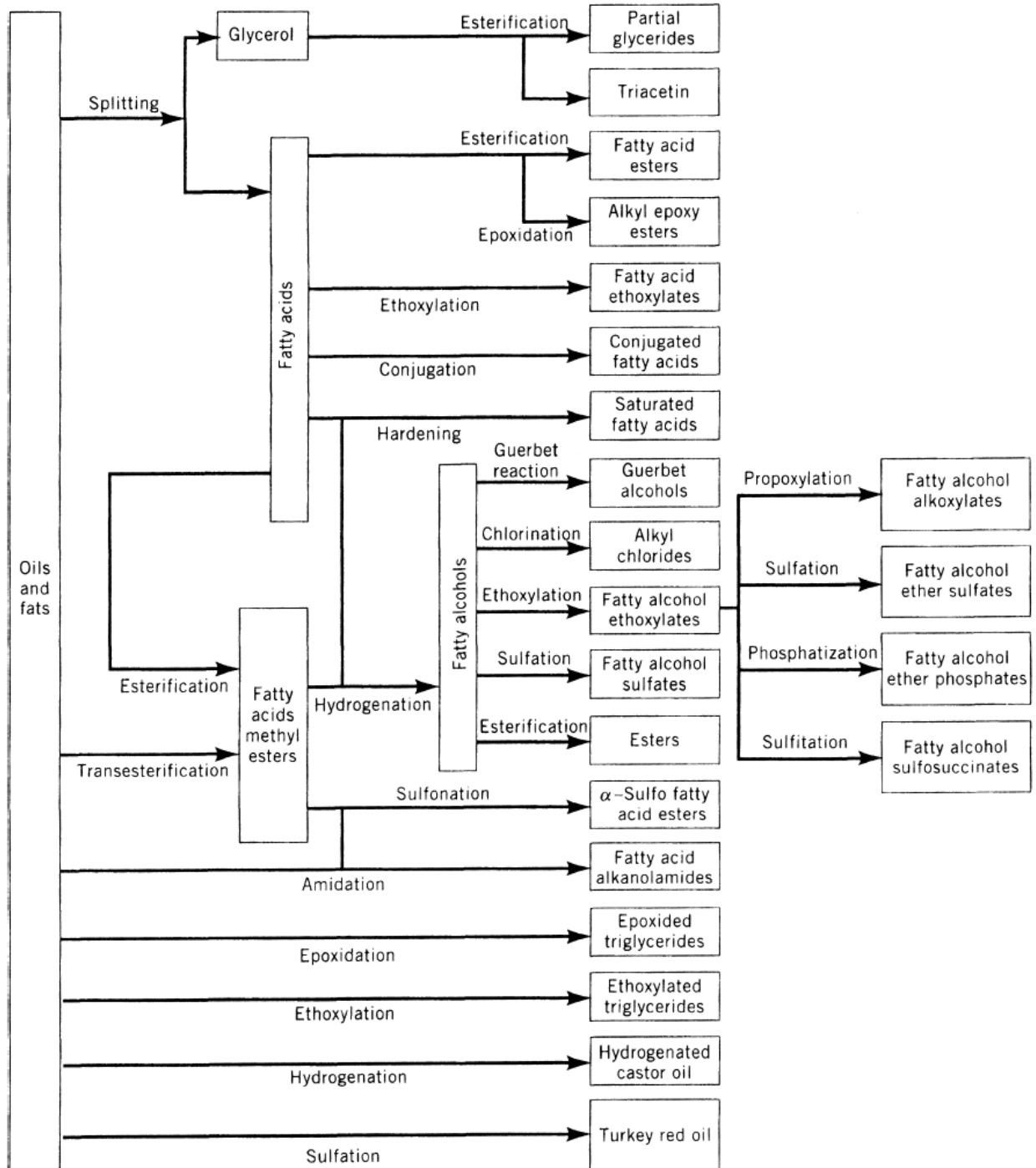
Fig. 1.3. *Fuels and chemicals from vegetable oils and fats [9]*

1.5. Processes for Converting Vegetable Oils into Biofuels

The idea to use vegetable oils as fuel for diesel engines is more than hundred years old. Rudolf Diesel ran the diesel engine on peanut oil at World's exhibition in Paris during 1900 [9]. But the availability of low cost petroleum-based hydrocarbon fuels left no interest in plant oils. After 1970's worldwide oil crisis and growing ecological awareness led to the rediscovery of vegetable oils as possible alternatives

to hydrocarbon-based fuels.

There are several hurdles in using vegetable oils as a fuel. Vegetable oils possess viscosities ten to twenty times higher than the viscosity of fossil fuel. This leads to poor fuel atomization and results in incomplete combustion. Extremely high flash points of vegetable oils and their tendency to thermal and oxidative polymerization aggravate the situation, leading to the formation of deposits on the injector nozzles, a gradual dilution and degradation of lubricating oil, and the sticking of piston ring.

These problems can be solved by either adapting the engine to fuel or by adapting the fuel to the engine. The first strategy led to the development of vegetable oil engines which are not commercially relevant today. The latter strategy aimed at modifying vegetable oils by various technologies to produce fuels which approximate the properties and performance of fossil diesel. The conversion of vegetable oil to fuel of identical properties to those of petroleum-diesel will entail the following:

• Cleavage of the triglyceride into its component fatty acid or linear hydrophobic components.

• Elimination of the polar interactions between them by deoxygenation of the fatty acids or triglycerides to linear hydrocarbons.

• Elimination of the reactive groups (unsaturation) to enhance the fuel storage life.

The ultimate goal is to achieve the above listed objectives in one or two step process units at a lower cost as much as possible. Following are the possible methods employed for using vegetable oil in diesel engines (Fig. 1.4) [10, 11].

A.Direct Use and Blending. Vegetable oils can be used as such or can be used after blending with petroleum-diesel. But, this is generally considered to be not satisfactory and impractical due to the high viscosity, free fatty acid content, gum formation due to oxidation and polymerization during storage [12].

B.Microemulsions. A microemulsion is defined as a colloidal equilibrium dispersion of optically isotropic fluid microstructures with dimensions generally in the 1 - 150 nm range formed spontaneously from two normally immiscible liquids with one of it being an ionic or non-ionic amphiphile [13]. The problem of the high viscosity of vegetable oils can be solved by forming microemulsions with solvents such as methanol, ethanol and 1-butanol. They can improve spray characteristics by

explosive vaporization of the low boiling constituents in the micelles. Microemulsions of aqueous ethanol in soybean oil were nearly as good as that of No. 2 diesel, in spite of lower cetane number and energy content.
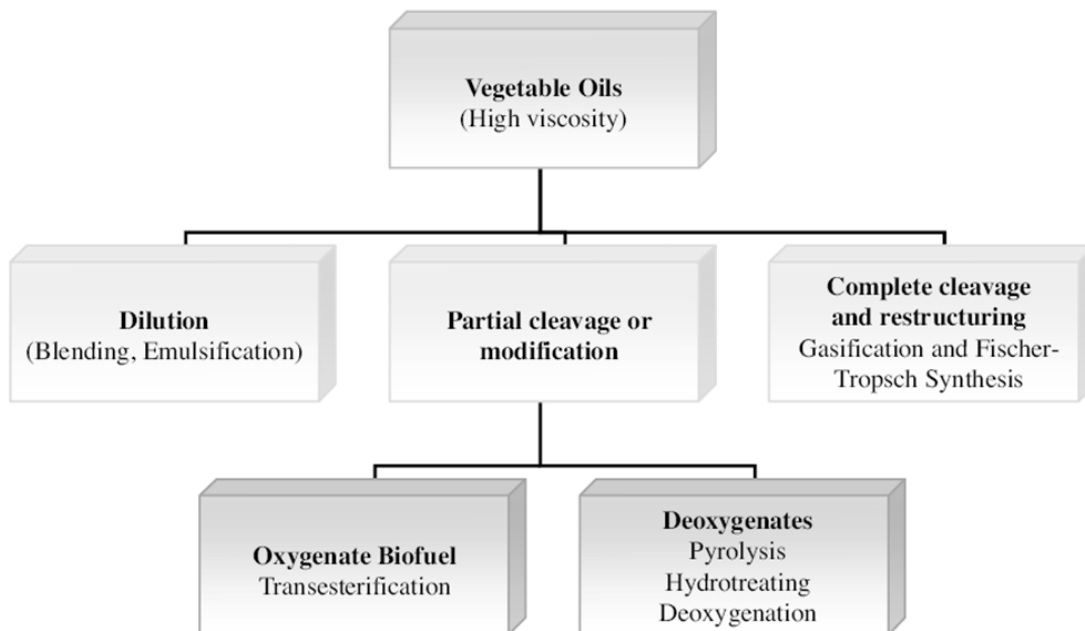
Fig. 1.4. *Classification of processes for converting vegetable oils into biofuels [10]*

C. **Pyrolysis.** Heavy molecules such as vegetable oils or animal fats are converted to smaller ones by means of heat or heat and catalyst (Scheme 1.2). The fuel obtained through this process is called "diesel-like fuels" since there are variety of components such as olefins and paraffin which are similar to the petroleum-based diesel. However, this process requires high temperature between 573 -773 K and products characterization is difficult due to a variety of reaction products [14]. The equipment for thermal cracking and pyrolysis is expensive for modest throughputs.
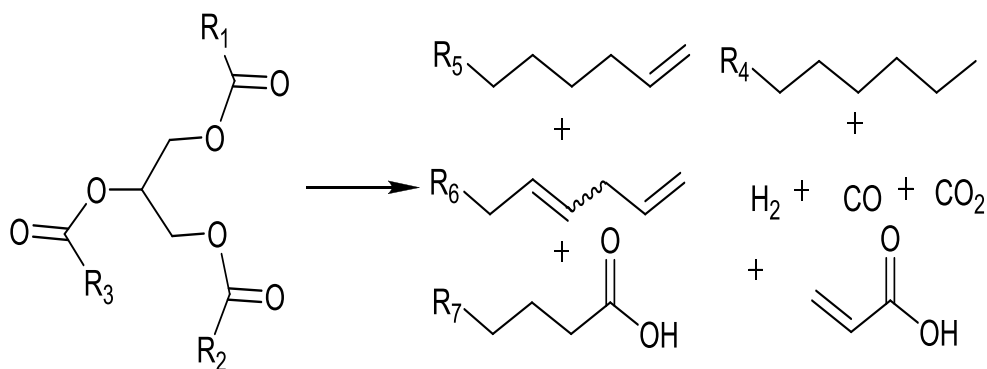
Scheme 1.2. *Products resulting from the pyrolysis of triglycerides*

In addition, while the products are chemically similar to petroleum-derived gasoline and diesel fuel, the removal of oxygen during the thermal processing also removes any environmental benefits of using an oxygenated fuel. It produces some low value materials and, sometimes, more gasoline than diesel fuel.

D. Alcoholysis of Vegetable Oils. It is one of the most practiced commercial methods to produce biodiesel. The process involves a reaction between ester (here triglyceride) and alcohol to form a new ester (biodiesel) and alcohol (glycerol). Different types of alcohols such as, methanol, ethanol, propanol and butanol have been used. However, methanol and ethanol are the most widely used, particularly methanol owing to its low price and availability [9]. This process has been widely used to reduce the high viscosity of triglycerides. If methanol is used in this process, it is called methanolysis.

E. Hydrotreatment. In this, oxygen found in vegetable oils and fats is removed by treatment with hydrogen. It involves deoxygenation and decarboxylation but mostly accompanied by cracking. It is a direct route to the hydrocarbon chains of the fatty components of the triglycerides. It is most ideal and also the shortest route to produce biofuel that will have identical properties with those of conventional diesel fuels. However, this route suffers from issues relating to process selectivity and economics. The processes commonly employed for obtaining deoxygenated biofuels from triglycerides include thermal and catalytic pyrolysis, but recently hydrotreating and deoxygenation are receiving increasing research attention [15].

1.6. Biodiesel

Fatty acid methyl/ethyl esters, commonly referred to as biodiesel, are promising candidate as alternative diesel fuel. The name biodiesel (Greek, bio- means life and diesel from Rudolf diesel/petrodiesel) has been given to transesterified vegetable oil to describe its use as a diesel fuel and renewable nature. Biodiesel can be produced from a variety of feedstocks. These feedstock include most common vegetable oils (e.g. soybean, cottonseed, palm, peanut, rapeseed/canola, sunflower, etc.) and animal fats (usually tallow, chicken fat, fish oils, etc) as well as waste cooking oil and grease. It can be produced either by transesterification of triglycerides or by esterification of fatty acids with low molecular weight alcohols. Chemically biodiesel is a mixture of fatty acid methyl esters (FAME) or fatty acid ethyl esters (FAEE). The main reason for the transesterification of vegetable oils and animal fats to alkyl esters

(biodiesel) is to reduce their kinematic viscosity. Biodiesel possess viscosity much closer to that of petrodiesel and can be used in diesel engine without any modification in the engine [11]. Table 1.3 compares the properties of biodiesel with petrodiesel which make biodiesel a good renewable alternative to petrodiesel [15]. Esters of higher alcohols with fatty acids can be used as biolubricants. This fuel is biodegradable and non-toxic and has low emission profiles than petroleum diesel. Biodiesel is miscible with petrodiesel in all proportions and can be used as such or mixed with petroleum diesel for direct application in diesel engines. In the case, when biodiesel is blended with petroleum diesel, it is represented as BX, where X is the percentage of biodiesel. For example B20 means 20% biodiesel and 80% petroleum diesel. B100 means 100% biodiesel itself.

Table 1.3. The American Society for Testing and Materials (ASTM) standards of maximum allowed quantities in diesel and biodiesel [16]

Property	Diesel	Biodiesel
Standard	ASTM D975	ASTM D6751
Composition	HC[a] (C10–C21)	FAME[b] (C12–C22)
Kin. viscosity (mm^2/s) at 313 K	1.9–4.1	1.9–6.0
Specific gravity (g/mL)	0.85	0.88
Flash point (K)	333-453	373-443
Cloud point (K)	258 to 278	270 to 285
Pour point (K)	238 to 258	258 to 289
Water, vol %	0.05	0.05
Carbon, wt %	87	77
Hydrogen, wt %	13	12
Oxygen, wt %	0	11
Sulfur, wt %	0.05	0.05
Cetane number	40–55	48–60
HFRR[c], microns	685	314
BOCLE[d] scuff (g)	3,600	47,000

[a]Hydrocarbons. [b]Fatty Acid Methyl Esters. [c]High Frequency Reciprocating Rig. [d]Ball-on-Cylinder Lubricity Evaluator.

1.6.1. Advantages of Biodiesel

✓ **Renewable**. Biodiesel is renewable as it is produced from plant oils which can be cultivated again in a short span of time. Animal fats are produced when the animal consumes plant oils and other fats which are renewable.

✓ **Biodegradable and Non-toxic**. It is biodegradable and non-toxic.

✓ **Carbon Neutral**. When plants like soybeans grow they take CO_2 from the air to make the stems, roots, leaves, and seeds (soybeans). After the oil is extracted from the soybeans, it is converted into biodiesel and burned to produce CO_2 and other emissions, which return to the atmosphere. This cycle does not add to the net CO_2 concentration in the air because the next soybean crop will reuse the CO_2 in order to grow. Hence, it is referred to as 'carbon neutral'. When fossil fuels are burned, 100% of the CO_2 released add to the CO_2 concentration levels in the air. When blends are used, the recycling of CO_2 is not 100%. B20 reduces CO_2 by 16% [17].

✓ **Reduction in Exhaust Emission**. It reduces tailpipe particulate matter (PM), hydrocarbon (HC), and carbon monoxide (CO) emissions from most modern four-stroke CI engines. These benefits occur because the fuel (B100) contains 11% oxygen by weight. The presence of fuel oxygen allows the fuel to burn more completely, so fewer unburnt fuel emissions result. The same phenomenon reduces air toxics, because the air toxics are associated with the unburnt or partially burnt HC and PM emissions. Testing has shown that PM, HC, and CO reductions are independent of the feedstock used to make biodiesel. However, an increase in NO_x is observed due to higher combustion engine temperature because of 11% oxygen content inbidiesel. Various gas emissions are compared in Table 1.4.

✓ **Higher Lubricity**. Due to environmental concerns, diesel is subjected to hydrodesulfurization process that leads to removal of compounds like dibenzothiophenes with alkyl (usually methyl) substituents. It is these compounds which provide lubricity to the diesel fuel and hence, ultra low sulphur diesel (ULSD) fuels possess poor lubricity. Adding biodiesel at levels of 2% or above restores lubricity. The presence of the ester moiety causes biodiesel to possess inherent lubricity [11].

✓ **Higher Cetane Number and Flash Point**. Biodiesel has a high cetane number (60 as compared to the value of 40 for petroleum diesel). This parameter is related to ignition quality and hence, biodiesel will allow cold starts and less idle noise. Higher flash point makes it safer in handling [19].

Table 1.4. Average B100 and B20 emissions compared to normal diesel [18]

Emission	B100	B20
Carbon monoxide	-48%	-12%
Total unburned hydrocarbons	-67%	-20%
Particulate matter	-47%	-12%
Nitrogen oxides	+10%	+2%
Sulphur oxides	-100%	-20%
Polycyclic aromatic hydrocarbons (PAHs)	-80%	-13%
Nitrated PAHs	-90%	-50%

1.6.2. Disadvantages of Biodiesel

× **Lower Energy Content**. Biodiesel contains 8% less energy per gallon than typical diesel. The difference between these two measurements is caused by the fact that biodiesel is slightly more dense than diesel fuel, so there are slightly more pounds in a gallon of fuel. All biodiesel, regardless of its feedstock, provides about the same amount of energy.

× **Inferior Cold-flow Properties**. A further drawback to biodiesel use is its less favourable cold-flow properties compared to conventional diesel. The cold-flow properties of biodiesel and conventional petro-diesel are extremely important. Unlike gasoline, biodiesel starts to freeze or gel as the temperature gets colder. If the fuel begins to gel, it can clog filters or eventually it can become thick enough that it cannot even be pumped from the fuel tank to the engine. The presence of higher amounts of saturated fatty esters is one of the causes of cold-flow problems [19]

× **Oxidative Stability**. The presence of polyunsaturated fatty esters is the cause of oxidative stability problems with biodiesel.

× **Higher Cost**. Higher cost of biodiesel is affecting its faster growth. But it will be more competitive if one uses less expensive feedstock (waste and inedible oil) and subsidies from governments are provided to encourage biofuels.

1.7. Methods of Biodiesel Production

There are two main factors that affect the cost of biodiesel production: the cost of raw materials (feedstock) and the cost of processing, though the commercialization of resultant glycerol can share the production costs with biodiesel, improving the overall process profitability. Most of the biodiesel is produced from the costly edible oils like soybean oil, sunflower oil, rapeseed/canola oil, palm oil, etc. But the use of edible oils for fuel production has also lead to a dilemma regarding the risk of diverting farm land or edible oil crops to biofuel production at the cost of food supply on a global scale which is usually referred to as the 'food *vs.* fuel' problem. This has lead researchers to search for alternative sources such as non-edible oils derived from Jatropha curcas (Ratanjyot), Pongamia pinnatta (Karanja), *Calophyllum inophyllum* (Nagchampa), *Hevea brasiliensis* (Rubber), *Madhua indica* (Mahua), used cooking oils, etc [20]. But the disadvantages of these oils are that they contain large amount of free fatty acids which affect the activity of the catalysts used and hence, the rate of transesterification reactions especially in case of homogeneous base catalyst. Depending on the quality of feedstock there are different routes used to produce biodiesel. Important routes (transesterification, esterification-transesterification and hydrolysis – esterification) for biodiesel production from edible and non-edible feedstock are shown in Fig. 1.5.
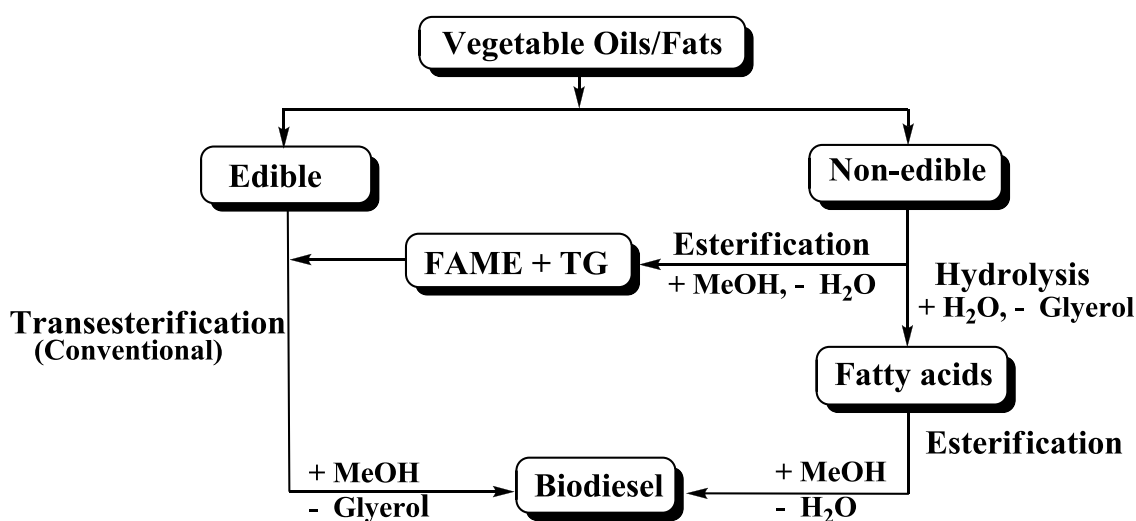
Fig. 1.5. *Different routes for biodiesel production*
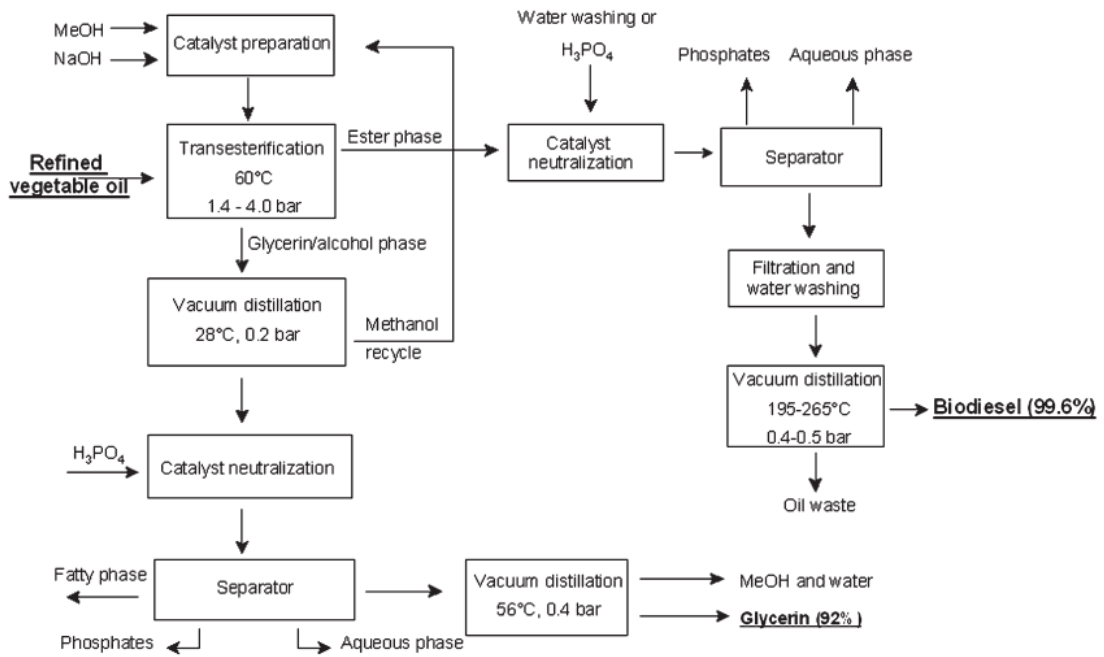
Fig. 1.6. *Flow diagram for a homogeneous base-catalyzed process for biodiesel production [22, 23]*
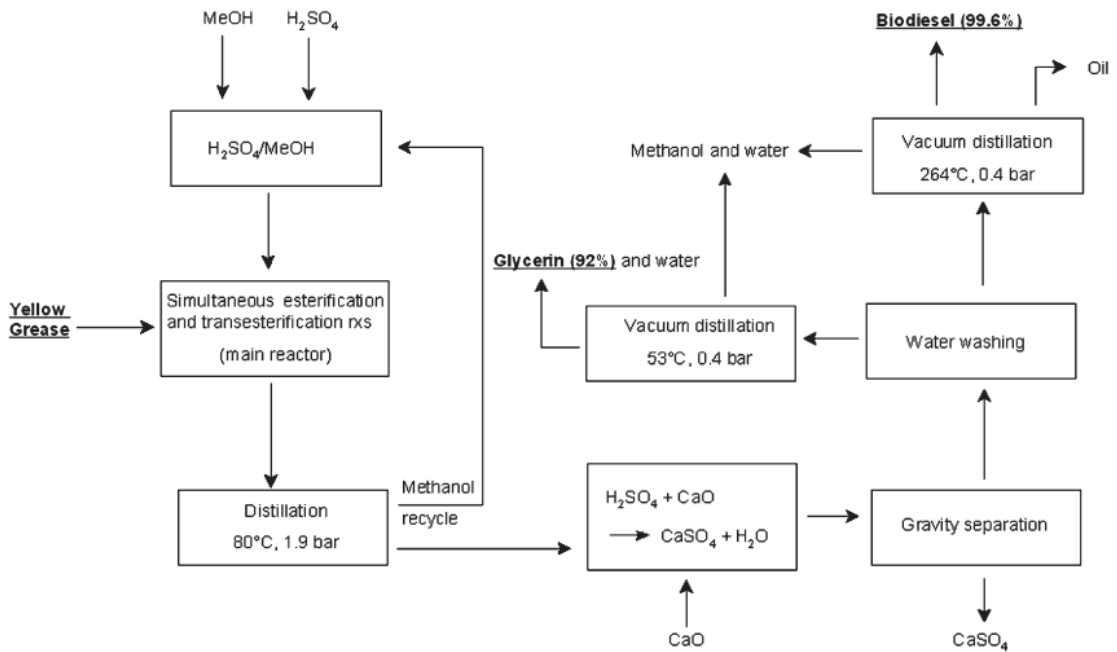
Fig. 1.7. *Flow diagram for a homogeneous acid-catalyzed process for biodiesel production [22-24]*

1.7.1. Transesterification

Transesterification is the most common method for the production of biodiesel. In this reaction, a fat or oil (triglyceride) reacts with three moles of light alcohol (C1 to C4) to give three moles fatty acid alkyl ester (biodiesel) and one mole of glycerol as the by-product (Scheme 1.3). It is called transesterification as one ester is converted into another. The most common alcohol used for biodiesel preparation is methanol as it is the least expensive alcohol although there are exceptions in some countries (ethanol in Brazil). Homogeneous alkali catalyst is most commonly used for transesterification reaction but heterogeneous catalyst and enzyme have also been reported in the literature. As base catalyst is mostly used for transesterification reaction, fats and oil used for it must be free from fatty acids i.e. it requires good quality feedstock (Fig. 1.6) [21- 23]. Acid-catalyzed process (Fig. 1.7), although slow and requires higher temperature, can be used with any type of feedstock. It is mostly used for transesterification of high FFA-containing feedstock such as yellow grease, crude palm oil, karanja etc., as in these cases base catalyst cannot be used. [22-24].
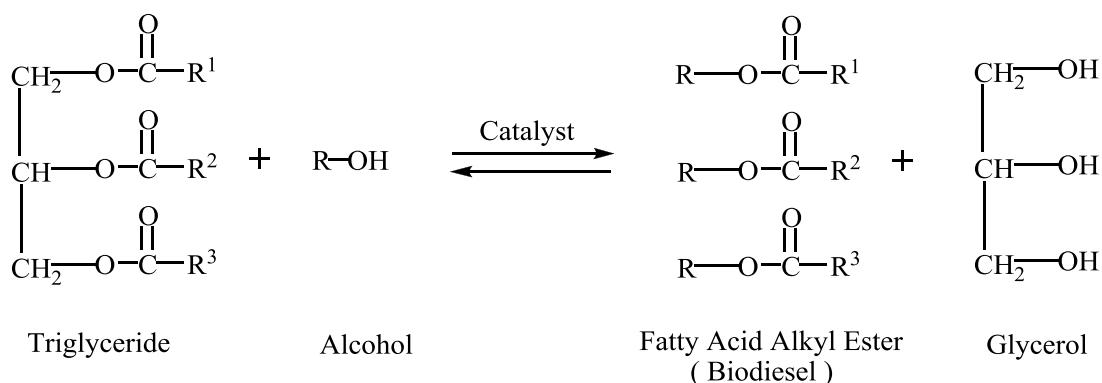
Scheme 1.3. Transesterification of triglyceride with alcohol

1.7.2. Esterification followed by Transesterification

To reduce the cost of biodiesel production one option is that we should use low quality feedstock as 70-80% of the cost of biodiesel mostly depends on the cost of the feedstock. Low quality feedstocks include non-edible vegetable oils, animal fats, waste cooking oils, grease, etc. These feedstocks contain significant amount of free fatty acids (FFA). When FFAs are present, base catalyst cannot be used due to soap formation. Acid catalysts work 4000 times slower than base catalyst in transesterification reaction. To avoid corrosion, expensive acid resistant reactors have to be used. Therefore, instead of converting FFAs containing triglycerides directly

into biodiesel using acid catalyst, first FFAs are esterified with methanol in the presence of an acid catalyst to obtain FAME and triglyceride mixture (Scheme 1.4) which, then, in the second step transesterified with methanol to obtain biodiesel and glycerol. Esterification step is sometimes also termed as the pre-treatment step as it is carried out to esterify only free fatty acids present before the main part of oil (triglycerides) is converted to fatty acid methyl ester by transesterification (Fig.1.8) [22, 25].

| FFA | Alcohol | Fatty Acid Alkyl Ester (Biodiesel) | Water |
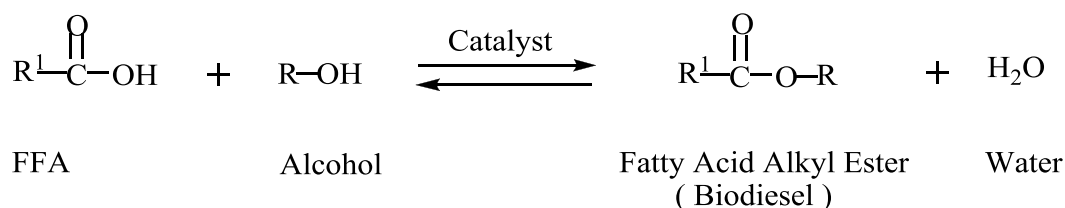
Scheme 1.4. *Esterification of fatty acids*
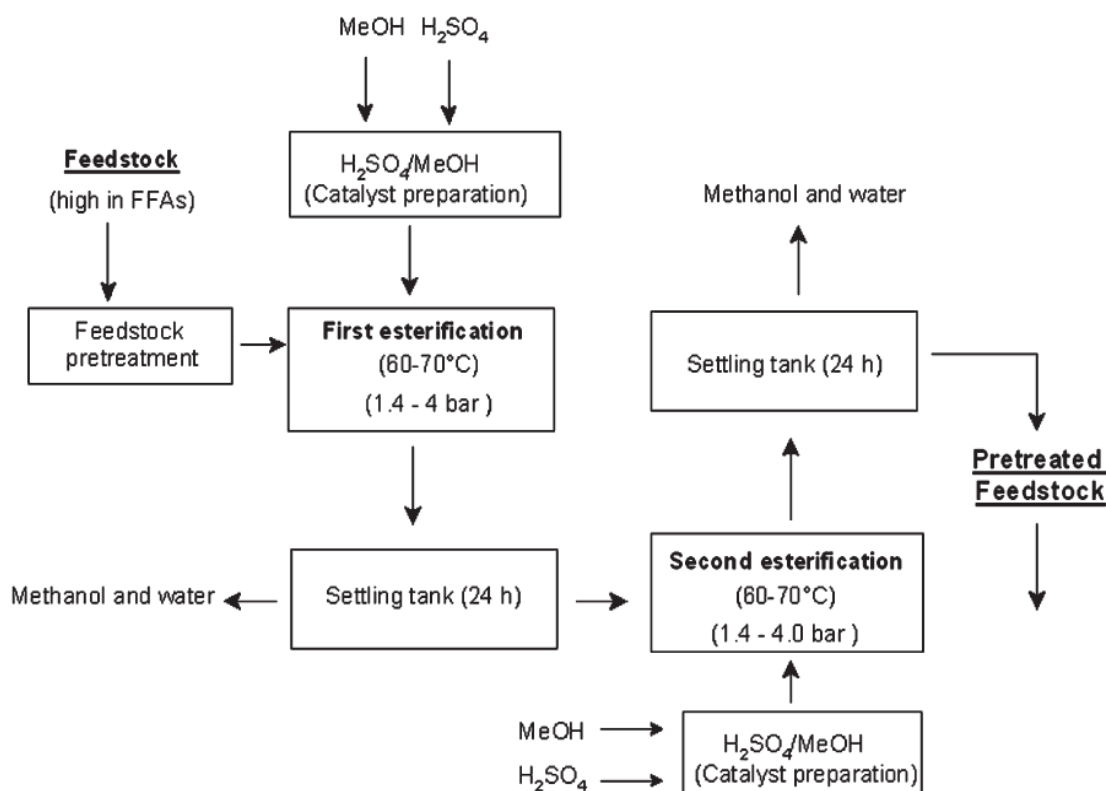
Fig. 1.8. *Pre-treatment of high FFA-containing vegetable oils [22, 25]*
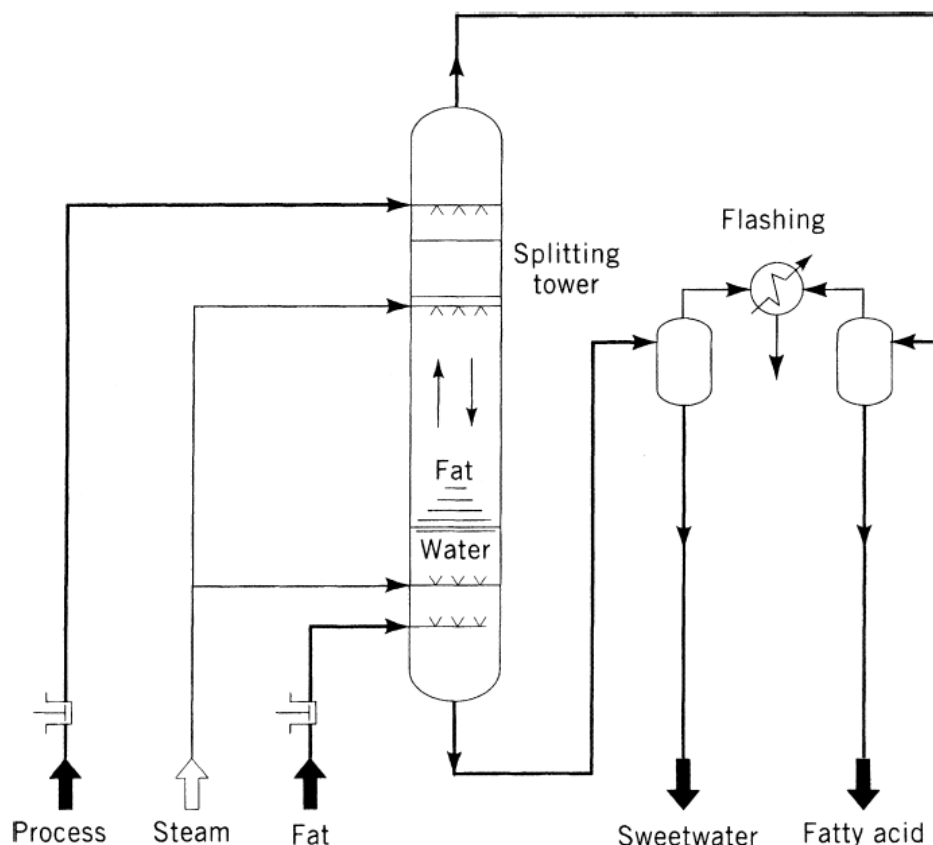
Fig. 1.9. *Flow diagram of Lurgi single-step counter-current fat splitting [26]*

| Triglyceride | Water | Fatty Acids | Glycerol |
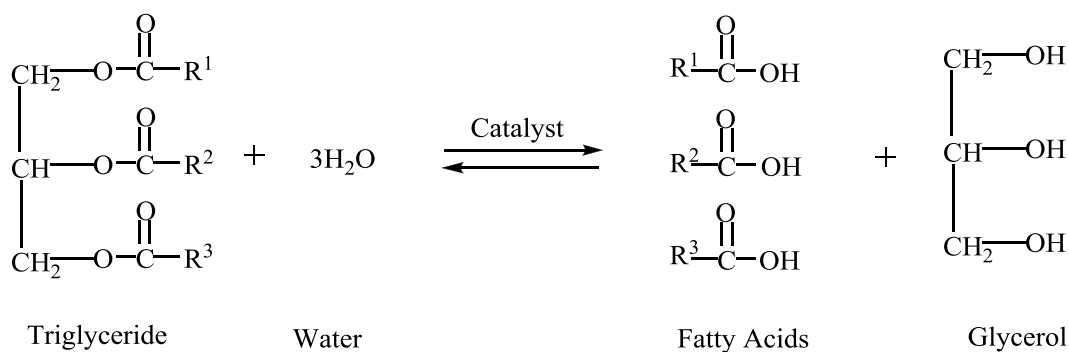
Scheme 1.5. Hydrolysis of triglyceride

1.7.3. Hydrolysis followed by Esterification

This route is used for the production of biodiesel from low quality feedstocks. In this alternate route, biodiesel is prepared by the hydrolysis of waste oils/fats to fatty acids (Scheme 1.5, Fig. 1.9) [26] followed by their esterification with alcohol to FAME. In this route, as both steps contain fatty acids (FA), base catalyst cannot be used due to soap formation. In the hydrolysis step, water and fats/oils are immiscible and water is used as a reactant while in esterification water is formed as a product, therefore, catalyst should be acidic and hydrophobic [27]. Besides biodiesel

production, fatty acids are major components used in the preparation of a wide variety of products, such as soaps, surfactants, lubricants, plasticizers, paints and coatings, pharmaceuticals, foods and agricultural, industrial and personal care products [28].

Table 1.5. Solid catalysts for biodiesel production

Catagory	Catalyst	Reference
Acid catalysts:		
Zeolites	Y, β, ZSM-5, MOR, MFI, FAU	[35-37]
Metal oxides (mixed & supported)	WO_x–ZrO_2/Al_2O_3, TiO_2–ZrO_2/Al_2O_3, TiO_2–Bi_2O_3/Al_2O_3	[38,39]
Modified catalysts (oxides, supports, mesoporous catalysts)	Sulfated zirconia, sulfated tin oxide, WO_3, ZrO_2-Al_2O_3, sulfonic acid functionalized silica, SBA-15-SO_3H, vanadium phosphate	[40-46]
Heteropolyacids	$H_3PW_{12}O_{40}$, $Cs_{2.5}H_{0.5}PW_{12}O_{40}$	[47,44]
Resins	Amberlyst-15, Nafion-1 series, Nafion NR50	[18,49-51]
Metal complex	Fe-Zn DMC	[52]
Base catalysts:		
Zeolites	Zeolite X exchanged with Na, K and Cs, 10%KOH-zeolite-X, ETS-10	[53-56]
Basic oxides	MgO, CaO, La_2O_3, ZnO, SrO, BaO, Mg-La mixed oxide, $CaCeO_3$, $CaMnO_3$, $CaZrO_3$, CaO/MgO	[57-64]
Modified catalysts (oxides, supports, mesoporous catalysts)	Alkali ion supported on Al_2O_3, ZnO, BaO and MgO, KF/KI-Al_2O_3, K_2CO_3-Al_2O_3, MgO-SBA-15, CaO-SBA-15, CaO-MCM-41, Eu_2O_3/Al_2O_3	[65-74]
Hydrotalcites and other basic clay	Crysotile, Sepiolite, hydrotalcite	[75-77]
Organic solid base	Guanidine [C(NH)(NH$_2$)$_2$] (amine), TBD (Triazo BicycloDecane), TBD-MCM-41, Zinc-Arginate (amino acid salt)	[78-80]
Enzyme catalysts:		
Lipases	*Candida antartica*, Novazyme 435 (immobilized)	[81]

1.8. Solid Catalysts for Biodiesel Production

A variety of catalysts have been used for the production of biodiesel. Conventionally most of the biodiesel is produced using homogeneous alkaline catalysts such as NaOH, KOH, Na_2CO_3, K_2CO_3, sodium and potassium alkoxide of methanol, ethanol, propanol and butanol or homogeneous acid catalyst such as sulphuric acid, hydrochloric acid, phosphoric acid, organic sulfonic acids if feedstock(low grade) contain free fatty acids (FFA) [29-32]. Base-catalyzed transesterification is many times faster than the acid-catalyzed one but cannot be used with low quality non-edible feedstock due to saponification. In addition to this saponification issue, homogeneously catalyzed transesterification, whether an acid or base catalyst is used, suffers from some drawbacks in terms of process integrity [33].

a) **Corrosion of Reactor Walls.** The first drawback is the corrosion of the reactor and pipelines by dissolved acid/base species, which inevitably raises the material cost in process construction.

b) **Catalyst Separation and Reusability.** The second is the difficulty in catalyst recovery from the reactant-product mixture.

c) **Waste.** Disposing of used catalyst and waste water required to remove catalyst at the end of the reaction raise problems with environmental pollution.

d) **Continuous Process.** A drawback of homogenously catalyzed transesterification is the limitation in establishing a continuous process.

In order to overcome these disadvantages of the homogeneous catalysts, significant amount of work has been done and is still in progress for the development of a heterogeneous catalyst for biodiesel production. Both base and acid heterogeneous catalysts have been prepared and tested. The most recognised problem with the heterogeneous catalysts is its slow rate of reaction as compared to the homogeneous ones. For this reason, the reaction conditions of heterogeneous catalysis are intensified to enhance its sluggish reaction rates by increasing reaction temperature (373–523 K), catalyst amount (3–10 wt %) and methanol/oil molar ratio (10 – 50). Another problem of the heterogeneous process is the leaching and deactivation of the catalysts which are important features of a catalyst for its continuous use [34]. Table 1.5 lists the broad classification and list of solid acid and base catalysts used for the production of biodiesel by transesterification.

Non-catalytic transesterification reaction is slow and normally needs high pressures and temperatures to be completed. Kusdiana and Saka [82] subjected rapeseed oil into transesterification process in the absence of catalyst and in the supercritical methanol and found that the amount of water in the reaction does not affect the conversion of oil. Conversely, the presence of certain amount of water increases the formation of methyl esters and esterification of free fatty acids takes place simultaneously in one stage. Although the products can be easily separated since there is no base or acid catalyst, the supercritical process needs to be carried out at high temperatures (523–673 K) and pressure (35–60 MPa). First, it operates at very high pressures (25–40 MPa). Second, the high temperatures bring along proportionally high heating and cooling costs. Third, high methanol : oil ratios (usually set at 42) involve high costs for the evaporation of the unreacted methanol. Fourth, the process as reported to date does not explain how to reduce free glycerol to less than 0.02% as suggested in the ASTM D6584 or other equivalent international standards [82].

Several solid base catalysts have been investigated for different transesterification reactions e.g., hydrotalcites, ETS-10, Na, K, Li-promoted calcium oxide, Na/NaOH/γ-Al$_2$O$_3$, K$_2$CO$_3$/alumina, MgO, nanocrystalline calcium oxide and quaternary ammonium functionalized on silica gel. Despite showing higher activity than acid catalysts they cannot be used for feedstock containing free fatty acids. They deactivate faster in the presence of air and moisture and FFA would react with the base catalyst forming soap.

Solid acid catalysts (tungsten oxides, sulphated zirconia, Amberlyst$^®$15, sulfonated saccharides-carbon, Nafion$^®$ resins and organosulfonic functionalized mesoporous silicas, etc.) that have been investigated as potential replacement for mineral acids for biodiesel related applications are listed in Table 1.5. Solid acid catalysts have some advantage over the base catalysts such as they are tolerant to FFA and moisture. These can also convert fatty acids and triglycerides into biodiesel simultaneously so can be used to convert non-edible oils/fats into biodiesel [83]. This not only solves the food *vs.* fuel issue but also helps in decreasing the production cost of biodiesel as 70-80% of biodiesel production cost depends on the feedstock it is produced from [84]. Solid acids contain a variety of acid sites with different strength of Brönsted or Lewis acidity, compared to the homogenous acid catalysts. Despite of the fact that a wide range of solid catalysts is available for the transesterification and

esterification reactions, most of them suffer from one or the other drawbacks. For example, zeolites are stable, robust and have good acidity but their small pore size causes the diffusional limitation resulting in slow rates [85]. Amberlyst-15 or -70, Nafion and resin-based catalyst possess high acidity and pore size but have to operate under mild reaction conditions to avoid the catalyst degradation due to their polymeric matrix structure. In addition, when using an organic catalyst, the swelling capacity becomes a critical issue since it dictates a substrate's accessibility to the acid sites. Unfortunately, TG is not a good swelling agent due to lengthy alkyl tails of substantial hydrophobicity, disfavouring the promise of organic resins as biodiesel catalysts [86]. In this case, inorganic solid acid catalysts are more desirable where high reaction temperatures are necessitated to enhance the catalyst performance. The inorganic acid catalysts operate at higher reaction temperatures than base catalysts because of their lower activity for transesterification.

Both solid acid and base catalysts have advantages and disadvantages in the transesterification reaction such as reactions over base catalysts are faster than acid catalysts but they are less tolerant to water and free fatty acids. Heterogeneous catalyst is reported to be used in the fatty acid methyl ester (FAME) plant of Diester Industrie (Paris) at Sete, France. The Esterfip-H process produces FAME by esterification of plant oils such as that from rapeseed, soybean or sunflower [87, 88]. The heterogeneous catalyst is a spinel mixed oxide of two (non-noble Zn & Al) metals, which eliminates several neutralization and washing steps needed for processes using homogeneous catalysts. The purity of methyl esters exceeds 99%, with yield close to 100%. In addition, the heterogeneous process produces glycerol as by-product with purity better than 98% compared to about 80% from the homogeneous process. The overall production economy improves through the utilization of the by-product [89].

Solid acid catalysts have the potential to replace strong liquid acids to eliminate the corrosion problems and consequent environmental hazards posed by the liquid acids. However, the efforts at exploiting solid acid catalysts for transesterification are limited due to the pessimistic expectations on the possibility of low reaction rates and adverse side reaction. The factors governing the reactivity of solid catalysts have not been fully understood. For example, simple correlations between acid strength and activity of the catalyst have not been clearly formulated. Second, due to diffusional restrictions the catalyst must have a porous system with interconnecting pores, so that

the entire surface of the solid is available for promoting the transesterification reaction. Even though, it is possible to generate these features in solids, it is not yet routinely possible to obtain uniform pore architecture with absolute control over size or radius or geometry of the pores as well as the stability of the solid in the system. Recently, increasing number of researchers have paid attention to the use of TG model compounds, e.g. triacetin [90] and tricaprylin [91], for biodiesel formation reactions in order to develop a better fundamental understanding relevant to catalyst activation and deactivation. By understanding catalyst deactivation, one should be able to design catalysts and catalytic systems which are more resistant to deactivation. Keeping the above discussion in mind, an ideal solid acid catalyst should have the following characteristics:

1. Interconnected system of large pores to minimize diffusional problems of molecules having long alkyl chains.

2. High surface area.

3. High concentration of moderate to strong acid sites to promote the transesterification/esterification reaction with significant rates.

4. High thermal stability of acid sites.

5. Hydrophobic surface to promote the preferential adsorption of oily hydrophobic species on the catalyst surface and avoiding possible deactivation of catalytic sites by strong adsorption of polar compounds such as water and glycerol.

1.9. Solid Catalyst-based Processes in Commercial/Pilot Plant Stage

Esterifip-H Process [92 - 94]. The Institut Français du Pétrole's (IFP) wholly owned subsidiary, Axens, has pushed forward commercialisation of IFP's R&D and concluded licensing contracts with producers. Axens' first breakthrough was a solid catalyst transesterification process known as Esterfip-H. It uses a combination of metal oxides, primarily zinc and aluminium, extruded into pellets and reactor design as shown in Fig.1.10. The main advantages are higher yield (nearly 100%) than with homogeneous catalysts, no side reactions producing soap and the catalyst remains stable for many years, keeping the catalyst cost below €4 per tonne of fuel produced. A total of eight Esterfip-H plants have been designed by Axens for projects around the world. Some are listed in Table 1.6.
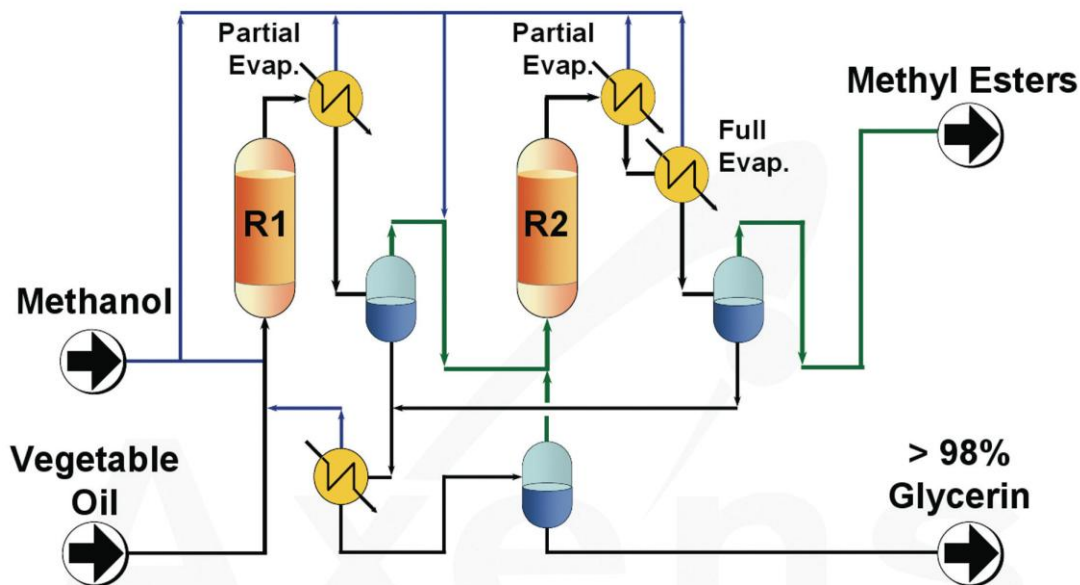
Fig. 1.10. *A schematic diagram of Axens' Esterfip-H process [92]*

Table 1.6. Some operational plants of Esterfip-H technology

Year	Company	Location/ Country	Catacity, tonnes/year
2006	Diester Sète	France	>200000
2007	Perstorp BioProducts	Stenungssund Sweden	160000
2009	Mission New Energy	Kuantan, Malaysia	250000

ENSEL Process [92, 95]. Benefuel Inc., USA has two catalysts - one is a double-metal cyanide (DMC) and the other a metal oxide catalyst developed by NCL, Pune. Benefuel Inc.'s catalysts are produced in powder or extruded forms: extrusions for fixed-bed continuous processing reactors (Fig.1.11) and powders for use in batch processing. There is less pre-treatment required and a washing or glycerine treatment plant is not needed. Due to three factors, favouring ENSEL: higher glycerin quality, low water consumption and lesser oil refining costs, the overall capital cost of a Benefuel facility is estimated to be lower than a conventional plant that is capable of processing high FFA feedstock. The ENSEL catalysts are able to convert lower grade (less refined) oils than the Axens process or conventional liquid catalyst technologies: higher FFA levels and water have no impact on ENSEL catalysts' capacity for transesterification. Even palm distillate having 85% FFA can be converted to biodiesel. Glycerin from the ENSEL process contains only traces of

water and ranges between 95-97% pure. Benefuel is currently designing commercial biodiesel plants for US-based companies, and several other deals are in its pipeline.
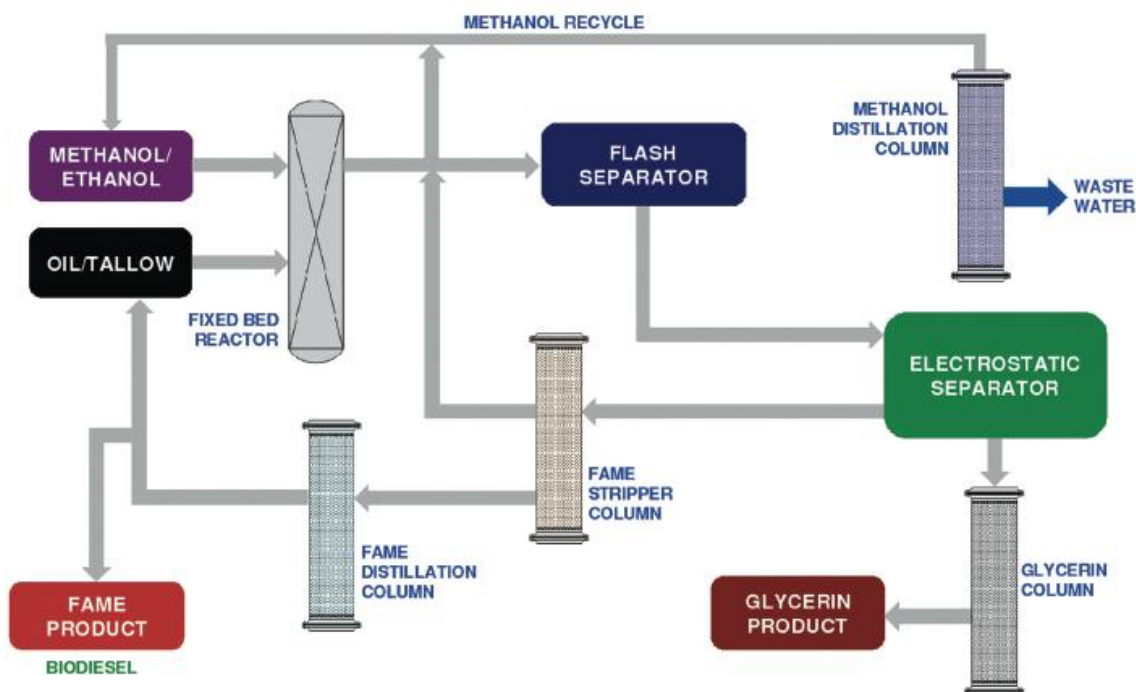
Fig. 1.11. *Biodiesel production using ENSEL process [92]*

Catilin's Process [96]. Catilin was set up as a company in 2007, based on the research work of Victor Lin at Iowa State University. Catilin is commercializing the research done in developing the new catalyst at Iowa State University in Ames and the U.S. DOE's Ames Laboratory. The T300 heterogeneous catalyst is non-toxic and can be a direct replacement for conventional catalysts used in biodiesel production. The drop-in solid catalyst operates at industry standard pressures and temperatures and is removed with filtration. As a result, current producers can retrofit their plants in a matter of days at very low cost. Another key advantage is that the glycerin co-product has purity greater than 98% and qualifies as technical grade, which significantly enhances its overall value. Catilin is currently running a batch production pilot plant in Ames, Iowa, which will be modified to a continuous process.

Nippon's Process [97]. Nippon Shokubai Co. Ltd., has developed a new catalyst and therewith a new process for simultaneous production of biodiesel fuel and glycerin from vegetable oils. This process based on a new technology is a landmark and cost competitive. It generates almost no waste and offers respective reductions of

about 10 and 15 percent in equipment and variable costs, compared to the conventional process. It can use all sorts of vegetable oils and yield biodiesel (3% higher) and high quality glycerin (98%).

Endicott Process [98, 99]. Endicott Biofuels headquartered in Houston, Texas, produces biofuels based in part on a license from Davy Process Technology Ltd. (Davy). This technology is an integral proven element of Davy's industry leading Natural Detergent Alcohol Process in which methanol vapour passes counter current to the fatty acid over solid esterification catalyst (ion exchange resin containing sulfonic/ carboxylic groups) ensuring almost complete conversion of the fatty acids to methyl esters. Endicott's G2Clear99™ biodiesel reduces greenhouse gases by >75% compared with petroleum diesel, as measured by its carbon intensity value. Endicott's production technology enables the conversion of any fat/oil or fatty acid feedstock, up to 100% fatty acids, to high quality biodiesel. Endicott can also switch from one blend of low cost feedstock to another while online and producing at full capacity. In the production of biodiesel (or petroleum diesel), feedstock comprise approximately 80% of total cost; therefore, the ability to convert low cost feedstock is a key competitive advantage.

Endicott's production technology is also ready to process future feedstock under development today including algae oil and lipids from cell ethanol production. Endicott's ability to process any lipid regardless of whether it is neutral or acidic gives future feedstock developers more freedom to operate. Endicott biofuels is currently developing its first facility, a state-of-the-art plant to produce 100,000 metric tons per year (30 million gallons) of fatty acid, any of the organic carboxylic acids present in fats and oils as esters of glycerol.

Despite having the various advantages over homogeneous process, only 10% of the total biodiesel is produced by heterogeneous catalysts and around 90% by using homogeneous catalysts – more than 80% of this quantity is made with methylates, the rest with hydroxides. Things change, though, biofuels are still a fast-moving industry in its infancy. Companies have shown that solid catalysts work on a commercial scale and with rising transport costs, increasing fuel prices and environmental concerns, biofuels' importance and market will grow in future.

1.10. Transition Metal Catalysts

One important use of transition metals and their compounds is the use as catalysts for a variety of industrial processes, mostly in the petroleum and polymer (plastics, fibres) industries, in which organic molecules are isomerised, built up from simple molecules, oxidized, hydrogenated, or caused to polymerize. The most important reason for the transition metals to be a good catalyst is the presence of *d* electrons and their unfilled *d* orbital. As a result, transition metals form compounds of variable oxidation states. Thus, these metals are *electron banks* that lend out electrons at appropriate time, and store them for chemical species at other times, depending on the nature of the reaction. The ability to be in a variety of oxidation states, to interchange between the oxidation states and to form complexes with the reagents and be a good source for electrons make transition metals good catalysts. Availability and costs are additional factors for the consideration [100]. The property of transition metals to be good catalysts also depends on the absorption or adsorption properties of the metal and the transition metal complex.

1.10.1. Double-Metal Cyanide Complexes
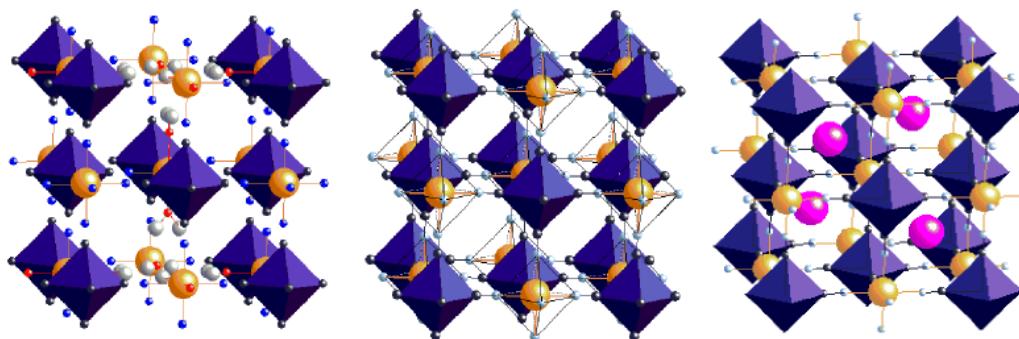
Fig. 1.12. *Structure of three cubic Prussian blue analogues: (a) $A^{II}[B^{III}(CN)_6]_{2/3}$. nH_2O, (b) $A^{III}[B^{III}(CN)_6]_{2/3}$, (c) $CsA^{II}[B^{III}(CN)_6]$.*

Double metal cyanides (DMC) are complexes of the general formula $[M^a]_m$ $[M^b(CN)_6]_n$, where M^a is an oxophilic metal and M^b is a transition metal [52]. These are also called Prussian blue analogues due to similarity with Prussian blue, a well known dye since old times. This family of zeolite-like porous materials can be considered as octahedral anionic blocks, $[B(CN)_6]^{4-}$, assembled by A^{2+} atoms linked at their nitrogen ends. A^{2+} atoms are found with a tetrahedral coordination (Fig.1.12) [101].
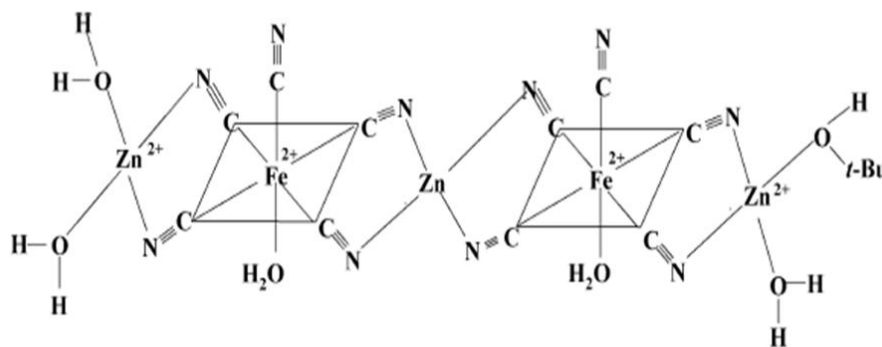
***Fig. 1.13.** Tentative structure of Fe-Zn DMC catalysts [52]*

In recent times, these materials have gained considerable attention for their interesting magnetic, electrochromic, magneto-optic, photomagnetic and nanomagnetic properties [52]. Fe–Zn double-metal cyanide complexes have the general molecular formula: $K_4Zn_4[Fe(CN)_6]_3.xH_2O$, where x = 6–12. The Fe–Zn complexes prepared in the presence of tert-butanol and the polymer surfactant contained, additionally, two butanol molecules in their molecular formula: $K_4Zn_4[Fe(CN)_6]_3.6H_2O.2(tert-BuOH)$ [52]. These catalysts are Lewis acidic, hydrophobic and insoluble in most of the solvents including aqua regia. Unlike most of the solid acid catalysts, these DMC catalysts transesterify oils containing significant amounts of free fatty acids (FFA) and water, probably due to the hydrophobicity of their surface. Tentative structure of the catalyst is as depicted in Fig. 1.13. Thermogravimetric studies showed that water present in the structure gets desorbed at 443 K and a catalyst activated at 443 K doesn't absorb moisture and hence is hydrophobic.

Double metal cyanides are used as catalysts in the manufacture of polyethers-polyols [103], in copolymerization of epoxides and CO_2 producing polycarbonates [104], hydrogen storage [105] and reaction of cyclic carbonates with alcohols yielding dialkyl carbonates [106]. Fe-Zn DMC catalysts reported by Sreeprasanth et al. [52] were efficient for the production of biodiesel by both transesterification of vegetable oils as well as esterification of free fatty acids and can convert a variety of edible and non-edible oil/fat feedstock to biodiesel successfully (Table 1.7). Due to its hydrophobic nature, insensitivity to high FFA content and water in the sample, stability and reusability, ability to catalyze both esterification and transesterification simultaneously and higher conversions. DMC is a superior catalyst for biodiesel production by fixed-bed as well as continuous-flow stirred tank operations.

Table 1.7. Biodiesel production from various feedstock over Fe-Zn DMC [102]

Vegetable oil	Conversion (mol %)[a]	Properties of the product			
		Density (kg.m^{-3})	Kinematic viscosity (m^2.sec^{-1})	Acid value (mg KOH.g^{-1})	Iodine number
Edible oils:					
Coconut	99.8	863.0	4.16	1.23	10.84
Palm	98.3	871.5	5.55	0.27	97.4
Sesame	98.2	873.0	5.25	1.38	106.5
Peanut	97.0	870.0	5.60	1.38	100.1
Sunflower	96.5	871.3	5.75	0.27	112.6
Safflower (Kardi)	97.0	878.0	5.41	0.61	122.4
Margarine	98.9	852.0	5.09	0.26	72.5
Used margarine	98.0	848.1	4.94	1.24	74.1
Castor	78.3	895.2	14.18	1.20	89.2
Non-edible oils:					
Rubber seed	97.1	874.0	5.18	2.11	118.7
Jatropha	86.9	868.2	5.81	1.40	97.4
Pinnai	84.2	886.9	6.91	4.84	116.7
Animal fat:					
Chicken fat	87.9	862.6	3.85	-	-

Reaction conditions: Catalyst (Fe-Zn-1) = 3 wt.% of oil, oil = 15 g, CH$_3$OH : oil molar ratio = 15, temperature = 443 K; reaction time = 8 h.

[a]Conversion estimated based on isolated glycerol yield.

1.10.2. Supported Metal Oxide Catalysts

A vast majority of catalysts used in modern chemical industry are oxides especially the transition metal oxides supported on high surface area support. Because of their ability to take part in the exchange of electrons as well as protons or oxide ions, oxides are used as catalysts in both redox and acid-base reactions. Properties of oxides are also important in the case of preparation of many metal and sulphide catalysts, which are obtained from an oxide precursor. Very often, highly dispersed metals are prepared by reduction of an appropriate oxide phase, and

sulphide catalysts are formed from the oxide precursor in the course of the hydrodesulphurization by interaction with the reaction medium. Finally, oxides play an important role as carriers for active metal or oxide phases, very often modifying strongly their catalytic properties.

1.11. Hydrocarbon-based Biofuels: Next Generation Renewable Fuels

Diesel-like hydrocarbons (paraffin) obtained by hydrotreating vegetable oils and fats are sometimes termed as second generation biodiesel or green diesel (Scheme 1.6). Unlike the first generation, this new generation biodiesel is more favourable for industrial applications being compatible with the current engines, even avoiding need to be blended with petrol fuels and resulting in formation of less by-products, like glycerol from transesterification [107]. This is an emerging area. In hydrotreating, removal of oxygen is accomplished through hydrodeoxygenation (HDO) and other direct mechanisms such as hydrodecarbonylation (HDCN), hydrodecarboxylation (HDCX) and hydrogenation (HYD). Deoxygenation in the presence of hydrogen is more useful than decarboxylation as no carbon is lost.

$$\text{Triglycerides} + H_2 \xrightarrow[\text{T \& P}]{\text{Catalyst}} \text{Paraffin} + \text{Propane} + \text{Water} + CO_2$$
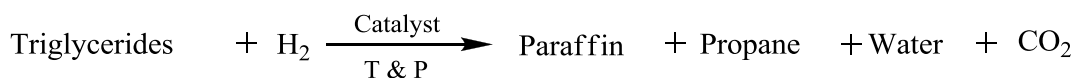
Scheme 1.6. *Hydrotreatment of vegetable oils/fats*

Deoxygenation provides straight chain hydrocarbons which are, then, isomerized to branched isomers to decrease the pour point of the paraffins obtained. Green diesel has a high cetane value and good cold-flow properties. It also has excellent storage stability and is completely compatible for blending with the standard mix of petroleum-derived diesel fuels [108]. In contrast to fatty acid methyl esters, green diesel's properties do not depend on feed origin and process configuration and the fully deoxygenated biofuel can readily be blended with diesel fuel. Table 1.8 compares the properties of green diesel with biodiesel. The light paraffin byproducts are valuable hydrocarbons that can be used in a variety of ways including as a feedstock to an olefins plant or a hydrogen plant. In some cases where a convenient supply of hydrogen is not available, an integrated hydrogen production facility can be used to supply all of the hydrogen needed in the process. This process has been commercially available since 2007, produced by Neste Oil in Porvoo, Finland and UOP-Eni since 2009. A number of manufacturers including ConocoPhillips (USA, Ireland), Petro bras (Brazil), Syntroleum (USA) are also developing

hydrodeoxygenation derived renewable biodiesel (2nd generation biodiesel) processes [109]. This process utilizes supported metal catalysts like Ni/silica, Ni-Mo/γ-alumina, Pd/C, Co-Mo/alumina etc [110, 111]. Hydroisomerisation yields biofuel that could meet the requirements of cold countries. However, one of the challenges in the HDRD process is to convert the deoxygenation and hydroisomerisation steps into a single step-process. This typically involves hydrogenation of triglycerides using existing refinery infrastructure and diesel can be used in the present automobile infrastructure without any modification. Gasoline can be produced using a similar refining process, but this process is in an early stage of development.

Table 1.8. Fuel properties: biodiesel vs. green diesel

Biodiesel	Green diesel
Vegetable oil + alcohol → ester	Vegetable oil + hydrogen → saturated HCs
100% yield	85% yield
Heating Value : 38 MJ/Kg	46 MJ/Kg
Oxidative degradable due to unsaturation	No unsaturation present
Easy to prepare but require new modified facilities	Can be produced in existing refinery infrastructure

1.12. Epoxidation of Fatty Acids and their Esters

Epoxides, also known as oxiranes, are cyclic ethers with three-membered ring. The highly strained ring in their molecule makes them more reactive than other ethers. Epoxidation is an important reaction in organic synthesis because the epoxides formed are intermediates to a variety of products. Epoxides of fats and oils and their FA derivatives are used as plasticizers and stabilizers of plastics [112, 113]. Since fatty epoxides can be converted to a number of chemical derivatives, there has been increasing interest in using these substances as intermediates in the production of new bio-based industrial materials.
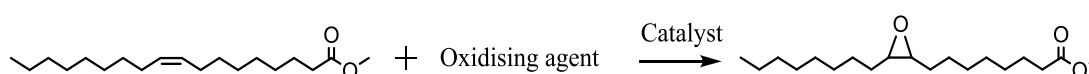
Scheme 1.7. Epoxidation of oleic acid methyl ester
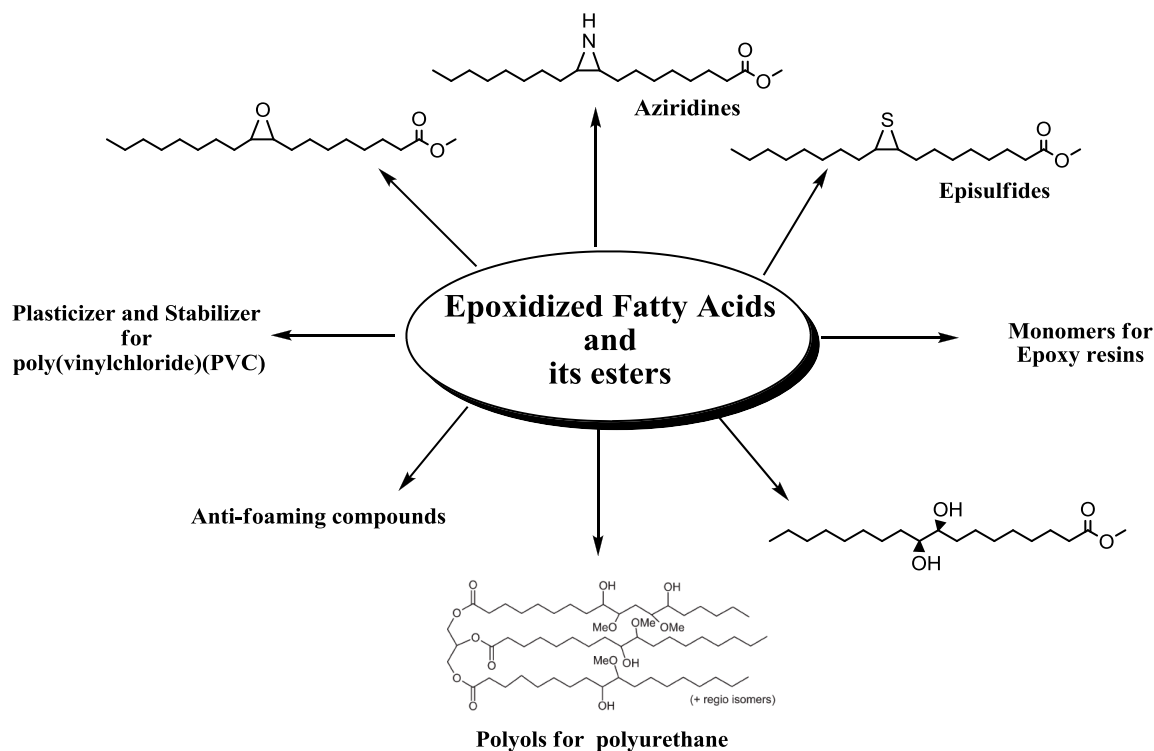
Fig. 1.14. *Some application of epoxidized fatty acids and their esters*

Currently fatty epoxides are prepared on an industrial scale using peracid formed *in situ* from hydrogen peroxide and acetic acid or formic acid in the presence of a strong mineral acid catalyst [114, 115]. This procedure has low selectivity, and the acids must be recycled or treated before discharge into the environment. The low selectivity is mainly the result of partial hydrolysis to diols by trace levels of water under acidic conditions. For the clean and efficient epoxidation of fatty acids and its esters, the available technologies needed to be explored are : 1) epoxidation with percarboxylic acids and 2) epoxidation with organic and inorganic peroxides. These technologies can be rendered cleaner when a heterogeneous catalyst is introduced replacing traditional homogeneous ones (Scheme 1.7) [113, 116].

The high environmental burden caused by the use of non-renewable petrochemical-based feedstock in the chemical industry, their depletion and increasing prices have led to the search for alternative renewable feedstock for various chemical products. In this perspective, fatty epoxides derived from renewable vegetable oils and fats are very important because they can be used as intermediates for the production of a variety of chemicals which are today produced from petrochemicals (Fig. 1.14).

1.13. Analytical Methods in Biodiesel Production

As biodiesel is gaining more and more importance, analytical method to monitor its production is also getting more attention. Various analytical methods [9] have been developed for monitoring biodiesel production by following the transesterification reaction mixture which consist of mostly fatty acid methyl esters and mono-, di- and triglycerides (MG, DG and TG). The ideal analytical method for a product such as biodiesel would be able to reliably and inexpensively quantify all contaminants even at trace levels with experimental ease in a matter of, at most, seconds or even faster for on–line reaction monitoring. No current analytical method meets these extreme demands. Therefore, compromises are necessary when selecting methods for analyzing biodiesel or monitoring the transesterification reaction [117, 118]. Some methods are discussed below:

1.13.1. TLC/FID Method

It is a quantitative method developed by Freedman *et al.* [119], in which analyses were performed by thin layer chromatography (TLC)/flame ionization detection (FID). Stearyl alcohol was used as an internal standard and MG, DG, TG and methyl ester of linoleic acid were used to calculate response factors. Hydrogen flow rate and developing solvent strongly influenced resolution and base line stability. Variation in scan speed affected compactness of burning and response factors, but not the measured composition. A computerized procedure for data analysis was developed so that 30 samples can be completed in 2–3 h. The major disadvantage of this method is the lower accuracy and precision compared to such techniques as gas chromatography (GC) and high performance liquid chromatography (HPLC) especially in case of minor components (1-2%).

1.13.2. Gas Chromatography (GC) Method

GC has been the most widely used method for the analysis of biodiesel due to its higher accuracy in quantifying minor components. Method for simultaneous determination of glycerol, MG, DG and TG in vegetable oil methyl esters has been reported by Plank and Lorbeen [120]. Trimethylsilylation of glycerol, mono-, and di-glyderides, followed by GC using a 10 m capillary coated with a 0.1 mm film of DB-5 allows the determination of all analytes in a single GC run. In principle, glycerol, MG, DG and TG can be analyzed on highly inert columns coated with apolar stationary phases without derivatization. The inertness of the column, required to

obtain good peak shapes and satisfactory recovery, cannot be easily maintained in routine analysis. Trimethylsilylation of the free hydroxyl groups of glycerol, MG and DG, however, ensures excellent peak shapes, good recoveries and low detection limits and enormously improves the ruggedness of the procedure. For complete silylation of glycerol and partial glycerides, the conditions of the derivatization reaction have to be controlled carefully. Extensive studies on the silylation of partial glycerides showed that silylation can be obtained under the following conditions; (i) bistrimethylsilyl trifluoroacetamide (BSTFA) as silylating agent, addition of pyridine or dimethylformamide and heating to 353 K for 15 min; (ii) BSTFA-1% trimethylchlorosilane as silylating agent, addition of pyridine and a reaction time of 15 min at room temperature; (iii) N-methyl N-trimethylsilyl-trifluoroacetamide (MSTFA) as silylating agent, addition of pyridine and reaction time of 15 min at room temperature; (iv) MSTFA as silylating agent and heating to 353 K for 15 min. The internal standard, 1, 2, 4-butanetriol, serves as a very sensitive indicator for incomplete derivatization [120]. In case of insufficient silylation, the peak of 1, 2, 4-butanetriol appears splitted and drastically reduced in height. It is necessary to use fresh BSTFA reagent to guarantee quantitative derivatization. The GC capillary column used was fused silica (60 m x 0.25 mm x 0.25 mm) DB 5 (J and W Scientific Inc.) where as Boocock [121] has used the DB-1 fused silica capillary column of dimension 2 m x 0.25 mm i.d. coated with 0.25 mm film of 100% polymethyl siloxane. Most reports on the use of GC for biodiesel analysis employ flame-ionization detectors (FID), although the use of mass spectrometric detector (MSD) would eliminate any ambiguities about the nature of the eluting materials since mass spectra unique to individual compounds would be obtained [118]. However, the accuracy of GC analyses can be influenced by factors such as baseline drift and overlapping signals.

1.13.3. High Performance Liquid Chromatography (HPLC) Method

A general advantage of HPLC compared to GC is that derivatization is not necessary, which reduces analysis time. The first literature on HPLC method describes the determination of overall content of MG, DG, TG and fatty acid methyl ester (FAME) by isocratic solvent system (0.6% ethanol in chloroform) on a cyano-modified silica column coupled with two GPC columns with a density detector [122]. HPLC with pulsed amperometric detection (PAD) (the detection limit is

usually 10–100 times lower than for amperometric detection and the detection limit is 1 mg/g) was used to determine the amount of free glycerol in vegetable oil esters. The major advantage of this method is its high sensitivity [123]. The simultaneous detection of residual alcohol is also possible with this technique. HPLC with evaporative light scattering detector (ELSD) was also used for analysis. This method can quantify product esters, FFA and various forms of acyl glycerols. A solvent system consisting of hexane and methyl tert.-butyl ether (each with 0.4% acetic acid) with gradient elution profile was used [124]. It can be applied to esters with higher than methyl. In a comparative study by Holcapek *et al.* [125], three detectors: (1) UV detection at 205 nm, (2) evaporative light scattering detection (ELSD) and (3) atmospheric pressure chemical ionization mass spectrometry (APCI-MS) in positive ion mode in reverse phase high performance liquid chromatography (RPHPLC) were used for the determination of compounds occurring during the production of biodiesel from rapeseed oil. Two gradient solvent systems were used: one consisting of methanol (A) with 2-propanol-hexane (5:4, v/v) (B) from 100% A to 50:50 A:B a non-aqueous reverse phase system and the other consisting of water (A), acetonitrile (B) and 5:4 2-propanol–hexane (C) with two linear gradient steps (30% A and 70% B in 0 min, 100% B in 10 min, 50% B and 50% C in 20 min followed by isocratic elution with 50% B and 50% C for last 5 min). The first solvent system was used for rapid quantitative determination of the yield of the transesterification reaction of rapeseed oil with methanol by comparing the sum of the areas of the peaks of methyl esters and triglycerides. The sensitivity and linearity of each detection method varied with the individual triglycerides. ELSD and APCI-MS sensitivity decreases with increasing number of double bonds in the fatty acid methyl esters. However, the sensitivity of UV detection is also different for individual triglycerides. APCI-MS is stated to be the most appropriate detection method for the analysis of rapeseed oil biodiesel.

1.13.4. Gel Permeation Chromatography (GPC) Method

A method for simultaneous analysis of transesterification reaction products – MG, DG, TG, glycerol and methyl esters, was developed using GPC (which is similar to HPLC in instrumentation except for the nature of the column and the underlying separation principle, namely, molecular weight of the analytes) coupled with refractive index detector [126]. The mobile phase was tetrahydrofuran at a flow

rate of 0.5 mL/min at room temperature and the sample injection size was 10 μL. Sample preparation involves only dilution and neutralization. Reproducibility of the method was good and analysis of palm oil transesterification products at different levels of conversion showed a relative standard deviation of 0.27–3.87%. Similarly, GPC was used to evaluate the influence of different variables affecting the transesterification of rapeseed oil with anhydrous ethanol and sodium ethoxide as catalyst [127]. GPC has made the quantification of ethyl esters, mono-, di- and tri-glycerides and glycerol possible.

1.13.5. ^{1}H NMR Method

Gelbard *et al* [128], first time in 1995, reported the application of ^{1}H NMR spectroscopy for the determination of the yield of transesterification reaction. The signal due to methylene protons adjacent to the ester group in triglycerides appears at 2.3 ppm and after the reaction the methoxy protons of the methyl esters appear at 3.7 ppm (Fig. 1.16). The areas of these signals were used in the formula given below to estimate the yield of transesterification.

$$C = 100 \times \left(\frac{2A_{ME}}{3A_{CH_2}}\right)$$

where

C = percentage conversion of triglycerides to corresponding methyl ester,

A_{ME} = integration value of the protons of the methyl esters (the strong singlet); and

A_{CH2} = integration value of the methylene protons.

The factors 2 and 3 are derived from the fact that the methylene carbon possesses two protons and the alcohol (methanol derived) carbon has three attached protons.

Fig. 1.16. Assignment of chemical shifts of protons in transesterification reaction

1.13.6. NIR Spectroscopy Method

More recently, NIR spectroscopy has been used to monitor the transesterification reaction [129]. The basis for quantification of turnover from triglyceride feedstock to methyl ester product is the differences in the NIR spectra of these classes of compounds. At 6005 cm^{-1} and 4425–4430 cm^{-1}, the methyl esters display peaks, while triglycerides display only shoulders. Ethyl esters could be distinguished in a similar fashion. Using Quantisation software, it is possible to develop a method for quantifying the turnover of triglycerides to methyl esters. The absorption at 6005 cm^{-1} gave better result than the one at 4425 cm^{-1}. The mid range IR spectra of triglycerides and methyl esters of fatty acids are almost identical and offer no possibility for distinguishing. NIR spectra were obtained with the aid of a fibre-optic probe coupled to the spectrometer, which render their acquisition particularly easy and time-efficient. While the first NIR report used a model system to describe monitoring of transesterification and for developing quantification methods, a second report applied the method to a transesterification reaction in progress on a 6L scale. Here, spectroscopic results were obtained not only by NIR but also by ^{1}H-NMR [130]. The results of both spectroscopic methods, which can be correlated by simple equations, were in good agreement. Two NMR approaches were used, one as described above. The second approach was the use of methyl ester protons and the protons of the glyceryl moiety (peaks at 4.1–4.4 ppm) in the triglycerides using the equation:

$$C = 100 \times \frac{5 \times I_{\text{ME}}}{5 \times I_{\text{CH}_2} + 9 \times I_{\text{TAG}}}$$

where **C** = percentage conversion of triglycerides to corresponding methyl ester;

I_{ME} = integration value of the methyl esters peak and

I_{TAG} = integration value of the glycerides peaks in the triacylglycerol.

The accuracy of NIR method in distinguishing triglycerides and methyl esters is in the range of 1-1.5%, although in most cases better results are achieved.

1.14. Scope and Objectives of the Present Work

Vegetable oils are gaining more and more attention not only as source of biofuels but also as feedstock for chemicals due to their renewability, higher energy density and long hydrocarbon chain. Biodiesel production from non-edible oils and fats (sustainable feedstock) by their hydrolysis into fatty acids followed by

esterification to fatty acid methyl esters (FAME) is a generic, preferred route. However, water involved as a reagent in the first-step and as a product in the second-step deactivates most of the acid catalysts. Fatty acid esterification using solid acids is not yet well established, as it is much more difficult to find a suitable solid acid for long-chain acid esterification compared to shorter acids such as acetic acid. The reaction mechanism for the heterogeneous acid-catalyzed esterification has also not been fully understood unlike the homogeneously catalyzed one. In view of all the above, the objectives of this research work are:

    i. To find suitable solid acid catalysts for hydrolysis and esterification of vegetable oil and fatty acids, respectively.

    ii. To examine the desirable catalyst characteristics (morphology, site nature, density, hydrophobicity and strength) for this particular application and to probe structure-function relationships.

    iii. To develop new analytical methods for monitoring the reaction and product estimation.

    iv. To convert vegetable oil into petrodiesel like hydrocarbon fuel (2nd generation biodiesel) over solid catalysts.

    v. To derive useful chemicals or their precursors from vegetable oil *via* the epoxidation route using solid catalysts.

1.15. Organization of Thesis

The thesis is divided into seven chapters including Chapter 1 on general introduction.

Chapter 2 describes synthetic methodologies of various catalysts used in the present study and their characterization by various physicochemical techniques. The various catalysts investigated in the present work include:

    (1) Fe-Zn and Co-Zn double metal cyanide (DMC) complexes

    (2) Sulfated zirconia (SZ)

    (3) Al-MCM 41

    (4) Zeolites : HY, Hβ, SAPO-11

    (5) Alumina-supported group VI metal oxides (group VI metal: Cr, Mo & W)

    (6) Alumina-supported Ni-Mo catalyst.

This chapter also includes a detailed description of analytical method used for the analysis of samples and a new ^{1}H NMR method developed for the estimation of FFA in vegetable oil, fats and biodiesel.

Chapter 3 deals with the hydrolysis of vegetable oils over solid acid catalysts. A range of vegetable oils (edible and non-edible) and animal fats were hydrolyzed to their fatty acids over DMC, HY, Hβ, SAPO-11, sulphated zirconia, MoO_x-Al_2O_3, ZnO and Amberlyst^{TM}70. Influence of reaction parameters (temperature, oil to water molar ratio, amount of catalyst, etc) on catalytic activity was examined. Factors responsible for the higher activity of DMC as compared to other catalysts were discussed.

Chapter 4 reports the esterification of fatty acids over solid acid catalysts, DMC, SZ and Al-MCM 41. The chain-length of fatty acids (octanoic acid to oleic acid) and alcohols (C1 − C8) was varied and their apparent activation energies for esterification over these catalysts were calculated. Influence of catalysts characteristics such surface area, acidity, pore size and hydrophobicity in esterification of fatty acids was examined. The mechanism of esterification was probed.

Chapter 5 describes the epoxidation of fatty acids and their esters with tert-butyl hydrogen peroxide over alumina supported group VI transition metal oxides catalysts, CrO_x-Al_2O_3, MoO_x-Al_2O_3 and WO_x-Al_2O_3. Effect of modification of alumina with phosphoric acid before loading metal oxide was also studied. Active sites and mechanism responsible for the higher activity of MoO_x-Al_2O_3 are investigated using *in situ* UV-visible and EPR spectroscopic techniques.

Chapter 6 reports the conversion of vegetable oil into diesel-like hydrocarbon (paraffin) fuel by deoxygenation in the presence of hydrogen over sulfided Ni-Mo catalyst supported on alumina. Vegetable oil was converted into cetane booster hydrocarbons and the effect of their blending with commercial petrodiesel on the pour point was investigated.

Chapter 7 provides an overall summary and conclusion of the work presented in the thesis.

By and large, this thesis contributes to the area of green chemistry and sustainable catalytic process for biodiesel production from non-edible vegetable oils/fats *via* hydrolysis–cum-esterification and hydrodeoxygenation routes and for chemicals production via epoxidation of fatty acids and their esters. It also probes into the factors influencing the reaction kinetics.

1.16. References

1. A. Demirbas, Biodiesel: A Realistic Fuel Alternative for Diesel Engines, Springer-Verlag, London (2008).

2. A.K. Dalai, A. Bassi, Energy Fuels 24 (2010) 4627.

3. Annual Energy Outlook 2006 by EIA. www.eia.doe.gov/oiaf/aeo/

4. T. Werpy and G. Petersen, "Top Value Added Chemicals From Biomass" Vol. 1 (2004). (report submitted to EERE, DOE).
   http://www1.eere.energy.gov/biomass/pdfs/35523.pdf.

5. (a) J.O. Metzger, Eur. J. Lipid Sci. Technol., 111 (2009) 865–876.
   (b) United States Department of Agriculture: Oil seeds: World Markets and Trade Monthly Circular.
   http://www.fas.usda.gov/oilseeds/circular/Current.asp.
   (c) F.D. Gunstone: Market Report. Lipid Technol. 20 (2008) 48.
   (d) Emerging Markets Online (EMO): Biodiesel 2020: A Global Market Survey. 2nd Edn. EMO, Houston, TX (USA) (2008).
   http://www.emerging-markets.com/biodiesel/.

6. M.W. Balakos, E.E. Hernandez, Catal. Today 35 (1997) 415.

7. A. Thomas, "Fats and Fatty oils" Ullmann's Encyclopaedia of Industrial Chemistry (2000).
   http://onlinelibrary.wiley.com/doi/10.1002/14356007.a10_173/pdf.

8. D.J. Anneken, S. Both, R. Christoph, G. Fieg, U. Steinberner, A. Westfechtel. "Fatty Acids" Ullmann's Encyclo. of Industrial Chem. (2006).
   http://onlinelibrary.wiley.com/doi/10.1002/14356007.a10_245.pub2/pdf.

9. (a) B. Brackman, J. Knaut, P. Wallscheid, Oleochemicals, Henkel KGA, Dusseldorf, 1984.
   (b) G. Knothe, J.V. Gerpen, J. Krahl, The Biodiesel Handbook, AOCS Press, Urbana, Illinois (2005).

10. J.O. Olusola, M.M. Adediran, A.K. Oluseyi, U.L. Ajao, Energy Environ. 20 (2009) 8 and 21 (2010) 1.

11. M. Mittelbach, C. Remschmidt, Biodiesel - The Comprehensive Handbook, 3rd Edition Boersedruck Ges.m.b.H, Viena (2006).

12. S. Bajpai, P.K. Sahoo, L.M. Das, Fuel, 88 (2009) 705.

13. A. Kerihuel, M.S. Kumar, J. Bellettre, M. Tazerout, Fuel, 84 (2005) 1713.

14   P. Tamunaidu, S. Bhatia, *Bioresource Technology*, 98 (2007) 3593.

15   I. Kubičková, M. Snåre, K. Eränen, P. Mäki-Arvela, D.Y. Murzin, Catal. Today 106 (2005) 197.

16.   E. Lotero, Y. Liu, D.E. Lopez, K. Suwannakarn, D.A. Bruce, J.G.J. Goodwin, Ind. Eng. Chem. Res. 44 (2005) 5353.

17.   F. Ma, M.A. Hanna, Bioresour. Technol. 70 (1999) 1.

18.   A.A. Kiss, A.C. Dimian, G. Rothenberg, Adv. Synth. Catal. 348 (2006) 75.

19.   Biodiesel Handling and Use Guide (Fourth Edition) (2008).US Department of Energy. http://www.nrel.gov/vehiclesandfuels/npbf/pdfs/43672.pdf.

20.   Report of the Committee on Development of Bio-fuel, 2003 April (Planning Commission of the Government of India).

21.   U. Schuchardt, R. Sercheli, R.M. Vargas, J. Braz. Chem. Soc. 9 (1998) 199.

22.   Catalysis, Volume 19, Publisher-The Royal Society of Chemistry (2006).

23.   Y. Zhang, M.A. Dube, D.D. McLean, M. Kates, Bioresource Technol. 89 (2003) 1.

24.   M. Canakci, J. Van Gerpen, T. ASAE 46 (2003) 945.

25.   Y. Wang, S.Y. Ou, P.Z. Liu, F. Xue, S.Z. Tang, J. Mol. Catal. A: Gen. 252 (2006) 107.

26.   Bailey's Industrial Oil and Fat Products, Sixth Edition, Six Volume Set. Edited by Fereidoon Shahidi, John Wiley & Sons, Inc. (2005).

27.   S. Yan, S.O. Salley, Ng K.Y. Simon, Appl. Catal. A: Gen. 353 (2009) 203.

28.   An Ullmann's Encyclopedia, Industrial Organic Chemicals: Starting Materials and Intermediates, Wiley-VCH, Weinheim, Germany, Vol. 4, 2481 (1999).

29.   A.W. Schwab, M.O. Bagby, B. Freedman, Fuel 66 (1987) 1372.

30.   B. Freedman, R.O. Butterfield, E.H. Pryde, J. Am. Oil Chem. Soc. 63 (1986) 1375.

31.   C. Stavarache, M. Vinatoru, R. Nishimura, Y. Maed, Ultrason. Sonochem. 12 (2005) 367.

32.   H.A. Aksoy, I. Becerik, F. Karaosmanoglu, H.C. Yamaz, H. Civelekoglu, Fuel 69 (1990) 600.

33.   E. Lotero, J.G. Goodwin Jr., D.A. Bruce, K. Suwannakarn, Y. Liu, D.E. López, The Catalysis of Biodiesel Synthesis, Vol. 19, Ed. by J. Spivey and K.M. Dooley, Royal Chemistry Society Publishing, Cambridge, UK (2006).

34. (a) A.K. Singh, S.D. Fernando, Chem. Engin. Tech. 30 (2007) 1.

(b) S. Gryglewicz, Biores. Tech. 70 (1999) 249.

35. A. Brito, M.E. Borges, N. Otero, Energy Fuels 21 (2007) 3280.

36. T.S. Koh, K.H. Chung, J. Kor. Ind. Eng. Chem. 19 (2008) 214.

37. Q. Shu, B. Yang, H. Yuan, S. Qing, G. Zhu, Catal. Commun. 8 (2007) 2159.

38. S. Furuta, H. Matsuhashi, K. Arata, Catal. Comm. 5 (2004) 721.

39. B. Delfort, D. Le Pennec, C. Lendresse, US Patent 7151187 B2 (2006).

40. F. Omota, A.C. demian, A. Bliek, Chem. Eng. Sci. 58 (2003) 3175.

41. S. Furuta, H. Matsuhashi, K. Arata, Appl. Catal. A 269 (2004) 187.

42. H. Matsuhashi, H. Miyazaki, Y. Kawamura, H. Nakamura, K. Arata, Chem. Mater. 13 (2001) 3038.

43. V.V. Brei, S.V. Prudius, O.S. Melezhyk, Appl. Catal. 239 (2003) 11.

44. G.D. Yadav, A.D. Murkute, J. Catal. 224 (2004) 218.

45. V.S.Y. Lin, D.R. Radu, US Patent 7122688 B2 (2006).

46. M.Di Serio, M. Cozzolino, R. Tesser, P. Patrono, F. Pinzari, B. Bonelli, E. Santacesaria, Appl. Catal. A: Gen. 320 (2007) 1.

47. F. Chai, F. Cao, F. Zhai, Y. Chen, X. Wang, Zhongmuisu, Adv. Synth. Catal. 349 (2007) 1057.

48. P. Morin, B. Hamad, G. Sapaly, M.G. Carneiro Rocha, P.G. Pries de Oliviera, W.A. Gonzales, E. Andrade Sales, N. Essayemet, Appl. Catal. A: Gen. 330 (2007) 69.

49. G. Vicente, A. Coteron, M. Martinez, J. Aracil, Ind. Crops Products 8 (1998) 29.

50. S.C.M. dos Reis, E.R. Lachter, R.S.V. Nascimento, J.A.J. Rodriguez, M. Garcia Reid, J. Am. Oil Chem. Soc. 82 (2005) 661.

51. Y. Liu, E. Lotero, J.G. Goodwin Jr., J. Catal. 243 (2006) 221.

52. P.S. Sreeprasanth, R. Srivastava, D. Srinivas, P. Ratnasamy, Appl. Catal. A: Gen. 314 (2006) 148.

53. G.J. Suppes, M.A. Dasari, E.J. Doskocil, P.J. Mankidy, M.J. Goff, Appl. Catal. A: Gen. 257(2004) 213.

54. D. Barthomeuf, Catal. Rev. Sci. Eng. 38(1996) 521.

55. E. Leclercq, A. Finiels, C. Moreau, J. Am. Oil. Chem. Soc. 78 (2001) 1161.

56. W. Xie, X. Huang, H. Li, Biores. Technol. 98 (2007) 936.

57. S. Bancquart, C. Vanhove, Y. Pouilloux, J. Barrault, Appl. Catal. A: Gen 218 (2001) 1.

58. S. Gryglewicz, Bioresour. Technol. 70 (1999) 249.

59. L. Wang, J. Yang, Fuel 86 (2007) 328.

60. A. Demirbas, Energy Conv. Manag. 48 (2007) 937.

61. X. Liu, H. He, Y. Wang, S. Zhu, Catal. Comm. 8 (2007) 1107.

62. N.S. Babu, R. Sree, P.S.S. Prasad, N. Lingaiah, Energy Fuels 22 (2008) 1965.

63. A. Kawashima, K. Matsubara, K. Honda, Biores. Technol. 99 (2008) 3439.

64. S. Yan, H. Lu, B. Liang, Energy Fuels 22 (2008) 646.

65. H.J. Kim, B.S. Kang, M.J. Kim, Y.M. Park, D.K. Kim, J.S. Lee, K.Y. Lee, Catal. Today 93 (2004) 315.

66. C.S. MacLeod, A.P. Harvey, A.F. Lee, K. Wilson, Chem. Eng. J. 135 (2008) 63.

67. (a) W. Xie, X. Huang, Catal. Lett. 107 (2006) 53.

    (b) W. Xie, Z. Yang, H. Chun, Ind. Eng. Chem. Res. 46 (2007) 7942.

68. B.M.E.Rusbueldt,W.F. Hoelderich, J. Catal. 271 (2010) 290.

69. A. D'Cruz, M.G. Kulkarni, L.C. Meher, A.K. Dalai, J. Am. Oil. Chem. Soc. 84 (2007) 937.

70. W. Xie, H. Li, J. Mol. Catal. A: Chem. 255 (2006) 1.

71. N. Boz, M. Kara, Chem. Eng. Comm. 196 (2009) 80.

72. E. Li, V. Rudolph, Energy Fuels 22 (2008) 145.

73. M.C.G. Albuquerque, I. Jiménez-Urbistondo, J. Santamaría-González, J.M. Mérida-Robles, R. Moreno-Tost, E. Rodríguez-Castellón, A. Jiménez-López, D.C.S. Azevedo, C.L. Cavalcante Jr., P. Maireles-Torres, Appl. Catal. A: Gen. 334 (2008) 35.

74. G.S. Macala, A.W. Robertson, C.L. Johnson, Z.B. Day, R.S. Lewis, M.G. White, A.V. Iretskii, P.C. Ford, Catal. Lett. 122 (2008) 205.

75. A. Corma, S.B.A. Hamid, S.Iborra, A.J. Velty, J. Catal. 234 (2005) 340.

76. W. Xie, H. Peng, L. Chen, J. Mol. Catal A: Chem. 246 (2006) 24.

77. M. Di Serio, M. Ledda, M. Cozzolino, G. Minutillo, R. Tesser, E. Santacesaria, Ind. Eng. Chem. Res. 45 (2006) 3009.

78. U. Schuchardt, R.M. Vargas, G. Gelbard, J. Mol. Catal. A: Chem. 99 (1995) 65.

79. R. Sercheli, R.M. Vargas, U. Schuchardt, J. Am. Oil Chem. Soc. 76 (1999) 1207.

80. S.K.F. Peter, R. Ganswindt, H.P. Neuner, E. Weidner, Eur. J. Lipid Sci. Technol. 104 (2002) 324.

81. H. Fuduka, A.K ondo, H. Noda, J. Biosci. Bioeng. 92 (2001) 405.

82. S. Saka, K. Dadan, Fuel 80 (2001) 225.

83. S.Yan, S.O. Salley, Ng K.Y. Simon, Appl. Catal. A: Gen. 353 (2009) 203.

84. Y. Zhang, M.A. Dube, D.D. McLean, M. Kates, Bioresour. Technol. 90 (2003) 229.

85. M.A. Camblor, A. Corma, A. Martinez, J. Perezpariente, J. Primo, Heterogeneous Catalysis and Fine Chemicals. 78 (1993) 393.

86. K. Suwannakarna, Ph.D. thesis (2008), Clemenson University.

87. R. Stern, G. Hillion, J.-J., Rouxel, S. Leporq, U.S. Patent 5908946 (1999).

88. L. Bournay, G. Hillion, P. Boucot, J.A. Chodorge, C. Bronner, A. Forestiere, U.S. Patent 6878837 (2005).

89. L. Bournay, D. Casanave, B. Delfort, G. Hillion, J.A. Chodorge, Catal. Today 106 (2005) 190.

90. D.E. Lopez, J.G. Goodwin Jr., D.A. Bruce, J. Catal. 245 (2007) 381.

91. D.E. Lopez, J.G. Goodwin Jr., D.A. Bruce, S. Furuta, Appl. Catal. A: Gen. 339 (2008) 7683.

92. Phil Thane, "Breaking Away from Potassium Hydrpoxide" Biofuels International, Nov. (2008) 53.

93. Axens - www.axens.net.

94. Biodiesel Production: Technologies and European Providers- A Report to IEA Bioenergy TASK 39, T39-B6, 06 July 2007

95. Benefuel - www.benefuel.net.

96. Catilin - www.catilin.com.

97. Nippons Process - http://www.shokubai.co.jp/cn/news/2008/080424.pdf.

98. Endicott Biofuels - http://www.endicottbiofuels.com.

99. Davy Process Technology - http://www.davyprotech.com.

100. H.H. Kung "Transition Metal Oxides: Surface Chemistry and Catalysis" Stud. Surf. Sci. Catal., 45 (1989) 1.

101. P.P. Gravereau, E. Garnier, Antonie Hardy, Acta Crystallogr. B 35 (1979)

2843.

102   D. Srinivas, J.K. Satyarthi, Catal. Surv. Asia. DOI 10.1007/s10563-010-9108-2.

103.   I. Kim, J.T. Ahn, C.S. Ha, C.S. Yang, I. Park, Polymer 44 (2003) 3417.

104.   S. Chen, Z. Hua, Z. Fang, G. Qi, Polymer 45 (2004) 6519.

105.   L. Reguera, J. Balmaseda, C.P. Krap, M. Avila, E. Reguera, J. Phys. Chem. C 112 (2008) 17443.

106.   R. Srivastava, D. Srinivas, P. Ratnasamy, J. Catal. 241 (2006) 34.

107.   P. Šimáček, D. Kubička, G. Šebor, M. Pospíšil, Fuel, 88 (2009) 456.

108.   T. Kalnes, T. Marker, D.R. Shonnard, International J. Chem. Reactor Engin. 5 (2007) A48.

109.   EERE, Department of Energy, U.S. Hydrogenation Derived Renewable Diesel.

http://www.eere.energy.gov/afdc/fuels/emerging_green_production.html.

110.   J. Gusmao, D. Brodzki, G. Djega-Mariadassou, R. Frety, Catal. Today 5 (1989) 533.

111.   S. Lestari, I. Simakova, A. Tokarev, P. Mäki-Arvela, K. Eränen, D. Yu Murzin, Catal. Lett.122 (2008) 247.

112.   G. Sienel, R. Rieth, K.T. Rowbottom, Epoxides, in Ulmann's Encyclopedia of Industrial Chemistry, 6th ed., Verlag Chemie, Weiheim (2003).

113.   (a) Ed.- S.T. Oyama "Mechanisms in Homogeneous and Heterogeneous Epoxidation Catalysis" First Ed. (2008) Elsevier.
(b) Höllriegelskreuth, Peroxygen Compounds in Organic Synthesis, Epoxidation, Chapter 6, 11-17 (1981).

114.   T.-C. Chou, J.-Y. Chang, Chem. Eng. Commun. 41 (1986) 253.

115.   F. van Rantwijk, R.A. Sheldon, Curr. Opin. Biotechnol. 11(2000) 554.

116.   R. Sheldon, Bull. Soc. Chim. Belg. 94 (1985) 651.

117.   L.C. Meher, D. Vidya Sagar, S.N. Naik, Renew. Sustain. Energy Rev. 10 (2006) 248.

118.   G. Knothe, Trans ASAE 44 (2001) 193.

119.   B. Freedman, E.H. Pryde, W.H. Kwolek, J. Am. Oil. Chem. Soc. 61 (1984) 1215.

120.   C. Plank, E. Lorbeer, J. Chromatogr. A 697 (1995) 461.

121.   (a) M. Mittelbach, Chromatographia 37 (1993) 623.

(b) D.G.B. Boocock, WO 0112581 (2001).

122.   B. Trathnigg, M. Mittelbach, J. Liq. Chromatogr. 13 (1990) 95.

123.   P. Lozano, N. Chirat, J. Graille, D. Pioch, Fresenius J. Anal. Chem. 354 (1996) 319.

124.   T. A. Foglia, K.C. Kwolek, J. Liq. Chromatogr. Relat. Technol. 61 (1997) 1829.

125.   M. Holcapek, P. Jandera, J. Fischer, B. Prokes, J. Chromatogr. A858 (1999) 13.

126.   D. Darnoko, M. Cheryan, E.G. Perkins, J. Liq. Chrom. Relat. Technol. 23 (2000) 2327.

127.   R. Fillieres, B.B. Mlayah, M. Delmas, J. Am. Oil. Chem. Soc. 72 (1995) 427.

128.   G. Gelbard, O. Bres, R.M. Vargas, F. Vielfaure, U.F. Schuchardt, J. Am. Oil Chem. Soc. 72(1995) 1239.

129.   G. Knothe, J. Am. Oil. Chem. Soc. 77 (2000) 489.

130.   G. Knothe, J. Am. Oil. Chem. Soc. 76 (1999) 795.

Chapter 2

Catalyst Preparation and Characterization

2.1. Introduction

This chapter describes the synthesis methodologies of various catalysts investigated in the present study. It also presents the methods of characterization of the catalyst materials and the details of analytical procedure used for the analysis of reaction products. As described in Chapter 1, the objective of the thesis is to develop efficient solid catalysts for (1) the conversion of vegetable oil into fatty acids (FA) by hydrolysis, (2) esterification of FA into fatty acid alkyl esters (biodiesel or biolubricants), (3) epoxidation of FA and their esters, and (4) conversion of vegetable oils into hydrocarbons (HCs) by hydrodeoxygenation (HDO). In this endeavour the various catalysts investigated in the present work include:

(1) Fe-Zn and Co-Zn double-metal cyanide (DMC) complexes

(2) Sulfated zirconia (SZ),

(3) Al-incorporated mesoporous silica (Al-MCM-41),

(4) ZnO,

(5) Zeolites : HY, Hβ and SAPO-11,

(6) Alumina-supported group VI metal oxides (group VI metal: Cr, Mo and W)

(7) Alumina-supported Ni-Mo catalyst., and

(8) Amberlyst[TM]70 resin.

Detailed synthesis procedure and characterization of various catalysts are described in the following sections.

2.2. Catalyst Preparation

2.2.1. Solid Double-Metal Cyanide (DMC) Complex

Double-metal cyanides have been widely investigated from the point of view of their structure and electronic properties [1]. One of the members of this family studied extensively is Prussian blue. Only recently, their catalytic properties have been reported in a commercially important organic transformation [2]. Fe- and Co-Zn double metal cyanides exhibited remarkable catalytic activity in polyethers synthesis by ring opening polymerization (ROP) of ethene and propene oxides [3]. Interestingly, this catalyst is insoluble in almost all solvents. It is insoluble even in strong acids and aqua-regia. Hence, it could be used as a solid, reusable catalyst. Zn coordinated to imine groups exhibited superior activity for CO_2 insertion in the epoxide ring to produce cyclic and polycarbonates [4]. A similar structural environment for Zn in Fe-Zn and Co-Zn double metal cyanide catalysts was

attributed the cause for its high catalytic activity in ROP [3]. Recently, Sreeprasanth et al [5] reported the activity of Fe-Zn catalysts for transesterification of vegetable oils into biodiesel and biolubricants. The superior catalytic activity of Fe-Zn DMC was attributed to its hydrophobic surface structure. In the present study, the application of DMC is reported, for the first time, for the hydrolysis of vegetable oils/fats and esterification of fatty acids. A detailed synthesis of different materials prepared under this category is presented below.

2.2.1.1 Fe-Zn DMC

Fe-Zn double-metal cyanide (DMC) complex was prepared using $K_4Fe(CN)_6 \cdot 3H_2O$ as a source of Fe, $ZnCl_2$ as a source of Zn and *tert.*-butanol as the complexing agent. In a typical preparation of DMC complex, 0.01 mol of potassium ferrocyanide, $K_4Fe(CN)_6 \cdot 3H_2O$, was dissolved in 40 mL of double-distilled water to prepare solution A. In a separate a beaker, solution B was prepared by dissolving 0.1 mol of $ZnCl_2$ in 100 mL of distilled water and 20 mL of *tert.*-butanol. Solution C was prepared by dissolving 15 g of a tri-block copolymer, poly(ethylene glycol)-block-poly(propylene glycol)-block-poly(ethylene glycol) (average molecular weight = 5800; Aldrich) in 2 mL of distilled water and 40 mL of *tert.*-butanol. Solution B was added to solution A slowly over 1 h at 323 K under vigorous stirring. Precipitation of a solid occurred during the addition. To that mixture, solution C was added over 5–10 min and stirring was continued for another 1 h. The solid was filtered, washed thoroughly with double-distilled water to remove all the uncomplexed ions, and dried at 298 K for several hours. This material was activated at 180 - 200ºC for 4 h prior to using it in the reactions.

2.2.1.2. Co-Zn DMC

The Co-Zn double-metal cyanide complex was prepared in the same manner as that of Fe-Zn DMC except for the use of $K_3[Co(CN)_6]$ instead of $K_4[Fe(CN)_6].3H_2O$. In a typical preparation, 0.01 mol of $K_3[Co(CN)_6]$ was dissolved 40 mL of double distilled water to prepare solution A. In a separate a beaker, solution B was prepared by dissolving 0.1 mol of $ZnCl_2$ in 100 mL of distilled water and 20 mL of *tert.*-butanol. Solution C was prepared by dissolving 15 g of a tri-block copolymer, poly(ethylene glycol)-block-poly(propylene glycol)-block-poly(ethylene glycol) (average molecular weight = 5800; Aldrich) in 2 mL of distilled water and 40 mL of *tert.*-butanol. Solution B was added to solution A slowly over 1 h at 323 K under

vigorous stirring. Then, solution C was added over 5–10 min and stirring was continued for another 1 h. The solid formed was filtered, washed with distilled water (500 mL) and dried at 298 K. This material was activated at 453 – 473 K for 4 h prior to using in reactions.

2.2.2. Al-incorporated Mesoporous Silica (Al-MCM-41)

Al-MCM-41 is one of the catalysts which possess large pore size (mesoporous), high surface area and good acidity (depending upon Al incorporation). It, therefore, can also be used for acid catalyzed reactions of large molecules such as fatty acids and vegetable oils/fats. Al MCM-41 has been used for many acid catalyzed reactions such as esterification [6, 7], cracking of straight chain naphtha [8], oligomerization of olefins [9], dealkylation [10], etc. Recently, it has also been reported for the esterification of palmitic acid with methanol for biodiesel production [11]. A general procedure for Al-MCM-41 synthesis is given below.

Al-MCM-41 was prepared according to known procedure [12] by hydrothermal synthesis route. In a typical preparation, 2.67 g of sodium hydroxide was dissolved in 147 g of distilled water. To it, 5.95 g of cetyl trimethyl ammonium bromide (Aldrich) was added and stirred for 1 h until a homogeneous solution was obtained. Then, 4 g of fumed silica (Aldrich) was added over 45 min and stirring was continued for another 1 h. The pH of the slurry was adjusted to 9.5 using a 4 N sulphuric acid solution. Sodium aluminate (0.112 g; alumina content = 44%; Aldrich) was dissolved in 10 mL of distilled water and added to the above slurry over 15 min. The resultant gel was stirred for 6 h, transferred to a Teflon-lined stainless-steel autoclave and subjected to hydrothermal synthesis at 373 K for 48 h. The solid formed was filtered, washed and dried at 373 K and then, calcined at 823 K for 6 h to remove the template molecules. Si/Al ratio in the final product was 48.

2.2.3. Alumina-supported Group VI Transition Metal Oxides

Transition metal oxides are used as catalysts in both redox and acid-base reactions because of their ability to take part in the exchange of electrons, as well as in the exchange of protons or oxide ions. The property of transition metals to be good catalysts also depends on the absorption or adsorption properties of the metal and the transition metal complex. Transition metal oxides possess low surface area and adsorption take place on the surface only, therefore these metal oxide are generally dispersed on high surface area supports such alumina or silica and can be used for

redox and acid-base reactions. In the present study, Group VI transition metal oxides were prepared by impregnation method. Following are their detailed preparation procedures.

2.2.3.1. MoO$_x$/Al$_2$O$_3$

First γ-alumina was activated at 473 K for 3 h to remove any adsorbed water and other species. Then, it was cooled to 298 K in a desiccator. In the preparation of 5% MoO$_x$/Al$_2$O$_3$, 0.646g of ammonium heptamolybdate tetrahydrate [(NH$_4$)$_6$Mo$_7$O$_{27}$.4H$_2$O] was dissolved in water so that total volume was made to 11 mL. This solution was added to 10 g of activated γ-alumina taken in a China-dish, slowly and uniformly. After this, the sample was left for dryness at 298 K for 5-6 h and then, dried at 373 K overnight. It was, then, calcined at 873 K for 6 h (temperature ramp rate = 2 K/min) and stored in a sealed bottle placed in a CaCl$_2$-desiccator.

10% MoO$_x$/Al$_2$O$_3$ and 15% MoO$_x$/Al$_2$O$_3$ were prepared in a similar manner by taking 1.363 and 2.165 g, respectively, of ammonium heptamolybdate tetrahydrate. After calcination, 5% MoO$_x$/Al$_2$O$_3$ was white while 10% and 15% MoO$_x$/Al$_2$O$_3$ were faint blue in colour.

2.2.3.2. CrO$_x$/Al$_2$O$_3$

In the preparation of CrO$_x$/Al$_2$O$_3$, chromium nitrate nonahydrate [Cr(NO$_3$).9H$_2$O] was used as the Cr source. In a typical preparation of 5% CrO$_x$/Al$_2$O$_3$, 1.386 g of chromium nitrate nonahydrate was dissolved in water so that total volume was made to 6 mL. This solution was added to 5 g of activated γ-alumina (prepared as above) taken in a China-dish, slowly and uniformly. After this, the sample was left to dryness at 298 K for 5-6 h. It was then dried at 373 K overnight. The dried sample was calcined at 873 K for 6 h (temperature ramp rate = 2 K/min) and stored in a sealed bottle placed in a CaCl$_2$-desiccator.

10% CrO$_x$/Al$_2$O$_3$ and 15% CrO$_x$/Al$_2$O$_3$ were prepared using the same procedure taking 2.924 and 4.656 g, respectively, of chromium nitrate nonahydrate. The calcined CrO$_x$/Al$_2$O$_3$ catalysts were green in colour.

2.2.3.3. WO$_x$/Al$_2$O$_3$

Here, the tungsten source used was ammonium tungstate [(NH$_4$)$_{10}$H$_2$(W$_2$O$_7$)$_6$]. As this compound is not soluble in water, it was treated with H$_2$O$_2$ to get a clear solution. In the preparation of 5%WO$_x$/Al$_2$O$_3$, 0.293 g of ammonium tungstate was

treated with minimum amount of 30% aq. H_2O_2 to get a clear solution. Then, the volume of the solution was made to 6 mL. This solution was added to 5 g of activated γ-alumina taken in a China-dish, slowly and uniformly. Rest of the procedure was same as used for the other supported oxides.

10% WO_x/Al_2O_3 and 15% WO_x/Al_2O_3 were prepared following the same procedure taking 0.613 and 0.971 g, respectively, of ammonium tungstate. After calcination all the tungsten catalysts were white in colour.

2.2.3.4. Phosphorous-modified MoO_x/Al_2O_3

To study the influence of phosphorous, before the impregnation of molybdenum, activated γ-alumina was first, impregnated with 1% phosphoric acid (H_3PO_4). For this, 0.345 g of 88% *ortho*-phosphoric acid was dissolved in 33 mL of water. 30 g of activated γ-alumina was dispersed in that solution. This sample was left to dryness at 298 K for 5-6 h. It was then, dried at 373 K overnight and calcined at 873 K for 6 h. This phosphorous-modified alumina was used instead of neat alumina to prepare the phosphorous-modified 5, 10 and 15% $MoO_x/P-Al_2O_3$ catalyst samples using the procedure described for MoO_x/Al_2O_3. The phosphorus-modified molybdenum catalysts were similar in colour as those without phosphorous.

2.2.4. ZnO

Nanoscopic ZnO was prepared as follows [13]: To a 10% solution of $Zn(NO_3)_2.6H_2O$, 45 g of polyethylene glycol (PEG-4000, Loba Chem.) was added slowly over a period of 1.5 h with stirring. The pH of the solution was adjusted to 6 – 7 and stirring was continued for another 24 h. The solid ZnO formed was filtered, washed with distilled water, dried at 373 K and calcined at 823 K for 6 h.

2.2.5. Other Catalysts

H-β ($SiO_2/Al_2O_3 = 28$) and H-Y ($SiO_2/Al_2O_3 = 5$) zeolites were supplied by the Catalyst Pilot Plant, National Chemical Laboratory, Pune. SAPO-11 (1.5 mm TRX) and some samples of MoO_x/Al_2O_3 (MoO_x content = 15 wt%, P content = 1.2 wt %) were obtained from Sud-Chemie India Ltd. Sulfated zirconia (1.5 mm pellets) was procured from Saint-Gobain, Norpro. High temperature, strongly acidic, macroporous polymer – Amberlyst[TM]70 was obtained from Rohm and Haas, USA.

2.3. Catalyst Characterization Techniques

2.3.1. X-ray Powder Diffraction (XRD)

XRD is an important tool, helps determining the crystallinity, phase purity, crystal structure and crystallite size of catalyst materials [14]. The XRD method

involves interaction between the incident monochromatized X-rays (like Cu Kα or Mo Kα) with the atoms of a periodic lattice. X-rays scattered by the atoms in an ordered lattice interfere constructively as described by Bragg's law: $n\lambda = 2d \sin\theta$, where, λ is the wavelength of the X-rays, d is the distance between two lattice planes, θ is the angle between the incoming X-rays and the normal to the reflecting lattice plane and *n* is an integer known as the order of reflection [14, 15].

The mesoporous materials were analyzed using an X'Pert Pro (Philips) diffractometer with Cu-Kα radiation ($\lambda = 0.15406$ nm) and a proportional counter as a detector. A divergent slit of 1/32° on the primary optics and an anti-scatter slit of 1/16° on the secondary optics were used to measure the data in the low-angle region. The rest of the catalysts were analyzed using a Rigaku Geigerflex X-ray diffractometer with Ni-filtered Cu-Kα radiation (40 kV, 30 mA). The XRD patterns were measured in the 2θ range of 0.5 − 10º in the case of mesoporous Al-MCM 41 and 5 − 80° in the case of rest of catalyst at a scan rate of 1 and 4°/min, respectively. Crystallite size of the materials was determined using the Scherrer equation: $L = K\lambda/\beta\cos\theta$, where θ and λ are the Brag angle and wavelength of incident X-ray radiation, respectively. K is a constant approximately taken as 0.9; β is the line width on the 2θ scale in radians. Unit cell parameter (a) for cubic systems (DMC catalysts) was found using the equation: $a = d(111)\sqrt{(h^2+k^2+l^2)}$. Here, d is the inter-planar distance obtained from the Bragg's equation while considering the value of n as unity.

2.3.2. Diffuse Reflectance UV-Visible Spectroscopy (DRUV-Vis)

This technique is based on the reflection of light in the ultraviolet (UV) and visible region by a powdered sample. In a DR spectrum, the ratio of the light reflected from a thick closely packed catalyst layer and the reflected light from an infinitely thick layer of an ideal non-absorbing (white) reference sample is measured as a function of wavelength, λ. DRUV-Vis spectroscopy is a highly sensitive and powerful technique for identification and characterization of the metal ion's coordination and location (framework or extra framework) in metal-containing solid catalysts [16]. Blue shift in charge transfer band of metal oxide can also be used to differentiate between bulk and well dispersed metal oxide on supports like silica or alumina. The measurements were conducted on a Shimadzu UV-2550 spectrophotometer equipped with an integrating sphere attachment (ISR 2200). In general, spectral grade $BaSO_4$ was used as the reference material.

2.3.3. Fourier Transform Infrared Spectroscopy (FTIR)

The formation of silicate framework and metal ion incorporation were determined using FTIR spectroscopy [17]. The spectra were recorded on a Shimadzu FTIR-8201 PC spectrophotometer in the wave number range of 400 – 4000 cm^{-1}. The samples were made into KBr pellets (1 wt %) or as such in DRIFT mode. In general, neat KBr was used as a reference material.

2.3.4. Energy Dispersive Analysis of X-ray (EDAX)

EDAX is a micro-chemical analysis technique. It is also sometimes referred to as EDX or EDS. It is a technique to identify the elemental composition of the specimen or for an area of interest. During EDAX analysis the specimen is bombarded with the incident electron beam. When a voltage of 10-20 keV is used in SEM, the incident electrons knock out the inner core level electrons of the sample. The electrons from the higher energy levels fill up the vacancy thus created. During this transition X-rays are emitted which is plotted as number of counts (intensity) with respect to the BE. The detector is made of the Li drifted Si detector, known as Si-Li detector and is operated at liquid nitrogen temperatures

EDAX measurements described in this thesis were performed on a Leica Stereoscan-440 scanning electron microscope instrument equipped with a Phoenix EDAX attachment. Samples for EDAX analysis were made by coating the sample solutions onto Si (111) wafers or sample holders. In some cases, powder samples were also used directly on the sample-holder for the measurement [18]. Elemental mapping was carried out in above mentioned SEM system equipped with an EDAX analyzer (Bruker, D451-10C Quantax 200 with X-flash detector) attachment. X-flash 4010 detector was employed for fast and high resolution real time spectrometry and elemental mapping. EDAX spectra were recorded in the spot-profile mode by focusing the electron beam onto specific regions of the sample. However, materials composition reported is based on the data collected over large areas (>300 μm2). Chemical mapping enables to determine the elements present within sample volumes of 10-30 cubic micrometers or less.

2.3.5. X-ray Photoelectron Spectroscopy (XPS)

The nature, oxidation state and dispersion of surface metal species were estimated by XPS [19]. The spectra of calcined powder samples were acquired on a VG Microtech Multilab ESCA 3000 instrument with a non-monochromatized Mg Kα radiation (hν = 1253.6 eV). Base pressure in the analysis chamber was maintained at

$3 - 6 \times 10^{-10}$ bar range. The energy resolution of the spectrometer was set at 0.8 eV at pass energy of 20 eV. Binding energy (BE) was calibrated with respect to Au 4f 7/2 core level (83.9 eV). The error in all the BE values reported is ± 0.1 eV.

2.3.6. Temperature-Programmed Desorption (TPD)

Acidity or basicity of solid catalysts can be investigated by adsorption/desorption techniques of basic or acidic probe molecule respectively. NH_3 was used as a probe molecule for measuring the acidity of catalysts. From the amount of desorption of the corresponding probe molecule, total acidity of the catalyst was estimated.

2.3.7. Nitrogen Physisorption – Textural Characterization

The most common method of measuring surface area and textural characteristics of catalyst materials is that based on the theory developed by Brunauer, Emmett and Teller (BET), considering the multilayer adsorption. The BET equation can be represented as: $P/V(P_o-P) = 1/cV_m + [(c-1)/cV_m] (P/P_o)$, where P is adsorption equilibrium pressure, P_o is saturation vapour pressure of the adsorbate at the experimental temperature, V is the volume of N_2 adsorbed at a pressure P, V_m is the volume of adsorbate required for monolayer coverage, and *c*, a constant that is related to the heat of adsorption and liquefaction [20]. A linear relationship between $P/V(P_o-P)$ and P/P_o is required to obtain the quantity of nitrogen adsorbed. The monolayer volume, V_m is given by $1/(S+I)$, where S is the slope and is equal to $(c-1)/cV_m$ and I is the intercept equal to $1/cV_m$. The surface area of the catalyst (S_{BET}) is related to V_m, by the equation: $S_{BET} = (V_m/22414)N_a\sigma$, where N_a is Avagadro number and σ is mean cross sectional area covered by one adsorbate molecule. The value of σ generally accepted for N_2 is 0.162 nm^2. Several computational procedures are available for the derivation of pore size distribution of mesoporous samples from physisorption isotherms. Most popular among them is the Barrett-Joyner-Halenda (BJH) model, which is based on speculative emptying of the pores by a stepwise reduction of P/P_o, and allowance being made for the contraction of the multilayer in those pores already emptied by the condensate [21]. The mesopore size distribution is usually expressed as a plot of $\Delta V_p/\Delta r_p$ versus r_p, where V_p is the mesopore volume, and r_p is the pore radius. Adsorption of nitrogen measured by Brunauer-Emmett-Teller (BET) equation at low pressure (10^{-4} Torr) and liquification temperature of N_2 (77 K) is the standard method for determination of surface area, pore volumes and pore size distribution of molecular sieves. All these measurements were conducted on a Coulter (Omnisorb 100 CX) instrument.

2.3.8. Scanning Electron Microscopy (SEM)

SEM probes the morphological characteristics of materials. SEM scans over a sample surface with a probe of electrons (5-50 eV) and detects the yield of either secondary or back-scattered electrons as a function of the position of the primary beam. Contrast is generally caused by the orientation that part of the surface facing the detector appears brighter than parts of the surface with their surface normal pointing away from the detector. The interaction between the electron beam and the sample produces different types of signals providing detailed information about the surface structure and morphology of the sample [22]. When an electron from the beam encounters a nucleus in the sample, the resultant Coulombic attraction leads to a deflection in the electron's path, known as Rutherford elastic scattering. A fraction of these electrons will be completely backscattered, re-emerging from the incident surface of the sample. Since the scattering angle depends on the atomic number of the nucleus, the primary electrons arriving at a given detector position can be used to produce images containing topological and compositional information [23]. A major advantage of SEM is that bulk samples can also be directly studied by this technique. SEM of the catalyst samples in this work were recorded using a SEM Leica 440 instrument operating at 100 kV.

2.3.9. Transmission Electron Microscopy (TEM)

TEM is typically used for high resolution imaging of thin films of a solid sample for micro structural and compositional analysis. The technique involves: (i) irradiation of a very thin sample by a high-energy electron beam, which is diffracted by the lattices of a crystalline or semi crystalline material and propagated along different directions, (ii) imaging and angular distribution analysis of the forward scattered electrons (unlike SEM where backscattered electrons are detected), and (iii) energy analysis of the emitted X rays [24]. In detail, a primary electron beam of high energy and high intensity passes through a condenser to produce parallel rays, which impinges on the sample. As the attenuation of the beam depends on the density and thickness, the transmitted electrons form a two-dimensional projection of the sample mass, which is subsequently magnified by the electron optics to produce the so-called bright field image. The dark field image is obtained from the diffracted electron beams, which are slightly off angle from the transmitted beam. Typical operating conditions of TEM instruments are 100-200 KeV electrons, 10^{-6} mbar vacuum, 0.5

nm resolution and a magnification of about 105. The topographic information obtained by TEM in the vicinity of atomic resolution can be utilized for structural characterization and identification of various phases of mesoporous materials, *viz.*, hexagonal, cubic or lamellar [25]. TEM also provides real space image on the atomic distribution in the bulk and surface of a nano-crystal [26]. TEM of the samples were recorded using a JEOL-model 1200 EX instrument operating at 100 KV.

Details of characterization results of different catalysts are reported in the respective chapters.

2.4. Reaction Procedure

2.4.1. Hydrolysis of Vegetable Oils/Fats

A known quantity of vegetable oil or fat (5 – 20 g), water (molar ratio of oil (fat) : water = 1: 5 to 1: 40) and catalyst in powdered form (1 – 10 wt% of oil) were taken in a Teflon-lined, stainless steel autoclave (100 mL). The reaction was conducted at 433 – 483 K and autogeneous pressure for a specific period of time (1 – 12 h) by mounting the autoclave in a rotating hydrothermal synthesis reactor (Hiro Co., Japan). At the end of the reaction, the autoclave was cooled to 298 K and the catalyst was separated by filtration. The reaction product consisted of two layers, an upper oily layer of fatty acids and mono-, di- and triglycerides and a lower, aqueous layer of water and glycerol. These layers were separated using a separating funnel or by decantation. Glycerol was obtained by removing the water from the lower layer by distillation under vacuum. Any trace of water in the upper layer was removed by distillation. In some cases, petroleum ether (5 – 10 mL) was added after the completion of reaction to facilitate separation of the solid catalyst. A few reactions were conducted in a 300 mL Paar stainless-steel stirred tank reactor. Several edible (coconut, palmolein, and soybean) and non-edible (castor, jatropha, karanja, palm and rubber seed) oils and chicken fat have been hydrolyzed.

With a view to improve the miscibility of oil/fat with water, some experiments were carried out in the presence of solvents (N, N-dimethylformamide (DMF), tetrahydrofuran (THF), acetone), phase transfer agents (tetrapropylammonium bromide, TPAB) or surfactants (Triton X-100). In other studies, prior to conducting the reactions, a portion of the product mixture or oleic acid (1 – 20 wt %) was added to the reactants.

In some studies, at the end of the hydrolysis reaction the solid catalyst was separated from the product mixture and, without any further treatment was used in another fresh batch of the hydrolysis reaction. The catalyst was reused in five consecutive recycles.

2.4.1.1. Product Analysis

High Performance Liquid Chromatography. The fatty acid products of the reaction were analyzed using a Perkin-Elmer (Series 200) high performance liquid chromatograph (HPLC) equipped with a quaternary pump, auto sampler, degasser, thermostated column compartment and TotalChrom navigator-PE-HPLC software. An ELSD detector from Gilson and a reverse-phase, Perkin-Elmer Brownlee column (C-18 Spheri-5, 250 x 4.6 mm with a 5 μm particle size) were used in the analysis.

^{1}H NMR (Bruker Avance 200 MHz) and Fourier transform infrared (Shimadzu FTIR 8300) spectroscopic techniques were also used to identify and estimate the products. The acid values of the product mixture and of the oil and fat were determined by titration with 0.1 N NaOH solution and using phenolphthalein as the indicator.

Determination of Acid Value. For determination of acid value [27] of the vegetable oils and hydrolyzed samples, 0.5 g or 1 g of sample was weighed in a conical flask and dissolved in a solvent mixture containing equal parts of toluene and isopropyl alcohol v/v; 3-5 drops of Phenolphthalein indicator (1%, Merck, India) was added and then titrated with 0.1 N standardized sodium hydroxide solution until the light pink coloration. Acid value of the sample can be calculated by the formula :

$$\text{Acid Value} = \frac{56.1 \times N_{NaOH} \times V_{NaOH}}{W_{Sample}}$$

where 56.1 is the molecular weight of potassium hydroxide as acid value is always reported as mg of KOH per g of sample.

N_{NaOH} = normality of NaOH V_{NaOH} – volume of NaOH used

W_{Sample} = weight of the sample taken for titration.

Percentage of FA can also be determined assuming that the average molecular weight of the fatty acids is 282

$$\text{\% of Fatty Acid} = \frac{N_{NaOH} \times V_{NaOH} \times 282}{W_{Sample}} \times 100$$

Determination of Iodine Number. For the determination of iodine value [27] of the vegetable oils and fatty acids, 0.2 g of sample was weighed out into a clean dry stoppered conical flask of 500 mL capacity. It was then dissolved in about 10 mL of carbon tetrachloride and 25 mL of Wij's solution (0.1 M iodine monochloride solution in glacial acetic acid) was added. The resulting mixture, if turbid, was cleared by adding more carbon tetrachloride. The conical flask was then kept aside for about half an hour in a dark place. Then 20 mL of 10% KI solution was added and the mixture was diluted by adding 100 mL of water. The mixture was then titrated with standard thiosulphate solution (which was already standardized by 0.1 N potassium dichromate solution iodometry titration) till pale yellow color then 0.5 mL of starch indicator (freshly prepared 1% starch solution) was added. Mixture turns blue and again titrated till first disappearance of blue color. A blank determination was carried out without the oil. Iodine value can be calculated from the following formula

$$\text{Iodine Value} = \frac{12.69 \times N_{\text{sod. thiosulphate}} \times (V_{\text{Blank}} - V_{\text{sod. thisulphate}})}{W_{\text{Sample}}}$$

where 12.69 is the atomic weight of iodine divided by 10 as iodine value is reported as centigram of iodine per gram of sample or gram of iodine consumed per 100 g of sample.

$V_{\text{Sod. thiosulphate}}$ = Volume of sodium thiosulphate used

$N_{\text{Sod. thiosulphate}}$ = Normality of sodium thiosulphate

V_{Blank} = Volume of sodium thiosulphate required for the blank

W_{Sample} = Weight of the sample taken for titration.

2.4.2. Esterification of Fatty Acids

Esterification of fatty acids with methanol was carried out in a batch reactor. 0.15 g of catalyst, 17.7 mmol of fatty acid and methanol (fatty acid: methanol molar ratio = 1: 1 - 20) were taken in a Teflon-lined, stainless steel autoclave (100 mL). The reaction was conducted by mounting the autoclave in a rotating hydrothermal reactor (Hiro Co., Japan). At the end of the reaction, the autoclave was cooled to 298 K and the catalyst was separated by filtration. Methanol from the reaction mixture was removed using a rotavapor. The acid values of the reaction mixture at the beginning and at the end of the reaction were determined by titration with 0.1 N NaOH solution

and using phenolphthalein as the indicator. ^{1}H NMR spectroscopy (Bruker AV 200 MHz) was also used to identify the product and to estimate the fatty acid conversion.

Esterification of octanoic ($C_{8.0}$), decanoic ($C_{10.0}$), dodecanoic ($C_{12.0}$), palmitic ($C_{16.0}$) and oleic ($C_{18.1}$) acids with methanol were conducted over DMC in the temperature range of 423 – 453 K. From the initial rates and using the differential rate law for the pseudo-first order esterification reaction, the rate constant (k) was determined at different temperatures. The activation energy (E_a) was determined using the Arrhenius equation. SZ and Al-MCM-41 were more active catalysts than DMC. The kinetic data for SZ and Al-MCM-41 were determined at similar conversion levels (20 – 40 mols %) by carrying out the reactions at lower temperatures (353 – 403 K).Esterification reactions were also conducted keeping acid (oleic acid) constant and changing the chain length of alcohol (methanol, ethanol, 1-propanol, 1-butanol, 1-hexanol and 1-octanol). Reactions were conducted at different temperature and the kinetic parameters were determined.

2.4.3. Epoxidation of Fatty Acids and their Esters

Epoxidation of methyl soyate (fatty acid methyl ester obtained from soybean oil) was carried out in a glass batch reactor connected with a water condenser. In a typical reaction, 1 g of methyl soyate was taken in a 50 mL double-necked round bottom flask. Dried tert.-butyl hydroperoxide (TBHP mole ratio 0.5 to 4 with respect to methyl soyate) in 10 mL toluene was added to it. Then the flask was placed in the oil bath maintained at a required temperature (333 - 393 K) for the desired period of time (30 min – 12 h). Samples were taken at different time intervals and analyzed by ^{1}H NMR spectroscopy and gas chromatography (GC).

Determination of Peroxide. For the determination of peroxide (TBHP) [27] in the reaction mixture, 1 g of the reaction mixture was taken in the conical flask and 30 mL 2 M H_2SO_4 and 2 g KI were added. The mixture was kept for 15-20 min in a dark place. Then, the mixture was titrated with 0.1 N sodium thiosulphate (which was already standardized by 0.1 N potassium dichromate solution; iodometry titration) to faint yellow or straw colour. Swirl or stir gently during titration to minimize iodine loss. 1 mL freshly prepared 1% starch indicator was added. The mixture turned blue. The mixture was again titrated with sodium thiosulphate solution till first disappearance of blue colour. One blank titration was also carried out without taking

any peroxide. Knowing the value of sodium thiosulphate consumed for blank, peroxide content can be estimated by the following formula:

$$\text{Peroxide \%} = \frac{MW_p \times N_{\text{sod. thiosulphate}} \times (V_{\text{Blank}} - V_{\text{sod. thisulphate}})}{W_{\text{Sample}}} \times 100$$

where MW_P = Molecular weight of peroxide (TBHP)

$N_{\text{Sod. thiosulphate}}$ = normality of sodium thiosulphate

$V_{\text{Sod. thiosulphate}}$ = volume of sodium thiosulphate used

V_{Blank} = volume of sodium thiosulphate required for the blank

W_{Sample} = weight of the sample taken for titration.

2.4.4. Hydrodeoxygenation of Vegetable Oils

The reaction was carried out in a fixed-bed reactor at 573 K with 480 mL/min of hydrogen flow with a feed of soybean oil with dimethyl disulfide (100-1000 ppm to keep the catalyst in sulfide state) at WHSV of 0.5 h^{-1} under 50 bar pressure. After stabilization of the conditions, samples were taken at the interval of 6 h. The liquid product contains two layers one is water and other one of hydrocarbons. Hydrocarbon layer was separated and analyzed by gas chromatography, FTIR and NMR spectroscopies.

2.5. New Methods Developed for Product Analysis

2.5.1. ^{1}H NMR Method for Estimation of Fatty Acids Content

NMR spectroscopy has emerged as a highly interdisciplinary area of research. It is unparalleled as a technique with regard to the breadth and depth of applications it has generated in different disciplines of science. The NMR can be used for quantitative analysis based on the fact that the amplitude of a proton nuclear magnetic resonance (^{1}H NMR) signal is proportional to the number of hydrogen nuclei contained in the molecule [28, 29]. Although gas chromatography (GC) and high performance liquid chromatography (HPLC) are more sensitive techniques than NMR, the latter is a more rapid and easy method to use than the former. The area of the NMR peak depends mainly on the number of protons and not on their response factor as in the case of GC and HPLC. Each and every component FFA in the sample has a different response factor which needs to be predetermined and used in the

quantitative determination by the chromatographic techniques. Such time consuming and laborious processes can be eliminated in the case of NMR detection.

A new ^{1}H NMR Method has been developed for the estimation of fatty acids content present in vegetable oils and biodiesel. Scheme 2.1 describes the typical chemical structures and Fig. 2.1 depicts the ^{1}H NMR spectra of vegetable oil, FFA, and fatty acid methyl ester (biodiesel). Assignments of the ^{1}H NMR peaks are listed in Table 2.1. Quantification of the FFA content in vegetable oil and biodiesel by ^{1}H NMR is based on the fact that α-CH$_2$ peaks of fatty acids appear at δ values higher than those of the methyl (biodiesel) or glyceryl (vegetable oil) esters. The difference in chemical shift (between the acid and ester) is due to the greater deshielding effect of the carboxylic group compared to the ester group. Due to this shift, one of the peaks of the triplet of FFA (at 2.38 ppm in Fig. 2.2(a)) shifts out of the α-CH$_2$ region of the ester, and the other two peaks (2.35 and 2.30 ppm, respectively) are merged with those due to the ester at 2.34 and 2.31 ppm, respectively (Fig. 2.2 (a)). In other words, a sample containing FFA and ester (vegetable oil or biodiesel) shows a quartet like spectral pattern in the α-CH$_2$ region of the ^{1}H NMR spectrum (Fig. 2.2(b)) with the intensity of the peaks depending on the content of FFA in esters. The unmerged peak of the FFA triplet can be used to determine the FFA content in vegetable oil, animal fat and biodiesel. The area (A$_{FFA}$) of unmerged peak of FFA triplet (appearing around 2.38 ppm, out of the ester triplet) can be determined by integration. The triplet appears with intensity ratio of 1:2:1. The total area corresponding to the α-CH$_2$ groups of the FFA, will thus, be four times the area of the single unmerged FFA peak around 2.38 ppm. The percent molar concentration of FFA in oil or biodiesel is thus,

$$\% \text{ of FFA} \ = \ \frac{4 \times \text{Area of unmerged peak of } \alpha\text{-CH}_2 \text{ of FFA}}{\text{Total Area of } \alpha\text{-CH}_2 \text{ of both FFA and Ester}} \times 100$$

Alternatively, the peaks due to the ester and acid can be deconvoluted and the FFA content can be calculated using the following equation

$$\% \text{ of FFA} \ = \ \frac{\text{Area of triplet of } \alpha\text{-CH}_2 \text{ of FFA}}{\text{Total Area of } \alpha\text{-CH}_2 \text{ of both FFA and Ester}} \times 100$$
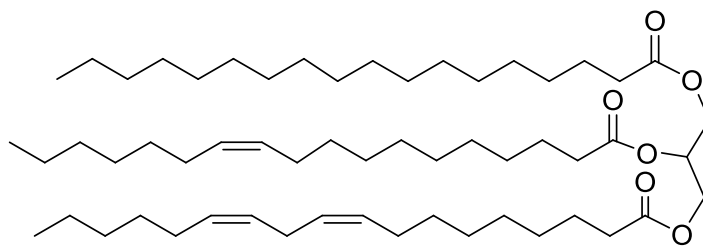
Triglyceride
Vegetable Oil and Fat

Stearic acid

Oleic acid

Linoleic acid

Linolenic acid

Fatty Acid

Methyl oleate

Methyl linoleate

Methyl linolenate

Methyl stearate
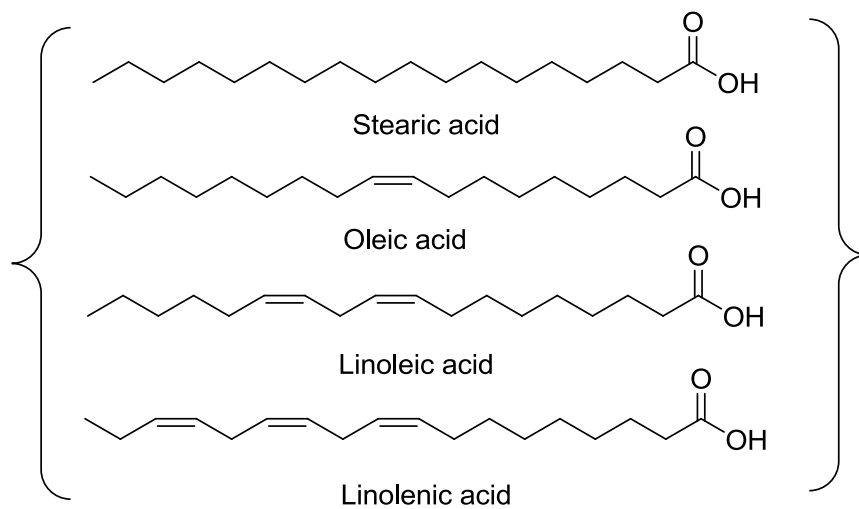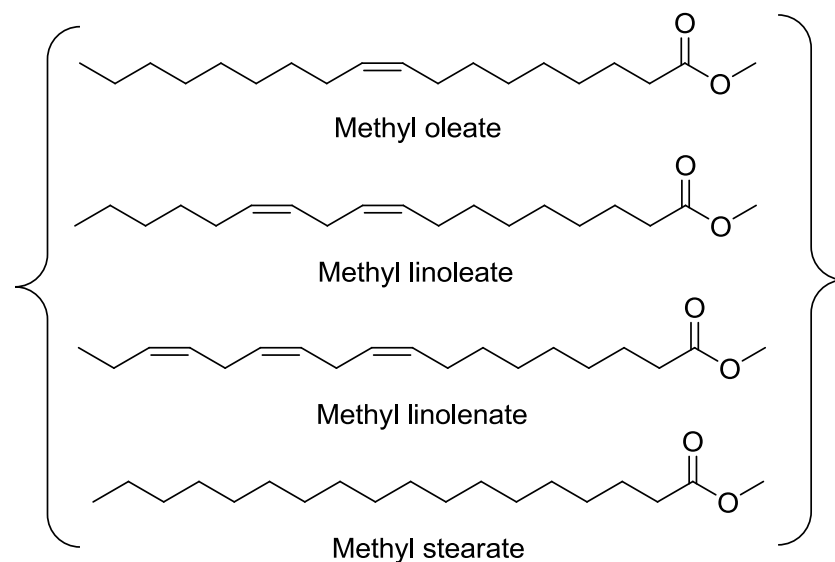
Biodiesel

Scheme 2.1. *Structure of vegetable oil, fatty acids and biodiesel*
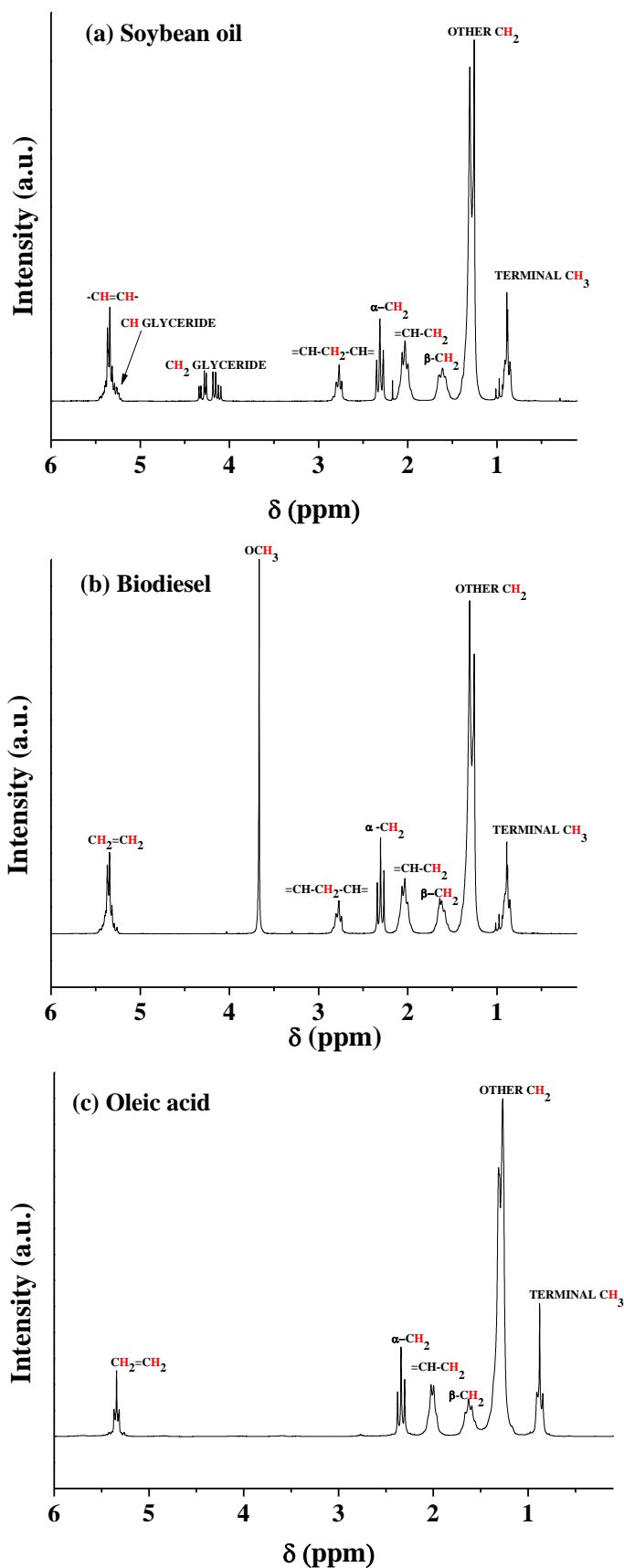
Fig. 2.1. *^1H NMR spectra and assignment of peaks: (a) soybean oil, (b) fatty acid methyl ester (biodiesel) and (c) oleic acid*

Table 2.1. Assignment of ^{1}H NMR peaks of FFA, vegetable oil and biodiesel

Proton(s)	Functional group	Compound / chemical shift, δ (ppm)		
		Oleic acid	Soybean oil	Biodiesel
CH₃-C	Terminal methyl group	0.88	0.80-1.01	0.8-1.0
-(**CH₂**)ₙ-	Backbone CH₂	1.14-1.43	1.20-1.41	1.22-1.42
- **CH₂**CH₂COOH	β-Methylene proton	1.541.69	1.53-1.70	1.55-1.69
=CH-**CH₂**-	α-Methylene group to one double bond	1.92-2.11	1.94-2.11	1.93-2.10
-**CH₂**COOH	α-Methylene group to acid	2.34	-	-
-**CH₂**COOR	α-Methylene group to ester	-	2.31	2.31
=CH-**CH₂**-CH=	α-Methylene group to two double bond	-	2.76	2.77
-COO**CH₃**	Methyl group of ester	-	-	3.67
- **CH₂** OCOR	Methylene group(C1 & C3) of glycerides	-	4.09-4.34	-
-**CH**OCOR	Methine proton at C2 of glycerides	-	5.25	-
-**CH**=**CH**-	Olefinic protons	5.3-5.4	5.28-5.43	5.27-5.41
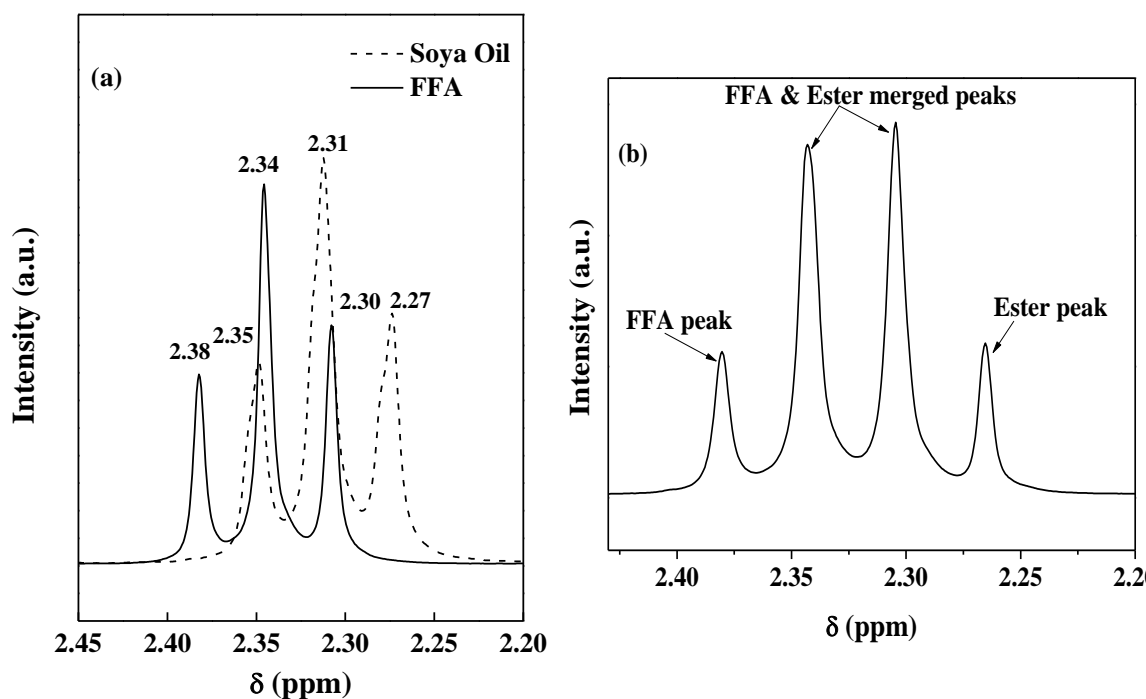
Fig. 2.2. *^{1}H NMR spectrum in α-CH₂ region: (a) soybean oil and oleic acid (FFA), and (b) mixture of oleic acid and its methyl ester*

For the calibration of the ^{1}H NMR method and for the quantification of FFA in oils or biodiesel, standard solutions of oleic acid in soybean oil with different compositions (5, 10, 20, 30 and 50%) were prepared and their compositions were determined by both ^{1}H NMR method and the conventional titration method by titrating a sample with 0.1 N NaOH using phenolphthalein solution (1%) as the indicator. For ^{1}H NMR, 20-25 mg of the sample was dissolved in $CDCl_3$ and the spectrum was recorded at 298 K on a Bruker 200 MHz spectrometer; 30 scans for each sample were taken during the measurement. Calibration curves were plotted and correlations among the titrimetric and ^{1}H NMR data were established. The FFA content of non-edible oils was determined by ^{1}H NMR and compared with the titration method. For the validation of this method, calibration curves for the standard solutions of oleic acid (as the representative FFA) and soybean oil (as a vegetable oil) were constructed based on both the ^{1}H NMR and titrimetric methods (Fig. 2.3). A good correlation is observed. Biodiesel can also contain FFA due the hydrolysis of the fatty acid methyl esters by moisture or incomplete conversion of FFA-containing non-edible oils. Standard mixtures containing 1 - 20% of oleic acid in commercial biodiesel were prepared and the FFA content was determined by both titration and ^{1}H NMR methods (Fig. 2.3(b)). Again there is a good correlation between the ^{1}H NMR and titrimetric methods.

Table 2.2. Evaluation of FFA content by titration and ^{1}H NMR: esterification of oleic acid with methanol

Time	Oleic acid conversion (mol %)	
(h)	Titration	^{1}H NMR
0.5	4.3	4.6
1	44.3	46.2
2	89.5	88.4
4	96.2	94.1
6	96.0	94.0
8	96.1	94.2

Reaction conditions: Oleic Acid = 10 g, Oleic Acid: Methanol molar ratio = 1: 5, Reaction Temperature = 190ᵒC, Catalyst = DMC.
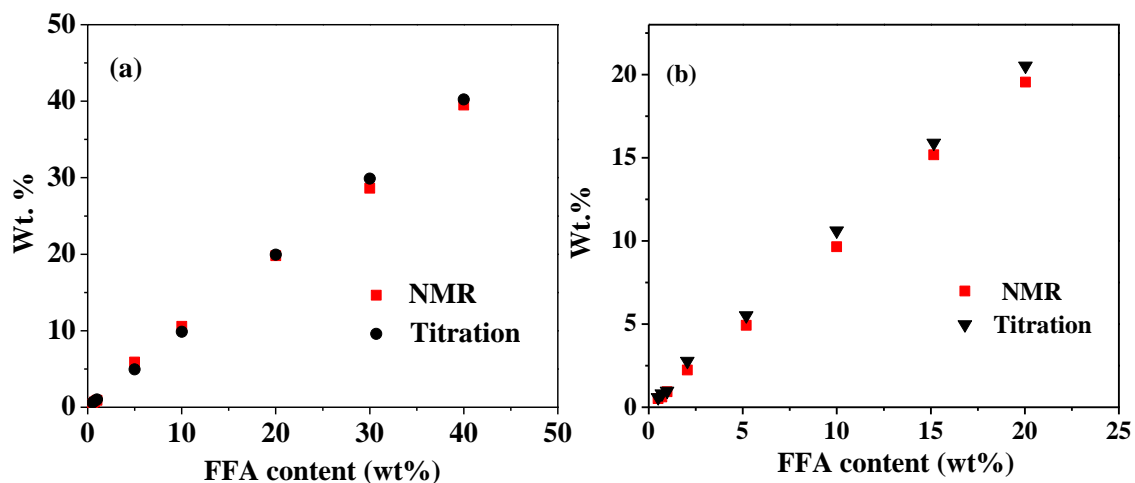
Fig. 2.3. *Correlation / calibration plots of FFA content in (a) soybean – oleic acid and (b) standard biodiesel – oleic acid mixtures by ^{1}H NMR and titration methods*
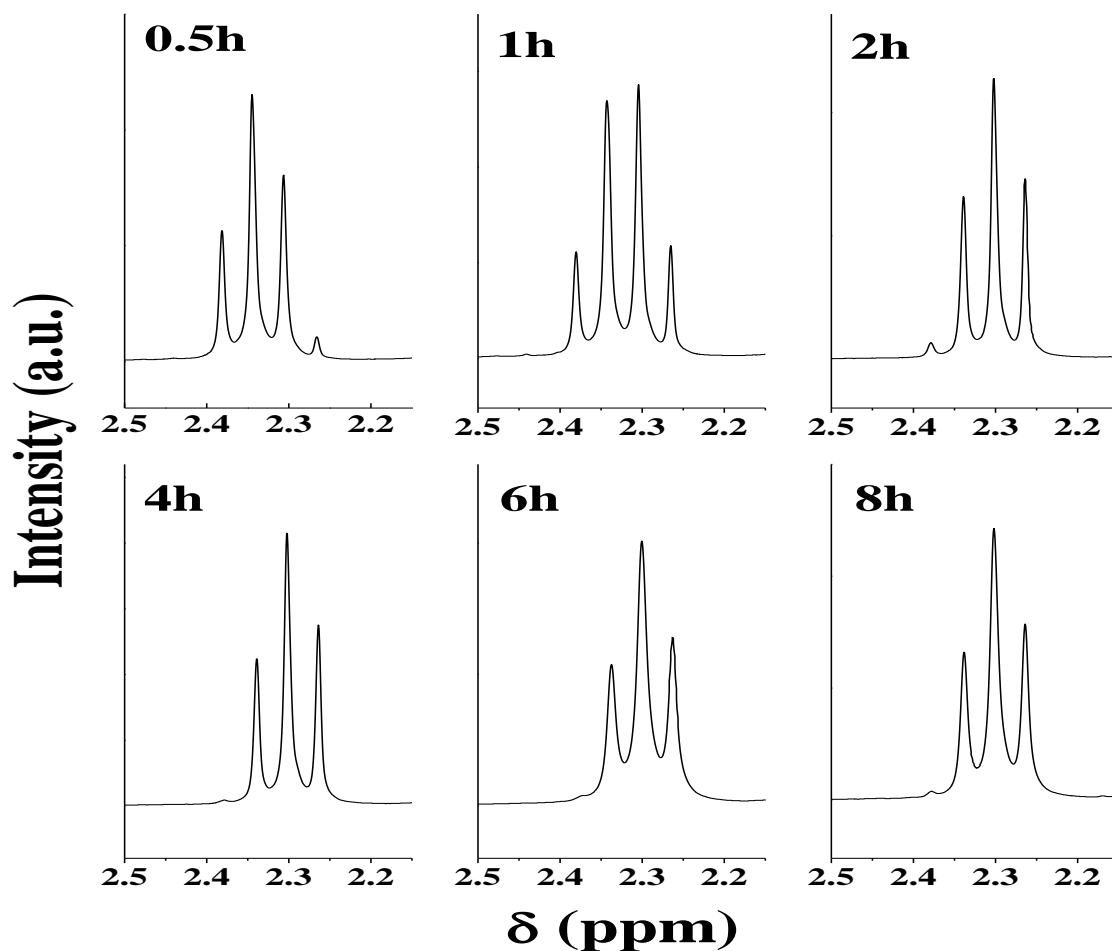
Fig. 2.4. ^{1}*H NMR spectra in the α-CH$_2$ region: Reaction of oleic acid with methanol as a function of time*

During the esterification of oleic acid with methanol, the decrease of the oleic acid content in the reaction mixture was followed, as a function of time, by both the ^{1}H NMR and titrimetric methods. At the start of the reaction, ^{1}H NMR spectrum in α-CH$_2$ region (2.3 – 2.4 ppm) showed a triplet pattern corresponding to oleic acid. As the reaction progressed, a quartet like pattern was detected. The intensity of the triplet signals due to oleic acid decreased and that of the methyl ester increased with the reaction time (Fig. 2.4). Finally, at the end of 8 h, the peaks corresponding to oleic acid had almost disappeared and only a triplet corresponding to that of the methyl ester (biodiesel) was detected. The FFA content in the reaction mixture at different time intervals determined by ^{1}H NMR spectroscopy correlated well with that determined by the titrimetric method (Table 2.2).

Non-edible oils and fats contain some amount of phospholipids and other acidic impurities along with the FFA, present in significant amounts. While the titrimetric method determines the total acid value in oils and fats, ^{1}H NMR detects the FFA content exclusively. The content of FFA in karanja oil (Table 2.3) estimated by titration (5.3%) is indeed higher than that determined by the ^{1}H NMR (4.5%) technique. To remove phospholipids, chicken fat was treated with water at 60 - 80°C for half an hour. Water was, then, separated and the oil was dried over anhydrous Na$_2$SO$_4$. The treated chicken fat oil is subjected to further analysis. The FFA content (by both the methods) had decreased after the water treatment (Table 2.3). The values estimated by the titrimetric method are still higher than those determined by ^{1}H NMR. After transesterification of those oils into biodiesel, the titration method still shows the presence of some acidity while no FFA is detected by ^{1}H NMR. These data, therefore, confirm that ^{1}H NMR spectroscopy determines the FFA in oils, fats and biodiesel more accurately than the titrimetric method.

Table 2.3. FFA content of karanja oil, chicken fat and their biodiesel

Oil/fat/biodiesel	FFA content (mol %)	
	Titration	^{1}H NMR
Karanja oil	5.3	4.5
Biodiesel from karanja oil	0.79	0
Chicken fat	11.7	10.4
Biodiesel from chicken fat	0.53	0
Water-treated chicken fat	10.4	9.6
Biodiiesel from water-treated chicken fat	0.52	0

2.5.2. ^{1}H NMR Method to Monitor Esterification Reaction with Different Alcohols

A conversion can also be independently estimated by ^{1}H NMR spectroscopy by an another way. In general, the α-CH_2 groups of oleic acid and ethyl oleate show ^{1}H NMR signals (triplet) in the chemical shift (δ) range of 2.4 - 2.2 ppm (Fig. 2.5). However, the triplet corresponding to oleic acid occurs at slightly higher δ value than that of ethyl oleate due to greater deshielding by carboxylic group compared to ester group. When both acid and ester are present in the sample, the spectrum looks like a multiplet pattern due to overlapping of the α-CH_2 triplet signals of ester and acid molecules. The –CH_2 of ethoxy group of ethyl oleate (Scheme 2.2) shows a quartet in the δ range of 4.2 - 4.0 ppm (Fig. 2.5). As the esterification reaction progresses, the intensity of the signals at 4.2 - 4.0 ppm increases while the overall area of the multiplet peaks at δ 2.4 - 2.2 remains the same (Fig. 2.5). Acid conversion can be estimated by comparing the areas of these signals due to α-CH_2 (δ 2.4 - 2.2) and –CH_2 of ethoxy part of ethyl oleate (δ 4.2 – 4.0) as defined by the equation given below.

$$Fatty\ acid\ conversion\ \% \ = \frac{A_{CH_2(ethoxy)}}{A_{\alpha-CH_2(total)}} \times 100$$

Where: $A_{CH_2(ethoxy)}$ = Area of methylene protons of ethoxy group in the ethyl or higher alcohol ester

$A_{\alpha-CH_2(total)}$ = Total area of α-CH_2 signals of acid and ester

While a similar expression is valid for esterification with other long chain alcohols used in this study, the following equation is be used for the reactions with methanol. The factors 2 and 3 in this equation arise because of the fact that the α-CH_2 group contains two protons while the methoxy group in the methyl ester contains three protons. The conversions determined by ^{1}H NMR and titration methods are in good agreement with each other.

For methyl esters:

$$Fatty\ acid\ conversion\ \% \ = \frac{2 \times A_{CH_3(methoxy)}}{3 \times A_{\alpha-CH_2(total)}} \times 100$$

where : $A_{CH_3(methoxy)}$ = area of protons of methoxy group in the methyl ester and $A_{\alpha-CH_2(total)}$ = total area of α-CH_2 signals of acid and ester
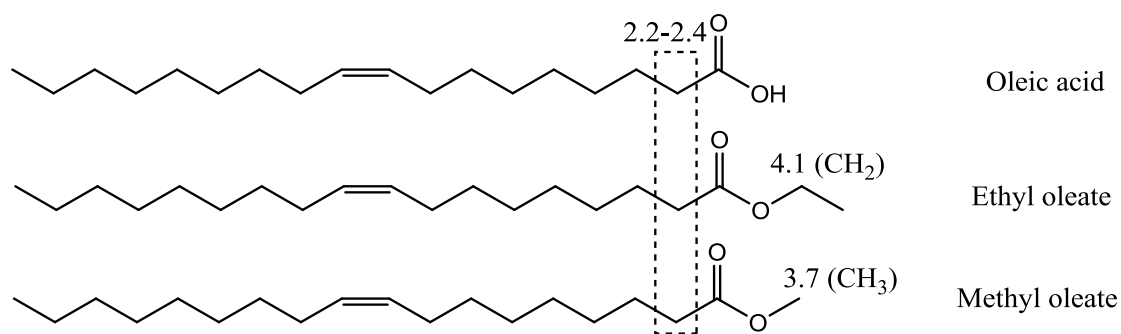
Scheme 2.2. *Structure oeic acid and its methyl and ethyl ester*
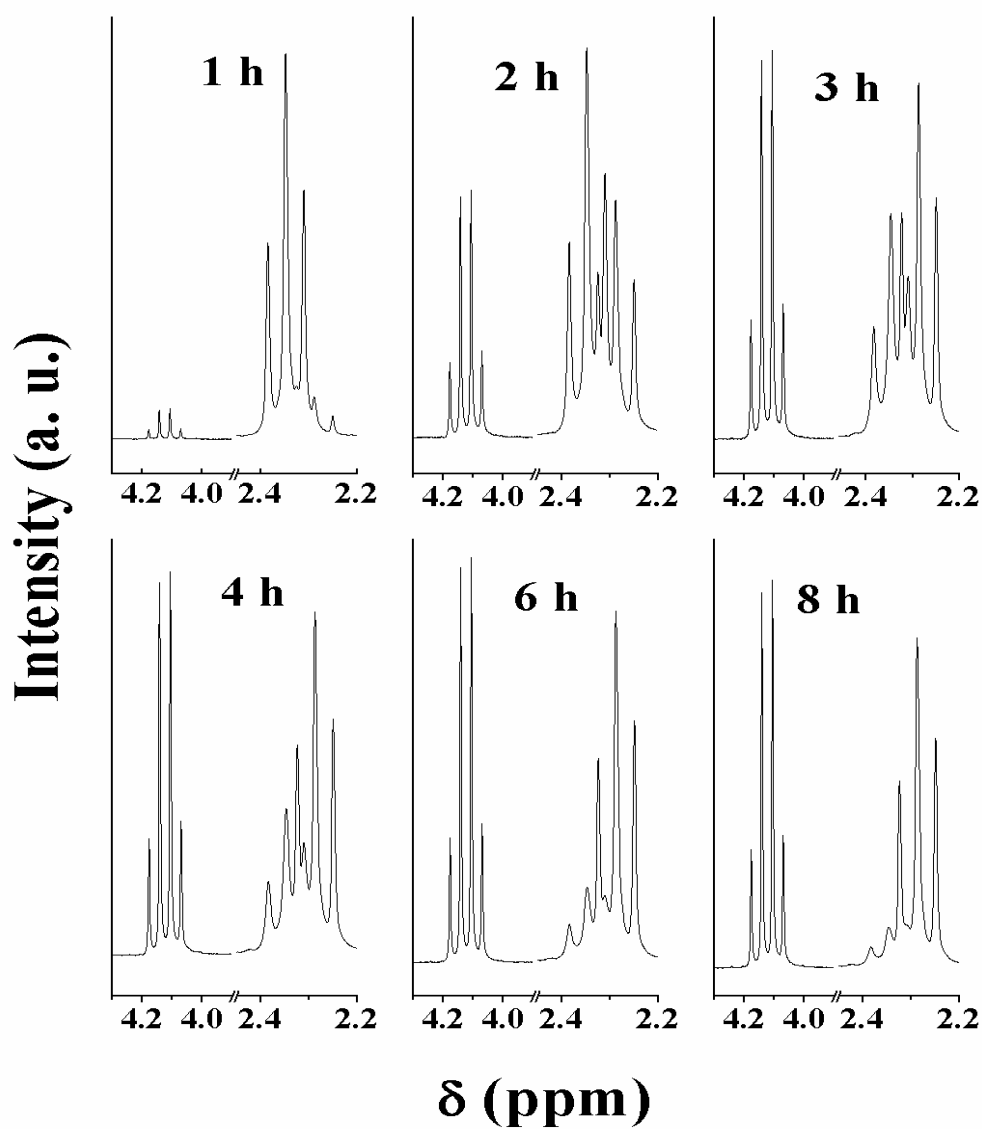
Fig. 2.5. *^1H NMR spectra: esterification of oleic acid with ethanol*

2.5.3. ^{1}H NMR Method for the Monitoring of Epoxidation of Fatty Acid, Biodiesel and Vegetable Oils

In Epoxidation of fatty acid, its methyl ester or vegetable oils, double bonds present in them react with oxidising agent to give epoxides. As a result double bonds in the sample keep decreasing while α-CH$_2$ peak at $\delta = 2.3$ ppm remains unaffected (Fig. 2.6). So this α-CH$_2$ peak at $\delta = 2.3$ ppm can be used as reference and the double bonds are conversion to epoxides can be monitored. Thus conversion of double bonds can be calculated by following equation

$$\text{Double bond conv. (mol.\%)} = \left[1 - \frac{(A_{DR} - A_{DP})}{A_{DR}} \right] \times 100$$

A_{DR} = Area of double bond peaks at $\delta = 5.2$ ppm with respect to α-CH$_2$ peak

at $\delta = 2.3$ ppm in reactants (fatty acids, biodiesel or vegetable oil/fats)

A_{DP} = Area of double bond peaks at $\delta = 5.2$ ppm with respect to α-CH$_2$ peak

at $\delta = 2.3$ ppm in products
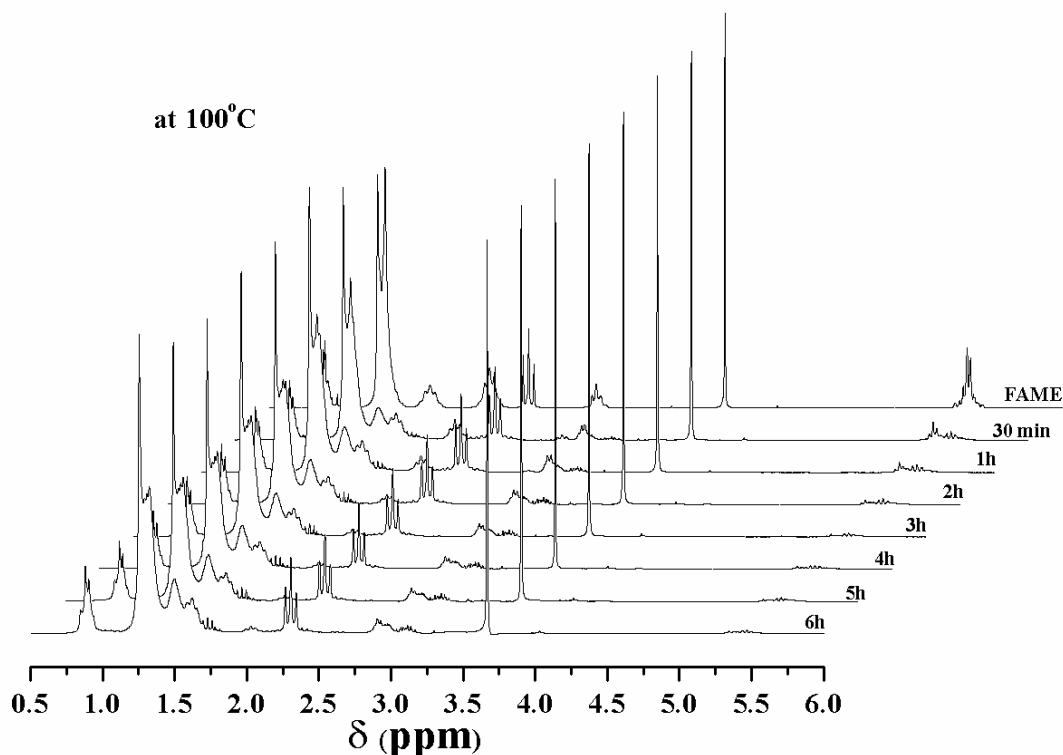
Fig. 2.6. [1]*H NMR spectra of epoxidation of biodiesel (fatty acid methyl ester)*

2.5.4. FTIR Method for Glycerides (MG, DG & TG) Estimation

In hydrodeoxygenation when triglyceride is treated with hydrogen, oxygen in ester groups is removed as water and hydrocarbons are formed. Therefore carbonyl group intensity in FTIR keeps on decreasing and can be used to determine the quantity of glycerides presents. For this, carbonyl (C=O) peak at 1750 cm^{-1} and C-H stretching peaks around 3000 cm^{-1} were selected. Area corresponding to CH stretching peaks in the region 2750-3150 cm^{-1} was taken as the reference as this area remains almost unaffected by the reaction and carbonyl peak decreases as the reaction proceeds (Fig. 2.7). Therefore conversion of TG into hydrocarbons can be monitored by measuring decrease in the area of carbonyl peak with respect to CH stretching peaks. Alternatively, using the liquid FTIR, one can prepare certain concentration of sample in an IR transparent solvent such as CCl_4 and can find out the quantity of vegetable oil present by comparing the peak area of carbonyl group with the standard calibration plot of vegetable oil in octadecane mixtures.
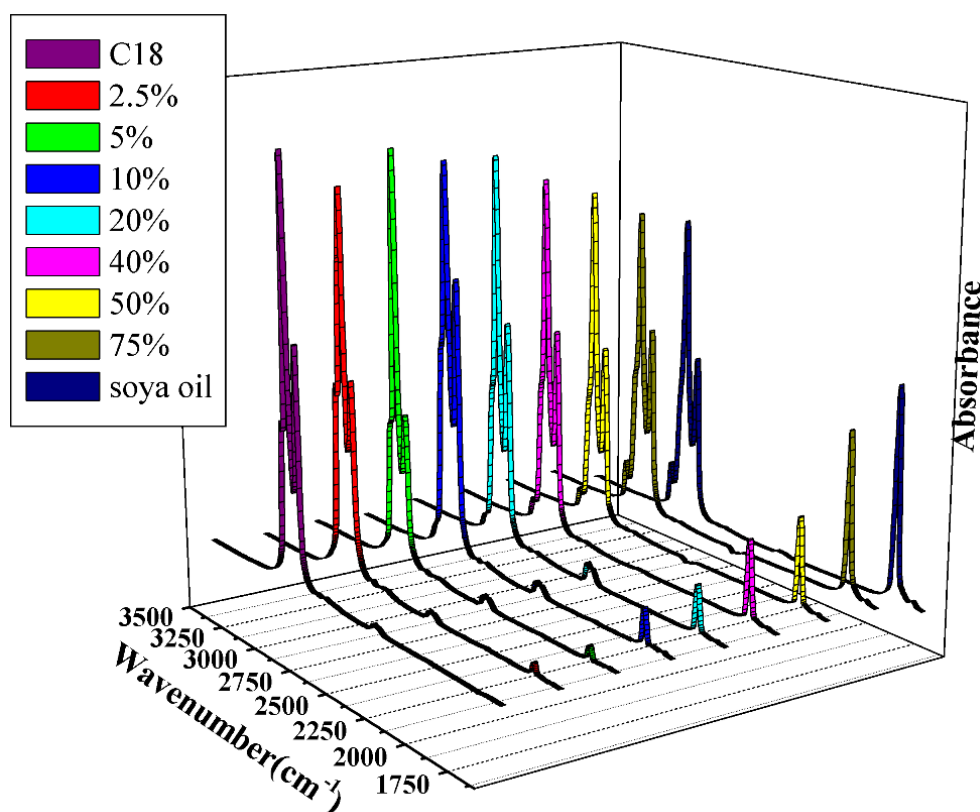
Fig. 2.7. *IR spectra of standard mixture of oil and octadecane*

For the standardization of the procedure a calibration curve was plotted between relative area of the C=O stretching vs. standard mixture of oil in octadecane (Fig. 2.8). For this, standard mixtures of oil in octadecane were prepared with oil

percentage of 2, 5, 10, 20, 40, 50 and 75. IR of pure C_{18} and pure soya oil were also taken (Fig. 2.7)**.** A good correlation was found between the percentage of oil present in the soybean oil-octadecane mixture and the area of the carbonyl peak. Therefore, this method can be used to estimate the unconverted vegetable oil present in the hydrodeoxygenated samples.
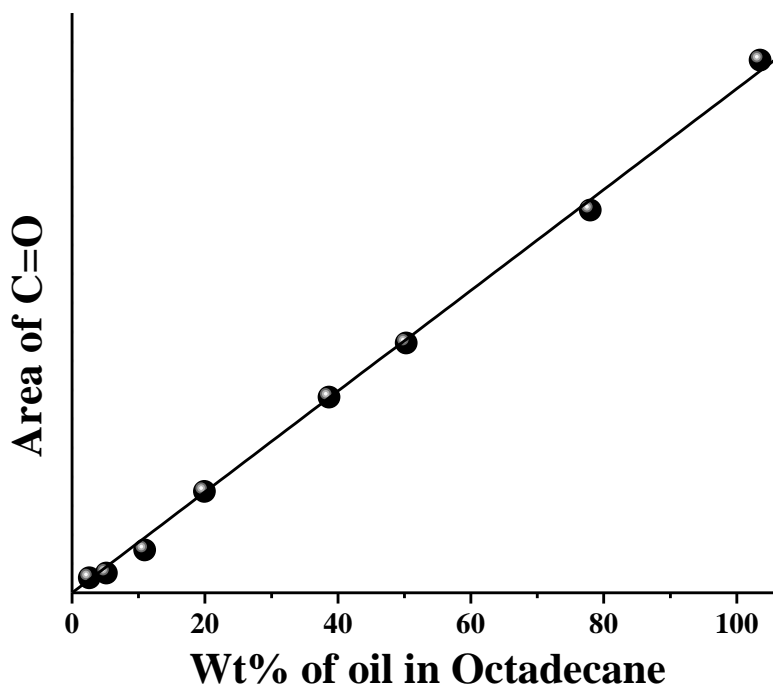
Fig. 2.8. *Calibration curve for glycerides conversion*

2.6. Conclusions

Various catalysts such as Fe-Zn DMC, Co-Zn DMC, Al-MCM 41, ZnO and group VI transition metal (Cr, Mo, & W) oxides supported on alumina were prepared characterize by several physicochemical techniques. Reaction procedures for hydrolysis of vegetable oils and fats, esterification of fatty acids, epoxidation of fatty acids and their esters and hydrodeoxygenation of vegetable oils were reported. Various methods used for the analysis of reaction mixtures and products were discussed.

2.7. References

1. (a) H.T. Takeyasu, T. Watabe, T. Doi, JP 2265921 (1990).

    (b) T. Watabe, H. Takeyasu, T. Doi, N. Kunii, Eur. Pat. Appl. EP 383333 (1990).

2. B. Le-Khac, US Patent 5789626 (1998).

3.   I. Kim, J-T. Ahn, C.S. Ha, C.S. Yang, I. Park, Polymer 44 (2003) 3417.

4.   K. Nakano, K. Nozaki, T. Hiyama, J. Am. Chem. Soc. 125 (2003) 5501.

5.   P.S. Sreeprasanth, R. Srivastava, D. Srinivas, P. Ratnasamy, Appl. Catal. A: Gen. 314 (2006) 148.

6.   N. Gokulakrishnan, A. Pandurangan, P.K. Sinha, J. Mol. Catal. A: Chem. 263 (2007) 55.

7.   A. Palani, M. Palanichamy, A. Pandurangan, Catal. Lett. 115 (2007) 40.

8.   Q.N. Le, R.T. Thomson, US Patent No. 5232580 (1993).

9.   Q.N. Le, R.T. Thomson, G.H. YoKomizo, US Patent No. 5134241 (1992).

10.   C.T. Kregse, M.E. Leonowicz, W.J. Roth, J.C. Vartuli, US Patent No. 5174888 (1992).

11.   A.C. Carmo Jr., L.K.C. de Souza, C.E.F. da Costa, E. Longo, J.R. Zamian, G.N. da Rocha Filho, Fuel 88 (2009) 461.

12.   (a) R. Schmidt, D. Akporiaye, m.Stocker, O.H. Ellestad, Stud. Surf. Sci. Catal. 84 (1994) 61.

      (b) R.B. Borade, A. Clearfield, Catal. Lett. 31 (1995) 267.

13.   P.M.S. Begum, K.K.M. Yusuff, R. Joseph, Intern. J. Poly. Mater. 57 (2008) 1083.

14.   W.H. Bragg, W.L. Bragg, The Crystalline State, Vol. 1, McMillan, New York (1949).

15.   G. Bergeret, in: Handbook of Heterogeneous Catalysis, Vol. 2, Eds: G. Ertl, H. Knozinger, J. Weitkamp, Wiley-VCH, Weinheim, pp. 464 (1997).

16.   C.N. Banwell, "Fundamentals of Molecular Spectroscopy" Tata McGraw-Hill Pub. Co. Ltd. New Delhi (1979).

17.   V.B. Kartha, "Spectroscopic Methods in Heterogeneous Catalysis" Eds N.M. Gupta, V.B. Kartha and R.A. Rajadhyaksha, Tata McGraw Hill, pp.1 (1991).

18.   (a) http://en.wikipedia.org/wiki/Scanning_electron_microscope#cite_ref-7. (b) http://www.uga.edu/caur/semnote1.htm

19.   D.K. Gosser, "Cyclic Voltametry Simulation and Analysis of Reaction Mechanisms" Wiley-VCH, Germany (1993).

20.   S. Brunauer, P.H. Emmett, E. Teller, J. Am. Chem. Soc. 60 (1938) 309.

21.   E.P. Barrett, L.G. Joyner, P.P. Halenda, J. Am. Chem. Soc. 73 (1951) 373.

22.   J.I. Goldstein, H. Yakowitz (Eds.), Practical Scanning Electron Microscopy,

Plenum Press, New York, 1975.

23. G. Lawes, Scanning Electron Microscopy and X-Ray Microanalysis, John Wiley and Sons Ltd., Chichester (1987).

24. J. R. Fryer, Chemical Applications of Transmission Electron Microscopy, Academic Press, San Diego (1979).

25. J.M. Thomas, O. Terasaki, P.L. Gai, W. Zhou, J. Gonzalez-Calbet, Acc. Chem.Res. 34 (2001) 583.

26. S. Brunauer, P.H. Emmett, E. Teller, J. Am. Chem. Soc. 60 (1938) 309.

27. J. Mendham, R.C. Denney, J.D. Barnes, M.J.K. Thomas, Vogel's Textbook of Quantitative Chemical Analysis, 6th Ed., Pearson Education limited (2006).

28. G. Gelbard, O. Brès, R.M. Vargas, F. Vielfaure, U.F. Schuchardt, J. Am. Oil Chem. Soc. 72 (1995) 1239.

29. (a) G. Knothe, Trans. of the ASAE 44 (2001) 193.
    (b) G. Knothe, J. Krahl, J. Van Gerpen, (Eds.) The Biodiesel Handbook, AOCS Press, Champaign, IL, USA (2005).

Chapter 3
Hydrolysis of Vegetable Oils and and Animal Fat

3.1. Introduction

Biodiesel is getting more and more attention due to its renewability, biodegradability, better lubricity and better emission properties. Depleting fossil fuels and their escalating prices are also favouring the use of biodiesel. It is generally prepared by transesterification of vegetable oils and fats in the presence of alkali catalysts. For an alkali-based process, feedstock should be free from water and fatty acids (<0.5 wt%) [1- 4]. This makes the biodiesel production costly and non-competitive to petrodiesel as 70-80% of the biodiesel production cost depends upon the feedstock used. An alternate, more generic process for the production of biodiesel is the hydrolysis of waste oils/fats to fatty acids followed by their esterification to fatty acid methyl esters, FAME (Fig. 3.1) [5]. Fatty acids produced from non-edible oils and fats are more advantageous as they cannot only make biodiesel more competitive but also avoid the food *vs* fuel issue. The hydrolysis of oils, prior to saponification, provides possibilities of overcoming many problems associated with the recovery of byproduct glycerol. Fatty acids and glycerol are valuable chemical intermediates with a variety of end uses. Fatty acids (FA) are major components used in the preparation of a wide variety of products, such as soaps, surfactants, lubricants, plasticizers, paints, coatings, pharmaceuticals, foods, agricultural, industrial and personal care products [6]. Yet quantitative information on the kinetics, thermodynamics, and engineering aspects of hydrolysis of vegetable oils and fats is limited.
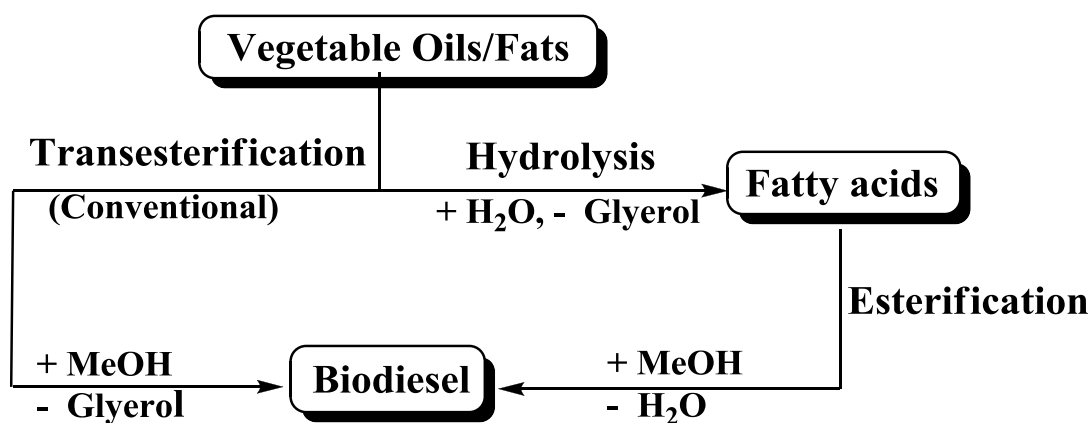
Fig. 3.1. Two routes for biodiesel production

In the widely used Colgate-Emery steam hydrolysis process, the reaction is conducted in continuous, counter-currents of fat and water (40–50 wt% of fat), in the absence of a catalyst, at high temperatures (523–603 K) and pressures (50–60 bar) [7,

8]. This pressure splitting process is efficient and vegetable oil/fat splitting yields of 95% and above are obtained. However, its applicability to low-cost, waste vegetable oils and animal fats especially those containing multiple/conjugated double bonds and hydroxyl groups (castor oil and fish oil, for example) is limited. At high temperatures, these triglycerides and the fatty acids derived from them undergo undesired thermal decomposition leading to deterioration in colour/odour and to a reduced yield of fatty acids [9]. Additional major drawbacks of the high temperature–pressure fat splitting process include: (a) it is an energy intensive process, (b) it uses considerable amount of superheated steam as a reagent, (c) it requires the use of large reactors made of expensive corrosion-resistant material of construction, (d) the quality of the product is poor and necessitates additional process steps to purify the fatty acids and glycerol escalating the cost of the overall manufacturing process.

The Twitchell fat splitting process operates at milder conditions (373 K and 1 bar) but needs longer contact times (12–24 h) and fat splitting is only 80–85% [10]. Fat splitting via saponification produces significant amount of acid sludge and hard water in the down-stream processing [11, 12]. The quality of glycerin by-product is also poor. Enzymatic splitting of fat (308 K) requires long contact times (16 h to several days) [13–15]. It is, therefore, desirable to have a more efficient hydrolysis process of vegetable oils which operates at moderate temperatures/pressures and produces higher yields of fatty acids and glycerin with minimum number of process steps.

Solid acid catalysts are more beneficial than homogenous catalysts due to engineering advantages and easy catalyst separation from the product stream. There are not many reports in the journal or patent literature wherein solid catalysts have been used successfully for the hydrolysis of oils and fats to fatty acids. Ngaosuwan et al. [16] reported tungstated zirconia and Nafion resin nanoparticles supported on mesoporous silica (SAC-13) catalysts for the hydrolysis of tricaprylin, a model compound. This chapter describes application of different solid acid catalysts for the hydrolysis of vegetable oils and fats as a means to ultimately lower the capital and operating costs by conducting the reaction under moderately low reaction conditions. Such a process could be applied in a novel two-step (hydrolysis-*cum*-esterification) biodiesel synthesis route using low-cost feedstocks containing 5-15% FFAs. Since the esterification of FFAs is faster than transesterification of triglycerides on acid catalysts, there could be a possibility to construct a more efficient biodiesel synthesis

process around the use of two-step hydrolysis-*cum*-esterification route using solid acid catalyst rather than what is currently done with homogeneous catalysts [17].

3.2. Experimental Section

3.2.1. Material Preparation

The Fe-Zn double-metal cyanide (DMC) complex, Co-Zn DMC complex and ZnO catalyst were prepared as reported in Chapter 2. Hβ ($SiO_2/Al_2O_3 = 28$) and HY ($SiO_2/Al_2O_3 = 5$) zeolites were supplied by the Catalyst Pilot Plant, National Chemical Laboratory, Pune. SAPO-11 (1.5 mm TRX) and MoO_x supported on phosphate-modified alumina (MoO_x/Al_2O_3; MoO_x content = 15 wt%, P content = 1.2 wt%) were obtained from Sud-Chemie India Ltd. Sulfated zirconia (1.5 mm pellets) was procured from Saint-Gobain, Norpro. High temperature, strongly acidic, macroporous polymer – Amberlyst^{TM}70 was obtained from Rohm and Haas, USA. Detailed characterization of the catalysts is reported in Chapter 2.

3.2.2. Characterization Techniques

X-ray diffractograms of the catalysts were recorded on an X'Pert Pro (Philips) diffractometer using Cu Kα radiation and a proportional counter as detector. Transmission electron micrographs (TEM) of the samples were scanned on a JEOL (model 1200 EX) microscope operating at 100 kV. The C, H, N & S composition was determined by a Carlo-Erba 1106 analyzer. The specific surface area (BET) of the samples was determined using a NOVA 1200 Quanta Chrome equipment.The acidic properties of the catalysts were determined using pyridine and NH_3 as probe molecules. The type and density of the acid sites were determined by diffuse reflectance infrared Fourier transform (DRIFT) spectroscopy of adsorbed pyridine and temperature-programmed desorption of ammonia (NH_3-TPD) techniques. In DRIFT measurements, the samples were initially activated at 473 K (in the case of DMC) or at 723 K (in the case of sulfated zirconia, Hβ, H-Y MoO_x/Al_2O_3 and ZnO). The temperature was brought down to 323 K and pyridine was adsorbed. Then, the temperature of the sample was raised and held at a desired value (373 K) for 30 min before starting the measurements (spectral resolution = 2 cm^{-1}; number of scans = 200). Difference FTIR spectra were obtained by subtracting the spectrum of the catalyst from that of the sample with adsorbed pyridine. NH_3-TPD measurements were performed on a Micromeritics AutoChem 2910 instrument. In a typical experiment, 0.1 g of catalyst was taken in a U-shaped, flow-thru, quartz sample tube.

Prior to measurements, the catalyst was pretreated in He (30 cm^3/min) at 473 K (in the case of DMC) or at 773 K (in the case of sulfated zirconia, Hβ, MoO$_x$/Al$_2$O$_3$ and ZnO) for 1 h. A mixture of NH$_3$ in He (10%) was passed (30 cm^3/min) at 323 K for 0.5 h. Then, the sample was, subsequently flushed with He (30 cm^3/min) for 1 h. The TPD measurements were carried out in the range 323 – 723 K at a heating rate of 10 K/min. Ammonia concentration in the effluent was monitored with a gold-plated, filament thermal conductivity detector. The amount of desorbed ammonia was determined based on the area under the peak.

3.2.3. Reaction Procedure – Hydrolysis of Oils / Fat

Catalytic activity of various solid acid catalysts was evaluated for the hydrolysis of vegetable oils or fat. A detailed reaction procedure is given in Chapter 2. The product was analyzed by high performance liquid chromatography (HPLC), titration and ^{1}H NMR spectroscopy. In some cases, petroleum ether (5 – 10 mL) was added after the completion of reaction to facilitate separation of the solid catalyst. A few reactions were conducted in a 300 mL Paar stainless steel stirred tank reactor. Several edible (coconut, palmolein, and soybean) and non-edible (castor, jatropha, karanja, palm and rubber seed) oils and chicken fat have been hydrolyzed. With a view to improve the miscibility of oil/fat and water, some experiments were carried out in the presence of solvents (N, N-dimethylformamide (DMF), tetrahydrofuran (THF), acetone), phase transfer agents (tetrapropylammonium bromide, TPAB) or surfactants (Triton X-100). In other studies, prior to conducting the reactions, a portion of the product mixture or oleic acid (1 – 20 wt%) was added to reactants. At the end of the hydrolysis reaction, the solid catalyst was separated from the product mixture and, without any further treatment was used in another fresh batch of hydrolysis reaction. The catalyst was reused in five consecutive recycles.

3.2.4. Product Analysis

The fatty acid products of the reaction were analyzed using a Perkin-Elmer (Series 200) HPLC equipped with a quaternary pump, auto sampler, degasser, thermostated column compartment and TotalChrom navigator-PE-HPLC software. An ELSD detector from Gilson and a reverse-phase, Perkin-Elmer Brownlee column (C-18 Spheri-5, 250 x 4.6 mm with a 5 μm particle size) were used in the analysis. ^{1}H NMR (Bruker Avance 200 MHz) [23] and Fourier transform infrared (Shimadzu FTIR 8300) spectroscopic techniques were also used to identify and estimate the

products. The acid values of the product mixture and of vegetable oils and fats were determined by titration with 0.1 N NaOH solution and using phenolphthalein as the indicator.

Quantification of fatty acids (FA) and glycerides (TG, DG and MG) in vegetable oil/fat and the hydrolyzed products by ^{1}H NMR is based on the fact that α-CH$_2$ peaks of FA appear at higher δ values than those of glycerides. The difference in chemical shift (between the FA and glycerides) is due to the greater de-shielding effect of the carboxylic group compared to the ester group. Due to this shift, one of the peaks of the triplet of FA (at 2.38 ppm) shifts out of the α-CH$_2$ region of the ester while the other two peaks (2.34 and 2.30 ppm, respectively) are merged with those due to the glycerides at 2.35 and 2.31 ppm, respectively. In other words, a sample containing both FA and glyceride (i.e., partially hydrolyzed product) shows a quartet spectral pattern in the α-CH$_2$ region of the ^{1}H NMR spectrum with the intensity of the peaks depending on the relative FA and glyceride concentrations. The unmerged peak of the FA triplet can be used to determine the FA content in vegetable oil, animal fat and hydrolyzed product. The area (A$_{FA}$) of the unmerged peak of FA triplet (appearing around 2.38 ppm, out of the glycerides triplet) can, thus, be determined by integration of the spectral region 2.37 – 2.41 ppm. The triplet appears with an intensity ratio of 1:2:1. Total area corresponding to the α-CH$_2$ groups of the FA, will thus, be four times the area of the single unmerged FA peak around 2.38 ppm. The total area corresponding to α-CH$_2$ of both FA and glycerides can be determined by integrating the spectral region 2.20 – 2.41 ppm. The concentration of FA (wt%) in oil or hydrolyzed product is, thus,

$$\% \text{ of FA } = \frac{4 \times \text{Area of unmerged peak of } \alpha\text{-CH}_2 \text{ of FA}}{\text{Total area of } \alpha\text{-CH}_2 \text{ of both FA and Glycerides}} \times 100$$

Alternatively, the peaks due to the glycerides and FA can be deconvoluted and the FA content can be calculated using the following equation:

$$\% \text{ of FA } = \frac{\text{Area of triplet of } \alpha\text{-CH}_2 \text{ of FA}}{\text{Total area of } \alpha\text{-CH}_2 \text{ of both FA and Glycerides}} \times 100$$

For validation of this method, calibration curves for the standard solutions of oleic acid (as the representative FA) and soybean oil were constructed based on both the ^{1}H NMR and titrimetric methods. A very good correlation was observed.

3.3. Results and Discussion

3.3.1. Physicochemical Properties

The textural and acidic properties of different solid catalysts used for the hydrolysis are listed in Table 3.1. Fe-Zn DMC has a molecular formula : $K_4Zn_4[Fe(CN)_6]_3.6H_2O.2$(tert.-BuOH) with two molecules of tert.-butanol included in its structure [18]. The complex crystallizes with a cubic unit cell (unit cell parameter = 0.904 nm). N_2 adsorption-desorption isotherms and high resolution transmission electron micrographs reveal that DMC is mostly microporous with some mesoporosity in its structure (average pore diameter = 2.1 nm and pore volume = 0.03 cc/g). It has a specific surface area; 52 m^2/g (Table 3.1). DMC is a Lewis acid catalyst. Tetracoordinated Zn ions are the acidic, active sites.

Sulfated zirconia possesses a tetragonal crystalline phase (a = 0.362 nm and c = 0.511 nm) and a long-range mesopore ordering (average pore diameter = 4.1 nm and pore volume = 0.14 cc/g, specific surface = 136 m^2/g). Sulfated zirconia, Hβ, HY and SAPO-11 contain both Lewis (IR bands at 1607, 1596 and 1443 cm^{-1} due to pyridine molecules adsorbed on Lewis acid sites) and Brönsted (IR bands at 1639 and 1542 cm^{-1} due to pyridinium ions) acid sites. The total amount of ammonia desorbed from sulfated zirconia, SAPO-11 and Hβ is lower (0.48, 0.42 and 0.68 mmol/g, respectively) than that from Fe-Zn DMC (0.84 mmol/g). However, the former group contains relatively stronger Brönsted acid sites. The Fe-Zn DMC contains only Lewis acid sites (absence of IR bands due to pyridinium ions).

Number of acid sites (1.28 mmol NH$_3$/g) in zeolite HY is higher but has smaller average pore diameter than Fe-Zn DMC. Sulfated zirconia has a Na$^+$ ion exchange capacity of 0.26 mmol/g [24]. Amberlyst^{TM}70 is a high temperature macroporous polymer with strong Brönsted acidic sites (0.26 mmol/g). It has a specific surface area of 36 m^2/g and a pore diameter of 22 nm. MoO$_x$/Al$_2$O$_3$ contains both Lewis and Brönsted acid sites (0.61 mmol/g). It has a specific surface area of 205 m^2/g and a pore volume of 0.28 cc/g.

Table 3.1. Surface and acidic properties of catalysts

Catalyst	Surface properties				Acidic properties		
	S_{BET} (m^2/g)	Av. pore diameter (BJH, nm)	Pore volume (cc/g)	Nature	Type[a]	Acid site density[b] mmol/g	$\mu mol/m^2$
Fe-Zn DMC	52	2.1	0.03	Hydrophobic	L	0.84	16.2
Amberlyst™70	36	22	-	Hydrophilic	B	0.26	7.2
Sulfated zirconia	136	4.1	0.14	Hydrophilic	L, B	0.48	3.5
MoO_x/Al_2O_3	205	5.5	0.28	Hydrophilic	L, B	0.61	3.0
SAPO-11	206	3.6[a]	0.19	Hydrophilic	L, B	0.42	2.0
HY (SiO_2/Al_2O_3= 5)	550	1.8[a]	0.50	Hydrophilic	L, B	1.28	2.3
H-β (SiO_2/Al_2O_3= 28)	577	2.7[a]	0.39	Hydrophilic-hydrophobic	L, B	0.68	1.2

[a]*L = Lewis, B = Brönsted.* [b]*Estimated from NH$_3$-TPD measurements.* [c]*Reaction conditions: Oil/fat = 10 g, water: oil/fat = 20, Fe-Zn DMC catalyst = 5 wt%, temperature = 463 K, reaction time = 8 h.* [d]*TG = triglycerides, FA = fatty acids.*

[a]*Average pore diameter of alumina extrudates and not the zeolites per se.*

Hydrolysis of vegetable oil:

Triglycerides + Water ⇌ Diglycerides + Fatty acid

Diglycerides + Water ⇌ Monoglycerides + Fatty acid

Monoglycerides + Water ⇌ Glycerol + Fatty acid

Triglycerides + 3 Water ⇌ Glycerol + 3 Fatty acid
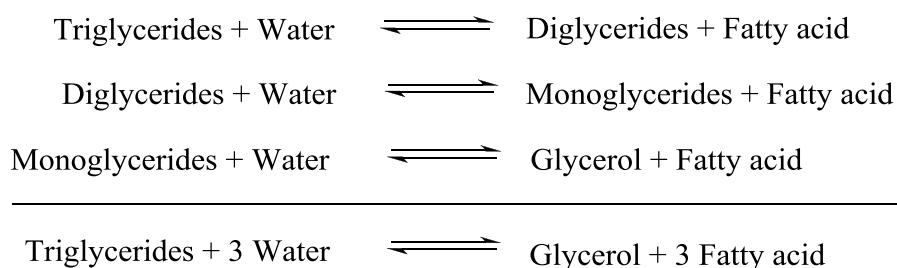
Scheme 3.1. Vegetable oil or fat hydrolysis

3.3.2. Catalytic Activity

The hydrolysis of triglycerides is a three-step, consecutive, reversible reaction. In the first step, the triglyceride (TG) is converted into diglycerides (DG), which is then in the second and third steps converted sequentially into monoglycerides (MG) and glycerol (G), respectively, producing one mole of fatty acid (FA) at each step (Scheme 3.1). Stoichiometrically, one mole of triglyceride requires three moles of water (oil : water molar ratio = 1 : 3) to produce three moles of fatty acids and one mole of glycerol. Excess water would drive the equilibrium towards the end-products – fatty acids and glycerol.

Representative triglyceride:

Glyceryl triacetate + Water ⇌ Glyceryl diacetate + Acetic acid $\triangle H = +11.5$ kJ/mol

Glyceryl diacetate + Water ⇌ Glyceryl monoacetate + Acetic acid $\triangle H = +13.0$ kJ/mol

Glyceryl monoacetate + Water ⇌ Glycerol + Acetic acid $\triangle H = +42.0$ kJ/mol

Glyceryl triacetate + 3 Water ⇌ Glycerol + 3 Acetic acid $\triangle H = +66.5$ kJ/mol
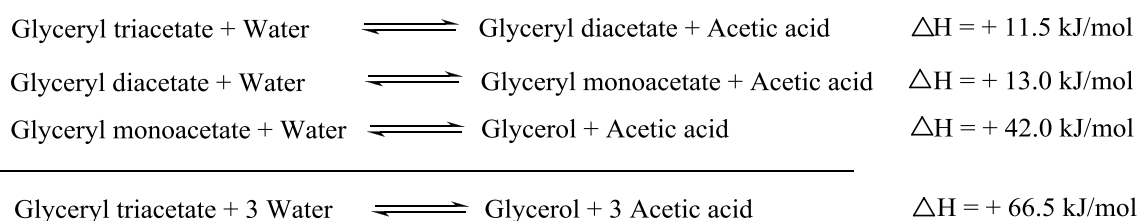
Scheme 3.2. Enthalpy of hydrolysis of glyceryl triacetate

It is an endothermic reaction as can be inferred from the calculated enthalpy for each step of hydrolysis of glyceryl triacetate (Scheme 3.2) [19]. The third step of the reaction i.e., conversion of MG into glycerin and FA is relatively more endothermic than the first two steps. Similar thermodynamics is expected for the vegetable oils and fats. Energy of activation for these transformations has been reported to be in range of 45 – 75 kJ/mol depending on the type of the catalyst and chain length of the fatty acid [16, 20]. Hydrolysis is accelerated by mineral acids, a number of metallic oxides or hydroxides, and various organic catalysts besides certain lypolytic enzymes of plant and animal origin. In practice the effectiveness of a catalyst is dependent not

only upon its fat-splitting action per se, but also to a great extent upon its ability to promote emulsion between the oily and aqueous phase undergoing reaction. The establishment of large water-oil interface is very necessary, because of the limited mutual solubility of the two phases [21].

Table 3.2. Hydrolysis of soybean oil over different catalysts[a]

Catalyst	TG conv. (wt%)	TON[b]	Products distribution (wt%)				Acid value of product (mgKOH/g)
			FA	MG	DG	TG	
No catalyst	34.5	-	14.4	0.8	19.3	65.5	28.4
HY	22.0	4	8.6	0.4	13.0	78.0	16.9
SAPO-11	27.0	14	10.9	0.8	15.3	73.0	21.5
Amberlyst™70	38.5	33	18.7	1.8	18.1	61.5	36.9
Sulfated zirconia	47.8	22	22.3	2.0	23.5	52.2	44.1
MoOx/Al$_2$O$_3$	64.7	24	31.9	4.0	28.8	35.3	63.0
Hβ	67.2	22	34.2	7.3	25.8	32.8	67.5
Co-Zn DMC	96.7	(7)	67.5	9.3	19.9	3.3	133.8
Fe-Zn DMC	93.9	25 (7)	71.8	4.5	17.7	6.1	141.7
ZnO	99.4	(2)	81.3	7.7	10.4	0.6	160.6
Conc. H$_2$SO$_4$	98.5	1	82.2	2.1	14.2	1.5	162.3

[a] *Reaction conditions: Soybean oil = 10 g, soybean oil : water (molar ratio) = 1 : 0, catalyst = 5 wt% of oil, temperature = 463 K, reaction time = 8 h, TG = triglycerides, DG = diglycerides, MG = monoglycerides, FA = fatty acids.*
[b] *Turnover number (TON) = moles of TG converted per mole of acid sites (NH$_3$-TPD) on the catalyst. Values in parentheses indicate TON calculated per mole of Zn^{2+} ions in the catalyst.*

3.3.2.1. Hydrolysis over Various Solid Acid Catalysts

Table 3.2 lists the catalytic activity data of different solid acid catalyst for the hydrolysis of soybean oil. Blank experiments under the reaction condition (463 K, reaction time = 8 h and oil : water molar ratio = 1 : 20, no catalyst), revealed that the

hydrolysis of soybean oil takes place even in the absence of any catalyst but to a small extent only (Table 3.2, TG conversion = 34.5% and fatty acids selectivity = 41.7%). However, the catalysts (except HY and SAPO-11) increase the TG conversion significantly. Near-quantitative conversion of TG was obtained over DMC and ZnO catalysts. TON (TON = moles of TG converted per mole of acid sites on the catalyst) values are significantly greater than one for most of the catalysts indicate that the reaction is catalytic and not stoichiometric in nature. Catalytic activity expressed in terms of turnover number indicates that Amberlyst^{TM}70 (TON = 33) is the most active catalyst for the conversion of the triglyceride among those investigated in this study. But the fatty acids yield over this catalyst is very low (18.7%), the mono- and diglycerides constituting the main products. DMC shows high activity (TON = 25) together with a high yield of fatty acids. Fe-Zn DMC was superior (fatty acids yield = 71.8%) to Co-Zn DMC (fatty acids yield = 67.5%). (Table 3.2). ZnO was efficient and comparable to the homogeneous concentrated sulfuric acid catalyst but its separation from the product mixture was difficult. A paste-like substance formed which required washing with ether or hexane several times before the catalyst could be separated. It is due to the fact that ZnO and MgO increases the solubility of water in oil phase by forming metal soaps [22].

3.3.2.2. Kinetics of Hydrolysis of Soybean Oil

Hydrolysis of soybean oil is conducted in a batch reactor and product yield monitored by acid-base titration, HPLC, FTIR and ^{1}H NMR spectroscopy. Fig. 3.2 shows the product composition in the hydrolysis of soybean oil as a function of reaction time over the Fe-Zn DMC catalyst analyzed by HPLC. Conversion of oil and yield of fatty acids increased with time and remained nearly constant after 8 h. Kinetic plot for the hydrolysis clearly indicates that it is a three-step, consecutive and reversible reaction (Scheme 3.1). The concentration of DG in the products increased with time, reaching a maximum at 7 h and then it decreased with further increase in reaction time (due to conversion into monoglycerides). The concentration of MG was negligible during the initial 5 h and then increased and remained at 7 – 9% beyond 8 h. This plot, suggesting that DG and MG are the intermediates while the fatty acids are the final products in the reaction sequence, is typical of sequential reactions (Scheme 3.1). In contrast to DG, no clear maximum was observed for MG in the kinetics plot because of the attainment of equilibrium between MG and FA at higher

conversion levels of triglycerides. Minami and Saka [23] reported a similar observation of equilibrium at around 90 wt% in yield of FA in the hydrolysis of rapeseed oil in subcritial water (reaction conditions: 593 K, 200 bar, oil to water molar ratio ~1: 55). DMC is a reusable catalyst. Hence, this behavior of MG variation in the kinetics plot is not due to deactivation of the catalyst but to attainment of equilibrium between MG and FA.
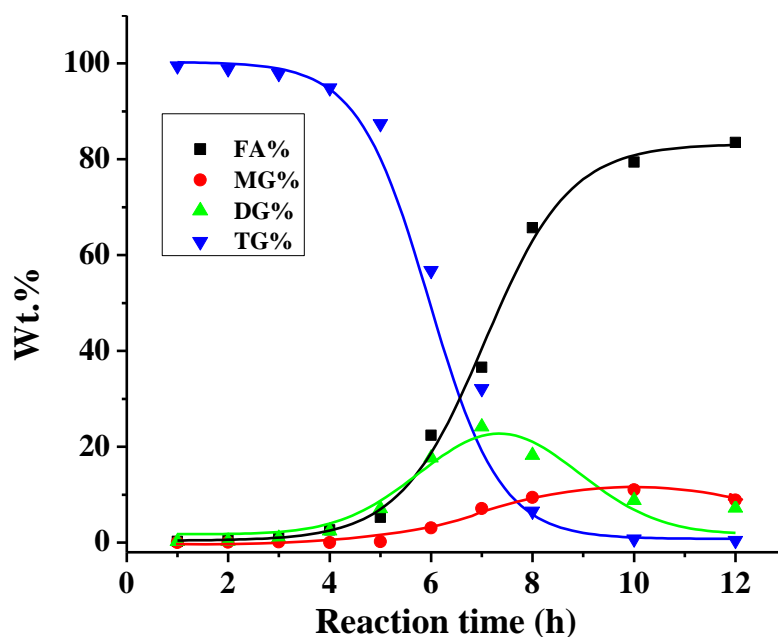
Fig. 3.2. Kinetics of hydrolysis of soybean oil over Fe-Zn DMC

FA - fatty acids, MG - monoglycerides, DG - diglycerides, TG - triglycerides

The kinetics of hydrolysis of soybean oil was also monitored by ^{1}H NMR (Fig. 3.3) and FTIR (Fig. 3.4) spectroscopic techniques. In ^{1}H NMR, the glycerides show characteristic signals at 4 – 4.5 ppm. As the reaction proceeded, intensity of these peaks decreased indicating their conversion into fatty acids. A significant increase in fatty acids yield was observed only after an induction period of 4 h (Figs. 3.3 and 3.4). No decrease in the intensity of peaks due to C=C groups (δ = 5.5 ppm) was observed indicating that there is no thermal polymerization or oxidation occurring as side reactions. Based on ^{1}H NMR spectroscopy, it can be concluded that the hydrolysis product at the end of 8 h contains mainly FA with negligible amounts of glycerides (Fig. 3.3). Fatty acid glycerides show a characteristic IR peak for the carboxylate group at 1750 cm^{-1}. The corresponding peak for FA appears at 1710 cm^{-1} (Fig. 3.4).   .
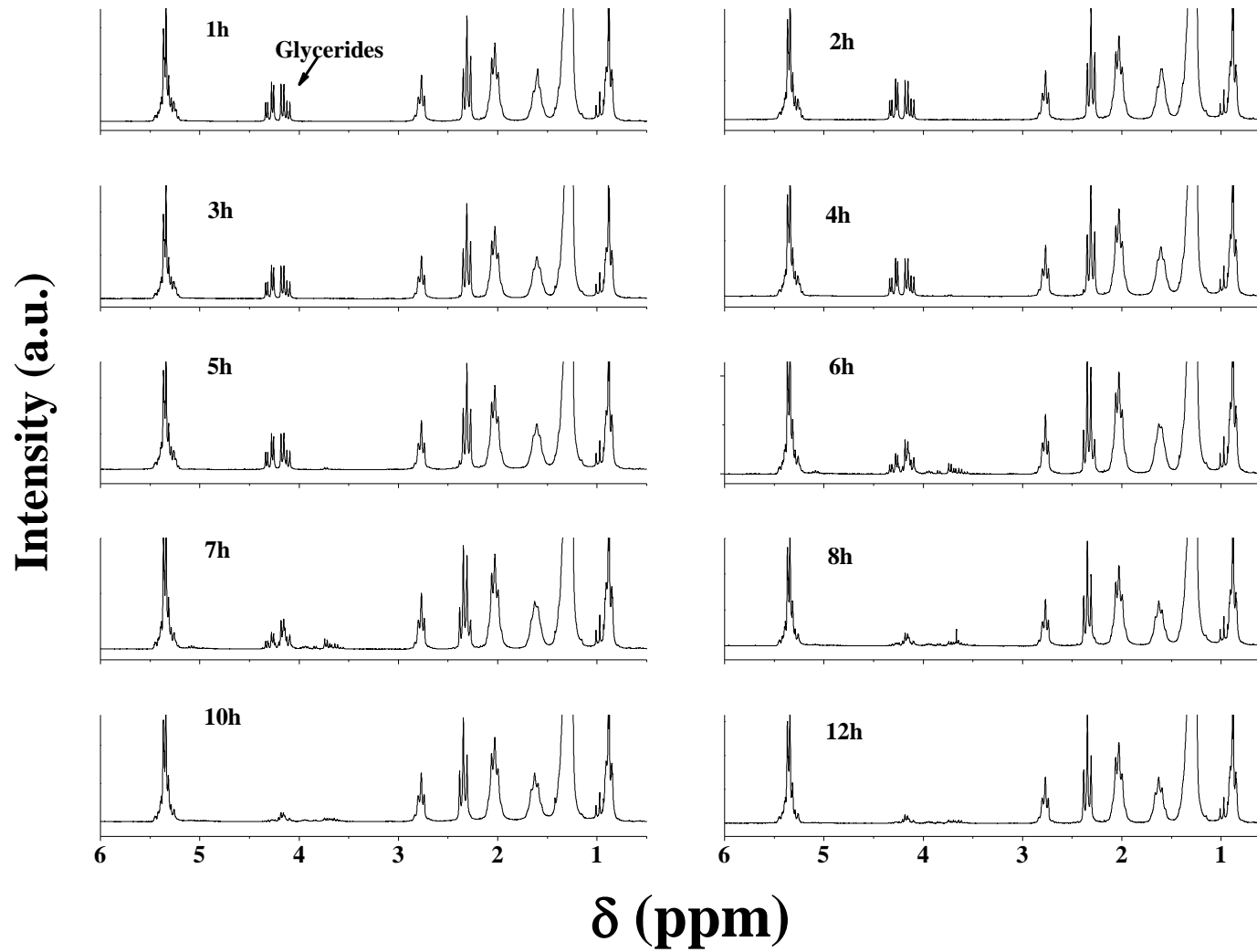
Fig. 3.3. *Kinetic study of hydrolysis of soybean oil by ^{1}H-NMR*

Table 3.3. Hydrolysis of soybean oil over Fe-Zn DMC catalyst : influence of amount of catalyst

Amount of catalyst (wt% of oil)	Reaction time = 5 h						Reaction time = 8 h					
	TG conv. (wt%)	Products distribution (wt%)				Acid value of product (mgKOH/g)	TG conv. (wt%)	Products distribution (wt%)				Acid value of product (mgKOH/g)
		FA	MG	DG	TG			FA	MG	DG	TG	
1	16.0	6.6	0.1	9.3	84.0	13.0	66.1	30.3	13.6	22.3	33.9	59.8
2	24.2	11.3	0.3	12.6	75.8	22.4	80.9	44.2	10.1	26.6	19.1	87.4
3	28.8	12.4	0.5	15.9	71.2	24.6	86.7	51.6	11.2	23.9	13.3	101.9
5	45.7	22.1	2.0	21.7	54.3	43.6	93.4	65.7	9.4	18.2	6.6	129.8
7	59.7	31.1	2.7	25.9	40.3	61.4	97.2	72.1	10.5	14.6	2.8	142.4
10	67.9	39.7	4.2	24.1	32.1	78.4	97.6	75.4	8.6	13.6	2.4	149.0

Reaction conditions: Soybean oil = 10 g, soybean oil : water (molar ratio) = 1 : 20, temperature = 463 K, reaction mode = batch process in a Teflon-lined stainless steel reactor (100 mL). Product distribution was analyzed by HPLC. FA content was also determined by titration method.

While the intensity of the former peak decreased, the intensity of the latter increased with reaction time in the FTIR spectrum. While ^{1}H NMR revealed complete conversion of glycerides to FA beyond 8 h of reaction, FTIR and HPLC do reveal the presence of some residual amounts of glycerides in the product. This disparity is due to differences in the sensitivity of the techniques for different products.
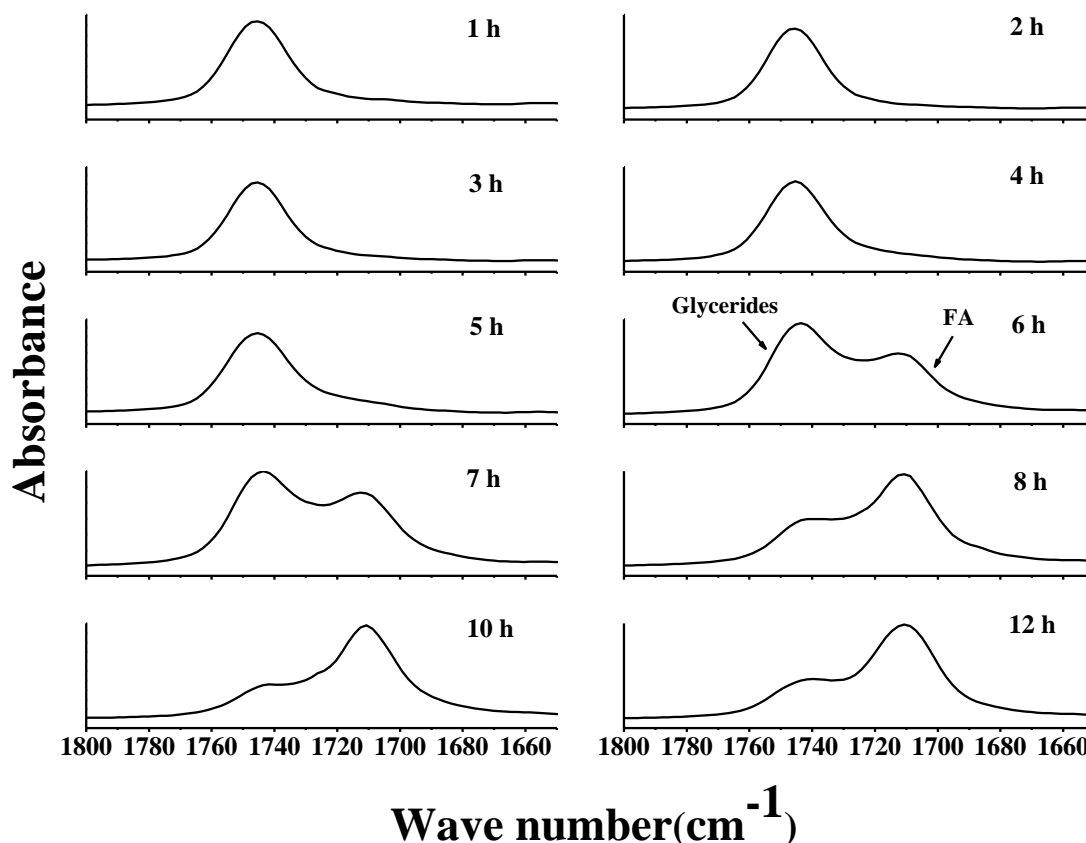
Fig. 3.4. Hydrolysis of soybean oil monitored by FTIR spectroscopy

3.3.2.3. Influence of Amount of Catalyst

TG conversion and FA selectivity increased markedly with an increase in the amount of catalyst up to 5 wt%. Beyond that, the change is only marginal (Table 3.3). According to the Madon and Boudart test [24], a modified form of the Koros and Nowak test [25], in the absence of any mass transfer limitations, the TG conversion should increase proportionately with the amount of the catalyst. We observed this increase in the range of $0 - 5$ wt% catalyst. The deviation from this linearity beyond 5 wt% of the catalyst indicates that, at higher catalyst concentrations, there exists mass transfer limitation on the reaction rate. At longer reaction time (8 h),

conversions are also influenced by equilibrium attainment. The non-homogeneity of the slurry at such high concentrations of the solid catalyst may also contribute to such a mass transfer limitation.

3.3.2.4. Influence of Reaction Temperature

Reaction temperature is another important parameter that influences the rate of hydrolysis. As expected, both TG conversion and FA yield increased with reaction temperature from 433 to 463 K. Above 463 K, however, the selectivity for FA declined due to equilibrium limitations (Table 3.4). At higher temperatures, the reverse esterification reaction of FA with glycerol becomes significant.

Table 3.4. Hydrolysis of soybean oil over Fe-Zn DMC catalyst: effect of reaction temperature[a]

Reaction temperature (K)	TG conv. (wt%)	TON[b]	Product distribution (wt%)				Acid value of the product (mgKOH/g)
			FA	MG	DG	TG	
433	24.3	7	8.6	1.2	16.5	73.7	16.9
443	90.3	24	73.0	6.3	11.0	9.7	144.2
463	84.1	23	72.3	5.8	6.0	15.9	121.5
473	89.7	24	69.4	11.8	8.6	10.3	137.1
483	93.2	25	66.3	20.1	6.8	6.8	131.0

[a]*Reaction conditions: Soybean oil = 20 g, soybean oil : water (molar ratio) = 1 : 30, reaction mode = batch process in a Ti-line stainless steel Paar reactor (300 mL, 300 revolutions per minute).*

[b]*Turnover number (TON) = moles of TG converted per mole of acid sites (NH_3-TPD) on the catalyst.*

3.3.2.5. Influence of Water to Oil Molar Ratio

Table 3.5 shows the influence of water to oil molar ratio on the hydrolysis of soybean oil over DMC catalyst. The yield of FA increased with water/oil molar ratio up to 20. Maximum FA yields could be obtained using 5 wt% of catalyst, an oil to water molar ratio of 1 : 20, a reaction temperature of 463 K and a reaction time of 8 h.

Table 3.5. Hydrolysis of soybean oil over Fe-Zn DMC catalyst : influence of water to oil molar ratio

Water : oil molar ratio	TG conv. (wt%)	TON[b]	Products distribution (wt%)				Acid value of the product (mgKOH/g)
			FA	MG	DG	TG	
5	92.7	25	49.4	14.3	29.0	7.3	97.7
10	92.6	25	53.4	7.5	31.7	7.5	105.5
15	96.2	26	66.0	8.8	21.4	3.8	130.3
20	93.4	25	65.7	9.4	18.2	6.6	129.8
30	97.0	26	69.1	7.3	20.5	3.0	136.6
40	96.4	26	68.9	7.2	20.4	3.6	136.1

[a]*Reaction conditions: Soybean oil = 10 g, catalyst = 5 wt% of oil, temperature = 463 K, reaction time = 8 h.*

[b]*Turnover number (TON) = moles of TG converted per mole of acid sites (NH₃-TPD) on the catalyst.*

3.3.2.6. Hydrolysis of Different Oils and Fat

Fe-Zn DMC was found to be very active in the hydrolysis of a range of edible (coconut, palmolein and soybean) and non-edible (castor, jatropha, karanja, palm and rubber seed) oils and chicken fat (Table 3.6). Non-edible oils (used soybean oil and fat) were converted with equal, if not higher efficiency than the edible oils under optimized conditions. Triglyceride conversion greater than 97% and FA selectivity greater than 76% were obtained. Non-edible oils and fats are low-quality feedstock compared to edible (refined) vegetable oils because of their free fatty acid content that may increase up to 15 wt% in contrast with edible oils which typically contain less than 0.5 wt% fatty acid. In addition, non-edible oils contain phospholipids, sterols, water, odorants and other impurities in small amounts (~2 wt%). These impurities deactivate conventional, homogeneous and heterogeneous catalysts. However, no such deactivation of DMC was observed when using non-edible oils.

Table 3.6. Hydrolysis of edible and non-edible oils and fat over Fe-Zn DMC catalysts

Oil/fat	FA content (wt%)		TG Conv. (wt%)	Product selectivity (wt%)			
	Before the reaction	After the reaction		FA	MG	DG	TG
Edible oils:							
Coconut oil	0.2	88.4	99.1	89.4	9.3	1.3	1.0
Palmolein oil	0.3	80.5	98.9	80.5	11.1	7.3	1.1
Soybean oil	0.3	77.2	98.5	77.2	12.0	9.3	1.5
Used soybean oil	0.5	83.2	99.2	83.2	9.6	6.3	0.8
Non-edible oils:							
Castor Oil	3.1	51.9					
Jatropha Oil	3.7	82.7	99.3	82.7	9.8	6.8	0.7
Karanja Oil	5.8	76.7	99.9	76.7	20.4	2.7	0.1
Palm oil	6.6	80.2	99.1	80.2	11.1	7.8	0.9
Rubber Seed Oil	17.0	84.4	94.3	84.4	5.6	4.3	5.7
Animal fat:							
Chicken Fat	10.5	78.5	97.2	78.5	11.5	7.2	2.8

Reaction conditions: Oil or fat = 10 g, oil or fat : water molar ratio = 1 : 30, catalyst = 5 wt% of oil, temperature = 463 K, reaction time = 12 h.
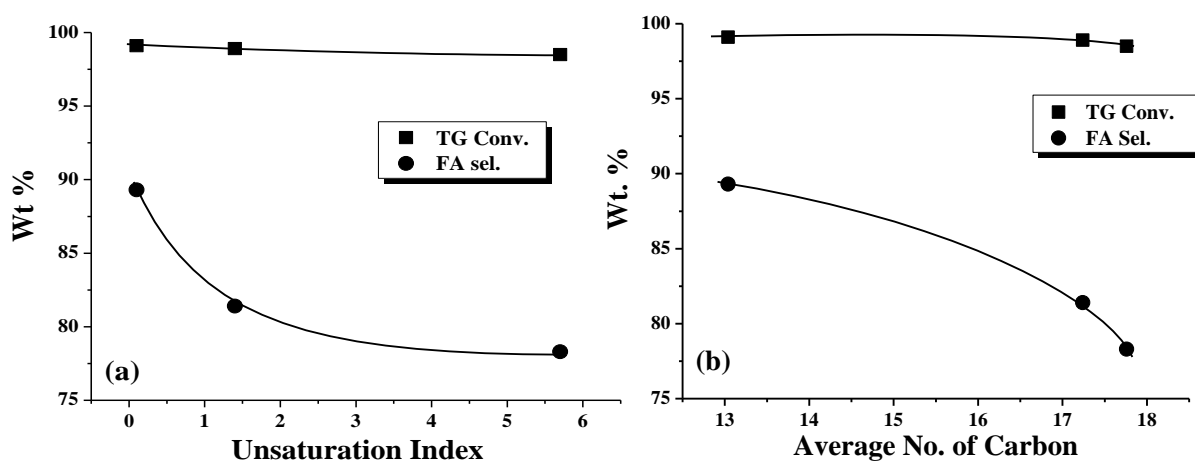
Fig. 3.5. *Influence of unsaturation and chain length of fatty acids on hydrolysis activity*

Unsaturation in vegetable oils and fatty acid chain length influenced the hydrolysis activity. Average fatty acid chain lengths of different oils were estimated based on their compositions projected in Table 1.2 in Chapter 1. Fig. 3.5(a) shows the influence of unsaturation index (ratio of unsaturated fatty acids to saturated fatty acids) on TG conversion. As the unsaturation of oils increases a slight decrease in TG conversion and FA yield was detected. A similar decrease was also observed with increasing fatty acid chain length (Fig. 3.5 (b)). The reason for this may be the electron rich double bond containing fats adsorb more strongly on the Lewis acidic catalyst surface than the saturated fats and thus show a lowering in the conversion.

3.3.2.7. Miscibility of Water with Oil

Miscibility of water with oil is a major issue in this reaction. Eklesberg et al [22] reported that the heterogeneous reaction between water and oil at the interface is of minor importance in the hydrolysis as compared with the homogenous reaction between oil and the water dissolved in the oil phase. Since water has limited solubility in oil, the reaction proceeds very slowly at the beginning, and a significant induction period is usually observed (Fig. 3.2). Miscibility of water with oil can be enhanced by adding suitable phase transfer agents or solvents. The following methods have been explored:

1) Addition of oleic acid
2) Addition of reaction product containing mono- and diglycerides along with fatty acids
3) Use of solvent
4) Use of surfactants

Table 3.7 shows the influence of the addition of oleic acid in different amounts to improve the miscibility of oil and water and thereby the conversion. Addition of $1-2$ wt% of oleic acid is sufficient to enhance the catalytic activity significantly. Addition of oleic acid significantly reduced the induction period. But, after 10% oleic acid addition there is not much increase in FA yield (Fig. 3.6). Higher efficiency and FA yield observed with non-edible oils compared to edible oils (Table 3.6) can therefore be attributed to the presence of free fatty acids in those oils. The fatty acids improve the miscibility of the oil phase with water. It is likely that the hydrolysis reactions occur in the oil phase. The low concentration of water in the oil will lead to slow reaction rates in the early stages of the reaction. An induction period (of about 4 h) is observed (Fig. 3.2).

Table 3.7. Influence of the addition of oleic acid on the hydrolysis of soybean oil

Oleic acid (%)	No catalyst					Fe-Zn DMC catalyst (5 wt% of oil)				
	Product distribution,[a] wt%				Acid value[a] (mgKOH/g)	Product distribution,[a] wt%				Acid value[a] (mgKOH/g)
	FA	MG	DG	TG		FA	MG	DG	TG	
0	1.2	0.0	0.8	98.0	2.4	2.6	0.0	2.5	94.9	5.2
1	6.5	0.3	6.4	86.8	12.8	50.7	8.0	28.6	12.7	100.2
2	10.3	0.9	13.9	74.9	20.3	50.3	8.9	28.5	12.3	99.4
5	17.4	2.0	22.6	58.0	34.3	54.6	9.0	26.7	9.8	107.8
10	28.1	5.5	30.8	35.6	55.4	54.6	8.8	27.7	8.9	107.6
15	28.0	9.6	32.7	29.7	55.0	53.3	10.0	29.4	7.3	104.9
20	32.6	8.1	35.3	24.0	64.0	52.4	9.4	31.4	6.8	103.0

[a]*After subtracting the corresponding value due to added oleic acid.*

Reaction conditions: (Soybean oil + oleic acid) = 10 g, (oil+OA) : water molar ratio = 1 : 20, temperature = 463 K
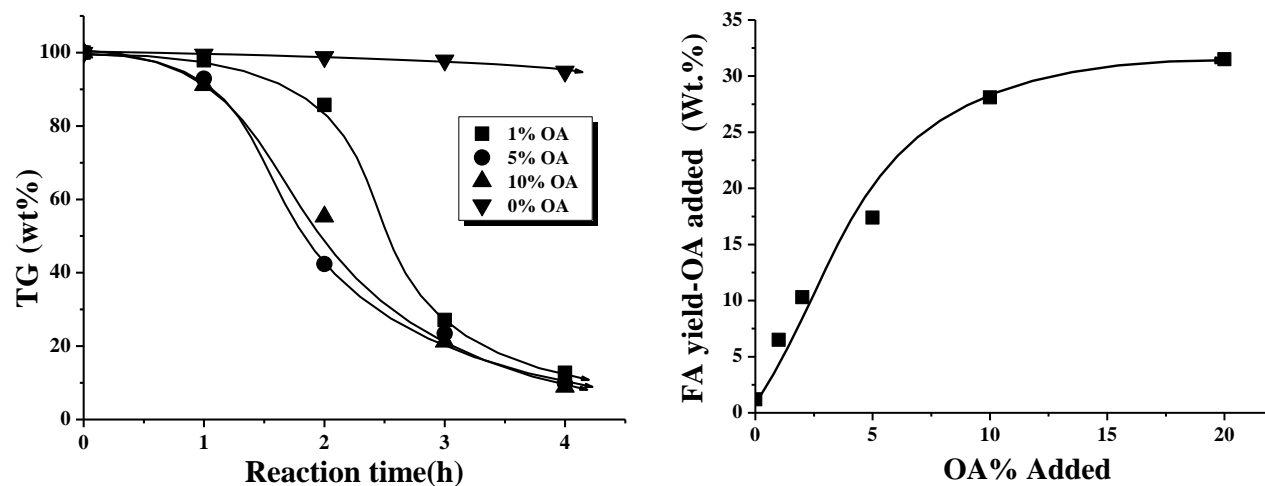
Fig. 3.6. *Effect of oleic acid addition on induction time and FFA yield*

Fig. 3.7 and Table 3.8 shows the effect of addition of 20 wt% of a partially hydrolyzed product (composition: FA - 35.3%, MG - 6.9%, DG - 21.2% and TG - 36.6%) to a fresh batch of reactants mixture. Reaction time was reduced considerably. The normal induction period of about 3 - 4 h (Fig. 3.2) was eliminated when 20 wt% of hydrolyzed product was added to the reaction mixture (Fig. 3.7). While the FA yield is about 2.6% at the end of 4 h in the absence of the added products, it increases to 60.9% when 20% of the hydrolyzed product was added. Water is a hydrophilic solvent. Oil and fat (TG) are aprotic (hydrophobic) and so immiscible with water. Mono and diglycerides are less hydrophobic than the starting triglycerides and are more miscible with water. As a result, the mono- and diglycerides function as emulsifiers and enhance mixing of the triglyceride layer with water and, thereby, the rate of the hydrolysis reaction.

Table 3.8. Hydrolysis of soybean oil over Fe-Zn DMC catalyst: influence of the addition of a part of hydrolysis product (20 wt%) to the reaction mixture

Reaction time (h)	Product distribution (wt%)							
	Without adding reaction mixture (oil: 10 g of soybean oil)				After addition of 20 wt% hydrolyzed product (feed: oil: 8 g of soybean oil + 2 g of hydrolyzed product)[a]			
	FA	MG	DG	TG	FA	MG	DG	TG
1	0.3	0.00	0.2	99.5	10.2	1.0	7.8	80.9
2	0.8	0.1	0.3	98.8	24.1	5.1	12.7	58.1
3	1.1	0.1	0.9	97.9	45.4	6.0	37.6	10.9
4	2.6	0.0	2.5	94.9	60.9	13.1	19.3	6.7

Reaction conditions: oil : water molar ratio = 1 : 30, catalyst = 5 wt% of oil, temperature = 463 K, wt% composition of hydrolyzed product added = FA(35.3) + MG (6.9) + DG (21.2) + TG (36.6). [a]Product composition includes the acid present in the added hydrolyzed product
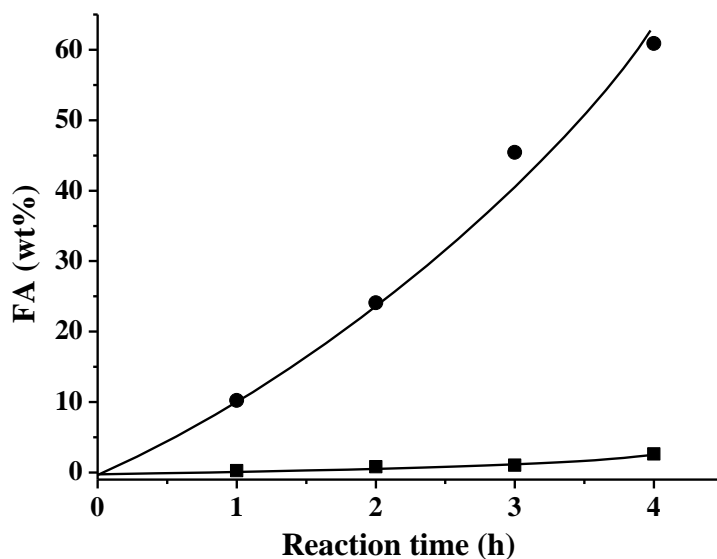
Fig. 3.7. *Hydrolysis of soybean oil with (●) and without (■) the addition of 20 wt% hydrolysis product*

Similar effects were also found when suitable solvents, phase transfer agents and surfactants were added (Table 3.9). Among the solvents investigated, DMF was the best. TG conversion was lower with acetone (7.4%) than without any solvent (12.6%). A similar observation was found also with Triton X 100 (8.8%). DMF was miscible with water in all proportions and up to 25% with soybean oil at 298 K. Acetone and THF are 100% miscible with both water and oil. When a known quantity of solvent was added to the reactants mixture (soybean oil: water molar ratio = 1: 20) at 298 K, a turbid layer formed at the interface of the reactants. The amount of such turbid layer is more in the case of DMF than with THF. When DMF was added the miscibility of these phases increased to 10 wt%, otherwise vegetable oil and water are immiscible. No such turbidity was detected with acetone solvent. The boiling point of different solvents decreases in the following order: DMF (426 K) > THF (339 K) > acetone (329 K). At our reaction conditions, in contract to acetone, DMF is mostly in the liquid phase in contact with the reactants enhancing their miscibility. This enhancement in reactants miscibility, formation of interface and high boiling point are the causes for the higher conversions observed in DMF than in THF and acetone solvents. Use of solvents, products containing partially hydrolyzed glycerides or fatty acids increase the miscibility of oil and water (form an active interface region) and greatly accelerate the reaction so that high conversion is reached in shorter time periods. Recycle of a portion of the products as a miscibility enhancer is more practical and beneficial.

Table 3.9. Influence of addition of solvent or surfactant[a]

Solvent or surfactant	TG conv. (wt%)	TON[b]	Products selectivity (wt%)				Acid value
			FA	MG	DG	TG	
No solvent	12.6	3	5.2	0.2	7.1	87.4	10.4
DMF	40.7	11	13.1	29.9	16.3	80.5	40.7
THF	32.7	9	16.5	3.4	12.8	67.3	32.6
Acetone	7.4	2	3.6	0.1	3.7	92.6	7.2
TPAB	43.8	12	21.0	3.2	19.5	56.2	41.6
Triton X 100	8.8	2	3.6	1.5	3.8	91.2	7.1

[a]Reaction conditions: Soybean oil = 5 g, oil : water molar ratio = 1 : 20, Fe-Zn DMC = 5 wt% of oil, solvent or surfactant = 5 wt% of oil, temperature = 463 K, reaction time = 5 h, reaction mode = batch process in a teflon-lined stainless steel reactor (100 mL).[b]Turnover number (TON) = moles of TG converted per mole of acid sites (NH_3-TPD) on the catalyst.

Table 3.10. Hydrolysis of soybean oil over Fe-Zn DMC : catalyst recyclability study[a]

Number of recycles	TG conv. (wt%)	TON[b]	Products selectivity (wt%)				Acid value of the product (mgKOH/g)
			FA	MG	DG	TG	
0th (Fresh)	93.9	25	71.8	4.5	17.7	6.1	141.7
1st	96.5	26	70.8	10.2	15.5	3.5	139.9
2nd	97.1	26	72.8	9.8	14.5	2.9	143.8
3rd	96.2	26	71.2	10.0	15.0	3.8	140.6
4th	97.1	26	72.9	10.1	14.1	2.9	143.9
5th	97.9	26	72.8	10.9	14.2	2.1	143.8

[a]Reaction conditions: Soybean oil = 10 g, oil : water molar ratio = 1 : 20, catalyst = 5 wt% of oil, temperature = 463 K, reaction time = 8 h, [b]Turnover number (TON) = moles of TG converted per mole of acid sites (NH_3-TPD) on the catalyst.

3.3.2.8 Recyclability of Fe-Zn DMC Catalyst

Recyclability is perhaps the most important parameter for any heterogeneous catalyst. Fe-Zn DMC catalyst was reused in five recycle experiments without any pretreatment (Table 3.10). No major loss in activity and selectivity for fatty acids were observed. This shows that DMC is a recyclable catalyst and does not get deactivated due to water (reactant in hydrolysis) and glycerol (a product of hydrolysis).

3.3.3. Structure–Activity Correlation

Adsorption and activation of the triglyceride molecule on the catalyst surface are the key steps in the hydrolysis of fats and oils over solid surfaces. Therefore, the nature of the catalyst surface plays crucial role in the hydrolysis of vegetable oils. In the case of hydrophilic catalysts, the surface is covered mostly with the water molecules and accessibility of the active sites for oil molecules is hindered. Hence, catalysts even with stronger acid sites will not be able to show higher activity. On the contrary, oil molecules will have greater access to acidic active sites on hydrophobic catalyst surfaces and therefore higher conversions are expected on those catalyst surfaces. The adsorption of this non-polar molecule will be facilitated on hydrophobic surfaces. To compare the relative surface hydrophobicity of our catalysts, a known amount of the powdered catalyst (DMC, Hβ, HY, SAPO-11, sulfated zirconia or MoO_x/Al_2O_3) was suspended in equal volumes of water-soybean oil mixture. Water and soybean oil are immiscible, with water forming the bottom and oil the top layers (Fig. 3.8). Interestingly, the DMC catalyst remained suspended in the oil layer, Hβ settles fast at the interface of the layers and the rest of the catalysts went into the water layer. The reason for this could be that the surface of DMC is hydrophobic and hence, it prefers to be in the hydrophobic oil layer. Hβ is less hydrophobic so settles at the interface and rest of the catalysts including sulfated zirconia are relatively hydrophilic and go into the water layer. Because of their hydrophilic nature their surface is covered with water molecules during the catalytic reaction thereby limiting access to the surface for oil molecules. On the contrary, on hydrophobic DMC surface, the hydrophobic oil/fat molecules are preferentially adsorbed and activated. The higher TG conversions and FA yield observed over Fe-Zn DMC are therefore due to its hydrophobic surface structure in addition to its higher acid site density.

Fig. 3.8. *Preferential dispersion of DMC in non-polar, soybean oil layer, Hβ near the interface and HY, SAPO-11, sulfated zirconia (SZ) and MoO$_x$/Al$_2$O$_3$ in polar water layer*

3.4. Conclusions

Hydrolysis of vegetable oils and fats has been investigated over different solid catalysts including acidic, macroporous polymeric resin (Amberlyst^{TM}70), zeolites (SAPO-11, HY and Hβ), supported oxide (MoO$_x$/Al$_2$O$_3$), sulfated zirconia, DMC and basic ZnO. Fe-Zn DMC exhibited the highest conversion and selectivity. Complete conversion of triglycerides and fatty acid yields greater than 73% were obtained at moderate temperature and pressure. The highly efficient activity of DMC has been attributed to its hydrophobic surface structure enabling it to adsorb and activate the triglyceride molecules selectively. The catalyst is reusable. Induction periods in hydrolysis reactions can be considerably curtailed / eliminated by including some amounts of the products (containing some fatty acids and mono- / diglycerides) in the initial reaction mixture. This is the first report on the application of DMC catalyst to hydrolysis of triglycerides.

3.5. References

1.   M. Di Serio, R. Tesser, L. Pengnice, E. Santacesaria, Energy Fuels 22 (2008) 207.

2.   M. DiSerio, M. Cozzolino, M. Giordano, R. Tesser, P. Patrono, E. Santacesaria, Ind. Eng. Chem. Res. 46 (2007) 6379.

3.   E. Lotero, Y. Liu, D.E. Lopez, K. Suwannakarn, D.A. Bruce, J.G. Goodwin, Jr., Ind. Eng. Chem. Res. 44 (2005) 5353.

4.   U. Schuchardt, R. Sercheli, R.M. Vargas, J. Braz. Chem. Soc. 9 (1998) 199.

5.   D. Kusdiana, S. Saka, Appl. Biochem. Biotech. 113-116 (2004) 781.

6.   An Ullmann's Encyclopedia, Industrial Organic Chemicals: Starting Materials and Intermediates, Wiley-VCH, Weinheim, Germany, Vol. 4 pp. 2481–2532 (1999).

7.   T.A. Patil, D.N. Butala, T.S. Raghunathan, H.S. Shankar, Ind. Eng. Chem. Res. 27 (1988) 727.

8.   H.L. Barnebey, JAOCS (1948) 95.

9.   R.L. Holliday, J.W. King, G.R. List, Ind. Eng. Chem. Res. 36 (1997) 932.

10.   L. Hartman, JAOCS (1953) 349.

11.   U.S. patent No. 6,646,146 B1 (2003) assigned to Haltermann Ascot GmbH, Hamburg, GE.

12.   US patent No. 5,383,678 (1995) assigned to Church & Dwight Co., Inc., Princeton, N.J.

13.   US patent No. 6,933,139 B2 (2005) assigned to T + T Oleochemie GmbH, Alzeunau, DE.

14.   W.M. Linfield, D.J. O'Brien, S. Serota, R.A. Barauskas, JAOCS 61 (1984) 1067.

15.   U.S. patent No. 6,258,575 B1 (2001) assigned to Kao Corp., Tokyo, JP.

16.   K. Ngaosuwan, E. Lotero, K. Suwannakaru, J.G. Goodwin Jr., P. Praserthdam, Ind. Eng. Chem. Res. 48 (2009) 4757.

17.   E. Minami, S.Saka, Fuel 85 (2006) 2479.

18.   P.S. Sreeprasanth, R. Srivastava, D. Srinivas and P. Ratnasamy, Appl. Catal. A: Gen. 314 (2006) 148.

19.   "Lange's Handbook of Chemistry," Ed. By J.A. Dean, McGraw-Hill Inc., New York, 15th ed. pp. 6.05-6.50 (1999)..

20.   P. Khuwijitjaru, T. Fujii, S. Adachi, Y. Kimura, R. Matsuno, Chem. Eng. J. 99 (2004) 1.

21.   A.E. Bailey, Industrial Oil and Fat products, Interscience publishers, New York (1945).

22.   O.J. Ackelsberg, J. Am. Oil chem. Soc. 35 (1958) 635.

23. E. Minami, S. Saka, Fuel 85 (2006) 2479.

24. R.J. Madon, M. Boudart, Ind. Eng. Chem. Fundam. 21 (1982) 438.

25. R.M. Koros, E.J. Nowak, Chem. Eng. Sci. 22 (1967) 470.

Chapter 4
Esterification of Fatty Acids into Biodiesel

4.1. Introduction

Biodiesel is comprised of fatty acid methyl or ethyl esters (FAME or FAEE) [1-5]. Currently, biodiesel is prepared from edible vegetable oils. Non-edible oils are sustainable feedstock for biodiesel production. However, non-edible oils contain significant amount of free fatty acids (FFAs). Conventional base catalysts cannot be used for biodiesel production from non-edible oils due to saponification of these FFAs by cations of the base [3] Solid acids which can catalyze simultaneously the esterification of FFA and transesterification of fatty acid glycerides into FAME biodiesel are considered as efficient catalysts for such low-grade, non-edible oil feedstocks. Alternatively, a two-step process has to be adopted, wherein the FA are esterified in the first-step using an acid catalyst prior to transesterification of the triglycerides by a base catalyst. The acids employed include sulfuric, phosphoric, hydrochloric and organic sulphonic acids [3]. Solid acid catalysts eliminate handling, corrosion and environmental problems associated with the use of these homogeneous mineral acids [6-16]. An understanding of the factors influencing esterification reaction is of great importance in designing more efficient solid acid catalysts.

Steric and diffusional effects play an important role on the esterification and transesterification reactions of vegetable oils over solid catalysts. Liu et al. [17] reported that chain length and steric effects of α-substituents in the fatty acid chain influence the kinetics of the reaction. Mbaraka et al. [18] demonstrated a strong dependence of reaction rates on the pore size of organosulfonic acid-functionalized mesoporous silica catalysts. Alonso et al. [19] reported that the polarity of the acid chain also influences the rate of esterification and transesterification reactions: for example, fatty acids containing Br and OH terminal polar groups reacted faster than normal fatty acid molecules. As an alternate approach to enhance the esterification rates of fatty acids, the catalyst surface can also be modified to achieve a faster esterification [20]. In this chapter, the influence of pore size and hydrophobicity of the catalyst and relative adsorption of reactants/products, besides acidity and surface area, on the kinetics of esterification of long-chain fatty acids over solid acid catalysts is investigated. For this, catalysts with different hydrophobicity viz., Fe-Zn double-metal cyanide (DMC), Hβ, sulfated zirconia (SZ) and Al-MCM-41 are chosen for the esterification of (1) $C_{8.0} - C_{18.1}$ fatty acids with methanol and (2) oleic acid with various linear alcohols (C_1 - C_8).

4.2. Experimental Section

4.2.1. Material Preparation

DMC [21, 22] and Al-MCM-41 (SiO_2/Al_2O_3 = 96) were prepared as reported in Chapter 2. Zeolite Hβ (SiO_2/Al_2O_3 = 28) was provided by the Catalyst Pilot Plant, National Chemical Laboratory, Pune. SZ was procured from a commercial source (Saint-Gobain, Norpro). Elemental analysis (wt%): DMC – C(18.1), H(1.7) and N(19.8) and SZ – S (1.35).

4.2.2. Catalyst Characterization

X-ray diffraction (XRD) patterns of the powdered samples were recorded in the 2θ range of 5 – 85° with a scan speed of 4°/min on a Philips X'Pert Pro diffractometer using Cu-K_{α} radiation (λ = 0.15406 nm) and a proportional counter detector. In the case of Al-MCM-41, the XRD patterns were recorded in the 2θ range of 1.5 – 10° with a scan speed of 1°/min. The specific surface area of the samples was determined by the BET method using NOVA 1200 Quanta Chrome equipment. The micropore volume was determined from the t-plot. A reference alumina sample supplied by Quanta Chrome was used for calibrating the instrument. The pore diameter was estimated using the Barret-Joyner-Halenda (BJH) model. Prior to N_2-adsorption, the samples were evacuated for several hours at 423 K in the case of DMC (150 mg) and 673 K in the case of Hβ, SZ and Al-MCM-41 (25 mg) catalysts. Morphological characteristics of the samples were determined using a scanning electron microscope (SEM; Leica 440) and high resolution transmission electron microscope (HRTEM; FEI Technai F 30). In HRTEM studies, the catalyst samples were dispersed in isopropyl alcohol, deposited on a Cu grid, dried and imaged. Diffuse reflectance infrared Fourier transform (DRIFT) spectra were recorded on a Perkin Elmer spectrophotometer in the region of 400 – 4000 cm^{-1}. Diffuse reflectance UV-visible (DRS) measurements were done in the 200 – 800 nm region using a Shimadzu spectrophotometer (model: UV-2550) and a spectral-grade $BaSO_4$ as reference material.

The acidic properties of the catalysts were determined using pyridine and NH_3 as probe molecules. The type and density of the acid sites were determined by DRIFT spectroscopy of adsorbed pyridine and temperature-programmed ammonia desorption (NH_3-TPD) techniques. The samples were initially activated at 473 K in the case of DMC and at 723 K in the case of Hβ, SZ and Al-MCM-41. The temperature was

brought down to 323 K and pyridine was adsorbed. The temperature of the sample was raised and held at a desired value (373 K) for 15 min before recording the spectrum (spectral resolution = 2 cm^{-1}; number of scans = 50). Difference spectra were obtained by subtracting the spectrum of the catalyst from that of the sample with adsorbed pyridine. NH$_3$-TPD experiments were performed on a Micromeritics AutoChem 2910 instrument. In a typical experiment, 0.1 g of catalyst was taken in a U-shaped, flow-thru, quartz sample tube. Prior to TPD experiments, the catalyst was pretreated in He (30 cm^3/min) at 473 K in the case of DMC and at 773 K in the case of Hβ, SZ and Al-MCM-41 for 1 h. A mixture of NH$_3$ in He (10: 90) was then passed (20 cm^3/min) at 323 K for 0.5 h. Then, the sample was, subsequently flushed in He (30 cm^3/min) at 323 K for 1 h. The TPD experiments were carried out in the range 323 – 723 K at a heating rate of 10 K/min. The ammonia concentration in the effluent was monitored with a gold-plated, filament thermal conductivity detector. The amount of desorbed ammonia was determined based on the area under the peak.

For ion-exchange capacity measurements, 0.1 g of activated catalyst was dispersed in 10 mL of 0.01 N NaCl and stirred for 1 h. The catalyst was separated by centrifugation, the liquid portion was titrated with 0.01 N NaOH using 1% phenolphthalein solutions as indicator and the ion-exchange capacity of the catalysts was determined.

4.2.3. Reaction Procedure

Esterification of fatty acids with methanol was carried out in a batch reactor. Titration and ^{1}H NMR spectroscopy (Bruker AV 200 MHz) were used to identify the product and to estimate the fatty acid conversion [23].

Esterification of fatty acids [octanoic acid (C$_{8.0}$), decanoic acid (C$_{10.0}$), dodecanoic acid (C$_{12.0}$), palmitic acid (C$_{16.0}$) and oleic acid (C$_{18.1}$)] with methanol was conducted in batch reactors over DMC, Hβ, Al-MCM-41 and SZ catalysts. In a typical reaction, 0.15 g of catalyst, 17.7 mmol of fatty acid and methanol (fatty acid : methanol molar ratio = 1:10) were taken in a Teflon-lined, stainless steel autoclave (100 ml). The reaction was conducted at a desired temperature and for a desired period of time by mounting the autoclave in a rotating hydrothermal reactor (Hiro Co., Japan). At the end of reaction, the autoclave was cooled to 298 K and the catalyst was separated by filtration. Methanol from the reaction mixture was removed using a rotavapor. The acid values of the reaction mixture at the beginning and at the

end of the reaction were determined by titration with 0.1 N NaOH solution and using phenolphthalein as indicator.

Kinetic parameters were determined by carrying out experiments at similar conversion levels (20 – 40 mol %). For each fatty acid ($C_{8.0}$ – $C_{18.1}$), the reactions were conducted at four different temperatures (423, 433, 443 and 453 over DMC, 363, 373, 383 and 393 K over Hβ, 393, 403, 413 and 423 K over Al-MCM-41 and 353, 363, 373 and 383 K over SZ, respectively). All the experimental data points collected over 8 h were fitted to a curve passing through origin. From this curve (conversion versus time plot), initial rates were determined. These were then used to calculate the rate constant (k) using the pseudo-first-order rate law. Employing the Arrhenius equation and the k values determined at different temperatures, activation energy (E_a) values were calculated.

In other studies, the reactions were carried out between oleic acid ($C_{18.1}$) and alcohols of varying chain length [methanol (C_1), ethanol (C_2), n-propanol (C_3), n-butanol (C_4), n-pentanol (C_5), n-hexanol (C_6) and n-octanol (C_8)]. The reactions were performed in a similar manner as mentioned above taking 0.06 g of catalyst (Hβ, Al-MCM-41 and DMC), 2 g of oleic acid and alcohol (fatty acid : alcohol molar ratio = 1: 10) and the kinetic data were estimated.

4.2.4. Adsorption Studies

4.2.4.1. Water - Methanol Adsorption

0.1 g of the catalyst was first activated at 393 K for 2 h. It was then, dispersed in a solution containing 2.5 g each of water and methanol. The amount of methanol adsorbed on the catalyst in the presence of water was determined by gas chromatography (Varian 3400; CP-SIL8CB column; 30 m-long, and 0.53 mm-i.d.) and gravimetry.

4.2.4.2. Adsorption of Fatty Acids

0.1 g of the catalyst (activated at 473 K) was dispersed (for 30 min at 298 K) in 5 mL of 0.1 M oleic acid ($C_{18.1}$) in decane or octanol/methanol. The solid was separated and the amount of fatty acid in the solution was estimated by titration with 0.01 N NaOH solution. A comparison of this value with that present originally in the solution before dispersing the catalyst yielded the amount of oleic acid adsorbed on the catalyst surface in the presence of a non-polar decane and the relatively more

polar octanol. Similar experiments were conducted also using the shorter chain octanoic acid ($C_{8.0}$) – methanol, octanol or decane mixtures.

4.3. Results and Discussion

4.3.1. Structural and Textural Properties of Catalysts
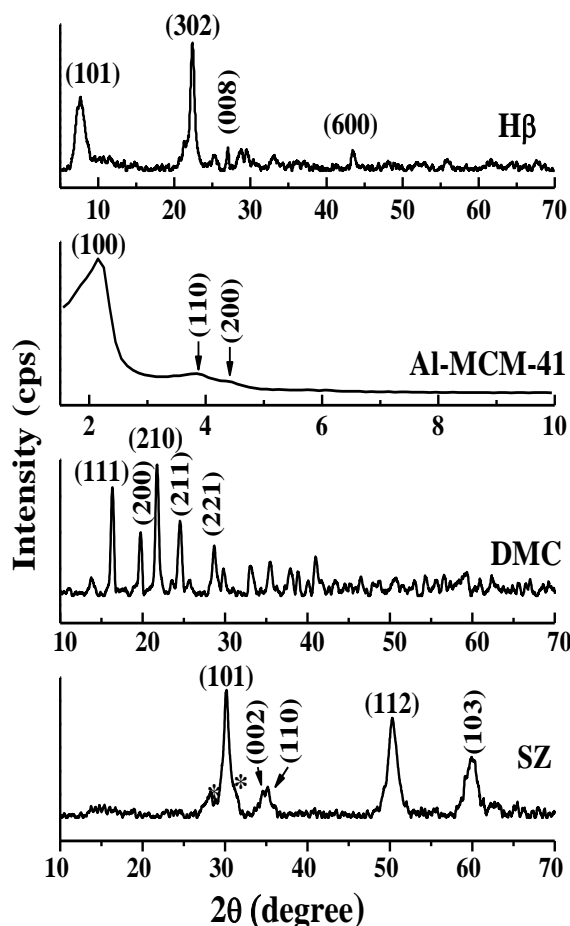
Fig. 4.1. *XRD patterns of Hβ, Al-MCM-41, DMC and SZ*

4.3.1.1. XRD

Table 4.1 lists the structural, textural and acidic properties of DMC, Hβ, Al-MCM-41 and SZ catalysts. DMC showed sharp characteristic XRD peaks at 2θ (hkl) values of 16.9° (111), 20.1° (200), 22.3° (210), 24.8° (211), and 29.1° (221) exhibiting a cubic symmetry (Fig. 4.1) [21]. The peaks of SZ were broader and corresponded mainly to a tetragonal phase (JCPDS No. 79-1768). Co-existence of a small amount of monoclinic phase of SZ (denoted by asterisks) along with the tetragonal phase was also be inferred. Al-MCM-41 showed low-angle XRD peaks

Table 4.1. Structural, textural and acidic properties

Catalyst	XRD			N_2 adsorption – desorption					microscopy		acidic properties		Na^+ ion exchange capacity $(mmol/g)^c$
	Crystal lattice	Crystallite size (nm)	Unit cell parameter (nm)	S_{BET} (m^2/g)	Average pore diameter (nm)	Pore volume (cc/g)	Surface area - external (m^2/g)	Micro pore surface area (m^2/g)	Particle size - SEM (μm)	Pore size- TEM (nm)	NH_3 TPD (mmol/ $g)^a$	Pyridine-IR (Lewis/ Brönsted)^b	
DMC	Cubic	18.9	a = 0.915	54	2.5	0.01	14	40	1.4	2.1	0.84	No B sites	-
SZ	Tetragonal	10.8	a = 0.362 c = 0.511	136	4.1	0.14	117	19	1.8	5.4	0.48	2.1	0.26
Al-MCM-41 (Si/Al = 48)	Hexagonal	5.7	a = 4.899	642	3.6	0.58	555	86	1.0	-	0.24	1.9	0.07
Hβ (Si/Al = 14)	-	14.0	-	577	1.2	0.39	169	408	0.7	-	0.68	8.6	-

^{a}Total acidity due to both Lewis and Brönsted acid sites. ^{b}Molar extinction coefficients for Lewis (1455 cm^{-1}) & Brönsted (1545 cm^{-1}) peaks were considered as 2.22 and 1.67 cm^{-1}. µmol^{-1}, respectively. ^{c}Na$^+$ exchange capacity in the case of Al-MCM-41 corresponds to concentration of framework substituted Al^{3+} ions and the corresponding Brönsted sites generated. For SZ, this value estimated by the titration method, is higher than expected from TPD and pyridine-IR but lower than the total sulfate content in SZ (0.42 mmol/g).

characteristic of a hexagonal structure and long-range mesoporous ordering. Hβ is highly crystalline and its XRD pattern was composed of sharp and broad (or diffused) reflections suggesting that structural disorder pervades the framework. It is known that there are three ordered poly-types (A, B and C) present in the structure of Hβ [24]. The sharp reflections can be indexed based on a tetragonal lattice ($P4_122$) and two different monoclinic lattices (C2/c and P2) which correspond to the A, B and C polytypes, respectively. The sample used in this study contains all these three polytypes. The average crystallite size of the catalysts estimated using the Scherrer equation decreased in the order: DMC (18.7 nm) > Hβ (14 nm) > SZ (11.8 nm) > Al-MCM-41 (5.7 nm). Unit cell parameter of DMC (cubic system) was found to be a = 0.915 nm. Al-MCM-41 (hexagonal system) has a cell parameter of 4.899 nm and SZ (tetragonal phase) has unit cell parameters of a = 0.362 nm and c = 0.511 nm (Table 4.1).
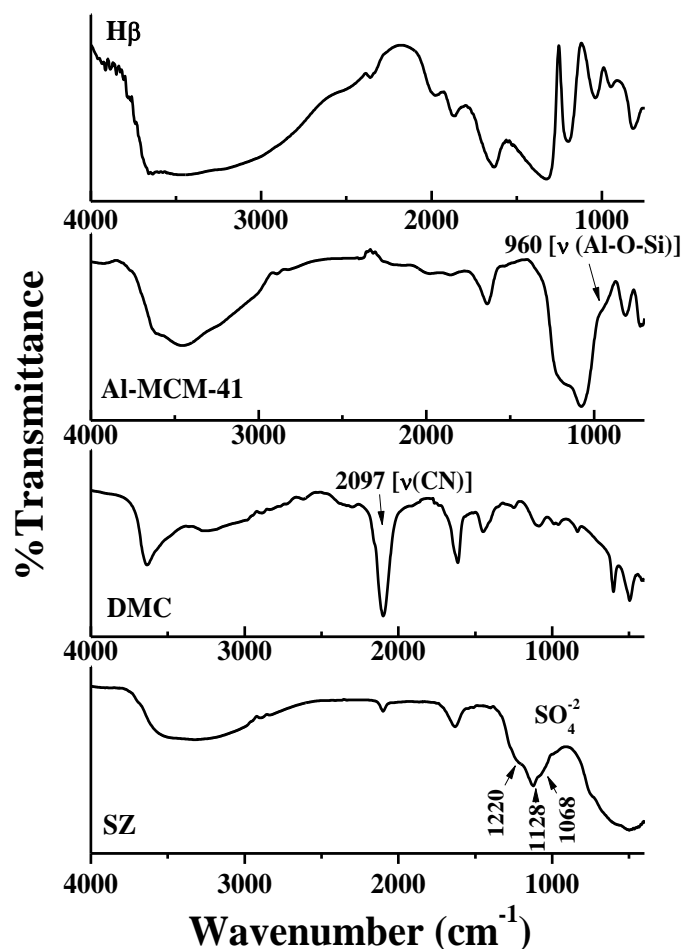
Fig 4.2. *FTIR spectra of Hβ, Al-MCM-41, DMC and SZ*

4.3.1.2. FTIR

DMC showed a characteristic band at 2097 cm^{-1} in the FTIR spectrum confirming the presence of bridging (Fe^{2+}-Zn^{2+}) cyanide groups [21]. SZ exhibited FT-IR bands at 1220, 1128 and 1068 cm^{-1} due to the presence of chelating, bidentate-type sulfate groups coordinated to Zr^{4+} cations. While the broad peak at 3500 cm^{-1} could be assigned to hydroxyl groups, that at 1638 cm^{-1} is due to adsorbed water molecules [25, 26]. Al-MCM-41 and Hβ showed a typical IR band at 950-960 cm^{-1} due to Al-O-Si vibration (Fig. 4.2).

4.3.1.3. Diffuse Reflectance UV-Visible

Three characteristic overlapping bands at 240, 265 and 310 nm were observed in the diffuse reflectance UV-visible spectrum of DMC (Fig. 4.3). While the former is attributed to π-π* charge transfer transitions in the cyanide group, the latter two bands are due to bridging CN^{-}-to-Fe^{2+} charge transfer (LMCT) transitions. Fe is in a $^{1}A_{1g}$ (low-spin) ground state as confirmed by the absence of any band in the visible region [21]. SZ depicted an intense band at 215 nm with a shoulder at 230 nm. While the band at 215 nm is due to O^{2-} to Zr^{4+} charge transfer transition, the shoulder band is assigned to Zr-O-Zr linkages [25].
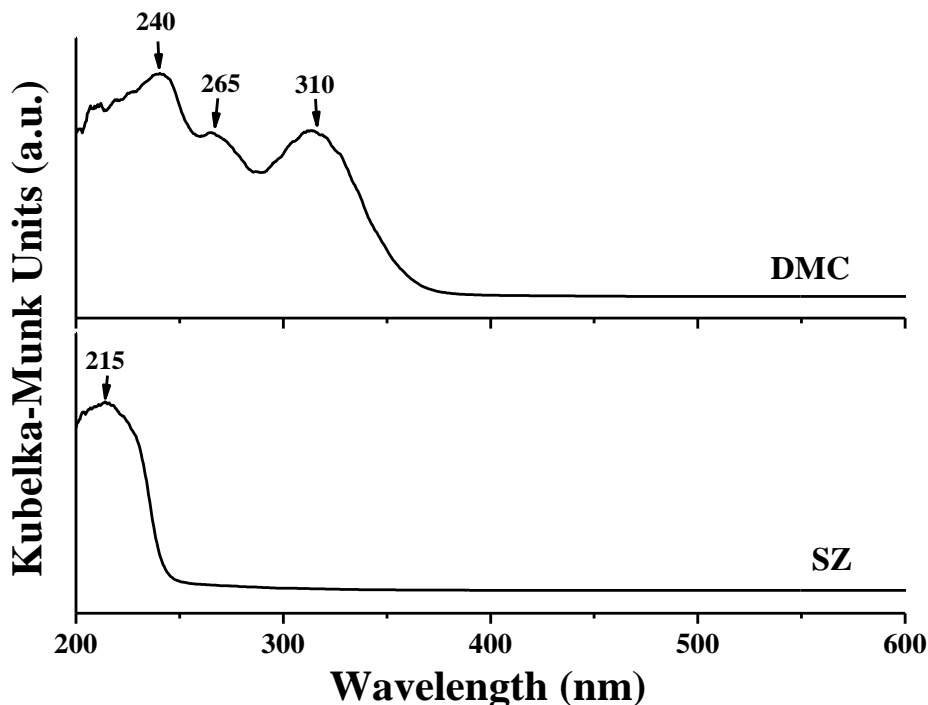
Fig. 4.3. *DRUV-visible spectra of DMC and SZ*
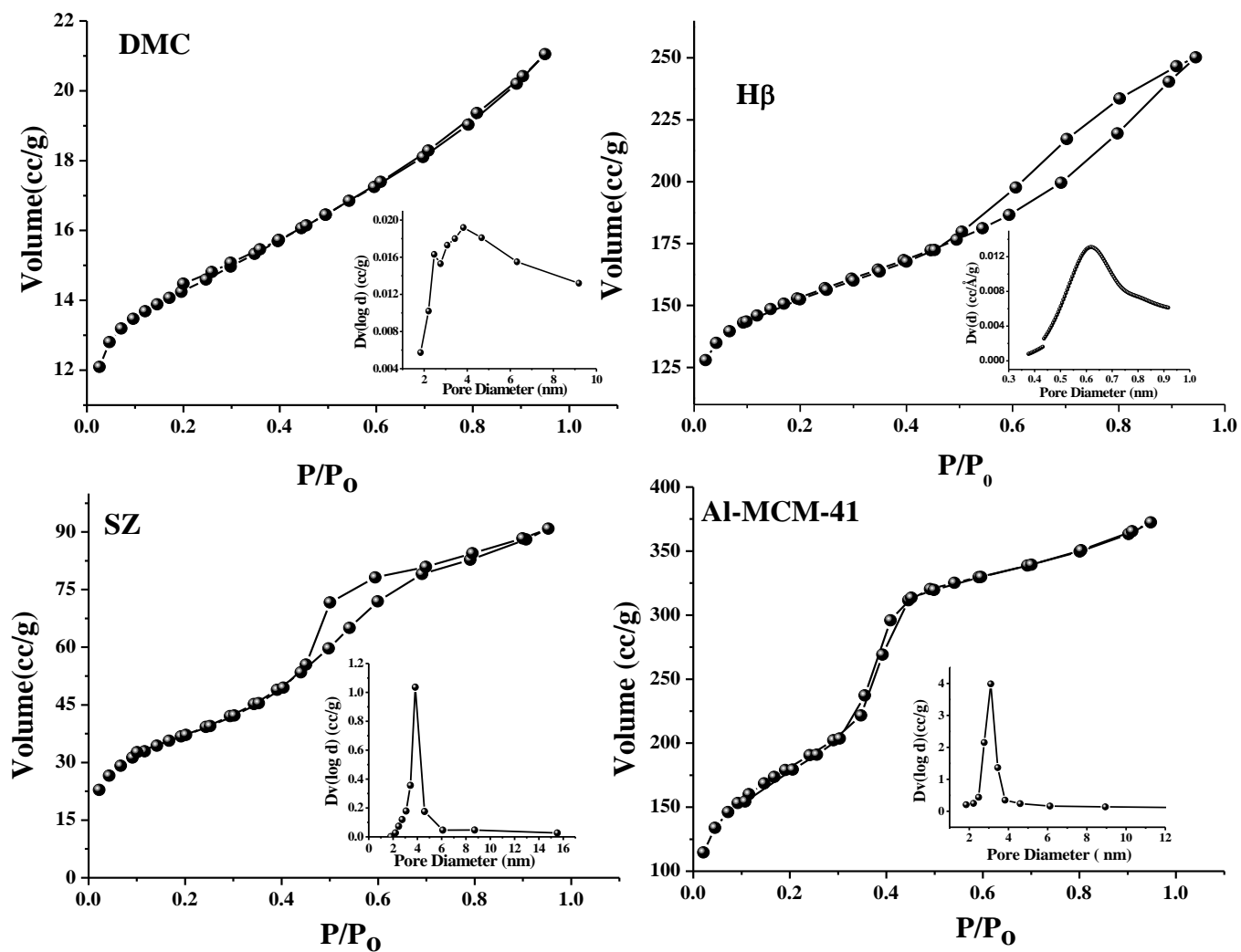
Fig. 4.4. *N_2 adsorption-desorption isotherms and pore size distribution curves of, DMC, Hβ, SZ and Al-MCM-41*
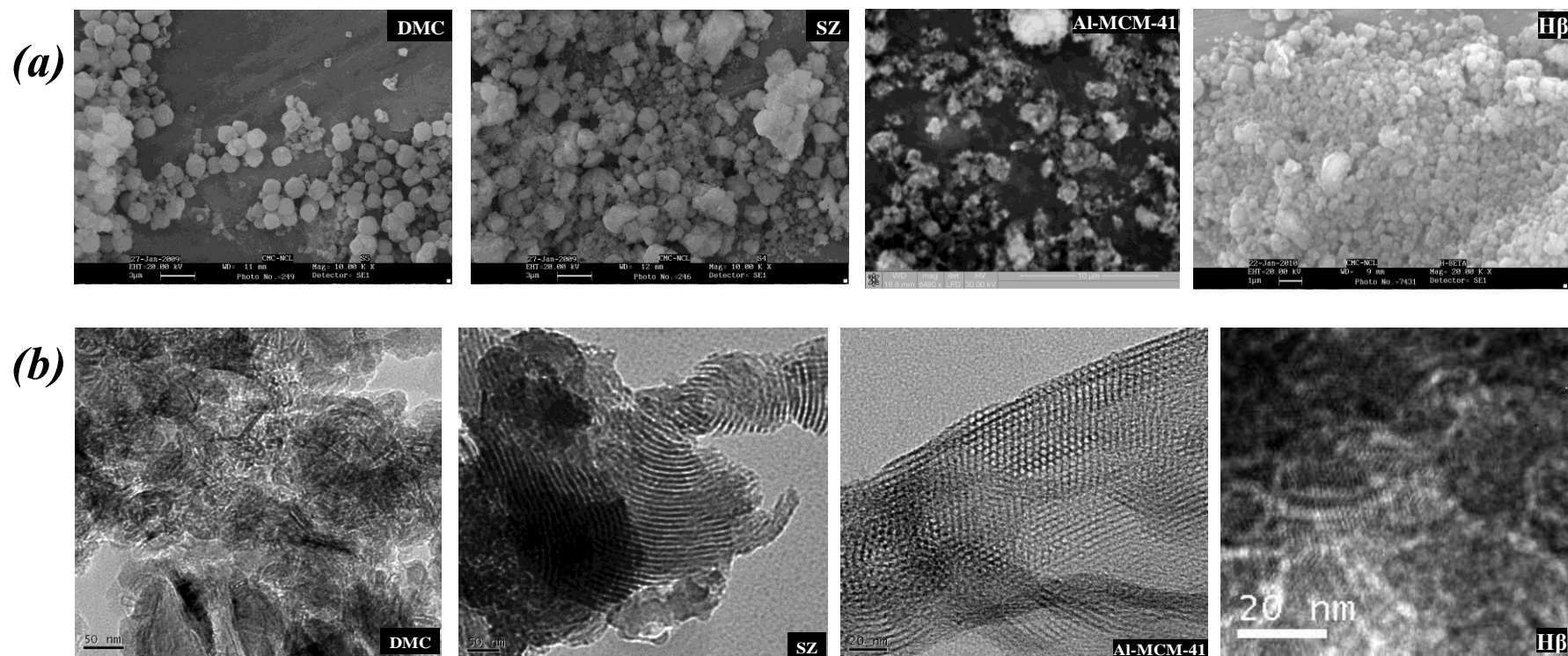
Fig. 4.5. *(a) Scanning electron microscopic (SEM) and (b) high resolution transmission electron microscopic (HRTEM) images of DMC, SZ, Al-MCM-41 and Hβ*

4.3.1.4. N$_2$ Adsorption-Desorption, SEM and HRTEM

Nitrogen adsorption-desorption isotherms revealed that SZ and Al-MCM-41 are mesoporous. The isotherms were typical of type IV nature (IUPAC) with H$_1$-type hysterisis loops (Fig. 4.4). The sharp steps of capillary condensation of N$_2$ were observed at a relative pressure (P/P$_0$) of 0.5 to 0.7 in the isotherms of SZ and at 0.3 to 0.5 for Al-MCM-41. DMC is mostly microporous as can be concluded based on the micropores area which is 74% of the total specific surface area (Table 4.1). As the average pore diameter is 2.5 nm, the presence of some mesoporosity in DMC structure can be inferred. The isotherms of Hβ are typical of a microporous material (average pore diameter = 1.2 nm). The surface area, average pore diameter and pore volume of SZ and Al-MCM-41 are larger than that of DMC (Table 4.1). Al-MCM-41 has a specific surface 642 m^2/g which is lower than that usually observed for all siliceous MCM-41 materials (~1000 m^2/g). However, such values for Al-MCM-41 have been reported by several researchers [27]. HRTEM images (Fig. 4.5), in agreement with the N$_2$ adsorption-desorption results, have also confirmed the presence of mesopores. However, the ordering of the pores is more regular in SZ and Al-MCM-41 than in DMC. The DMC (average particle size = 1.4 μm) and Hβ (average particle size = 0.7 μm) catalysts have a spherical shape. No regular shape was observed for SZ (average particle size = 1.2 μm) and Al-MCM-41 (average particle size = 1 μm) in SEM analysis (Fig. 4.5).

4.3.2. Acidic Properties of Catalysts

Pyridine and ammonia were used as probe molecules. DRIFT spectroscopy of adsorbed pyridine on DMC revealed the presence of Lewis acid (L) sites (Fig. 4.6). The IR peaks at 1613 and 1451 cm^{-1} are due to strong Lewis acid sites and those at 1443 cm^{-1} are due to weak Lewis sites (Fig. 4.6). The concentration of the former is higher (by 3.6 times) than that of the latter. Hβ, SZ and Al-MCM-41 contained both Lewis (IR peaks: 1607, 1596 and 1443 cm^{-1}) and Brönsted acid (B) sites (IR peaks: 1639 and 1542 cm^{-1}) [26]. The latter are not present in DMC. The peak at 1488 cm^{-1} has been attributed in the past to both Brönsted and Lewis acid sites [26]. Based on the area of IR peaks at 1542 (for B sites) and 1443 cm^{-1} (for L sites) and molar extinction coefficients reported by Emeis [28], the compositions of B and L-sites in SZ and Al-MCM-41 were estimated to be 21 - 24 and 76 -79%, respectively of the

total acid sites measured by IR of pyridine. The ratio of L/B was estimated to be 8.4 1.9 and 2.1 for Hβ, Al-MCM-41 and SZ, respectively.
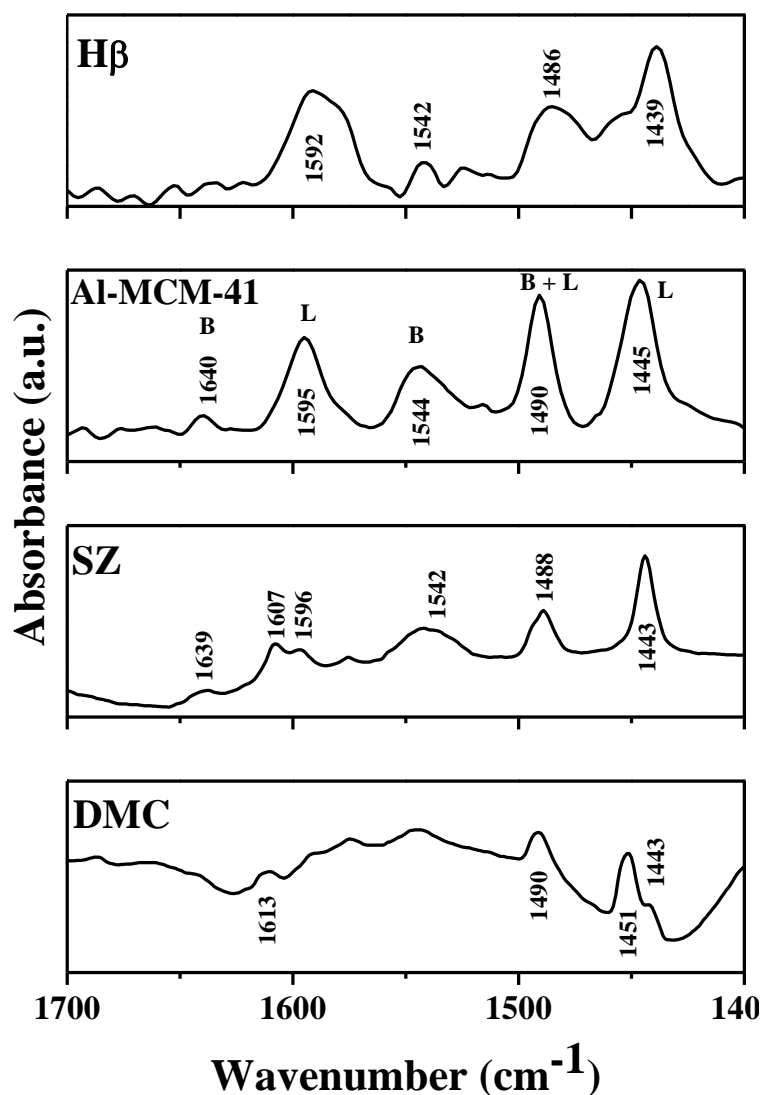
Fig. 4.6. *FTIR spectra of pyridine adsorbed Hβ, Al-MCM-41, SZ and DMC*

NH$_3$-TPD of DMC showed broad, asymmetric peaks at 400 and 453 K (Fig. 4.7). While the former is attributed to physisorbed NH$_3$, the latter corresponds to NH$_3$ desorbed from Lewis acid sites [21]. SZ showed a broader distribution of acidity [25]. While the peak at 485 K is due to NH$_3$ desorbed from Lewis acid sites, the broad desorption in the region 600 – 850 K, present only in SZ but not in DMC, is attributed to stronger Brönsted acid sites (Fig.4.7). Hβ and Al-MCM-41 also showed desorption peaks similar to those of SZ at 555 K and 476 K, respectively (Lewis acid sites) and at 600 – 900 K for Brönsted acid sites. Although the total amount of NH$_3$ desorbed from DMC (0.84 mmol/g) was found higher than Hβ (0.68 mmol/g), SZ

(0.48 mmol/g) and Al-MCM-41 (0.24 mmol/g), the latter two catalysts contained relatively stronger (Brönsted) acid sites than the former. SZ has a higher ion exchange (Na^+) capacity (0.26 mmol/g) than Al-MCM-41 (0.07 mmol/g). The sulfate content in SZ was estimated to be 0.42 mmol/g (sulfur analysis). These values agree well with those reported by others [25, 29, 30]. Na^+ exchange capacity in the case of Al-MCM-41 corresponds to a concentration of framework-substituted Al^{3+} ions and the corresponding Brönsted sites generated. For SZ, the ion exchange capacity estimated by the titration method is higher than expected from TPD and pyridine-IR but lower than the total sulfate content in SZ (0.42 mmol/g).
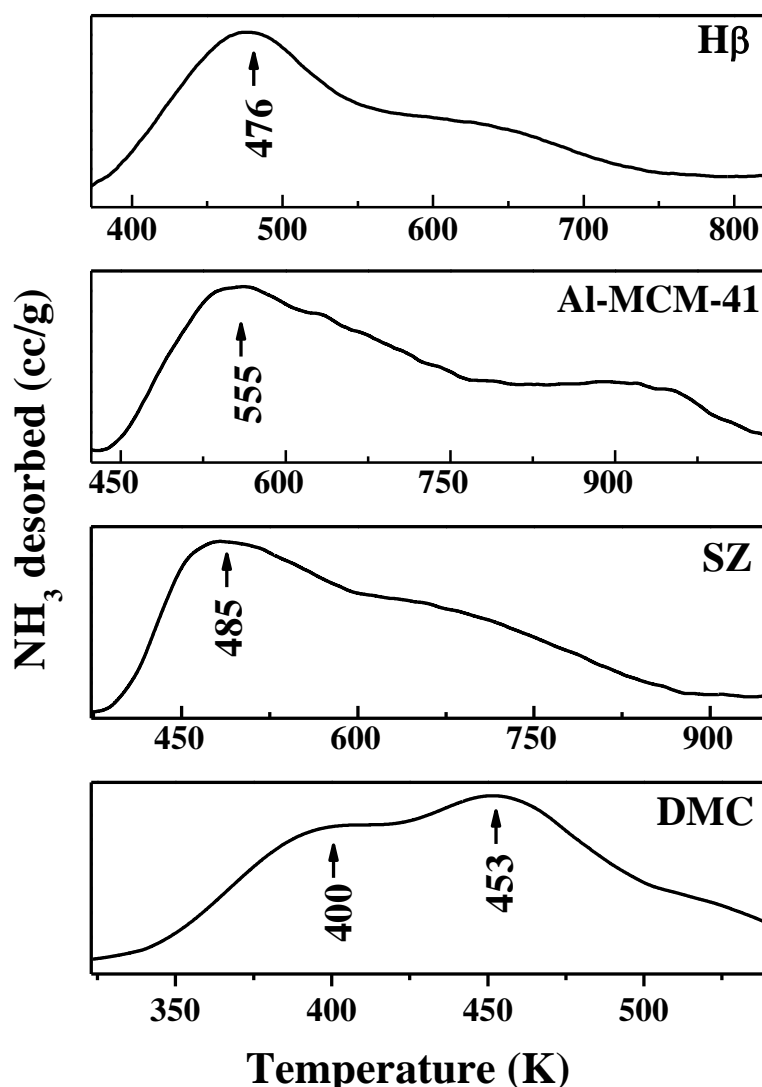
Fig. 4.7. *NH₃-TPD profile of Hβ, Al-MCM-41, SZ, and DMC*

4.3.3. Adsorption Studies

In esterification over solid catalysts, water, a co-product, limits the conversion not only due to equilibrium considerations but also by strongly adsorbing on the active, catalytic sites [31]. Adsorption of H_2O will depend on the hydrophilicity of the catalyst surface. On highly hydrophilic zeolite BEA, for example, Schildhauer *et al*. [31] found that the adsorption of H_2O was 35 times higher than that of 1-octanol while the adsorption of hexanoic acid and ester were negligible. In esterification, due to the different polarity and dielectric constant values of methanol and water, the strength of their interaction with the active (acidic) sites will vary. Water, with its higher dielectric constant, can successfully compete with methanol, for adsorption on the acid sites [31]. To probe this further, competitive adsorption of methanol in the presence of water over DMC, SZ and Al-MCM-41 catalysts was investigated. Adsorption of methanol in the presence of water was found to be 10 times higher on DMC than on SZ and Al-MCM-41 (Table 4.2). The relative adsorption of methanol with respect to water (defined as the hydrophobicity index) increased in the order: Al-MCM-41 (0.4) < SZ (0.6) < DMC (1.2) (Table 4.2). Water therefore, competes with methanol for adsorption on the active sites and, in the process, lowers the concentration of methanol on the catalyst surface. This effect is more in the case of Al-MCM-41 and SZ than in DMC. Adsorption of oleic acid in the presence of methanol, n-octanol and decane over different catalysts increased in the same order as their hydrophobicity index. The surface acidity of the catalysts estimated by NH_3-TPD and FTIR of adsorbed pyridine techniques also varied in the same order (Al-MCM-41 < SZ < DMC) (Tables 4.1 & 4.2, Fig. 4.8). NH_3 and pyridine (molecules having lower polarity and dielectric constant than water) are expected to adsorb preferentially on more hydrophobic surfaces like DMC than on SZ and Al-MCM-41. As seen from Fig. 4.8, pyridine adsorption levels off beyond a certain hydrophobicity index while that of NH_3 still increases. This could be due to two reasons: (1) steric effects – pyridine is bulkier than NH_3. DMC has smaller pore diameter than SZ and Al-MCM-41, and (2) polarity of adsorbing molecules – pyridine is more polar than ammonia and hence, its adsorption would be lower and levels off beyond a certain hydrophobicity index. From curve (c) in Fig. 4.8, it can be inferred that on hydrophilic and hydroxylic surfaces like Al-MCM-41 and SZ, methanol may not be an effective esterification reagent if water is also present. The superior catalytic activity of DMC in the esterification reactions is probably due to the greater surface

Table 4.2. Competitive adsorption of reactants and products on solid catalysts

Catalyst	Water – Methanol		Fatty acid – alcohol or decane adsorption ($\mu mol/m^2$)					
	Methanol adsorbed ($mmol/m^2$)[a]	Hydrophobicity index : Ratio of (CH_3OH/ H_2O) adsorbed	Oleic acid ($C_{18.1}$) adsorbed in presence of			Octanoic acid ($C_{8.0}$) adsorbed in presence of		
			Methanol[b]	Octanol[c]	Decane[c]	Methanol[b]	Octanol[c]	Decane[c]
DMC	1.55	1.22	0.76	1.3	8.0	-1.0	2.7	12.9
SZ	0.15	0.59	0.67	1.1	5.4	1.1	0.7	7.7
Al-MCM-41	0.13	0.42	0	0.05	1.3	0	0.02	1.7

[a]0.1 g of the catalyst was dispersed in a solution containing 2.5 g each of H_2O and CH_3OH (298 K, 1 h), the catalyst was separated and the amount of methanol adsorbed was estimated by gas chromatography and thermogravimetric analysis. [b]1 g of catalyst was dispersed in 5 mL of fatty acid – methanol solution (fatty acid : methanol molar ratio = 1 : 10; 298 K, 0.5 h), the catalyst was separated and the fatty acid content in the liquid portion was estimated by titration with 0.1 N NaOH solution. [c]0.1 g of catalyst was dispersed in 5 mL of 0.1 M solution of fatty acid in octanol or decane (298 K, 0.5 h), the catalyst was separated and the fatty acid content in the liquid portion was estimated by titration with 0.01 N NaOH solution.

coverage of methanol and the relatively more hydrophobic (compared to water) fatty acid molecules. The leveling off of oleic acid (but not octanoic acid) is again a steric effect in the narrower pores of DMC. DMC contains both meso and micropores. While NH_3 and octanoic acid may adsorb in both easily, pyridine and oleic acid probably adsorb only in the mesopores; hence, this leveling off in the case of oleic acid and pyridine adsorptions over DMC (Fig. 4.8).
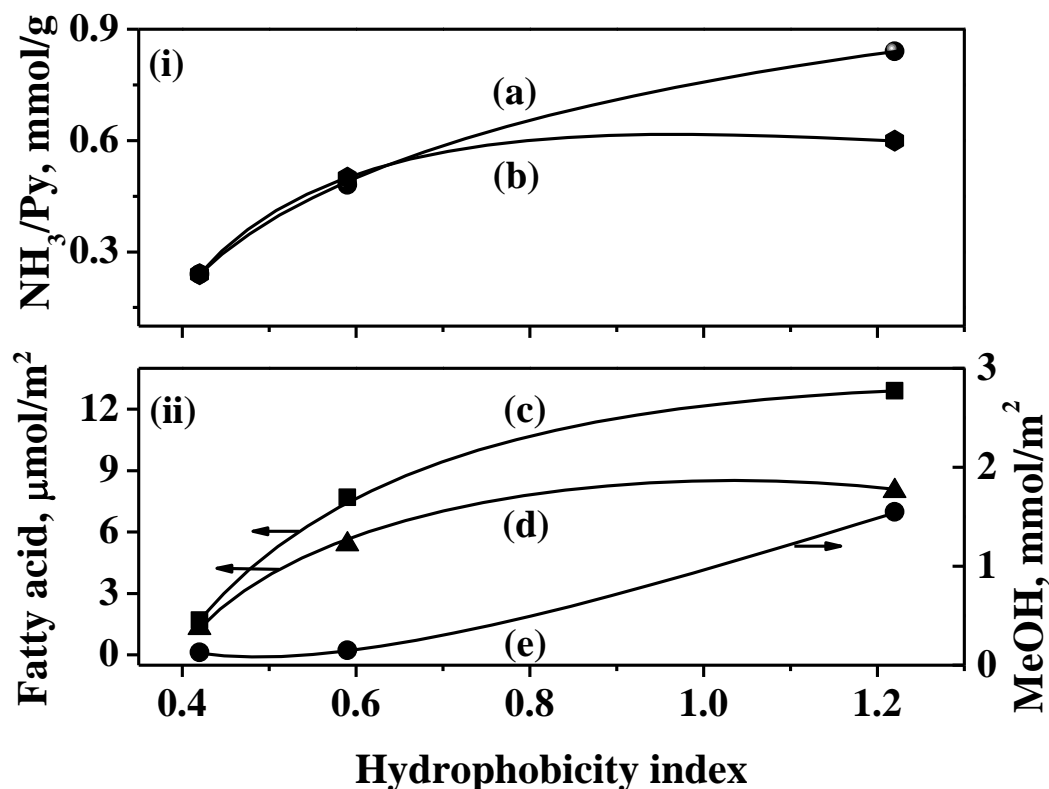
Fig. 4.8. *Plot of hydrophobicity index vs (i) total acidity [estimated from (a) NH_3 desorbed and (b) pyridine (Py) adsorbed] and (ii) adsorption of reactants [(c) octanoic acid in presence of decane, (d) oleic acid in presence of decane and (e) methanol in presence of water]*

The hydrophobicity of different catalysts used in this study was also confirmed from a different experiment wherein 25 mg of activated catalyst powder was suspended in water-toluene and water-CCl$_4$ (1 : 1 v/v) mixtures. These solvent mixtures are immiscible and form two separate layers; in one case with toluene being the top layer and water being the bottom layer and in the other case water being the top layer and CCl$_4$ being the bottom layer. DMC remains suspended in the organic, non-polar toluene and CCl$_4$ layers while SZ and Al-MCM-41 prefer to remain in the

water layer in the both the solvent mixtures (Fig. 4.9) confirming the higher hydrophobicity of DMC compared to SZ, Al-MCM-41 and Hβ.
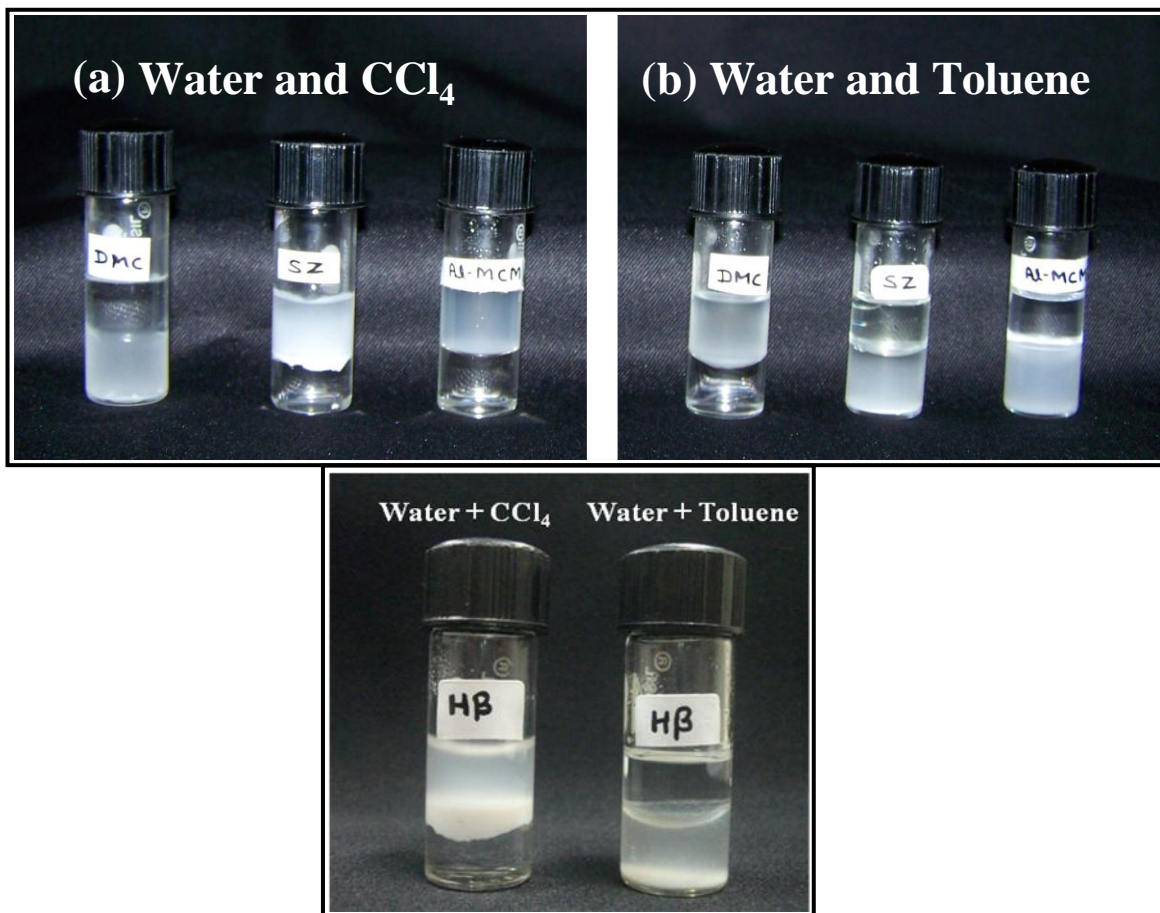
Fig. 4.9. *Preferential dispersion of DMC in non-polar, organic and SZ , Al-MCM-41 and Hβ in polar aqueous phases : (a) water-CCl$_4$ and (b) water-toluene mixtures*

4.4. Esterification of Fatty Acids of Varying Chain Length with Methanol

DMC, Hβ, SZ and Al-MCM-41 are known to be active catalysts for esterification reactions [20, 21, 29, 30]. In the present study, the relative catalytic performance of hydrophobic DMC and hydrophilic Hβ, SZ and Al-MCM-41 for the esterification of fatty acids of varying chain length (octanoic acid − C$_{8.0}$, decanoic acid − C$_{10.0}$, dodecanoic acid − C$_{12.0}$, palmitic acid − C$_{16.0}$, oleic acid − C$_{18.1}$) with methanol is reported for the first time. The reactions were conducted with fatty acid to methanol molar ratios of 1 : 1 to 1 : 20 (Fig. 4.10). Beyond a molar ratio of 1 : 5, no significant increase in the catalytic activity was detected. Dimethyl ether was not detected in the products under our reaction conditions.
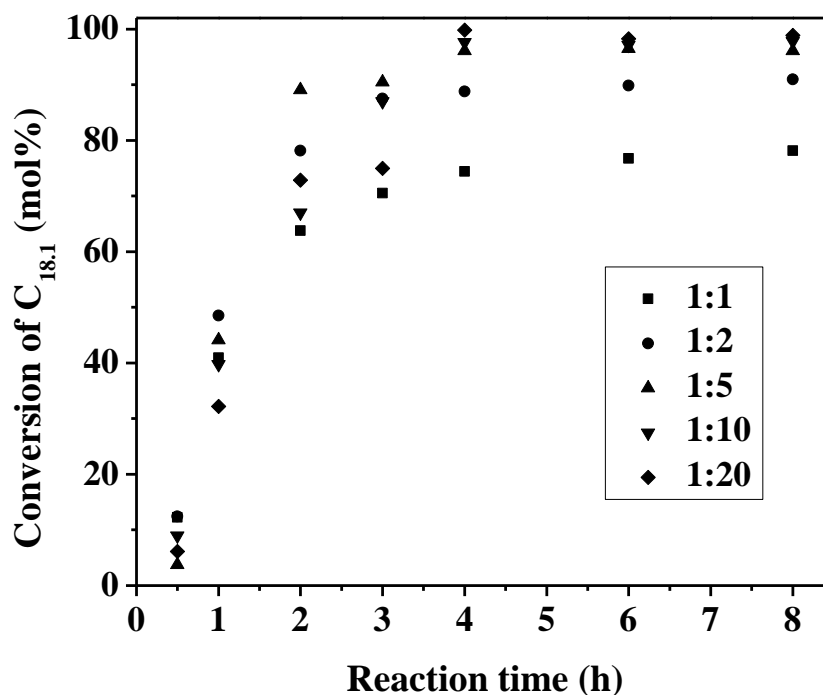
Fig. 4.10. *Effect of oleic acid to methanol molar ratio on the esterification reaction over DMC. Reaction conditions: catalyst (0.15 g), oleic acid (5 g), reaction temperature (443 K)*

In kinetic studies, methanol was taken in excess (10 times) to that of fatty acid so that the reaction follows a pseudo-first-order rate equation. The reaction is faster over Hβ, SZ and Al-MCM-41 than on DMC. While a conversion of about 95% of $C_{18.1}$ was achieved at 443 K in 4 - 5 h over DMC, a similar conversion was obtained at 393 K itself, in 3 - 4 h, over SZ (Fig. 4.11). For each fatty acid ($C_{8.0}$ - $C_{18.1}$), the reactions were conducted at four different temperatures over DMC (423, 433, 443 and 453 K), Hβ (363, 373, 383 and 393 K), SZ (353, 363, 373, 383 and 393 K) and Al-MCM-41 (393, 403, 413 and 423 K) catalysts. From the conversion vs time plots, the initial rates were determined. These were then used to calculate rate constants (k) using the pseudo-first order rate law. Employing the Arrhenius equation, activation energy (E_a) values were also determined (Table 4.3). These values are well within the range reported for other solid acid catalysts (Table 4.4). The rate constants for the esterification reaction are also comparable with those reported by Peters et al [35] for various commercial solid acid catalysts. Fig. 4.12 presents representative conversion vs time plots (left) and Arrhenius plot (right) for esterification of $C_{12.0}$ with methanol over DMC. The following conclusions can be drawn from Table 4.3.
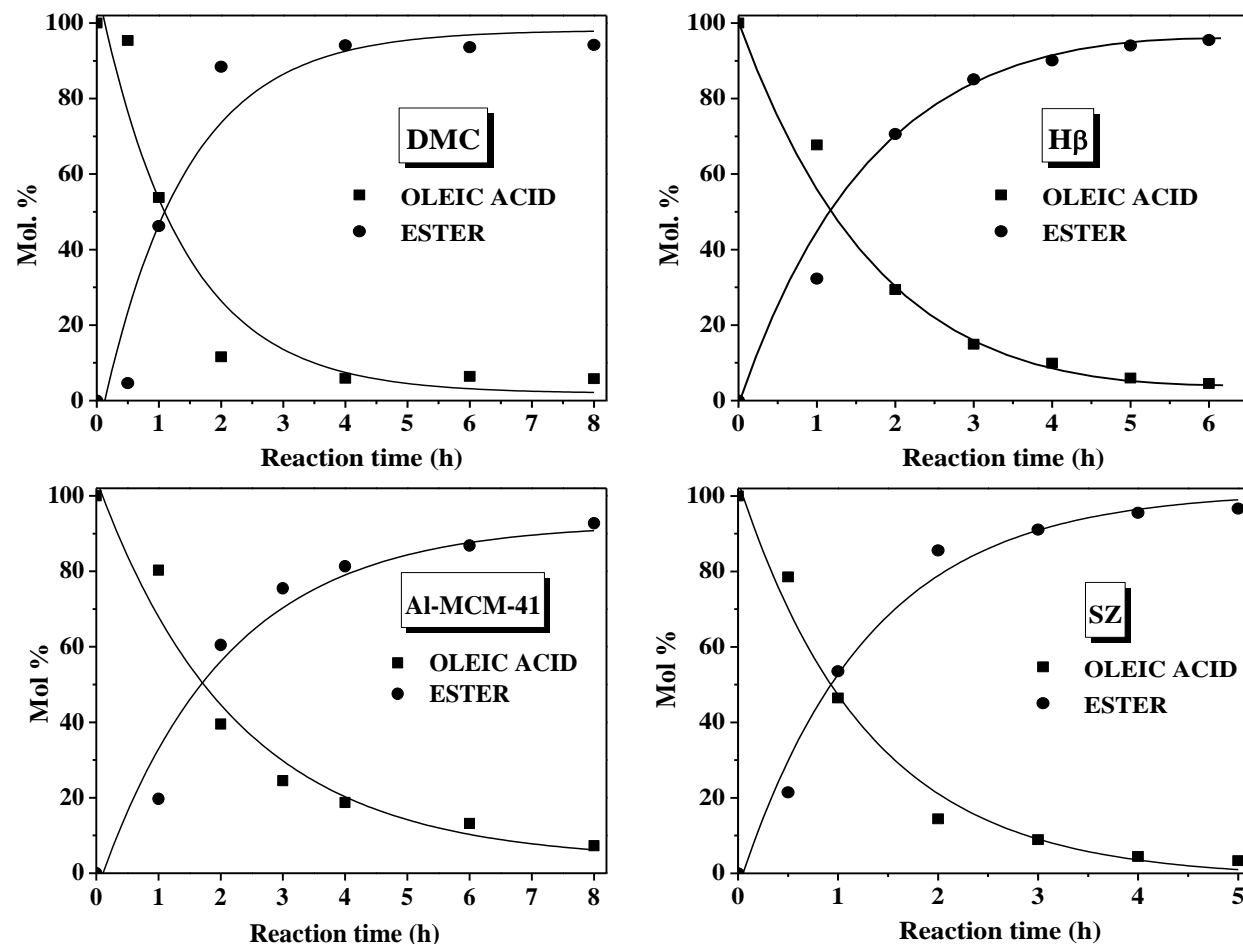
Fig. 4.11. *Esterification of oleic acid with methanol over DMC, Hβ, Al-MCM-41 and SZ catalysts, Reaction conditions: catalyst (0.15 g), oleic acid (5 g), oleic acid : methanol molar ratio = 1 : 10, reaction temperature (DMC - 443 K, Al-MCM-41 – 423 K, SZ – 393 K, Hβ – 423K)*
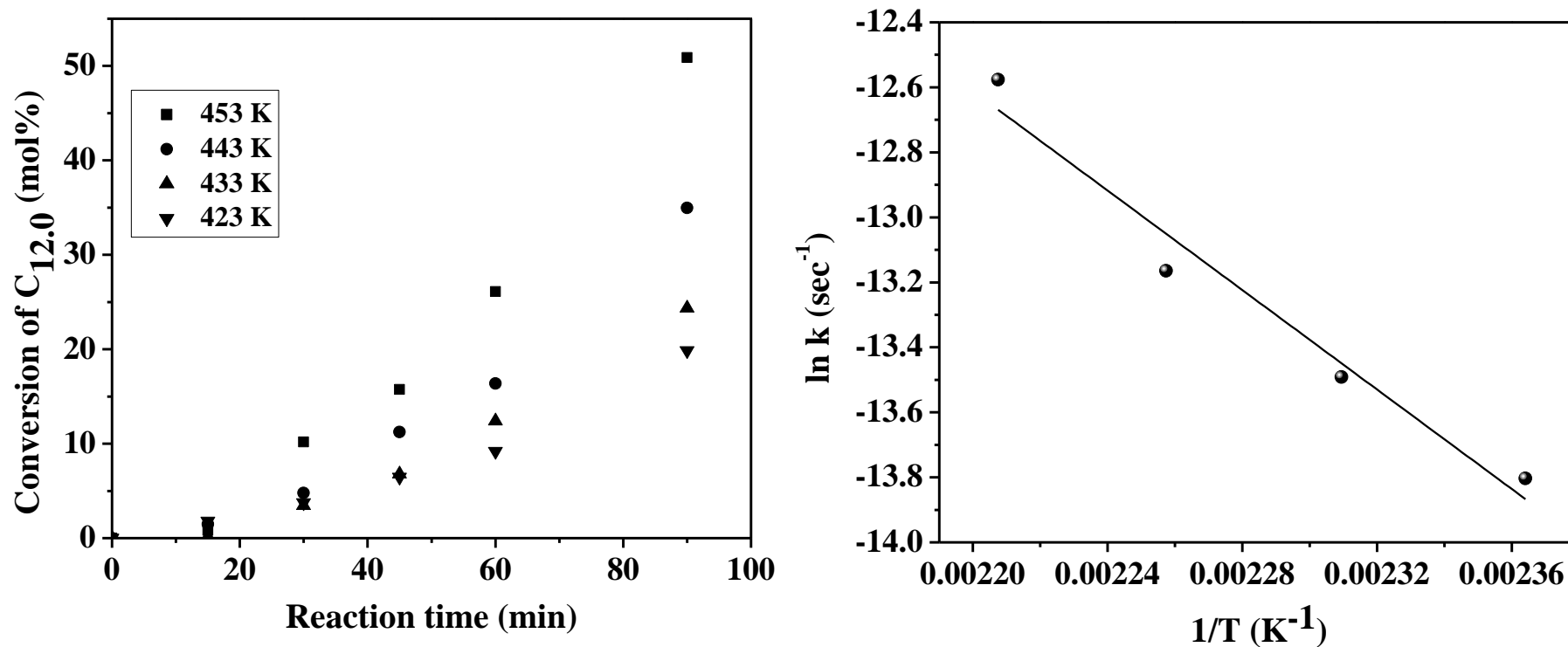
Fig. 4.12. Left: Conversion - time plots at different temperatures. Right: Arrhenius plot for the methanolysis of dodecanoic acid over DMC. Reaction conditions: DMC (0.15 g), dodecanoic acid (0.0177 mol), acid : methanol molar ratio = 1 : 10

Table 4.3. Kinetic parameters for the esterification of fatty acids

fatty acid	DMC T (K)	k (x 10^{-7})	TOF (x 10^{-3})	E_a	Hβ T (K)	k (x 10^{-8})	TOF (x 10^{-3})	E_a	Al-MCM-41 T (K)	k (x 10^{-8})	TOF (x 10^{-3})	E_a	SZ T (K)	k (x10^{-7})	TOF (x10^{-3})	E_a
$C_{8.0}$	423	-	--		363	1.0	3.2		393	1.9	6.9		353	4.9	35.9	
	433	1.4	4.0		373	1.4	6.4	24.7	403	3.3	8.3	24.1	363	8.9	38.8	5.4
	443	2.1	5.9	90.9	383	2.4	8.4		413	4.3	16.0		373	9.2	45.8	
	453	2.4	6.9		393	-	-		423	4.7	12.2		383	9.8	44.7	
$C_{10.0}$	423	1.1	5.1		363	0.9	4.7		393	1.9	11.1		353	3.6	23.8	
	433	2.6	8.5		373	1.0	4.9	26.9	403	3.1	19.7	29.4	363	3.9	27.0	18.2
	443	4.8	15.9	78.6	383	1.4	8.4		413	4.1	19.7		373	5.1	33.9	
	453	6.8	10.5		393	2.2	-		423	-	21.3		383	6.7	44.3	
$C_{12.0}$	423	1.3	3.6		363	2.2	5.4		403	3.5	18.3		353	5.1	41.1	
	433	11.8	4.8		373	3.5	7.8	34.7	413	4.9	29.9	25.3	363	-	26.7	16.7
	443	2.4	6.5	63.6	383	3.9	9.4		423	-	29.1		373	6.7	43.7	
	453	4.4	10.1		393	5.6	-		433	6.0	39.1		383	7.4	44.4	
$C_{16.0}$	423	2.9	7.9		373	2.1	5.2		403	6.3	27.8		363	4.7	25.5	
	433	3.8	8.4		383	3.7	9.1	46.0	413	6.2	36.3	37.9	373	5.7	30.7	24.2
	443	4.0	7.4	52.8	393	4.7	-		423	6.8	49.9		383	6.6	32.0	
	453	7.7	13.3		403	6.5	-		433	10.4	44.2		393	8.8	48.0	
$C_{18.1}$	423	1.7	3.8		363	1.0	2.1		403	4.2	18.3		373	4.6	28.4	
	433	1.7	4.1		373	1.6	3.3	54.7	413	6.2	20.2	38.9	383	5.5	31.2	24.4
	443	3.2	6.7	52.8	383	1.6	4.2		423	6.9	26.9		393	6.4	36.5	
	453	4.6	9.9		393	3.9	9.4		433	9.9	43.2		403	8.4	44.3	

Rate constant (k) is reported as $L.mol^{-1}.s^{-1}.m^{-2}$ and activation energy (E_a) as $KJ.mol^{-1}$. Turnover frequency (TOF, s^{-1}) = moles of fatty acid converted per mol of acid sites on the catalyst per sec.
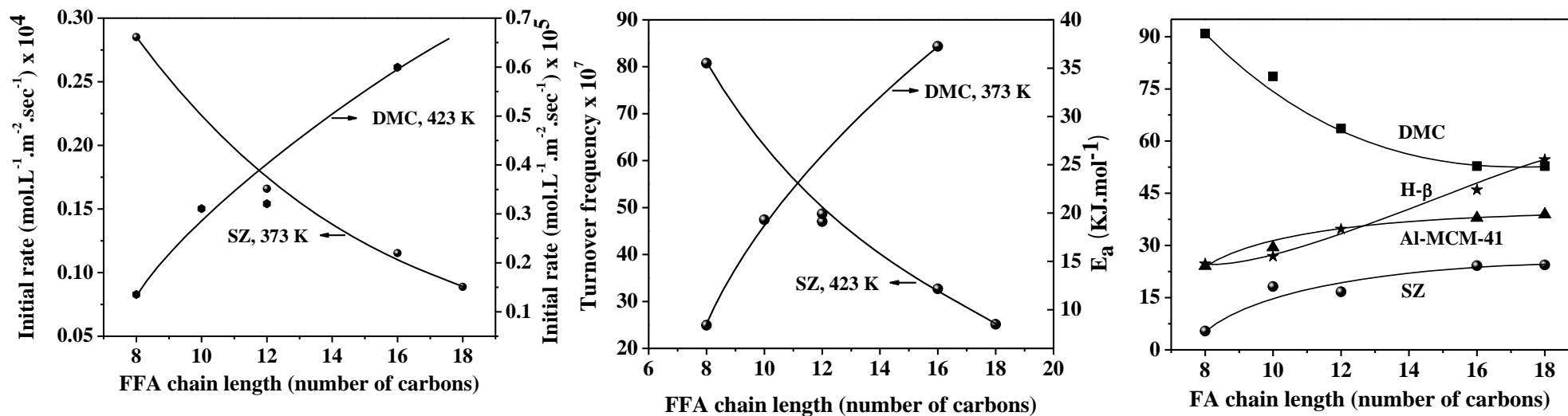
Fig. 4.13. *Influence of chain length of fatty acid on the initial rate (left), turnover number (middle) and activation energy (E_a right) for the esterification reactions over DMC, Hβ, SZ and Al-MCM-41 catalysts*

Table 4.4. Activation energy (E_a) for esterification of fatty acids with methanol over different acid catalysts

catalyst	fatty acid	E_a (kJ/mol)	reference
Nafion	palmitic acid ($C_{16.0}$)	60 ± 9	(18)
HMS-SO$_3$H-C12	palmitic acid ($C_{16.0}$)	75 ± 10	(18)
SBA-15-SO$_3$H-L64	palmitic acid ($C_{16.0}$)	55 ± 5	(18)
SBA-15-SO$_3$H-P123	palmitic acid ($C_{16.0}$)	40 ± 1	(18)
acidic ion exchange polymeric resin (Relite CFS by Resindion)	oleic acid ($C_{18.1}$)	58.8	(32)
Amberlyst-15	oleic acid ($C_{18.1}$)	74.4	(33)
sulfuric acid	palm fatty acids	27.3	(34)
Methanesulfonic acid	palm fatty acids	15.8	(34)

(a) The turnover frequency (TOF) is higher over SZ and Al-MCM-41 than on DMC and Hβ.

(b) The rate of esterification (k) per unit surface area of the catalyst is higher over SZ than on DMC and Hβ.

(c) The apparent activation energy (E_a) for esterification is lower for SZ and Al-MCM-41 than for DMC. For Hβ, for lower fatty acids ($C_{8.0}$), E_a is lower than DMC and comparable to Al-MCM-41 but for higher fatty acids ($C_{18.0}$), E_a is comparable to DMC but higher than Al-MCM-41.

(d) Over DMC, the apparent activation energy (E_a) decreases with increasing chain length of fatty acid. A reverse trend, however, is observed over Hβ, SZ and Al-MCM-41 (Fig. 4.13).

(e) Activation energy values for shorter chain length fatty acids ($C_{8.0}$ and $C_{10.0}$) are nearly the same over Hβ and Al-MCM-41. However, the difference increased with increase in the chain length of FA.

4.5. Esterification of Oleic Acid with Alcohol of Varying Chain Length

Oleic acid was esterified with methanol (C_1), ethanol (C_2), n-propanol (C_3), n-butanol (C_4), n-pentanol (C_5), n-hexanol (C_6) and n-octanol (C_8). Each reaction was conducted at four different temperatures for $1 - 8$ h over Hβ, Al-MCM-41 and DMC catalysts. As in the above experiments, alcohol was taken in excess (10 times) so that a pseudo-first order rate law is obeyed. Fig. 4.14 shows representative kinetic plots obtained over DMC catalyst. The kinetic data and energy of activation

Fig. 4.14. *Conversion vs time plots for esterification of oleic acid with different alcohols (temperature = 423 K; left) and at different temperature (middle) over DMC catalyst. Right panel shows the Arrhenius plot for esterification with n-butanol*

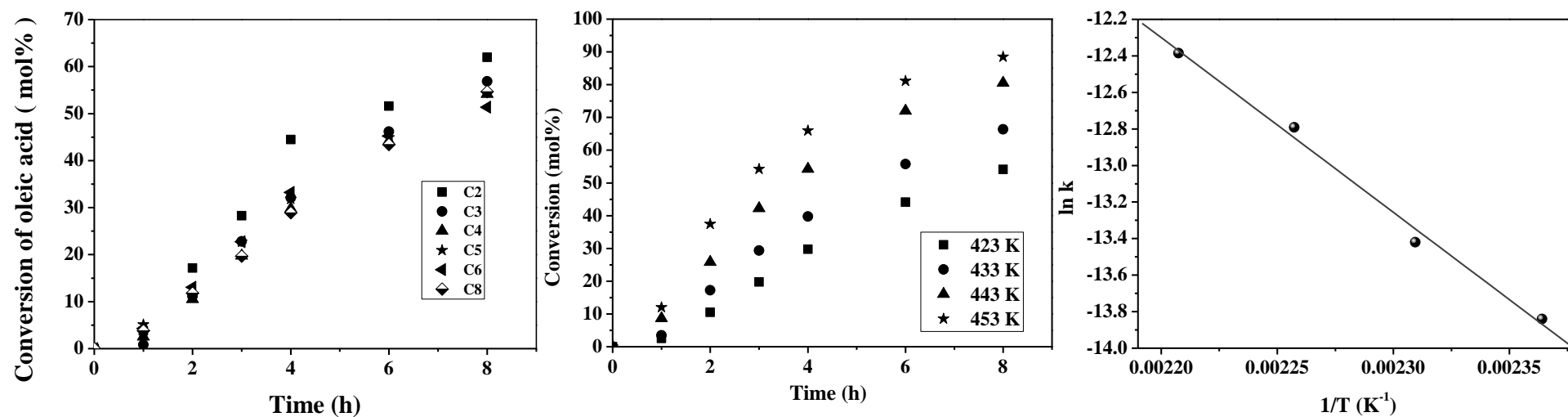**Table 4.5.** Rate constant (k, L.mol^{-1}.s^{-1}.m^{-2}) and E_a (kJmol^{-1}) for the esterification of oleic acid with different alcohols

Alcohol	DMC				Al-MCM-41				Hβ			
	T (K)	k (x10^{-7})	TOF (x10^{-3}) (s^{-1})	E_a (kJ.mol^{-1})	T (K)	k (x10^{-8})	TOF (x10^{-3}) (s^{-1})	E_a (kJ.mol^{-1})	T (K)	k (x10^{-8})	TOF (x10^{-3}) (s^{-1})	E_a (kJ.mol^{-1})
methanol	423	4.2	3.8		403	10.4	18.3		363	2.5	2.1	
	433	4.3	4.1	52.8	413	15.6	20.2	38.9	373	4.0	3.3	54.7
	443	8.1	6.7		423	17.2	26.9		383	3.9	4.2	
	453	11.5	9.9		433	24.7	43.2		393	9.8	9.4	
ethanol	423	3.7	1.5		393	0.9	21.6		373	0.5	3.7	
	433	5.7	2.6	54.7	403	1.6	36.6	40.8	383	1.4	9.6	49.9
	443	7.8	3.4		413	2.0	55.4		393	1.9	14.8	
	453	10.3	4.4		423	2.9	76.8		403	2.6	15.8	
n-propanol	423	4.0	0.3		393	1.0	19.0		373	1.1	3.1	
	433	5.2	1.1	57.1	403	1.2	31.6	38.7	383	1.3	5.7	28.2
	443	6.7	3.2		413	1.6	38.0		393	1.1	8.5	
	453	11.6	4.1		423	2.4	56.5		403	2.1	11.8	
n-butanol	423	4.2	1.0		393	1.1	9.2		373	0.9	3.7	
	433	5.3	1.4	61.5	403	1.4	20.8	38.4	383	1.1	-	22.4
	443	12.2	3.4		413	1.9	28.1		393	1.1	4.9	
	453	12.6	4.7		423	1.8	47.4		403	1.9	6.5	
n-pentanol	423	5.0	2.0		403	3.2	33.5		383	1.0	4.3	
	433	8.4	2.5	53.0	413	3.5	39.3	42.1	393	1.2	5.7	28.4
	443	11.3	3.0		423	5.8	53.4		403	1.6	9.6	
	453	13.5	3.6		433	6.3	80.6		413	2.7	15.4	
n-hexanol	423	5.9	1.7		403	2.6	30.9		383	0.7	3.9	
	433	9.0	3.1	46.8	413	4.5	41.9	54.3	393	2.0	5.2	21.2
	443	12.2	3.7		423	6.8	56.7		403	2.2	9.6	
	453	14.1	4.4		433	7.8	77.7		413	2.7	13.7	
n-octanol	423	7.0	1.5		403	1.9	30.3		383	2.1	4.8	
	433	10.8	2.5	43.8	413	2.1	41.7	55.9	393	2.3	6.8	24.0
	443	13.8	3.0		423	2.9	60.8		403	3.2	7.6	
	453	16.0	3.6		433	3.2	76.3		413	3.6	13.7	

for all the three catalysts are compiled in Table 4.5. Even in this experiment, the kinetic parameters (k and TOF) of Al-MCM-41 are higher than those of Hβ, while the parameters of DMC are higher than both Hβ and Al-MCM-41. While an increase in the value of k with an increase in the chain length of alcohol was observed over DMC, no systematic variation was found with Al-MCM-41 and Hβ catalysts. The variation of activation energy (E_a) with the chain length of alcohols is different over each catalyst (Fig. 4.15). Over Al-MCM-41, the value of E_a increased slowly from methanol to n-butanol and then steeply from n-butanol to n-octanol. Over DMC, the value of E_a increased with increasing chain length of alcohol up to n-butanol and then decreased beyond that. In the case of Hβ, the E_a values decreased with an increase in the chain length of alcohol. This decrease is, however, more noticeable up to n-butanol.
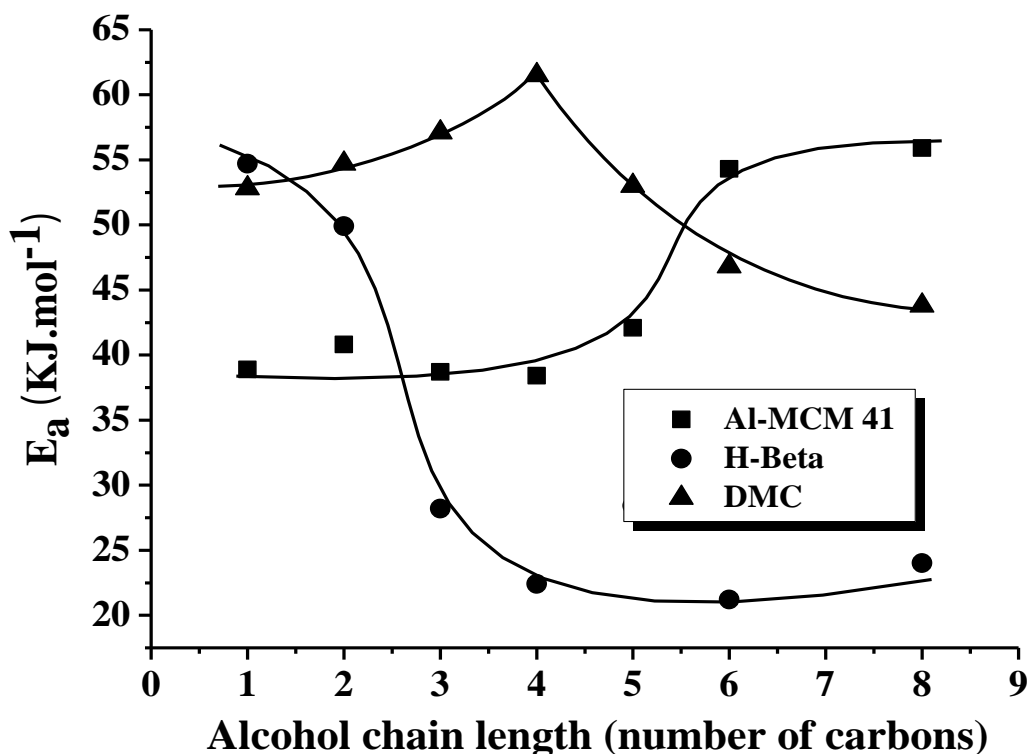
Fig. 4.15. *Variation of energy of activation (E_a) with the chain length of alcohols for esterification of oleic acid over different solid acid catalyst*

4.6. Catalyst Reusability Studies

The reusability of DMC, SZ and Al-MCM-41 catalysts was investigated in five recycling experiments. After each reaction, the catalyst was separated from the reaction mixture by filtration and then used without any further treatment in subsequent recycling studies. As seen from Fig. 4.16, while DMC is more stable and

reusable, SZ (to a larger extent) and Al-MCM-41 (to a lower extent) lose their catalytic activity in recycling experiments. Non- or limited reusability of catalysts in batch reactions, usually, translates into deactivation in long duration trials in fixed-bed reactors as has, indeed, been observed for SZ catalysts. Leaching of sulfate ions during use in the presence of H_2O molecules has already been reported [26] and is, probably, the main cause of its activity loss on recycles.
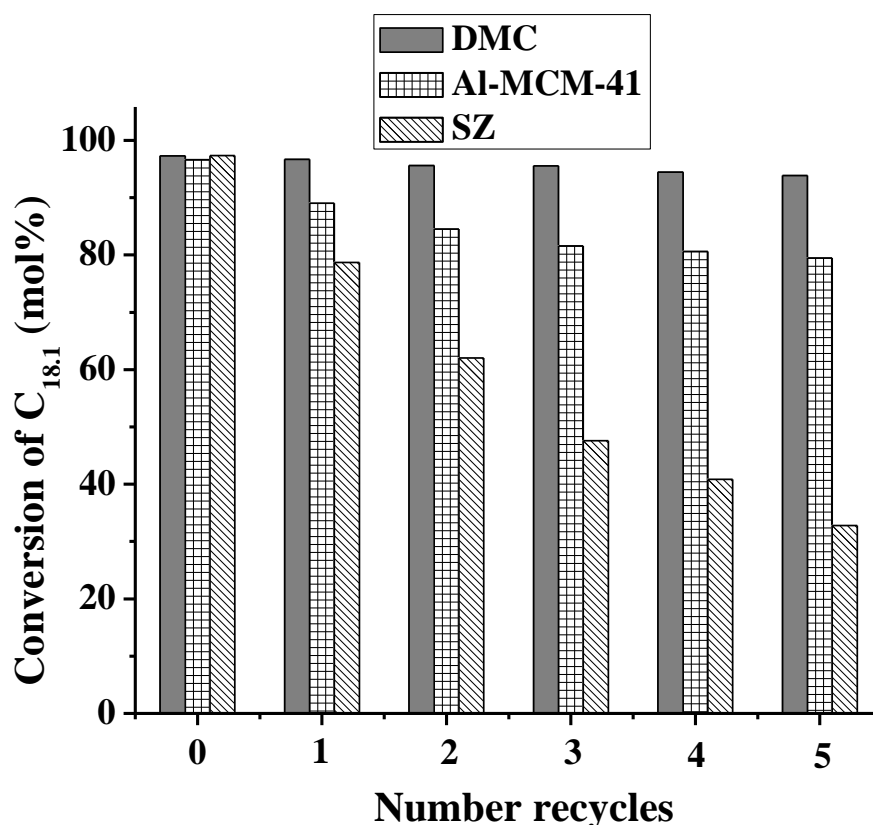
Fig. 4.16. Recyclability studies of DMC, SZ and Al-MCM-41 catalysts in the esterification of oleic acid with methanol

After calcination, Al-MCM-41 regained its original activity indicating that leaching of Al^{3+} was probably, not the major cause of its deactivation. In order to probe this deactivation phenomenon further, we have carried out "hot filtration" experiments wherein the catalyst was removed from the reaction mixture at the end of 1 h and the reaction was continued further without the catalyst. In the case of SZ, the reactions were conducted at 373 K and with Al-MCM-41 and DMC the studies were performed at 423 K. Esterification proceeded at significant rate even after the removal of the SZ catalyst (Fig. 4.17). However, with Al-MCM-41 and DMC, the reaction rate, after the removal of the catalyst, was similar to that observed in the absence of the solid catalyst. Deactivation of SZ observed in recycling experiments

is, hence, due to leaching of the catalytically active species. Leaching of the Al ions are not, probably, the major cause of the non-reusability of Al-MCM-41. The lowest values of activation energy for SZ (Table 4.3) comparable to that of sulfuric acid (Table 4.4) do suggest leaching of sulfate groups of SZ into the liquid phase and some amount of homogeneous reaction in this case. The values of activation energy for Al-MCM-41 and DMC fall within the range for solid acid catalysts. A heterogeneous DMC catalyst cannot be compared in a true sense with SZ which leaches during the reaction. In view of this, Al-MCM-41 was chosen as an alternative to compare its activity trend with DMC. Similar to SZ, Al-MCM-41 is also hydrophilic but non-leachable during the reaction condition and showing an opposite activation trend to hydrophobic DMC catalysts.
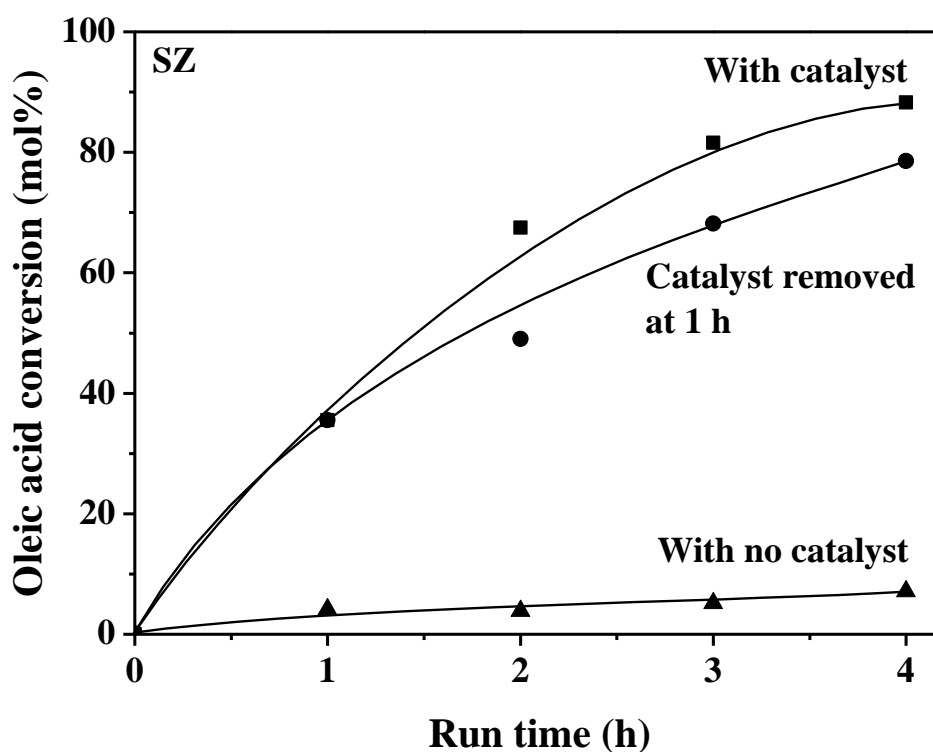
Fig. 4.17. *Catalyst leaching (hot filtration) experiment*

In this study, an attempt was also made to delineate the relative roles of the Lewis and Brönsted acid sites in the esterification reaction. Calcined and activated SZ and Al-MCM-41 were exposed to the vapors of pyridine at 373 K. Then the catalysts were flushed with nitrogen and then, the temperature was raised to 573 K to desorb all the pyridine from the Lewis acid sites. At this stage only the Brönsted acid sites were poisoned by pyridine molecules (DRIFT spectroscopy). These catalysts were then used in the esterification reactions. It was found that oleic acid conversion

decreased from 82.6 to 33.5% over SZ (reaction temperature = 373 K, run time = 3 h). In the case of Al-MCM-41, this decrease was from 81.3 to 58.9% (reaction temperature = 423 K, run time = 4 h). The lower drop in case of Al-MCM-41 is due to the lower fraction of its Brönsted acid sites.

4.7. Structure – Activity Correlations

The surface area, pore volume and pore dimensions of DMC are smaller than those of SZ and Al-MCM-41. Hβ has smallest pore size (microporous). The crystallite and particle sizes of DMC are also bigger than those of Hβ, SZ and Al-MCM-41. While Hβ, SZ and Al-MCM-41 contained stronger Brönsted and Lewis acid sites, DMC contains only the relatively weaker Lewis acid sites. Although the pore size of DMC is smaller than that of SZ, it is still large enough for the fatty acid molecules ($C_{18.1}$, for example) to approach the active sites and get converted to the corresponding fatty acid methyl esters. Hence, the rates of reactions are probably not diffusion controlled. It may be noted that methanol and fatty acid are completely miscible above 313 K. The stirring speed (400 rpm) was chosen such that the kinetic data are not affected by mass transfer limitations.

4.7.1. Influence of Hydrophobicity of Catalyst Surface

The higher activity of SZ, Hβ and Al-MCM-41 than DMC can be attributed to their higher acid strength, specific surface area. But the variations in apparent activation energy with the chain length of fatty acid (Fig. 4.13) cannot be explained based only on the textural and acidic properties of the catalysts. For a given pore size, E_a is expected to increase with increasing chain length of the fatty acid as indeed observed for Hβ, SZ and Al-MCM-41 (Fig. 4.13). The observation of a decrease in E_a with chain length of FFA for DMC indicates that other factors, like surface polarity/hydrophobicity also play an important role. Adsorption data (Table 4.2) indicated that the surface of DMC is more hydrophobic (the *relative* adsorption of methanol is higher than that of water, Table 4.2). As the chain length of the fatty acid increases it is less miscible with water. Hence, its adsorption on the hydrophobic DMC is expected to be thermodynamically more favored than on the relatively more hydrophilic (and hydroxylic) SZ and Al-MCM-41. Adsorption studies have indeed revealed higher amounts of oleic acid adsorption on DMC than on SZ and Al-MCM-41. More facile adsorption of fatty acid with increasing chain length over hydrophobic surfaces (as in the case of DMC) results in a more facile reaction and lower activation energy. The relative performance of these catalysts were also

investigated in transesterification of soybean oil (more hydrophobic molecule than fatty acid) with methanol (oil : methanol molar ratio = 1 : 15, catalyst = 3 wt% of oil, temperature = 443, reaction time = 8 h). Fatty acid methyl ester (FAME) yield was determined using ^{1}H NMR spectroscopy. The catalytic activity (FAME yield) varied in the order: SZ (91%) > DMC (77%) > Al-MCM-41 (11%). Leaching of acid sites and contribution due to homogeneous reaction are the causes for the higher catalytic activity of SZ. Unlike DMC, it could not be reused in recycling experiments (Fig. 4.16 and 4.17). This agrees with the independent report by Garcia et al. [36] on SZ. Al-MCM-41 showed higher catalytic activity than DMC in esterification reactions but a reverse trend was observed in transesterification of soybean oil with methanol. This reverse trend in transesterification can be explained only on the basis of hydrophobicity of catalyst surfaces. As triglycerides are more hydrophobic than fatty acids, their adsorption on hydrophilic Al-MCM-41 is more difficult than fatty acids resulting in lower activity of Al-MCM-41 compared to DMC.

The trend observed in esterification of oleic acid with different alcohols over Al-MCM-41 and DMC can also be explained on the basis of their hydrophobic nature. Over Al-MCM-41, E_a increased from methanol to n-butanol and then steeply from n-butanol to n-octanol and over DMC, the value of E_a increased with increasing chain length of alcohol up to n-butanol and then decreased beyond that. As we know the pK_a of alcohols increases with increasing chain length. Due to this long-chain alcohols are less nucleophilic and thereby, exhibit lower conversion and higher E_a value. This behaviour is observed up to n-butanol for both Al-MCM-41 and DMC. But for higher alcohols, pk_a remains the same and their hydrophobicity keeps increasing. Hydrophobicity of these solid catalysts decreases in the order: DMC > Al-MCM-41. Hence, Al-MCM-41, having a hydrophilic surface is expected to show higher E_a values with increasing chain length of alcohols due to less adsorption of those molecules resulting in a sharp increase in E_a beyond n-butanol. While DMC is a hydrophobic catalyst, after n-butanol as the hydrophobicity of reactant molecules increases their adsorption becomes more favourable and that's why decrease in E_a was observed.

4.7.2. Influence of Pore Size of Catalyst

Activation energy values for shorter chain length fatty acids ($C_{8.0}$ and $C_{10.0}$) are nearly the same over Hβ and Al-MCM-41 (Fig. 4.13). However, the difference increased with increase in the chain length of fatty acid. This is because of the

variation in the pore size of these catalysts (Table 4.1). In general, activation energy increases with the chain length of fatty acid [37, 38]. This increase is expected due to increased diffusional and steric hindrances with the increase in chain length of the acid. As Al-MCM-41 is a mesoporous and Hβ is a microporous catalyst, as the length of reactant molecules increases diffusional hindrances increase more in case of Hβ resulting in higher increase in E_a. In other words, the present study demonstrates that the porosity of the catalyst affects the kinetics of esterification of fatty acids. Despite having higher acidity lower values of kinetic parameters for Hβ indicate the importance of pore size of the catalysts. Over microporous Hβ, with methanol as alcohol, the reaction might be taking place both inside the pores and on the external surface. As the chain length of alcohol increases contribution of the reaction occurring inside the pore decreases and that at the external surface increases. This variation as well as its hydrophobic nature (compared to Al-MCM-41) is possibly the cause for the low E_a values in reactions with long chain length alcohols.

Variation in the properties of the catalysts and chain length of fatty acid as well as alcohols enabled to demonstrate that the pore size and hydrophobicity of the catalyst surface are two additional important parameters that influence fatty acid esterification reaction.

4.8. Conclusions

Esterification of long chain fatty acids was investigated over Lewis acidic DMC and Lewis-Brönsted acidic Hβ, sulfated zirconia and Al-MCM-41 catalysts. Apart from acidic and textural features, the hydrophobicity and pore size of the catalyst surface influences, significantly, the rate of esterification of long-chain fatty acids. DMC having a more hydrophobic surface and medium pore size shows superior catalytic activity and reusability than SZ, Hβ and Al-MCM-41 catalysts. In the case of more hydrophilic SZ and Al-MCM-41, co-product water molecules compete for strong adsorption on the acid sites.

4.9. References

1. U. Schuchardt, R. Sercheli, R.M. Vargas, J. Braz. Chem. Soc. 9 (1998) 199.

2. A.C. Pinto, L.L.N. Guarieiro, M.J.C. Rezende, N.M. Ribeiro, E.A. Torres, W.A. Lopes, P.A.P. Pereira, J.B. de Andrade, J. Braz. Chem. Soc. 16 (2005) 1313.

3. F.R. Ma, M.A. Hanna, Bioresource Technol. 70 (1999) 1.

4. J. Van Gerpen, Fuel Process. Technol. 86 (2005) 1097.

5. M. Di Serio, R. Tesser, L. Pengmei, E. Santacesaria, Ener. Fuel 22 (2007) 207.

6. M. Toda, A. Takagaki, M. Okamura, J.N. Kondo, S. Hayashi, K. Domen, M. Hara, Nature 438 (2005) 178.

7. M.-H. Zong, Z.-Q. Duan, W.-Y. Lou, T.J. Smith, H. Wu, Green Chem. 9 (2007) 434.

8. X. Mo, D.E. López, K. Suwannakarn, Y. Liu, E. Lotero, J.G. Goodwin Jr., C. Lu, J. Catal. 254 (2008) 332.

9. D.E. López, K. Suwannakarn, D.A. Bruce, J.G. Goodwin Jr., J. Catal. 247 (2007) 43.

10. D.E. López, J.G. Goodwin Jr., D.A. Bruce, J. Catal. 245 (2007) 381.

11. Y. Liu, E. Lotero, J.G. Goodwin Jr., J. Catal. 242 (2006) 278.

12. D.E. López, J.G. Goodwin Jr., D.A. Bruce, S. Furuta, Appl. Catal. A: Gen. 339 (2008) 76.

13. D.E. López, J.G. Goodwin Jr., D.A. Bruce, E. Lotero, Appl. Catal. A: Gen. 295 (2005) 97.

14. T.A. Peters, N.E. Benes, A. Holmen, J.T.F. Keurentjes, Appl. Catal. A: Gen. 297 (2006) 182.

15. A.A. Kiss, F. Omota, A.C. Dimian, G. Rothenberg, Topics Catal. 40 (2006) 141.

16. A.A. Kiss, A.C. Dimian, G. Rothenberg, Energy & Fuels 22 (2008) 598.

17. Y. Liu, E. Lotero, J.G. Goodwin Jr., J. Catal. 243 (2006) 221.

18. I.K. Mbaraka, D.R. Radu, V.S.-Y. Lin, B.H. Shanks, J. Catal. 219 (2003) 329.

19. D.M. Alonso, M.L. Granados, R. Mariscal, A. Douhal, J. Catal. 262 (2009) 18.

20. A.A. Kiss, A.C. Dimian, G. Rothenberg, Adv. Synth. Catal. 348 (2006) 75.

21. P.S. Sreeprasanth, R. Srivastava, D. Srinivas, P. Ratnasamy, Appl. Catal. A: Gen. 314 (2006) 148.

22. R. Srivastava, D. Srinivas, P. Ratnasamy, J. Catal. 241 (2006) 34.

23. J.K. Satyarthi, D. Srinivas, P. Ratnasamy, Energy Fuels 23 (2009) 2273.

24. J.B. Higgins, R.B. Lapierre, J.L. Schlenker, A.C. Rohrman, J.D. Wood,

G.T. Kerr, W.J. Rohrbaugh, Zeolites 8 (1988) 446.

25. X.-R. Chen, Y.-H. Ju, C.-Y. Mou, J. Phys. Chem. C 111 (2007) 18731.

26. X.B. Li, K. Nagaoka, J.A. Lercher, J. Catal. 227 (2004) 130.

27. Wang, G.; Wang, Y.; Liu, Y.; Liu, Z.; Guo, Y.; Liu, G.; Yang, Z.; Xu, M.; Wang, L. Appl. Clay Sci. 44 (2009) 185.

28. C.A. Emeis, J. Catal. 141 (1993) 347.

29. K. Suwannakarn, E. Lotero, J.C. Goodwin Jr., C. Lu, J. Catal. 255 (2008) 279.

30. J. Jitputti, B. Kitiyanan, P. Rangsunvigit, K. Bunyakiat, L. Attanatho, P. Jenvanitpanjakul, Chem. Eng. J. 116 (2006) 61.

31. T.J. Schildhauer, I. Hoek, F. Kapteijn, J.A. Moulijn, Appl. Catal. A: Gen. 358 (2009) 141.

32. R.Tesser, M. Di Serio, M. Guida, M. Nastasi, E. Santacesaria, Ind. Eng. Chem. Res. *44* (2005) 7978.

33. R. Tesser, L. Casale, D. Verde, M. Di Serio, E. Santacesaria, Chem. Eng. J. 154 (2009) 25.

34. D.A.G Aranda, R.T.P Santos, N.C.O Tapanes, A.D. Ramos, O.A.C. Antunes, Catal. Lett. 122 (2008) 20.

35. T.A. Peters, N.E. Benes, A. Holmen, J.T.F. Keurentjes, Appl. Catal. A: Gen. 297 (2006) 182.

36. C.M. Garcia, S. Teixeira, L.L. Marciniuk, U. Schuchardt, Bioresource Tech. 99 (2008) 6608.

37. K. Srilatha, N. Lingaiah, P.S. Sai Prasad, B.L.A. Prabhavathi Devi, R.B.N. Prasad, S. Venkateswar, Ind. Eng. Chem. Res. 48 (2008) 10816.

38. J. Lilja, D.Y. Murzin, T. Salmi, J. Aumo, P. Mäki-Arvela, M. Sundell, J. Mol. Catal. A: Chem. 182-183 (2002) 555.

Chapter 5

Epoxidation of Fatty Acids and their Esters

5.1. Introduction

Chemical modification of vegetable oils (a renewable feedstock) is an important approach to obtain industrial products [1]. There is still a high potential to develop new, efficient and environmentally friendly reaction pathways leading to new products or to find new applications for already existing oleochemicals [2]. This strategy can contribute to decrease our dependence on non-renewable, limited, natural resources such as mineral oil. On the industrial level, chemical reactions on hydrocarbon chain/unsaturation are in second place (10%) after the reactions involving carboxylic/ester groups of fatty acids and their esters. In industry, the most extensively applied reactions on the unsaturation are hydrogenation and epoxidation. Other reactions with a lower industrial use are isomerization, hydroxylation, oxidative cleavage, metathesis, Diels-Alder reactions, carboxylation (hydroformylation and hydrocarboxylation) and radical and cationic additions [3].

Epoxidation of fatty acids and their esters (biodiesel and triglycerides) provides intermediates useful for the manufacture of commercially important materials. Fatty acid epoxides have numerous applications such as polyether polyols produced from methyl oleate by the Prileshajev epoxidation (using peracetic acid) [4], defence compounds in infected plants [5] (e.g., to combat fungal infection), epoxidized soybean oil (ESBO) used as a plasticizer and stabilizer for poly(vinylchloride) (PVC) to improve flexibility, elasticity and toughness [1]. The ESBO market is second to that of epoxy resins and its worldwide production in 1999 was 2 x 10^5 tons [6]. Fatty acid epoxides are also used to form coating compositions by reactions with urethanes and alcohols [7], plasticizers by reaction with triacetin to form epoxidized glyceride acetate [8], and antifoaming compounds by reaction with alcohols and alkylamides [9].

Commercially, epoxidation of fatty acids and its esters is carried out with peracid formed in situ from hydrogen peroxide and acetic acid or formic acid, using a strong mineral acid catalyst [10, 11]. However, this procedure causes several concerns about safety and corrosion problems related to the percarboxylic acids. Low selectivity, side reactions (diols by hydrolysis, polymerization, etc) and separation of homogeneous mineral acids after reaction are the main drawbacks of this process [12]. Therefore, it is desirable to have a heterogeneous catalyst that provides a selective and clean process for epoxidation of fatty acids and its esters. Some attempts in this direction have been made using the catalysts such as Ti(IV)-grafted on silica [13], Ti-MCM-

41 [14], Ti-amorphous silicas [15], peroxo phosphotungstate [16], a tungsten based tetrakis catalyst [17], acidic ion exchange resin [18], alumina [19], methyltrioxorhenium(VII) supported on niobia [20], transition metal complexes [21], chemo-enzymatic "self"-epoxidation catalysed by immobilized Novozym 435[®] [22] etc. Several transition complexes of molybdenum, titanium, tungsten, rhenium [23] etc. are also being studied as catalysts nowadays.

In the present study, group VI transition metal oxides (Cr, Mo and W) supported on alumina, are evaluated as catalysts for the epoxidation of fatty acids and their esters (methyl and glyceryl). The effect of modification of alumina with phosphoric acid on epoxidation activity was also investigated. Active sites and mechanism responsible for higher activity of MoO_x/Al_2O_3 were investigated using diffused reflectance UV-visible spectroscopy.

5.2. Experimental Section

Group VI transition metal oxides supported on alumina (CrO_x/Al_2O_3, MoO_x/Al_2O_3, WO_x/Al_2O_3 and $MoO_x/P-Al_2O_3$) were prepared with 5%, 10% and 15% loading by impregnation technique as per the procedure reported in Chapter 2.

The catalysts were characterized using various physicochemical techniques. Procedure for catalytic reaction is given in Chapter 2.

Decomposition of tert.-butyl hydroperoxide over various alumina-supported catalysts was investigated. For this, 100 mg of catalyst was dispersed in 5 g of anhydrous 3% TBHP solution in toluene and stirred at 373 K for 30 min. After removal of the catalyst by filtration, TBHP was estimated by iodometric titration. For reference TBHP was also determined before dispersion of catalyst. Difference in titration value was used to calculate the TBHP decomposition.

5.3. Results and Discussion

5.3.1. Structural and Spectroscopic Characterization

5.3.1.1. XRD

Fig. 5.1 shows the X-ray diffractograms of alumina-supported group IV metal oxide catalysts. No additional peaks other those due to γ-Al_2O_3 were observed indicating that the metal oxides are well dispersed on the alumina support.
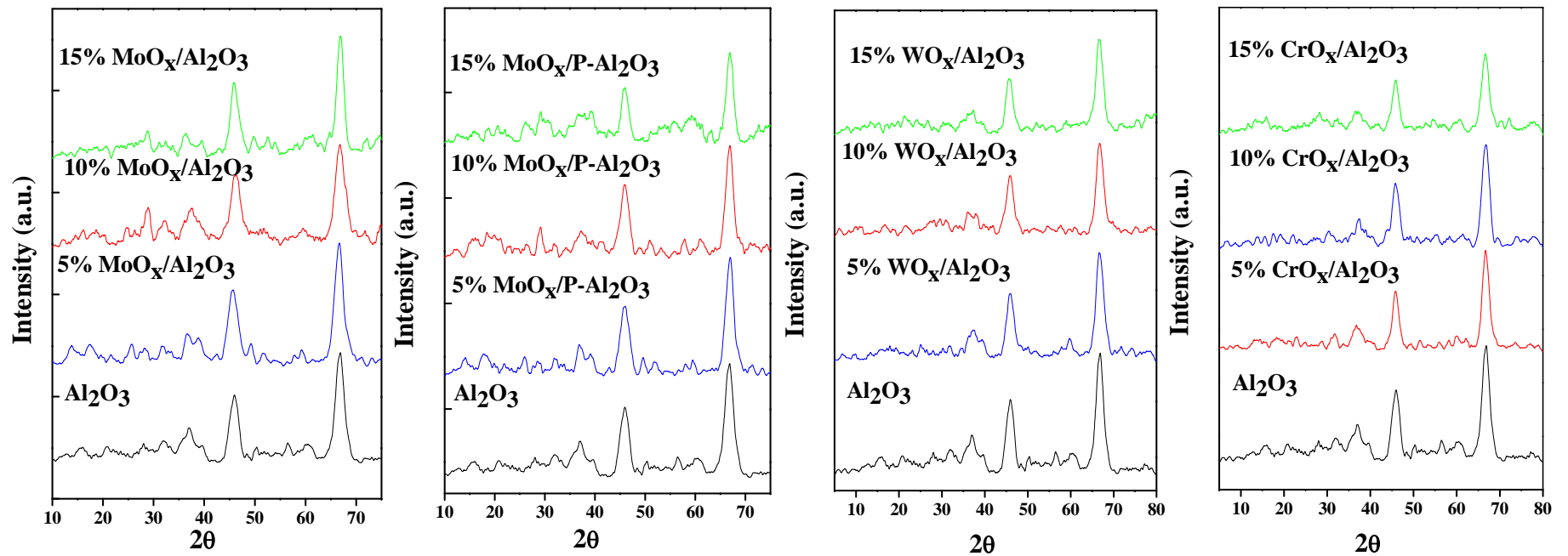
Fig. 5.1. *XRD pattern of alumina-supported group VI metal oxide catalysts*
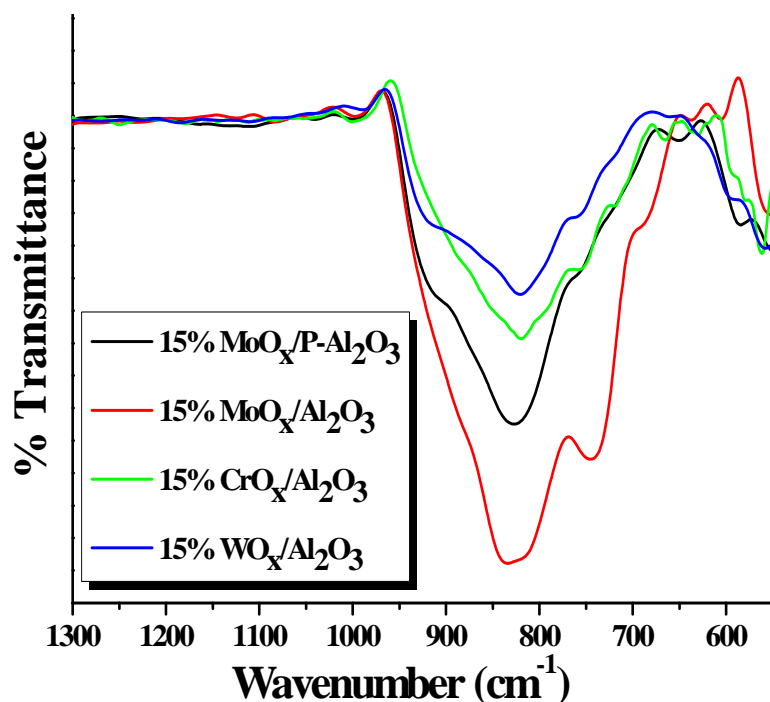
Fig. 5.2. *FTIR spectra of alumina-supported group VI metal oxide catalysts*

5.3.1.2. FTIR

The supported metal oxides showed intense overlapping FTIR peaks in the region 650- 1000 cm^{-1} corresponding to Al-O-Al, Al-O-M and M-O-M and M=O stretching vibrations (Fig. 5.2). In spite of similar metal oxide loadings (15 wt%), the supported catalysts showed IR peaks with different intensities. This is perhaps due to the difference in the extinction coefficients of different M-O-M and M=O vibrations.

5.3.1.3. DRUV-Vis

Diffuse reflectance UV-visible (DRUV-Vis) spectroscopy can differentiate the dispersed metal oxides from the bulk-phase oxides [24]. Neat CrO$_x$ shows three overlapping bands at 370, 465 and 604 nm. These, in the case of supported oxides (CrO$_x$/Al$_2$O$_3$) shifted to 276, 372 and 462 nm, respectively (Fig. 5.2). This blue shift in UV-visible bands position is attributed to dispersion of CrO$_x$ on the alumina support. In the case of MoO$_x$/Al$_2$O$_3$ and WO$_x$/Al$_2$O$_3$, the oxygen to metal charge transfer band shifted from 352 to 295 nm and 385 to 232 nm, respectively (Fig. 5.2). At lower loadings (ca. 5 wt%), a split in charge transfer band was observed. This is indicates the presence of at least two types of metal oxide species: (1) metal oxide interacting directly with aluminum (Al-O-M) and (2) isolated metal oxide nanoparticles (M-O-M). Intensity of the charge transfer band also increased with increasing metal oxide loading.
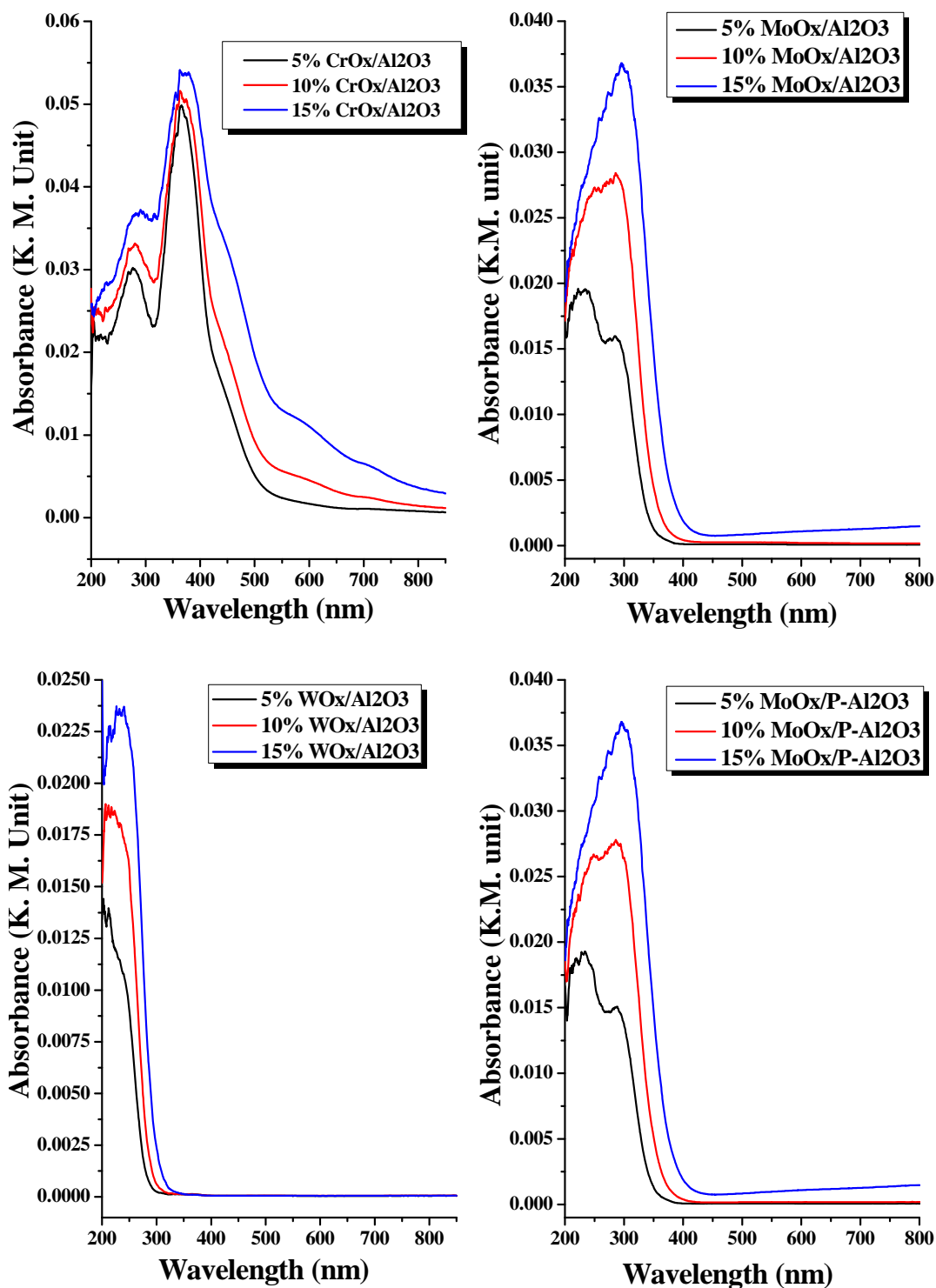
Fig. 5.3. *DRUV-Vis spectra of alumina-supported group VI metal oxide catalysts*

5.3.1.4. XPS

The oxidation state of supported metal was confirmed by X-ray photoelectron spectroscopy. 15% CrO_x/Al_2O_3 showed two peaks at 586.7 and 577.7 eV corresponding to $2p_{3/2}$ and $2p_{1/2}$ of Cr^{3+}, respectively (Fig 5.4). The supported MoO_x showed peaks at 235.6 and 232.9 eV corresponding to $3d_{5/2}$ and $3d_{3/2}$, respectively of molybdenum in +6 oxidation state [25, 26]. The supported WO_x showed a broad peak at 35 eV which could be deconvoluted into two peaks corresponding to $4f_{5/2}$ and $4f_{7/2}$ of W^{6+}. Intensity of these peaks increased with increasing metal loading.
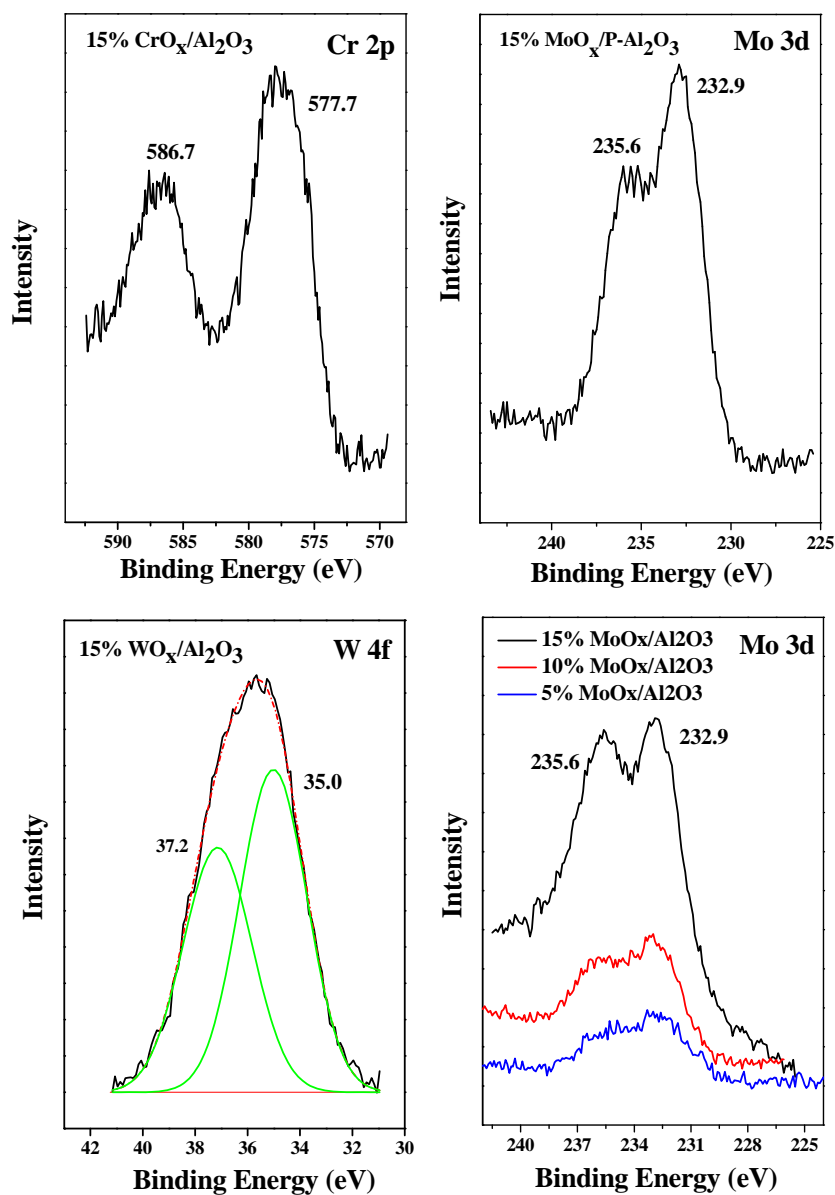
Fig. 5.4. *XPS spectra of alumina-supported group VI metal oxide catalysts*
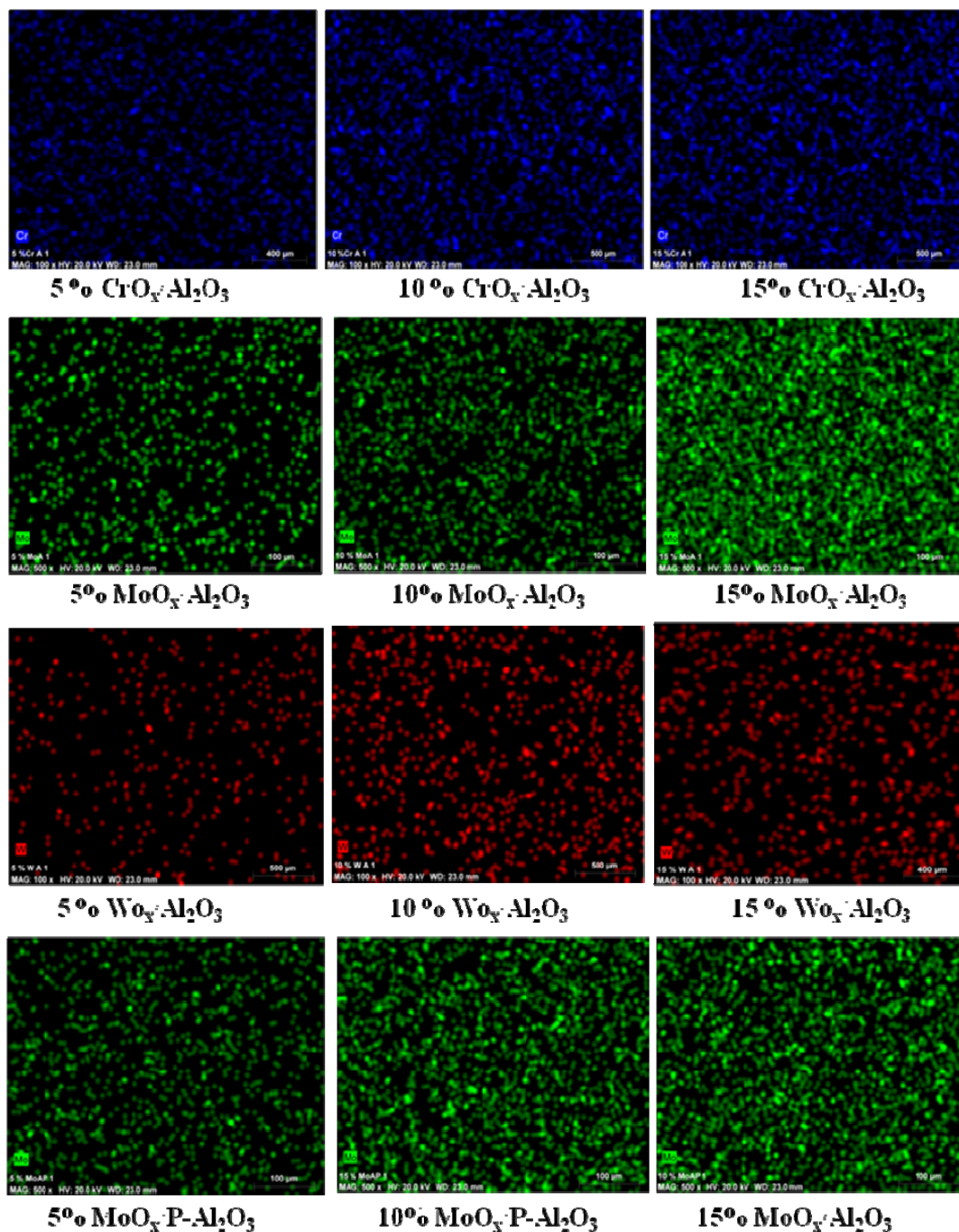
Fig. 5.5. *Elemetal mapping of alumina-supported group VI metal oxide catalysts*

5.3.1.5. Elemental Mapping

Fig. 5.5 shows the chemical mapping of metal (by EDAX) in supported metal oxide catalysts. This analysis provides the information on the homogeneity and distribution of meal oxides over alumina. The intensity of coloured dots corresponds to the metal and its concentration. More intense the dot higher is the concentration of

metal at that particular area. From Fig. 5.5 it can be concluded that the metal oxide dispersion on alumina increases in the following order: $WO_x < MoO_x < CrO_x$ Incorporation of phosphorous in the support enhances the supported metal oxide dispersion.

5.3.1.6. Textural Properties

N_2-physisorption studies revealed that surface area of the catalysts decreased with an increase in the loading of supported metal oxide. This decrease is more in the case of MoO_x than in WO_x and CrO_x. Chen et al. [27], Giordano et al. [28] and Benitez et al. [29] have also reported a similar observation. No systematic trend in variation of pore size and pore volume was noticed (Table 5.1).

Table 5.1. Surface properties of alumina-supported group VI metal oxide catalysts

Catalyst	S_{BET} (m^2/g)	Pore volume (cc/g)	Pore size (nm)	Acidity (NH$_3$-TPD) (mmol/g)
Al$_2$O$_3$	229	0.44	7.7	0.38
5% MoO$_x$/Al$_2$O$_3$	204	0.34	6.7	0.59
10% MoOx/Al2O3	180	0.42	9.2	0.65
15% MoO$_x$/Al$_2$O$_3$	133	0.30	8.9	0.61
5% MoO$_x$/P-Al$_2$O$_3$	193	0.39	8.1	0.57
10% MoO$_x$/P-Al$_2$O$_3$	180	0.35	7.7	0.60
15% MoO$_x$/P-Al$_2$O$_3$	158	0.33	8.4	0.64
5% CrO$_x$/Al$_2$O$_3$	214	-	-	0.52
10% CrO$_x$/Al$_2$O$_3$	196	-	-	0.56
15% CrO$_x$/Al$_2$O$_3$	192	-	-	0.50
5% WO$_x$/Al$_2$O$_3$	228	-	-	0.53
10% WO$_x$/Al$_2$O$_3$	222	-	-	0.49
15% WO$_x$/Al$_2$O$_3$	197	-	-	0.55

5.3.1.7. Acidity Measurement

Acidity of the catalysts was determined using pyridine and ammonia as probe molecules. Fourier transform infrared spectra of pyridine adsorbed on catalysts showed that catalyst possess both Lewis and Brönsted type acid sites but the concentration of the former is higher than that of the latter (Fig. 5.6).
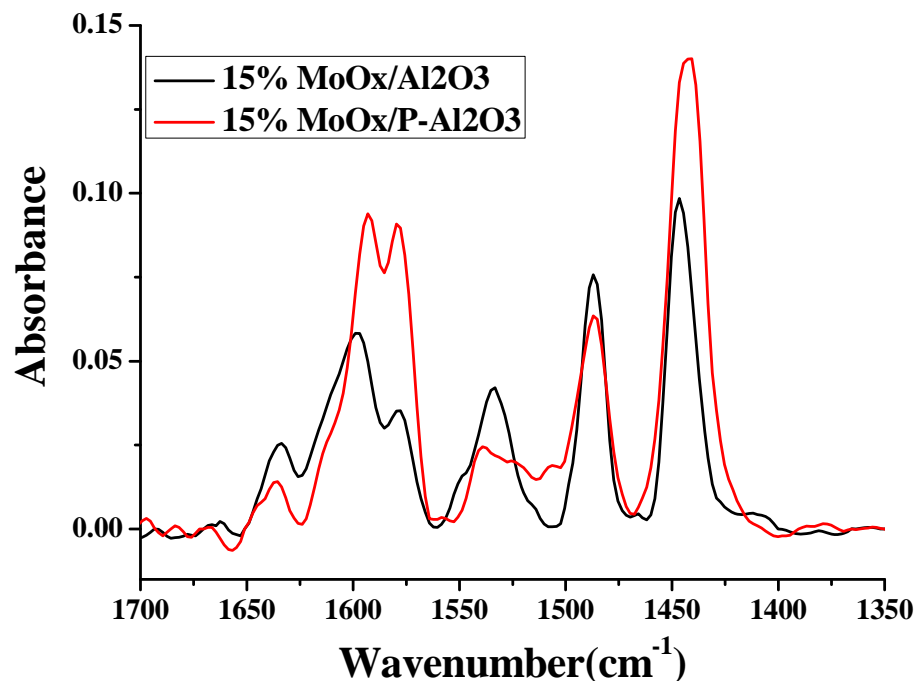
Fig. 5.6. *FTIR spectra of pyridine adsorbed MoO$_x$/Al$_2$O$_3$ and MoO$_x$/P-Al$_2$O$_3$*

Temperature-programmed desorption of ammonia showed two desorption peaks corresponding to presence of at least two types of acid sites, weak (180-200°C) and strong (350-400°C). Metal oxide loading enhanced the acidity of γ-alumina. The total acidity of the supported catalysts increased with an increase in metal oxide loading up to 10 wt% and then decreased (Table 5.1). The concentration of the strong acid sites decreased with increasing metal loading (Fig. 5.7). Acidity of MoO$_x$/Al$_2$O$_3$ is marginally higher than the other two supported metal oxides. Modification with phosphoric acid (2 wt%) has little effect on the overall acidity. The acidity of the catalyst correlates with the dispersion of metal oxide.

5.4. Catalytic Activity

Epoxidation of oleic acid, methyl soyate and soybean oil were carried out over these supported catalysts. Fatty acid profile of soybean oil was determined to be (GC analysis): palmitic acid (C$_{16.0}$) − 12 wt%, stearic acid (C$_{18.0}$) − 3 wt%, oleic acid (C$_{18.1}$) − 27 wt%, linoleic acid (C$_{18.2}$) − 52 wt% and linolenic acid (C$_{18.2}$) − 6 wt%. The structures of different fatty acid methyl esters of soybean oil are shown in Scheme 5.1. Average molecular weight of methyl soyate was calculated to be 292.1 g while the average molecular weight of soybean oil was found to be 872.4 g. Number of double bond per mole of methyl soyate was estimated to 1.49.
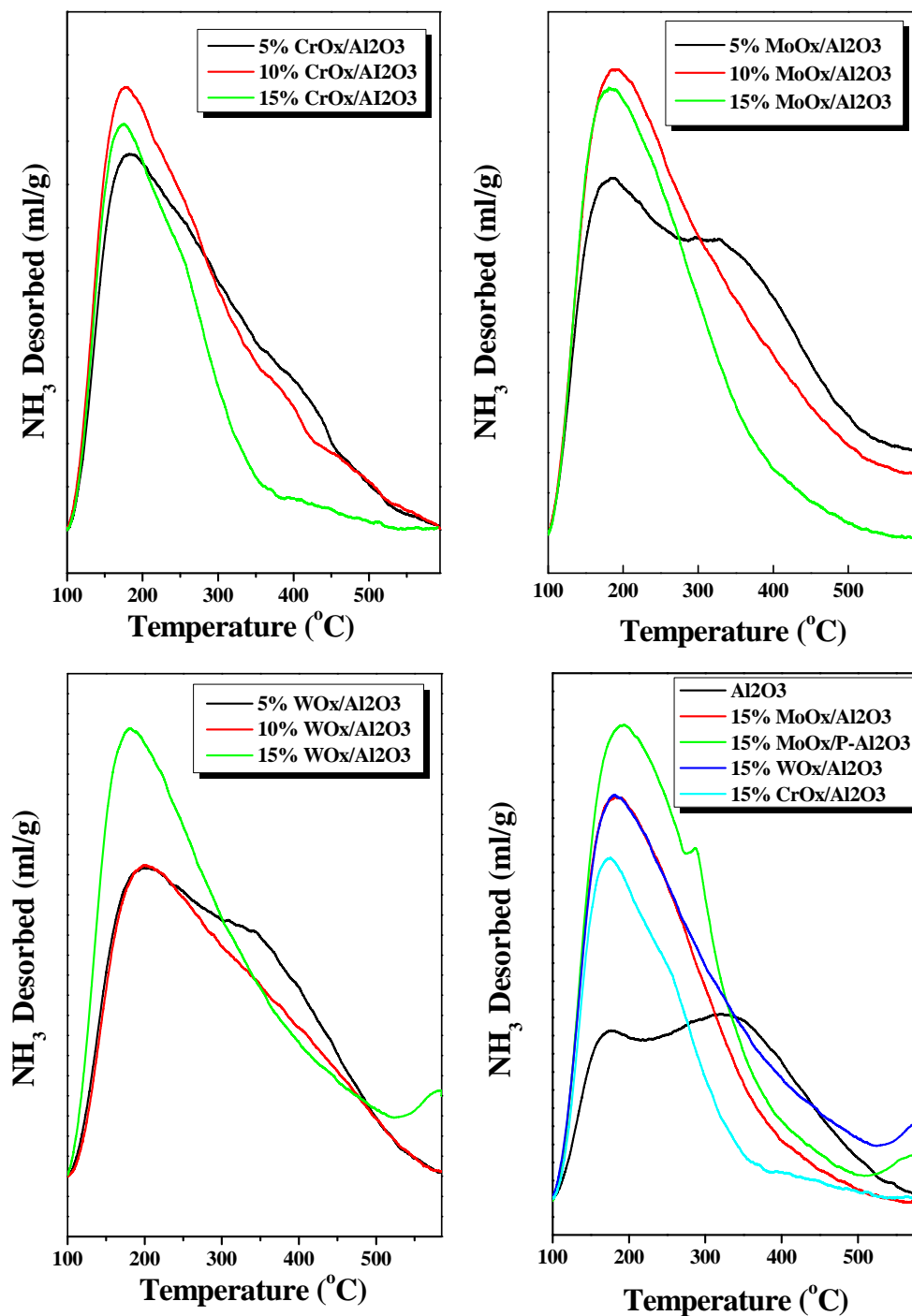
***Fig. 5.7.** NH₃ profile of alumina-supported group VI metal oxide catalysts*

Epoxidation of methyl soyate was carried out with *tert.*-butyl hydroperoxide (TBHP). 70% aq. TBHP was extracted with toluene as reported in Chapter 2 and the anhydrous TBHP thus prepared was used in the reactions. Progress of the reaction

was monitored by ^{1}H NMR spectroscopy (Chapter 2). The possible epoxide products from the reaction of methyl soyate are depicted in Scheme 5.2.

methyl oleate

methyl linoleate

methyl linolenate

methyl stearate

methyl palmitate
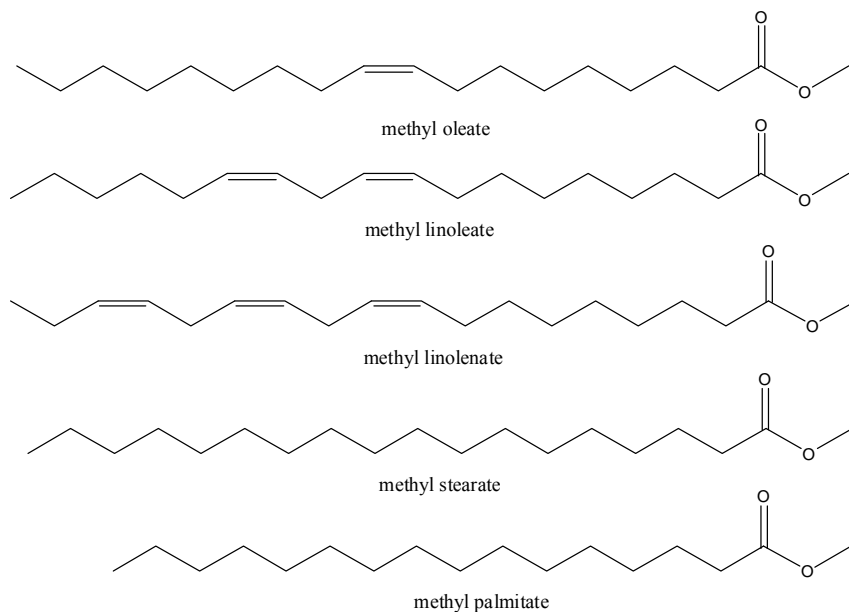
***Scheme 5.1.** Methyl esters of fatty acids in soybean oil*

methyl 8-(3-octyloxiran-2-yl)octanoate

(*Z*)-methyl 8-(3-(oct-2-enyl)oxiran-2-yl)octanoate

methyl 8-(3-((3-pentyloxiran-2-yl)methyl)oxiran-2-yl)octanoate

methyl 8-(3-((2*Z*,5*Z*)-octa-2,5-dienyl)oxiran-2-yl)octanoate

(*Z*)-methyl 8-(3-((3-(pent-2-enyl)oxiran-2-yl)methyl)oxiran-2-yl)octanoate

methyl 8-(3-((3-((3-ethyloxiran-2-yl)methyl)oxiran-2-yl)methyl)oxiran-2-yl)octanoate
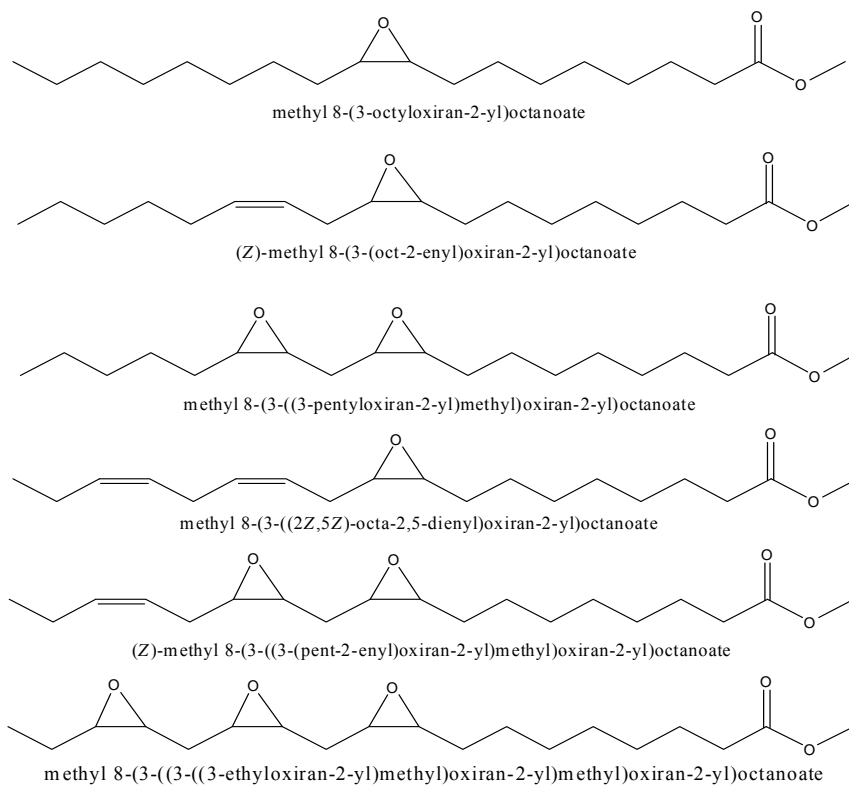
***Scheme 5.2.** Epoxidized products of fatty acid methyl esters*

Epoxidation methyl soyate occurred to a small extent (13 mol%) even without a catalyst. The conversion of double bonds in the epoxidation of methyl soyate over neat γ-alumina was found to be (as determined by ^{1}H NMR method) very small (8.6 mol%). A significant enhancement in double bonds conversion of methyl soyate (by nearly 10 times) was observed when alumina-supported metal oxides were used as catalysts. Among all the catalyst investigated (Table 5.2) MoO_x/Al_2O_3 was found to be more efficient. The conversion increased with increasing MoO_x loading. Conversion of methyl soyate over "neat" MoO_3 was found lower (52.1 mol%) than that obtained with alumina-supported MoO_x (81.1 mol%). Dispersion on support surface is perhaps the cause its enhanced catalytic activity. Even 50 mg 15% MoO_x/Al_2O_3 was found to yield higher conversions than 50 mg "neat" MoO_3.

Table 5.2. Catalytic activity of supported metal oxides in epoxidation and TBHP decomposition

Catalyst	Double bond conv. (mol %)[a]	TBHP decomposed (mol%)[b]
5% MoO_x/Al_2O_3	20.5	7.0
10% MoO_x/Al_2O_3	61.9	32.9
15% MoO_x/Al_2O_3	81.1	80.3
5% $MoO_x/P-Al_2O_3$	23.8	25.6
10% $Mo/P-Al_2O_3$	75.2	50.4
15% $MoO_x/P-Al_2O_3$	78.1	82.9
5% CrO_x/Al_2O_3	40.1	100
10% CrO_x/Al_2O_3	41.0	100
15% CrO_x/Al_2O_3	55.4	100
5% WO_x/Al_2O_3	13.7	10.1
10% WO_x/Al_2O_3	14.7	13.2
15% WO_x/Al_2O_3	17.3	16.3
MoO_3 (1 mg)	52.1	-
MoO_3 (50 mg)	65.1	-
Al_2O_3	8.6	-
Without catalyst	13.0	-

[a]*Reaction conditions: Methyl soyate = 1 g, double bond : TBHP = 1 : 1.5, catalyst = 10 wt% with respect to methyl soyate, toluene – 10 mL, temperature = 373 K, reaction time = 2 h.*

[b]*Reaction conditions: 100 mg of catalyst was dispersed in 5 g of TBHP + toluene solution and TBHP was estimated by iodometric titration before and after TBHP decomposition by catalyst at 373K for 30 min.*

Fig. 5.8 shows the influence of metal oxide and amount metal loading on the epoxidation activity. Under similar conditions, 15 wt% MoO_x/Al_2O_3 was found to be the most active catalyst. Although, at 5 wt% loading, CrO_x/Al_2O_3 was found to be more active than MoO_x/Al_2O_3, at higher metal loadings a reverse trend was observed. WO_x/Al_2O_3 were found to be the least active catalyst for the epoxidation of methyl soyate. It is known that WO_3 is a good catalyst in epoxidation reaction with hydrogen peroxide. But it doesn't have the synthetic utility when alkyl hydroperoxides are employed as oxidants [30-32]. However, there are issues of hydrolysis of epoxide ring when H_2O_2 and polar solvents are used [30-32]. At lower loading (5 – 10 wt%), modification of alumina with phosphorous did improve the catalytic activity. But at 15 wt% of MoO_x, modification with phosphorous had little effect.
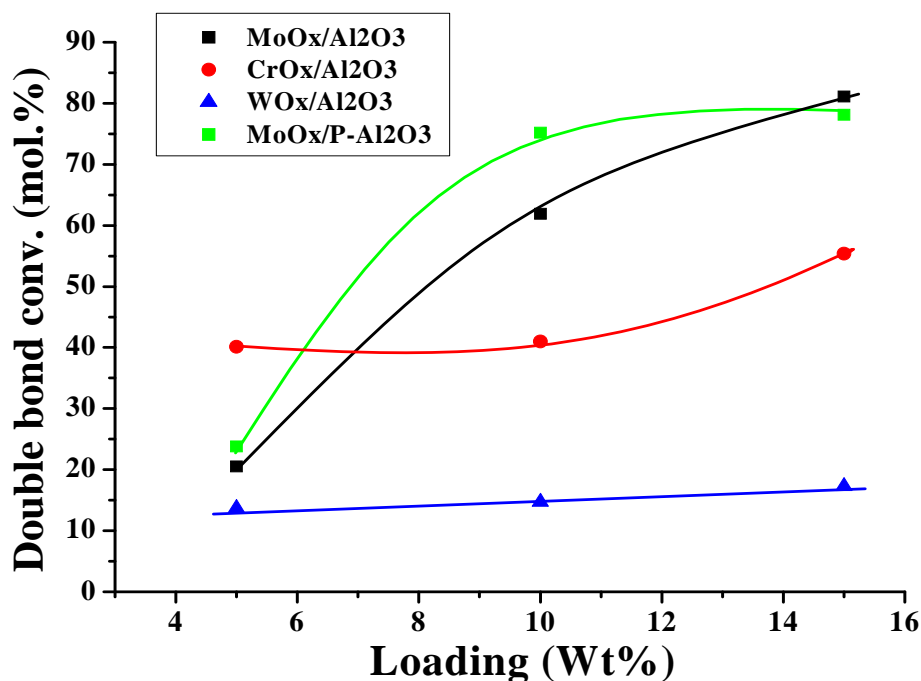
Fig. 5.8. *Influence of metal oxide and loading*

TBHP decomposition over these catalysts was determined (Table 5.2) and it was found that CrO_x/Al_2O_3 is more efficient for decomposing TBHP into molecular oxygen and *tert.*-butanol. MoO_x catalysts showed an intermediate activity while the WO_x catalysts showed a very low activity. Hence, the lack of ability of WO_x/Al_2O_3 to activate TBHP either to decompose or to utilize the oxidant is the cause for its lowest epoxidation activity. On the other hand, TBHP decomposes at a higher rate on

CrO_x/Al_2O_3. It is not efficiently utilized for epoxidation. Thus shows an intermediate activity. MoO_x/Al_2O_3 is more efficient in epoxidation rather than in decomposition of TBHP. Hence, among the metal oxides studied it was found to be the best in the epoxidation activity.

5.4.1. Kinetics of Epoxidation

Epoxidation of methyl soyate was carried out in a batch reactor and the course of reaction was monitored by ^{1}H NMR spectroscopy (Fig. 5.9) and gas chromatography. Gas chromatography always provided higher values as compared to ^{1}H NMR (Table 5.3). This is due to the fact that gas chromatography provides conversion of methyl soyate while ^{1}H NMR estimates the conversion of the double bond. If a fatty acid methyl ester in methyl soyate contains more than one double bond and even if one bond is epoxidized GC counts it as conversion of whole fatty acid methyl ester as its peak shifted to mono epoxidized products. While in ^{1}H NMR the double bond conversion is estimated. Hence, GC shows higher values of conversion then ^{1}H NMR. The latter is therefore, a more reliable way of estimation of the conversion of fatty acids or their esters to epoxides. Details of ^{1}H NMR method of estimation are given in Chapter 2.

Table 5.3. Epoxidation of methyl soyate monitored by ^{1}H NMR and GC techniques

Run time (h)	^{1}H NMR (Double bond conversion)	Gas Chromatography (FAME conversion)
0.5	59.8	79.2
1	73.0	91.5
2	81.1	88.1
3	85.6	94.2
4	87.1	93.3
5	87.1	93.4
6	90.1	93.1

Reaction conditions: Catalyst : methyl soyate = 1 g, TBHP : double bond = 1.5 : 1, 15% MoO_x/Al_2O_3 =10 wt% of methyl soyate, temperature = 373 K, solvent (toluene) = 10 mL.

As the reaction proceeds peak area corresponding to protons of double bonds (-C**H**=C**H**-) at δ = 5.4 ppm, protons of CH_2 group next to double bond (–C**H₂**-CH=CH-C**H₂**-) at δ = 2.0 ppm and protons of methylene (=CH-C**H₂**-CH=) at δ = 2.7 ppm keep on decreasing. New signal corresponding to protons of epoxides (-C**H**OC**H**-) at δ = 2.9 ppm and CH_2 next to epoxides (–C**H₂**-CHOCH-C**H₂**-) at δ = 1.5 ppm, appeared (Fig. 5.9). Area of the signal (triplet) due to α-CH_2 (-C**H₂**-COO) at δ = 2.3 ppm and methoxy group (-OC**H₃**) at δ = 3.7 ppm in methyl esters remains the same. No peaks corresponding to ring opening of epoxides were observed. The decrease in the area of proton peaks at δ = 5.4 ppm with respect to α-CH_2 peaks was used to calculate the conversion of double bonds in methyl soyate.
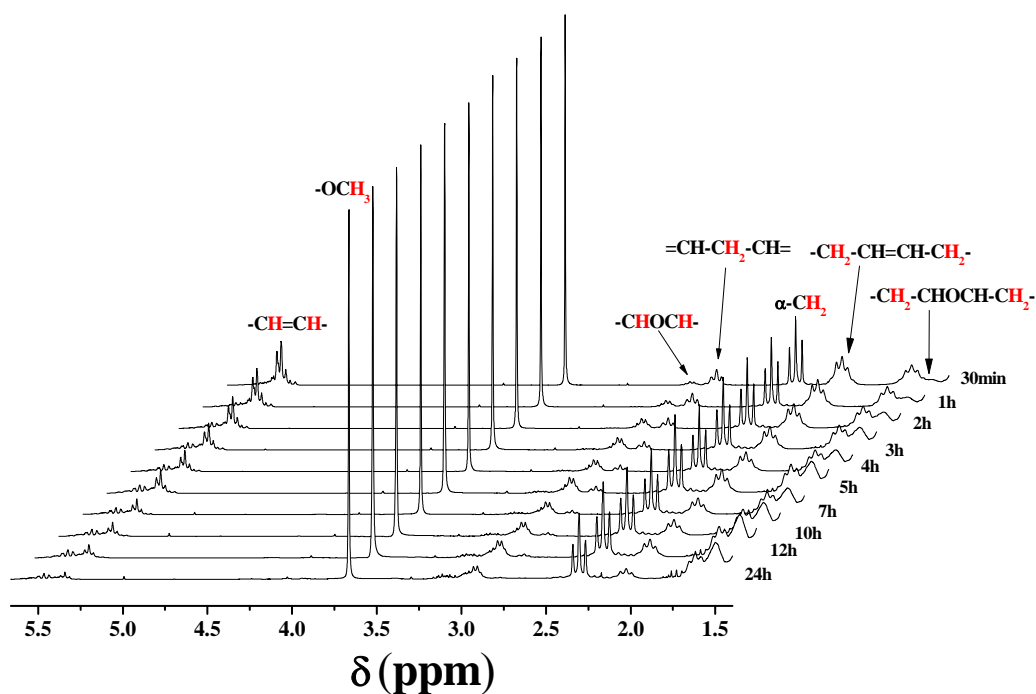
Fig. 5.9. *Time-on study for the epoxidation of methyl soyate*

5.4.2. Epoxidation of Different Substrates

Table 5.4 lists the catalytic activity of 15% MoO_x/Al_2O_3 for the epoxidation of oleic acid, methyl soyate, soybean oil and oleic acid-methyl soyate mixtures. These substrate are chosen to evaluate the efficiency of the catalyst for various fatty acid feedstock such as vegetable oils (soybean oil), biodiesel (methyl soyate, FAME), oleic acid (Free fatty acids) and non-edible oils (oleic acid + FAME). 15% MoO_x/Al_2O_3 showed comparable activity for all these different substrates.

Table 5.4. Epoxidation of different substrates over 15% MoO_x/Al_2O_3

Substrate	Double bond conversion (mol %)
FAME	85.6
Soya oil	82.2
Oleic Acid	81.2
Oleic acid : FAME = 1:1	81.1

Reaction conditions: substrate = 0.5 g, double bond : TBHP = 1 : 1.5, catalyst (15% MoO_x/Al_2O_3) = 10 wt%, solvent (toluene) = 5 mL, temperature = 373 K, reaction time = 3 h.

5.4.3. Influence of Catalyst Amount

Fig. 5.10 shows the influence of catalyst amount on the epoxidation of methyl soyate over 15% MoO_x/Al_2O_3. Double bond conversion increases with the increase in catalyst amount but after 5 wt% the increase was not significant.
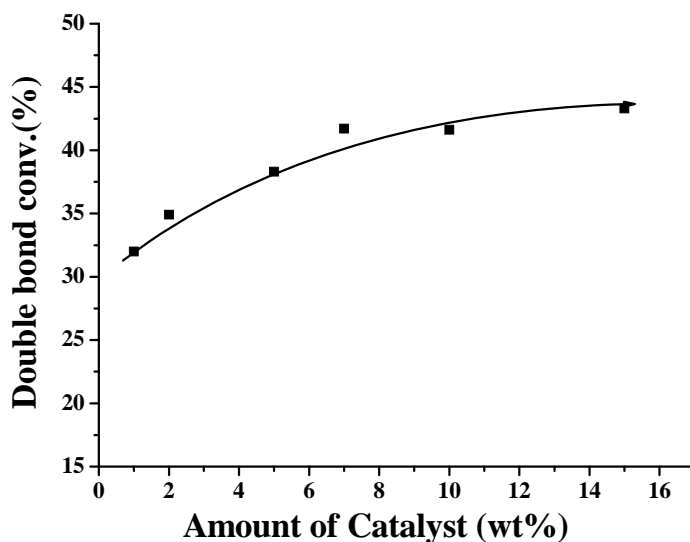
Fig. 5.10. Influence of catalyst amount on epoxidation of methyl soyate. Reaction conditions: methyl soyate = 0.5 g, double bond : TBHP = 1:1.5, solvent (toluene) = 5 mL, catalyst =15% MoO_x/Al_2O_3.

5.4.4. Influence of Peroxide Amount

Amount of peroxide is an important factor which influences the epoxidation. Peroxide is always required in slight excess as decomposition of peroxide occurs as a side reaction. Fig. 5.11 presents the influence of double bond to TBHP molar ratio. This ratio of 1 : 2.5 was found to give high yields of epoxides over 15% MoO_x/Al_2O_3 catalyst.
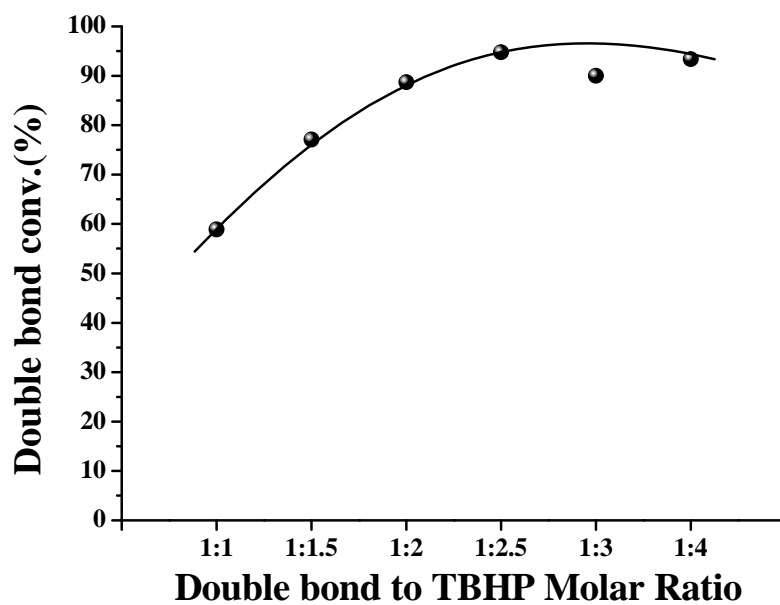
Fig. 5.11. *Influence of peroxide amount. Reaction conditions: methyl soyate = 0.5 g, catalyst (15% MoO$_x$/Al$_2$O$_3$) = 5 wt%, solvent (toluene) = 5 mL, reaction temperature =373 K, reaction time = 1 h.*
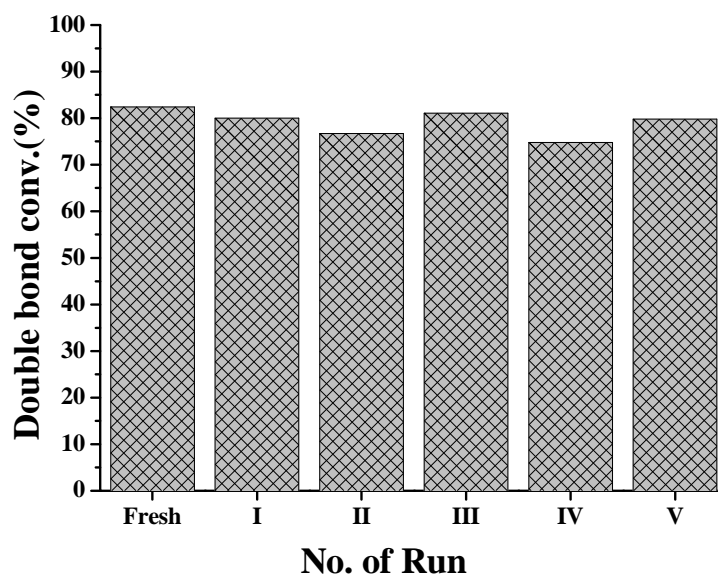
Fig. 5.12. *Reusability of catalyst. Reaction conditions : methyl soyate = 1 g, double bond : TBHP = 1:1.5, catalyst (15% MoO$_x$/Al$_2$O$_3$) = 5 wt%, solvent (toluene) = 10 mL, reaction time = 2 h, reaction temperature =373 K.*

5.4.5. Catalyst Reusability

Reusability of 15% MoO$_x$/Al$_2$O$_3$ was tested in six consecutive runs. At the end of each run, catalyst was separated by filtration, washed with pet-ether, dried at 373 K and reused in the next run. No apparent loss in catalytic activity was observed (Fig. 5.12). To check any leaching of active sites into the reaction medium during the reaction, the catalyst was filtered and separated at the end of 30 min and the reaction was continued without any catalyst. Hot filtration study of 15% MoO$_x$/Al$_2$O$_3$ and 15% MoO$_x$/P-Al$_2$O$_3$ is presented in Fig. 5.13. In case 15% MoO$_x$/Al$_2$O$_3$, the reaction proceeded with the same rate as without a catalyst after its removal while in case of 15% MoO$_x$/P-Al$_2$O$_3$ reaction proceed at higher rate indicating some leaching.
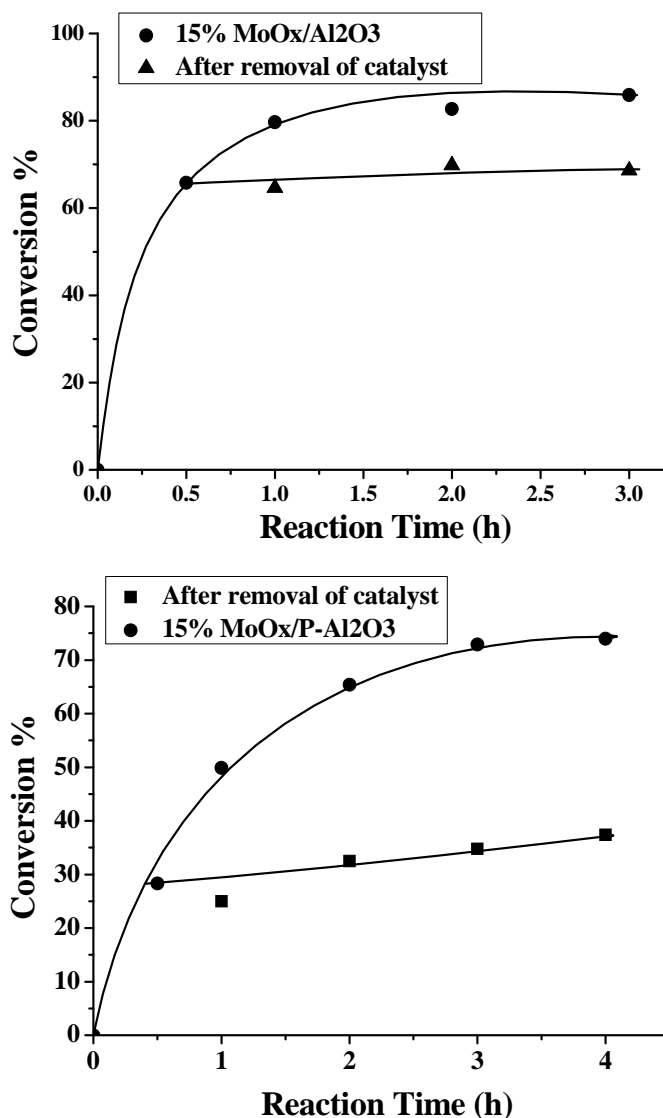
Fig. 5.13. *Leaching study (hot filtration method)*

5.5. Mechanistic Investigation

In-situ diffuse reflectance UV-visible spectroscopy (DRUV) (Fig 5.14) was used to probe the mechanism of epoxidation and the transient species formed during the interaction of alumina-supported group VI metal oxide catalysts with peroxide. On contact with TBHP no change in color of the catalyst was observed. However, on contact with aqueous H_2O_2, a new band was observed at 460 nm, intensity of which decreased with increase in Mo loading. The catalyst with 5 wt% MoO_x turned pink from white, 10 wt% MoO_x turned to pinkish yellow from white and 15 wt% MoO_x turned to light bluish green from light blue. A new band appeared at 460 nm for MoO_x/Al_2O_3 and 355 nm in the case of WO_x/Al_2O_3. By analogy with the literature, this band is attributed to formation of metal-peroxo species [33, 34]. As the loading of molybdenum oxide increased intensity of this new peak decreased in the order: 5% MoO_x-Al_2O_3 > 10% MoO_x-Al_2O_3 > 15% MoO_x-Al_2O_3, which indicates that the stability of peroxo species is in reverse order and transfer of oxygen to double bond is also in the reverse order. Hence, higher activity was observed as the metal oxide loading increased.

When intensity of the new visible band (460 nm and 355 nm) increased for different catalysts in the order: MoO_x > WO_x, stability of the peroxo-M species increased in the order: MoO_x < WO_x. Hence, reactivity of the peroxo-M increases as : WO_x < MoO_x i.e. transfer of oxygen from peroxy species of tungsten to double bond is less facile compared to peroxy species of molybdenum.

UV-visible spectra of CrO_x/Al_2O_3 contain more than one type of species of which some (polymeric) are not involved in the epoxidation reaction but decomposed the oxidant. Hence, shows lower activity than MoO_x/Al_2O_3. Cr(VI), which is a strong Lewis acid, is expected to be a good catalyst, but this is not the case and must be ascribed to the fact that Cr(VI) is a strong oxidant and promotes the decomposition of TBHP [30, 35]. This was also supported by the observation that the decomposition of TBHP experiments (no TBHP left after 30 min) (Table 5.2). When TBHP and H_2O_2 were contacted with CrO_x/Al_2O_3, H_2O_2 decomposition was very vigorous and even some white fumes (water vapours) appeared and colour changes from green to dark violet green for short time before turning back to green. We could conclude that 15% MoO_x/Al_2O_3 has the optimum peroxide species stability and moderate peroxide decomposition which are responsible for its high activity for the epoxidation of fatty acids and its esters.
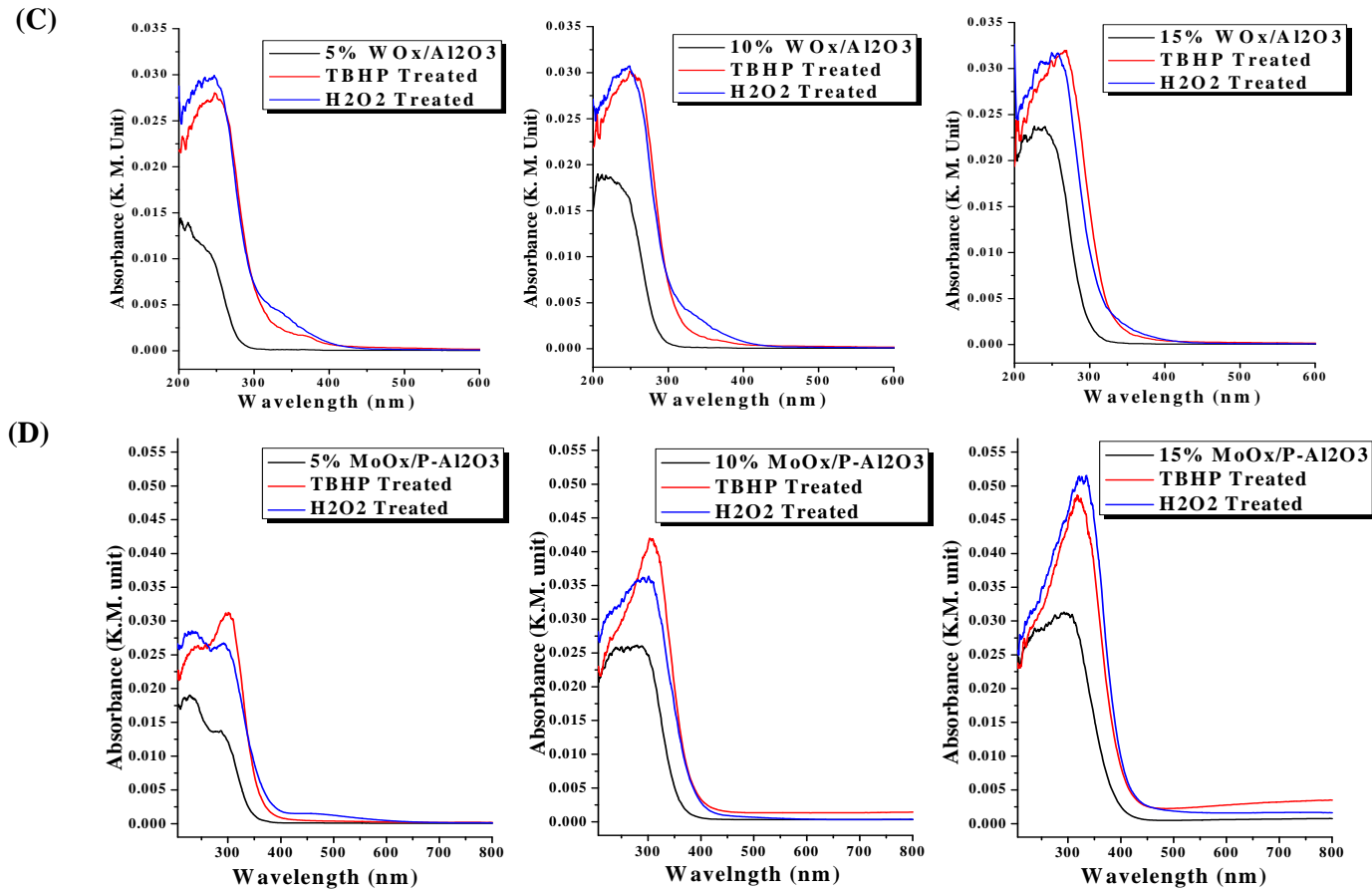
(A)

(B)

(C)

(D)
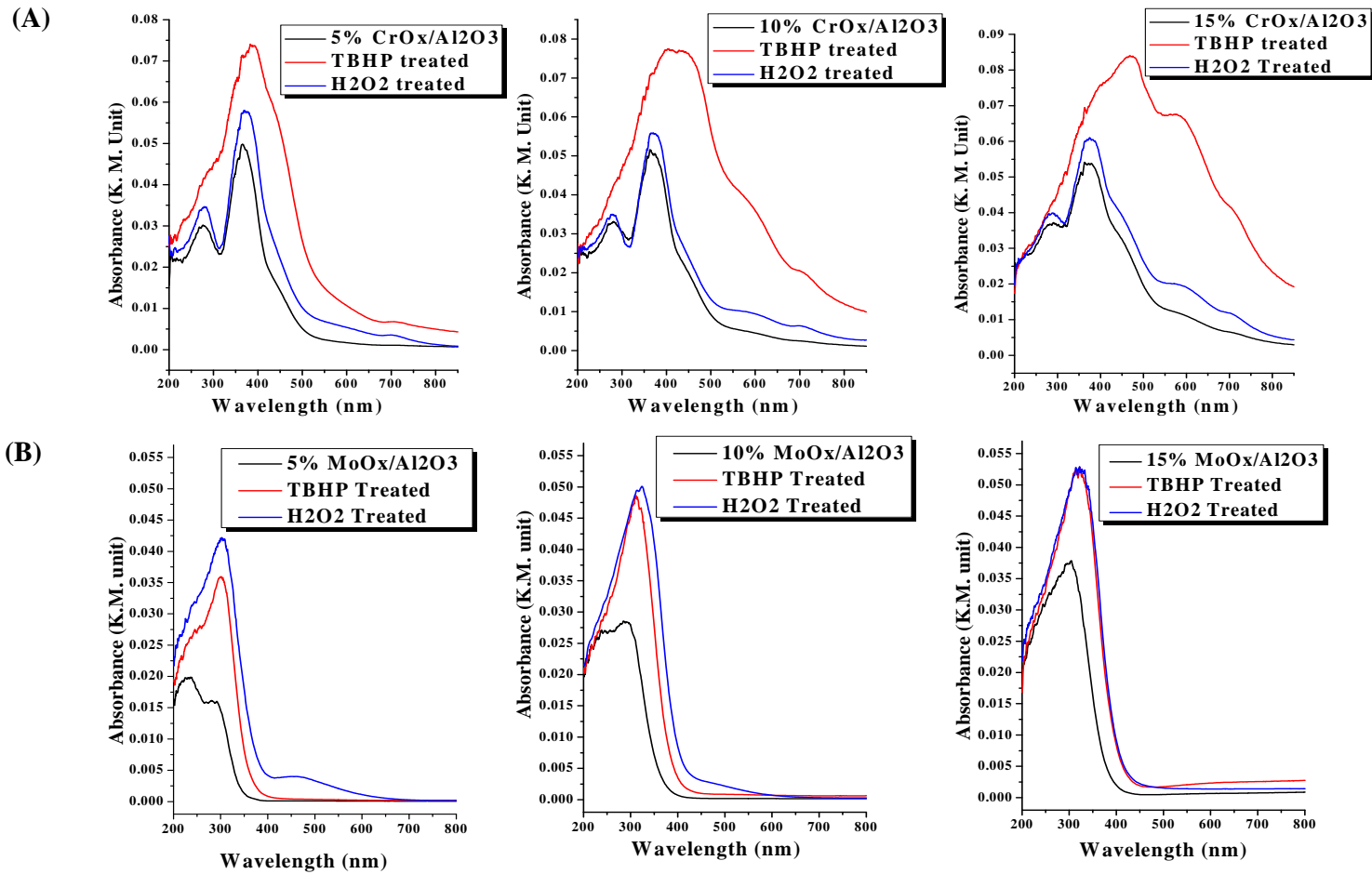
Fig. 5.14. *DRUV-Vis spectra of alumina-supported group VI metal oxides contacted with TBHP and H₂O₂*

5.6. Conclusions

The catalytic activity of alumina-supported group VI metal oxides (CrO_x/Al_2O_3, MoO_x/Al_2O_3 and WO_x/Al_2O_3) in the epoxidation of fatty acids and their esters was investigated. A catalyst with 15 wt% of MoO_x supported on γ-Al_2O_3 was found to be highly active in the epoxidation reaction. In situ spectroscopic studies revealed that peroxide species formed on molybdenum oxide have optimum stability which is the cause for the superior activity of MoO_x/Al_2O_3 catalyst than the supported group VI metal oxides.

5.7. References

1. G. Sienel, R. Rieth, K.T. Rowbottom, Epoxides, in : Ulmann's Encyclopedia of Industrial Chemistry, 6th ed., verlag chemie, Weiheim, p. 269 (2003).

2. "Mechanisms in homogeneous and heterogeneous epoxidation catalysis" Ed. –S. Ted Oyama, First edition, Elsevier (2008).

3. U. Biermann, W. Friedt, S. Lang, W. Luhs, G. Machmuller, J.O. Metzger, M.R. gen. Klass, H.J. Schäfer, M.P. Schneider. Angew. Chem. Int. Ed. 39 (2000) 2206.

4. Z.S. Petrovic, A. Zlatanic, C.C. Lava, S. Sinadinovic-Fiser, Eur. J. Lipid Sci. Technol. 104 (2002) 293.

5. T. Kato, Y. Yamaguchi, T. Hirano, T. Yokoyama, T. Uyehara, T. Namai, S. Yamanaka, N. Harada, Chem. Lett. 26 (1984) 409.

6. M. R. Klaas, S. Warwel, Complete and partial epoxidation of plant oils by lipase catalysed perhydrolysis, Ind. Crops. Prod. 9 (1999) 125.

7. R. Gruetzmacher, U. Nagorny, W. Gress, R. Hoefer, A. Heidbreder, B. Hirschberger, US patent 6433125, August 13 (2002) to Henkel Kommanditgesellschaft auf Aktien.

8. P. Daute, R. Picard, J.-D. Klamann, P. Wedl, A. Peters, US patent 7071343 B2 July 4 (2006) to Cognis Deutschland GmbH & Co. KG.

9. A. B. Cook, J.J. Palmer, J.M. Rodriguez, US patent 5465762 July 8 (1997) to Henkel Corporation (Plymouth Meeting, PA).

10. M. Wiebe, J. Kümmel, J. Prüß, H.-J. Warnecke, Lipids 100 (1998) 404.

11. T.-C. Chou, J.-Y. Chang, Chem. Eng. Commun. 41 (1986) 253.

12. G. J. Piazza, T. A. Foglia, J. Am. Oil Chem. Soc. 83 (2006) 1021.

13. M. Guidotti, N. Ravasio, R. Psaro, E. Gianotti, S. Coluccia , L. Marchese, J.

Mol. Catal. A: Chem. 250 (2006) 218.

14.   L.A. Rios, P. Weckes, H. Schuster, W.F. Hoelderich, J. Catal. 232 (2005) 19.

15.   A. Campanella, M.A. Baltanás, M.C. Capel-Sánchez, J.M. Campos-Martín, J.L.G. Fierro, Green Chem.6 (2004) 330.

16.   I.V. Kozhevnikov, G.P. Mulder, M.C. Steverink-de Zoete, M.G. Oostwal, J. Mol. Catal. A: Chem. 134 (1998) 223.

17.   E. Poli, J.-M. Clacens, J. Barrault, Y. Pouilloux, Catal. Today 140 (2009) 19.

18.   R. Mungroo, N.C. Pradhan, V.V. Goud, A.K. Dalai, J. Am. Oil Chem. Soc. 85 (2008) 887.

19.   J. Sepulveda, S. Teixeira, Ulf Schuchardt, Appl. Catal. A: Gen. 318 (2007) 213.

20.   A.O. Bouh, J.H. Espenson, J. Mol. Catal. A: Chem. 200 (2003) 43.

21.   G. Du, A. Tekin, E.G. Hammond, L. K. Woo, JAOCS 81 (2004) 477.

22.   S. Warwel, M.R. gen. Klaas, J. Mol. Catal. B: Enzymatic 1 (1995) 29.

23.   S.F. Cai, L.S. Wang, C.L. Fan, Molecules 14 (2009) 2935.

24.   Z. Zhang, J. Suo, X. Zhang, S. Li, Appl. Catal. A: Gen. 179 (1999) 11.

25.   P.A. Spevack, N. S. McIntyre, J. Phys. Chem., 97 (1993) 11020.

26.   M. Shimoda, T. Hirata, K. Yagisawa, M. Okochi, A. Yoshikawa, J. Mater. Sci. Lett.8 (1989) 1089.

27.   K. Chen, S. Xie, A.T. Bell, E. Iglesia, J. Catal. 198 (2001) 232.

28.   N. Giordano, J.C.J. Bart, A. Vaghi, A. Castellani, G. Matinotti, J. Catal. 36 (1975) 81.

29.   V.M. Benitez, C.A. Querini, N.S. Figoli, Appl. Catal. A: Gen. 252 (2003) 427.

30.   K.A. Jørgensen Chem. Rev. 89 (1989) 431.

31.   R.A. Sheldon, J.A. Kochi, "Metal-Catalyzed Oxidations of Organic Compounds"; Academic Press: New York, (1981).

32.   D.I. Metelitza, Usp. Khim. 41 (1972) 1737.

33.   B.F. Sels, D.E. De Vos, M. Buntinx, P.A. Jacobs, J. Catal. 216 (2003) 288.

34.   B.F. Sels, D.E. De Vos, P.A. Jacobs, J. Am. Chem. Soc. 123 (2001) 8350.

35.   R.A. Sheldon, J.A. van Doorn, J. Catal. 31 (1973) 427.

Chapter 6

Hydrodeoxygenation of Vegetable Oils into Hydrocarbon-based Biofuels

6.1. Introduction

The efforts of biofuel developers are now basically directed toward production of biodiesel (aliphatic acid monoalkyl esters) obtained from plant or animal feedstock by reacting them with alcohols (transesterification method) [1-5]. But stability (due to unsaturation units in the structure), low energy content (due to oxygen/ester moiety) and cold-flow properties are some of the issues that work against the use of biodiesel especially in the cold climates. A different processing route to convert vegetable oils into a high quality diesel fuel or diesel blend stock that is fully compatible with petroleum-derived diesel fuel is desired [6]. The new types of bio-renewable fuels entering the fuel market must satisfy the following conditions [7]:

(1) There should be no requirement of expensive changes to the existing diesel-engines.

(2) They should not significantly reduce the engine power.

(3) They should be easily integrated into the existing market structure and should be easily blended with petro-diesel in any proportions.

(4) They should meet high fuel quality and form environmentally cleaner combustion products.

The direct route to diesel-like hydrocarbon fuel from the triglycerides is via removal of oxygen. Hence, it is most ideal and also the shortest route at arriving biofuel that will have identical properties with those of conventional diesel fuels. The processes commonly employed for obtaining deoxygenated biofuels from triglycerides include thermal and catalytic pyrolysis [8-12], but these processes provide low atom economy, poor selectivity due to uncontrollable side reactions such as cracking or polymerization of the hydrocarbons, formation of undesired hydrocarbon gases coupled with poor yield of diesel range product [13].

Alternative method of converting triglycerides into hydrocarbon-based diesel fuel is through a hydrotreating process. The hydrotreating process requires hydrogen gas to selectively eliminate the linkage oxygen as water and carbon dioxide. The resulting products are the respective diesel-like hydrocarbons. Paraffin-like liquid fuel obtained by hydrotreating vegetable oil and fats is sometimes termed as *second generation* biodiesel or *green diesel* [14]. Unlike the first generation (ester-based biodiesel), this new generation of biodiesel (hydrocarbons) is more favourable for industrial applications being compatible with the current engines, even avoiding need to be blended with petrol fuels if isomerised [15, 16]. This is an emerging area. In

hydrotreating, removal of oxygen is accomplished through hydrodeoxygenation (HDO) and other direct mechanisms such as hydrodecarbonylation (HDCN), hydrodecarboxylation (HDCX) and hydrogenation (Scheme 6.1) [17]. These processes can be performed using existing petroleum refineries. Hydrotreating is used in the petroleum refinery to remove S, N and metals from petroleum-derived feedstocks including heavy gas-oil or vacuum gas-oil. NExBTL [18, 19] and UOP/Eni Ecofining[TM] [20] are commercialized process for converting vegetable oil feedstock into iso-paraffin-rich diesel substitute (green diesel) which is aromatic and sulfur free-diesel fuel and has a very high cetane value. The cold-flow properties of the fuel can be adjusted in the process to meet climate-specific cloud point in either neat or blended forms. Diesel yields vary from 88-99 vol% depending upon the level of hydroisomerisation and cloud point specification [14]. Recently, several studies for conversion of different fatty acids and their esters (triglycerides and methyl ester) into a mixture of hydrocarbons have been published (Table 6.1) [21-28]
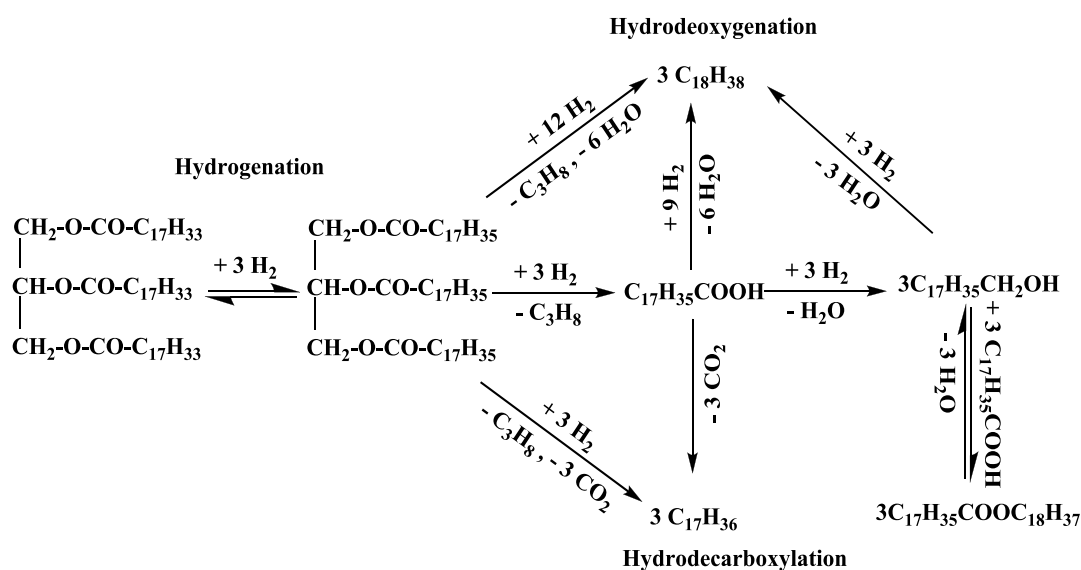
Scheme 6.1. *Hydrotreatment of vegetable [10]*

But due to the highly exothermic nature of these reactions, the control of reaction heat is extremely important. Impure plant oil or animal fat, high reaction temperatures, insufficient control of reaction temperature or low hydrogen availability in the feed stream may cause unwanted side reactions, such as cracking, polymerization, ketonization, cyclization and aromatization, and coking of the catalyst. Deoxygenation in the presence of hydrogen is more useful than decarboxylation as no carbon is lost. Continuous sulfidation of catalyst during the

reaction was reported to improve the selectivity in the hydrodesulphurization reaction [28]. This chapter reports the application of Ni-Mo/γ-Al$_2$O$_3$ catalyst for hydrodeoxygenation of soybean oil. A new FT-IR method is developed to monitor the progress of the reaction.

Table 6.1. Summary of deoxygenation/decarboxylation for fatty acid or its esters

Catalyst	Reaction conditions	Main HC product	Conv.- X Sel. - S (wt.%)	Ref.
5% Pd/C (Aldrich)	Oleic acid, 15-27 bar, 573-633 K, 6 h	C$_{17}$	X = 35% S = 87%	[21]
4% Pd/C mesoporous	Stearic and palmitic acid, 573 K, 17 bar (5% H$_2$ in Ar),	C$_{17}$ C$_{15}$	X = 98% S = 99%	[22]
1% Pt-Re/H-ZSM-5	Vegetable oil, 65 bar (85% H$_2$ in N$_2$), 543 K, 12 h	C$_{10}$ - C$_{20}$	X=100% S = 90%	[23]
1% Pt/Al$_2$O$_3$	Methyl stearate, 6.9 bar (H$_2$), 598 K, 5h	C$_{17}$	X = 64% S = 93%	[24]
Ni-Mo/SiO$_2$ or Al$_2$O$_3$	Jatropha oil, H$_2$/oil = 800 mL/mL, LHSV = 7.6/h, 623 K	C$_{11}$- C$_{20}$	X=100% S = 83%	[25]
Topsøe TK-575 NiMo/γ-alumina	Rapeseed (15% in n-heptane, 45 bar, 623 K, LHSV = 1.5/h,	C$_{17}$ - C$_{22}$	X=100% S = 94%	[26]

6.2. Experimental Section

6.2.1. Catalyst Preparation

Ni-Mo/γ-Al$_2$O$_3$ was procured from Süd-Chemie India Ltd. The catalyst was first activated in-situ by heating at 623 K in nitrogen flow (20 mL/min) overnight at 5 bar pressure. It was cooled to 323 K. Nitrogen was replaced with H$_2$ (50 mL/min). Temperature of the catalyst bed was raised to 623 K and the reduction in hydrogen was continued for 6 h at 5 bar pressure. For sulfidation, 1% dimethyl disulfide (DMDS) in diesel was passed over the catalyst at a weight hourly space velocity of 1 h^{-1} for 18 h at 533 K and 40 bar. Hydrogen flow was set at 50 mL/min. Then the temperature was raised to 613 K and kept at that condition for another 6 h. After that, 0.5% DMDS in diesel was passed for another 6 h maintaining the same conditions.

6.2.2. Reaction Procedure for Hydrotreating of Vegetable Oils

Hydrotreatment of soybean oil was carried out as per the procedure described in Chapter 2. The liquid product formed was first filtered (G3 glass sintered funnel) and analyzed by FTIR and gas chromatography. FTIR was used to estimate the unconverted carbonyl groups which are present in tri-, di- and monoglycerides as per the method described in Chapter 2.

The composition of the hydrocarbon portion was determined by gas chromatography (Varian 3800 GC with HP-1 column, length - 30 m and internal diameter - 0.53 mm, column temperature program: start temperature (323 K)-5 min hold-563 K (5°/min)-20 min hold). The hydrocarbon products were identified using standard compounds procured from Aldrich Co.
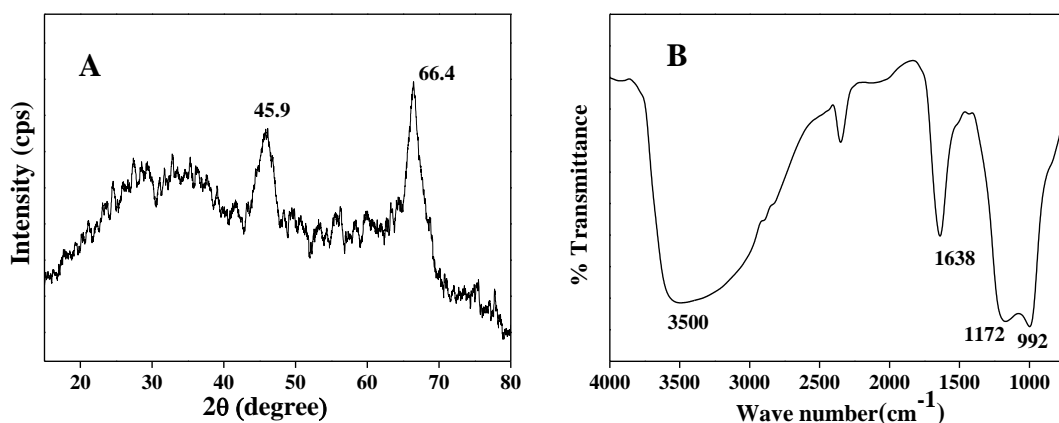
Fig. 6.1. *XRD and FTIR of Ni-Mo/Al₂O₃ catalyst*

6.3. Results and Discussion

6.3.1. Catalyst Characterization

The as-received form of Ni-Mo/γ-Al$_2$O$_3$ catalyst was characterized by XRD, FTIR, TPR and EDAX techniques. The XRD (Fig. 6.1 A) of the sample showed two prominent reflections at 2θ = 45.9 and 66.4°, typical of γ-alumina. No separate peaks corresponding to Ni or Mo oxides were detected. This reveals that these oxide phases are well dispersed over the alumina surface. The peaks at 1638 and 3500 cm^{-1} in the FTIR spectrum (Fig. 6.1 B) of the catalyst prior to activation and reduction indicate the presence of some moisture on the catalyst surface. Peaks corresponding to M-O stretching frequencies appeared at 950 – 1200 cm^{-1}.

Elemental composition by energy dispersive X-ray (EDAX) analysis (Fig. 6.2) revealed the presence of 6.88 wt% of Ni and 24.1wt% of Mo and rest corresponding to Al and O. No other element was detected. The temperature-programmed reduction

(TPR) (Fig. 6.3) of Ni-Mo/γ-Al$_2$O$_3$ showed a broad, unresolved profile in the temperature range 500 – 1100 K. Burch and Collins [29] reported that Ni reduces at higher temperature than Mo but in Ni-Mo/γ-Al$_2$O$_3$, most of the Ni reduces simultaneously with the Mo at around 700 K. However, some proportion of Ni didn't reduce until the temperature exceeded 800 K.
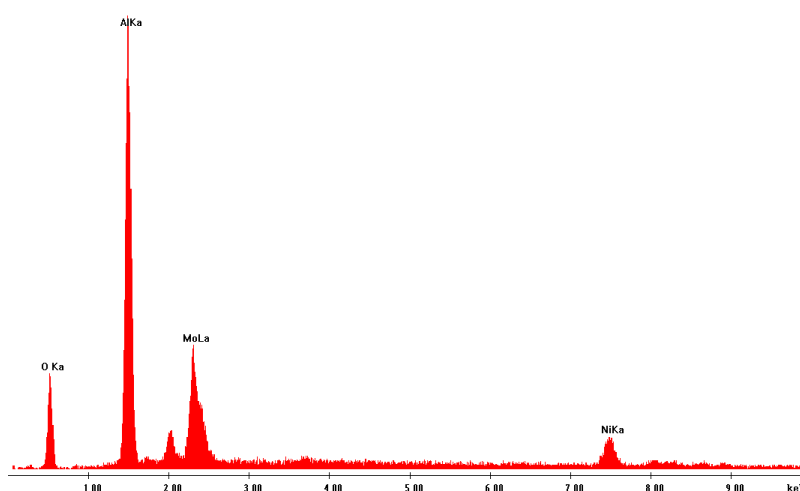
Fig .6.2. *EDAX of Ni-Mo/ γ-Al$_2$O$_3$*

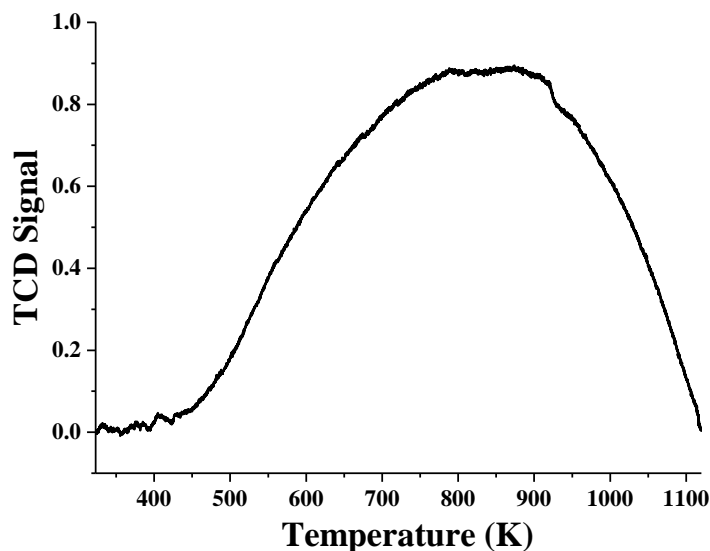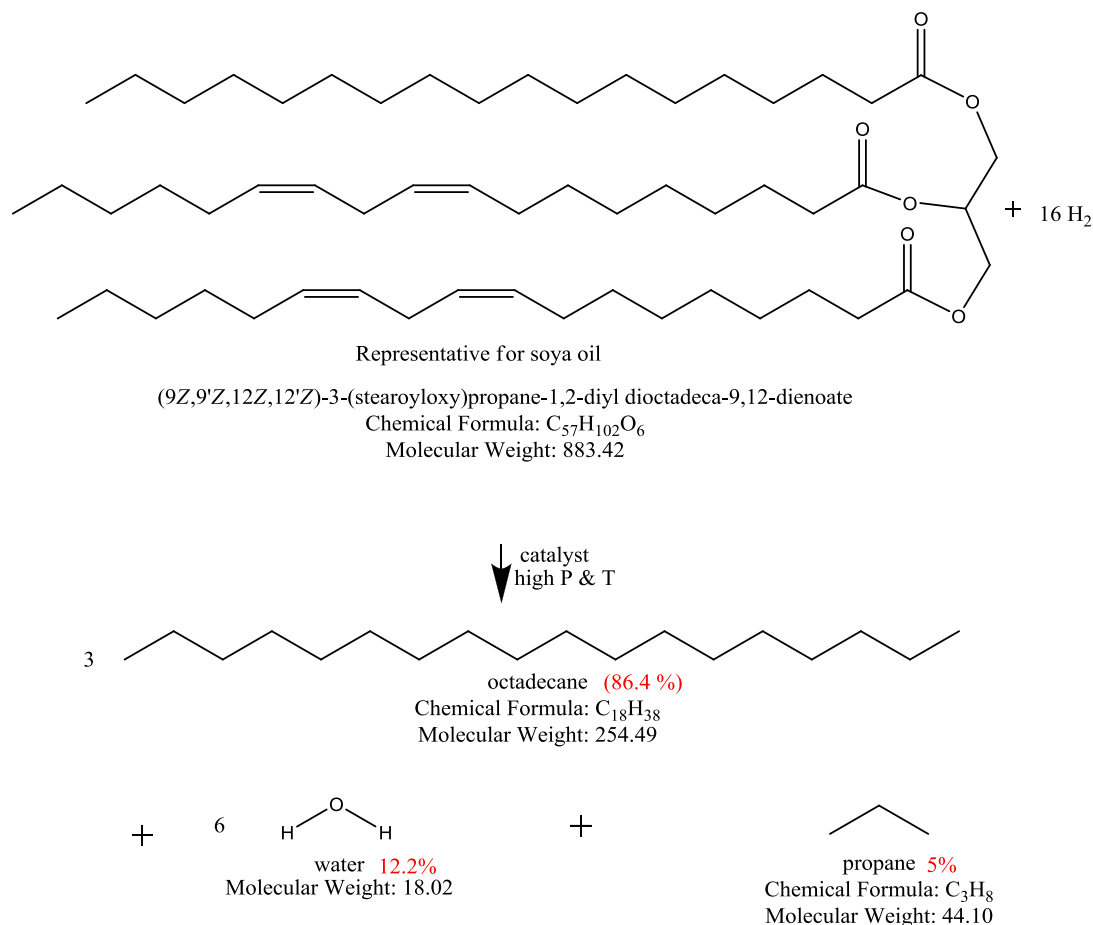***Fig. 6.3.*** *TPR profile of Ni-Mo/γ-Al$_2$O$_3$*

6.3.2. Catalytic Acitivity

Hydrotreatment of vegetable oils involves many reactions such as hydrodeoxygenation, hydrodecarboxylation, hydrogenation of double bonds, hydroisomerisation, cracking, etc. Hydrodeoxygenation of vegetable oils is preferred over hydrodecarboxylation as one carbon atom is lost as carbon dioxide. Scheme 6.2

provides the hydrodeoxygenation of triglycerides in soybean oil (a representative example) to corresponding hydrocarbons and their theoretical yield. In this scheme only deoxygenation is shown as in deoxygenation we get the maximum hydrocarbon yield as compared to decarboxylation where one carbon is lost as carbon dioxide.

Representative for soya oil

(9Z,9'Z,12Z,12'Z)-3-(stearoyloxy)propane-1,2-diyl dioctadeca-9,12-dienoate
Chemical Formula: $C_{57}H_{102}O_6$
Molecular Weight: 883.42

catalyst
high P & T

octadecane (86.4 %)
Chemical Formula: $C_{18}H_{38}$
Molecular Weight: 254.49

water 12.2%
Molecular Weight: 18.02

propane 5%
Chemical Formula: C_3H_8
Molecular Weight: 44.10

Scheme 6.2. *Reaction scheme for hydrodeoxygenation and theoretical yield of different products*

In hydrotreatment of vegetable oils, hydrogen has to be taken in excess to avoid decarboxylation. Excess hydrogen flow also helps in removing water (by-product of deoxygenation) and thereby avoids deactivation of catalyst. This excess hydrogen can be recycled after purification (Fig. 6.4) and thus there is no wastage of hydrogen. Excess hydrogen also removes the sulphur from the catalyst; therefore to keep the catalyst in sulfided form, 100-1000 ppm of dimethyl disulfide is added to the feed which generates H_2S by decomposition at temperature higher than 483 K in presence of hydrogen.
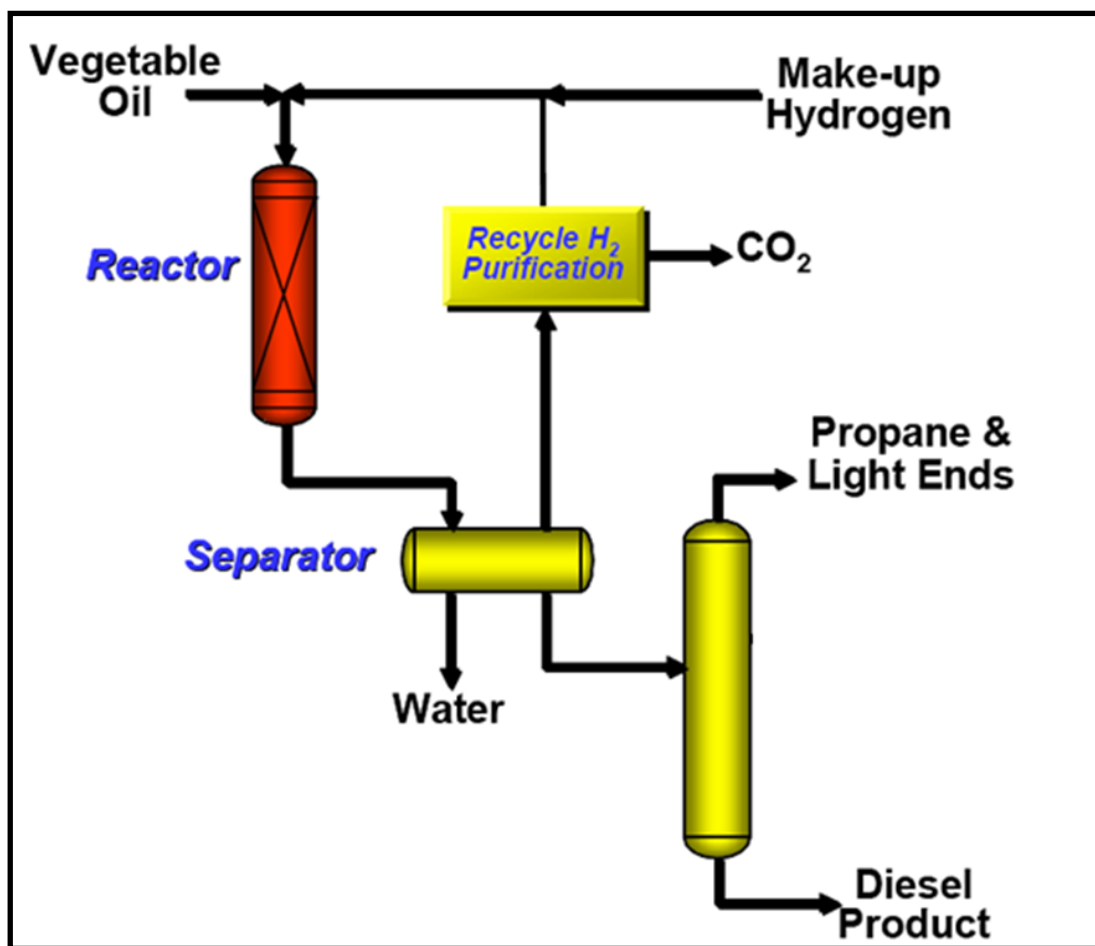
Fig. 6.4. *Process diagram for hydrotreatment of vegetable oils*

Hydrotreatment of 20, 40 and 80 wt% soybean oil in octanol and 100% pure soybean oil was carried out in a fixed-bed reactor loaded with Ni-Mo/γ-Al$_2$O$_3$ catalyst. Liquid product obtained was colourless (Fig. 6.5) and has two layers with the lower being water and the upper layer being (hydrocarbon product (bio-HC) + any unconverted soybean oil). Absence of organic impurities in water layer was confirmed by ^{1}H NMR spectroscopy. The upper layer was analyzed by FTIR (Chapter 2), NMR and GC. FTIR was used to detect unconverted glycerides present in the product sample. At chosen reaction conditions, vegetable oil and its blends got completely converted into hydrocarbons (Table 6.2). In the FTIR spectrum (Fig. 6.6) a complete disappearance of carbonyl (at 1746 cm^{-1}) and olefinic (3010 cm^{-1}) peaks was observed indicating 100% removal of oxygen and unsaturation, respectively, of soybean oil. The ^{1}H NMR spectrum of the product (Fig. 6.7) also confirmed the formation of saturated hydrocarbons. Upon hydrotreating, the ^{1}H NMR signals due to glycerides (δ = 4.1-4.4 ppm) and double bonds (δ = 5.3 ppm) have completely disappeared and the product showed signals corresponding to only methylene (–CH$_2$-

; δ = 1.28 ppm) and methyl (-CH$_3$; δ = 0.88 ppm) groups. This observation reconfirms the conclusions drawn from FTIR spectroscopy that all the soybean oil got converted to saturated hydrocarbons at the chosen reaction conditions.
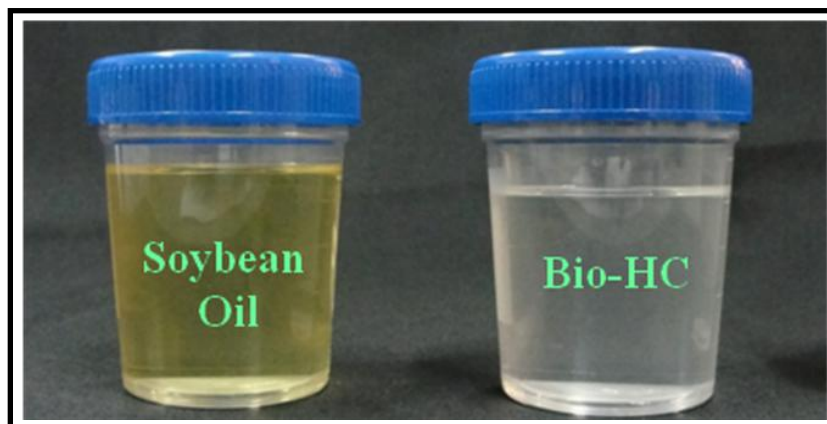
Fig. 6.5. Soybean oil and HDO product
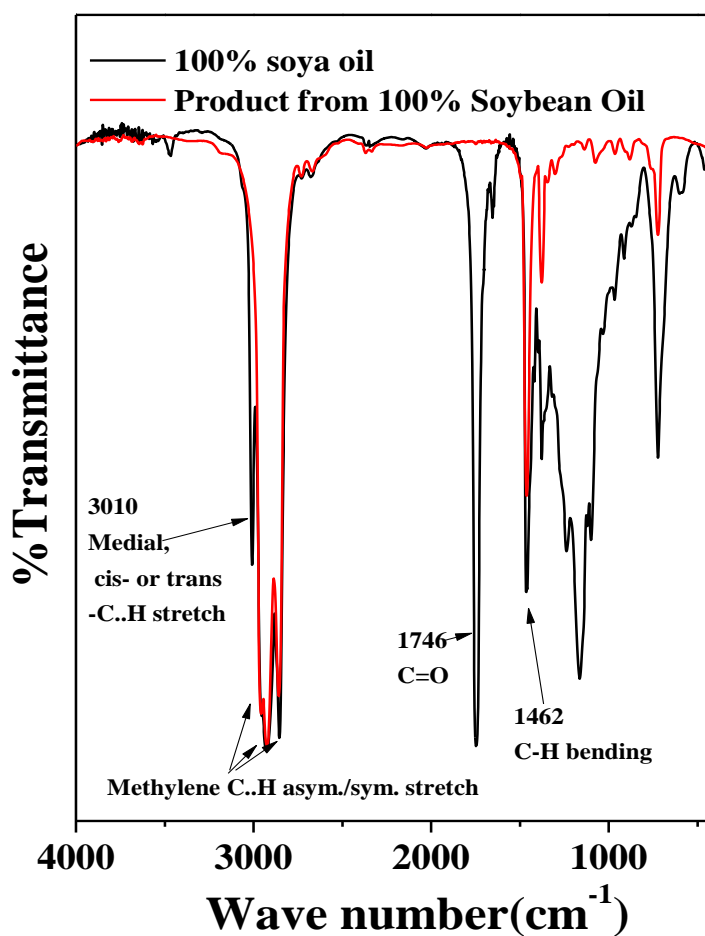
Fig. 6.6. FTIR spectra of soybean oil and hydrocarbon product

Table 6.2. Different feed and liquid yield

wt% of soybean oil in feed	H$_2$ flow rate (mL/min)	Unconverted oil (wt%)	HDO product (wt%)
20%	480	0	100
40%	480	0	100
80%	480	0.3	99.7
100%	480	0	100
100%	320	0	100
100%	200	4.7	95.3

Reacion conditions : H$_2$ flow = 480 mL/min, temperature= 573K, pressure = 50 bar, WHSV = 0.5 h^{-1}.
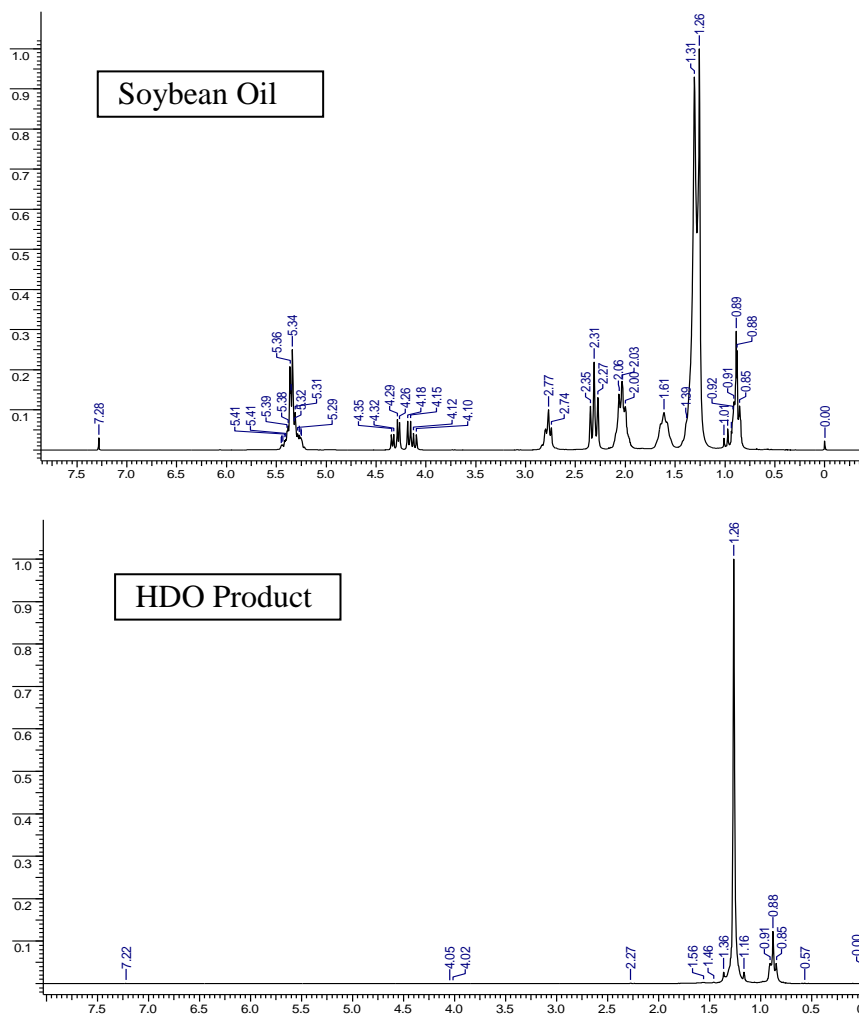
Fig. 6.7. ^{1}*H NMR spectra of soybean oil and HDO product*

Table 6.3. Product distribution of hydrocarbons derived from soybean oil (SO) by hydrotreating

Product from Feed	H_2 Flow (mL/min)	Product distribution (wt%)					
		C_{15}	C_{16}	C_{17}	C_{18}	$C_{<15}$	$C_{>18}$
20% SO	480	0.8	1.5	4.2	10.7	80.9	1.9
40% SO	480	1.1	2.7	3.4	17.5	67.9	7.4
80% SO	480	0.9	7.7	7.7	60.2	20.5	3.1
100% SO	480	1.8	7.5	17.7	69.0	0.52	3.4
100% SO	320	1.9	7.9	18.3	69.1	0.6	2.1
100% SO	200	3.5	7.8	26.7	56.8	0.4	4.8

Reacion conditions : H_2 flow = 480 mL/min, temperature= 573K, pressure = 50 bar, WHSV = 0.5 h^{-1}.

The composition of various hydrocarbons in the product was determined by gas chromatography (Fig. 6.8). Octadecane (C_{18}), heptadecane (C_{17}), hexadecane (C_{16}) and pentadecane (C_{15}) were the four major products constituting >95% of the total bio-hydrocarbon product. Hydrocarbon fraction with greater than 18 carbon atoms in the chain was found to be 3-4% and the fraction with less than 15 carbon atoms in the chain was <1%. Soybean oil contains palmitic acid (C_{16}) of 10-12% and the rest is oleic, linoleic and linolenic acids (C_{18}). Deoxygenation of C_{18} fatty acid gives octadecane and decarboxylation forms heptadecane. Similarly, palmitic acid turns into hexadecane and pentadecane. Under chosen reaction conditions, octadecane was the main product suggesting that deoxygenation is the main reaction occurring on Ni-Mo/γ-Al_2O_3 catalyst. Presence of heptadecane and pentadecane do suggest that decarboxylation is also occurring to a smaller extent. Hydrogen flow has a pronounced effect on product distribution. The concentration of decarboxylation products (pentadecane and heptadecane) increased when the flow rate of hydrogen was decreased from 320-480 mL/min to 200 mL/min, (Table 6.3).
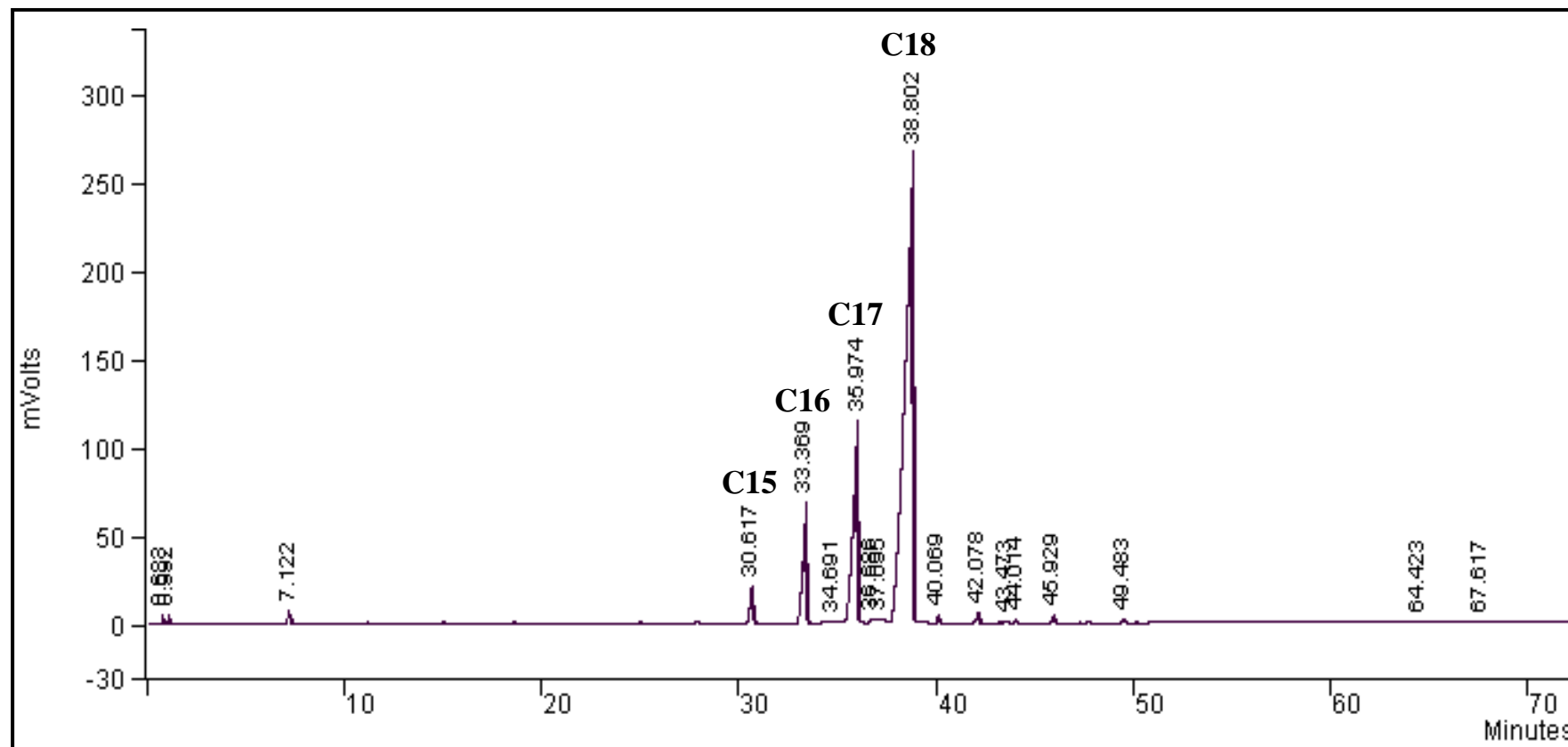
Fig. 6.8. *Gas chromatogram of the hydrocarbon product from 100 % soybean oil*

Table 6.4. Time-on-stream study: composition of liquid hydrocarbon product

Time on stream (h)	Product distribution (wt%)					
	C_{15}	C_{16}	C_{17}	C_{18}	$C_{<15}$	$C_{>18}$
80% Soybean oil in n-octanol						
19	0.8	7.0	7.0	61.4	22.2	1.7
25	0.7	6.9	6.6	62.6	21.2	3.1
31	0.7	7.0	6.3	62.0	22.1	2.3
37	0.9	7.6	7.4	59.9	21.1	2.1
43	0.9	7.6	7.3	60.5	20.5	2.1
49	0.9	7.6	7.3	60.4	20.6	3.3
55	0.9	7.7	7.7	60.2	20.5	3.1
61	0.9	7.7	7.4	60.0	20.8	3.3
67	0.9	7.8	7.2	59.57	21.4	3.2
73	0.9	7.8	7.3	61.1	20.0	3.0
79	0.7	7.1	6.5	62.5	21.4	1.8
85	0.7	7.1	6.0	62.8	21.6	1.8
91	0.7	6.9	6.3	61.8	22.0	2.4
100% Soybean oil						
12	1.5	7.6	14.3	69.8	3.3	3.5
18	1.7	7.7	16.3	69.5	1.2	3.5
24	1.9	7.6	17.2	69.3	0.7	3.4
30	1.9	7.7	17.6	68.1	0.5	4.2
37	1.8	7.5	17.8	68.8	0.5	3.6
42	2.0	7.7	19.1	66.9	0.6	3.8
48	1.9	7.8	18.3	68.6	0.4	3.1
54	1.8	7.5	17.7	69.0	0.5	3.4
66	1.9	7.6	19.7	67.6	0.6	2.7
72	1.8	7.6	18.5	68.7	0.5	2.9
78	1.9	7.9	18.3	69.2	0.6	2.1

Reacion conditions : H_2 flow = 480 mL/min, temperature= 573K, pressure = 50 bar, WHSV = 0.5 h^{-1}.

Time-on-stream studies (Table 6.4 and Fig. 6.9) with 80 and 100% soybean oil feeds revealed that the catalysts is stable during 200 h of investigation and product selectivity is nearly unaltered during this period. In the product with 100% soybean oil, the composition of $C_{<15}$ is lower than 1%. However, this in the case of 80%

soybean oil feed it was found to be 20 – 22%. This suggests that n-octanol used as a diluent also got reduced to octane and is included in the product distribution.
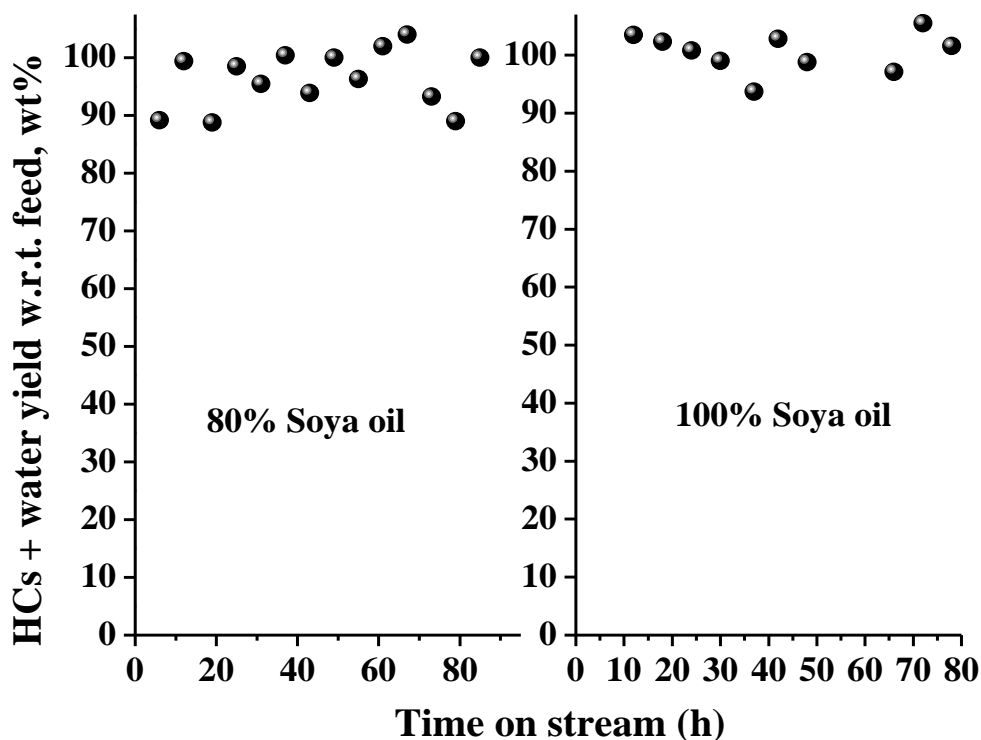

Fig. 6.9. *Catalyst stability study during hydrotreating reaction*

Table 6.5 reports the pour points of hydrocarbon products obtained from different feedstocks. The product obtained from 100% soybean oil has a high pour point than that from soybean oil diluted with n-octanol. The product obtained from 20, 40 and 80% soybean oil was distilled at 403 K to remove lighter fraction ($C_{<15}$). The distilled out product has pour point same as that of the 100% soybean oil product (Table 6.10). This trend in pour point variation is as per expectation.

Table 6.5. Pour point of HDO products from different feeds

S. no.	Sample name	Pour point (K)
1.	Product from 20% feed	266
2.	Product from 40% feed	270
3.	Product from 80% feed	293
4.	Product from 100% feed	298
5.	Soybean Oil	264
6.	Distilled Product of (1+2+3)	299

In another experiment, the distilled HDO product was mixed with commercial diesel in different proportions and the pour point was determined (Table 6.6). Up to 20% blending the pour point of the HDO product-diesel blend is below 273 K. While this study reports that Ni-Mo/γ-Al$_2$O$_3$ catalyst is highly efficient for hydrodeoxygenation to produce saturated hydrocarbons, the product has high pour point and needs to be isomerized for direct use.

Table 6.6. Pour point HDO product-commercial diesel blends

HDO product (wt%)	Commercial diesel (wt%)	Pour point (K)
0	100	268
10	90	269
20	80	272
30	70	276
40	60	277
50	50	284
60	40	287
70	30	291
80	20	293
90	10	295
95	5	297
100	0	298

6.4. Conclusions

Soybean oil was quantitatively converted into diesel-like hydrocarbons selectively by deoxygenation route in the presence of hydrogen over sulfided Ni-Mo supported on γ-alumina. The catalyst was stable in a continuous 200 h time-on-steam run. Pour point of the product can be improved by isomerisation for direct application in diesel engines.

6.5. References

1. A. Sivasamy, K.Y. Cheah, P. Fornasiero, F. Kemausuor, S. Zinoviev, S. Miertus, Chem. Sus. Chem. 2 (2009) 278.

2. M. Di serio, R. Tesser, L. Pengmei, E. Santacesaria, Energy Fuels 22 (2008) 207.

3. A.A. Kiss, A.C. Dimian, G. Rothenberg, Adv. Synth. Catal. 348 (2006) 75.

4. D. Srinivas, J.K. Satyarthi, Catal. Surv. Asia, (2010) DOI 10.1007/s10563-010-9108-2.

5. J.A. Melero, J. Iglesias, G. Morales, Green Chem. 11 (2009) 1285.

6. B. Smith, H.C. Greenwell, A. Whiting, Energy Environ. Sci. 2 (2009) 262.

7. T.A. Mamedova, N.K. Andryushchenko, E.N. Askerova, Kh.R. Veliev, V.M. Abbasov, M.I. Rustamov, Chem. Techn. Fuels Oils 46 (2010) 149.

8. C.C. Chang, S.W. Wan, Ind. Eng. Chem. 42 (1942) 1543.

9. J.T. Kloprogge, L.V. Duong, R.L. Frost, Environ. Geol. 47 (2005) 967.

10. A.W. Schwab, G.J. Dykstra, E. Selke, S.C. Sorenson, E.H. Pryde, J. Am. Oil Chem. Soc. 65 (1988) 1781.

11. J.D. Adjaye, N.N. Bakhshi, Fuel Process. Technol. 45 (1995) 185.

12. Y.S. Ooi, S. Bhatia, Microporous Mesoporous Mater. 102 (2007) 310.

13. J.O. Olusola, M.M. Adediran, A.K. Oluseyi, U.L. Ajao, Energy Environ. 20 (2009)/21 (2010) 1325.

14. T. Kalnes, T. Marker, D.R. Shonnard, Intern. J. Chemical Reactor Engin. 5 (2007) A48.

15. J. Holmgren, C. Gosling, K. Couch, T. Kalnes, T. Marker, M. McCall, R. Marinangeli, Petrol. Technol. Quart. 3 (2007) 119..

16. J. Holmgren, C. Gosling, R. Marinangeli, T. Marker, G. Faraci, C. Perego, Hydrocarbon Process. 9 (2007) 67.

17. David Kubička, L. Kaluza, Appl. Catal. A: Gen. 372 (2010) 199.

18. http://www.nesteoil.com

19. L. Rantanen, R. Linnaila, P. Aakko, T. Harju, SAE Technical Paper 01 (2005) 3771.

20. http://www.uop.com

21. M. Snåre, I. Kubičková, P. Mäki-Arvela, D. Chichova, K. Eränen, D.Yu. Murzin, Fuel 87 (2008) 933.

22. S. Lestari, P. Mäki-Arvela, I. Simakova, J. Beltramini, G. Q. Max Lu, D. Yu. Murzin, Catal. Lett. 130 (2009) 48.

23. K. Murata, Y. Liu, M. Inaba, I. Takahara, Energy Fuels 24 (2010) 2404.

24. P.T. Do, M. Chiappero, L.L. Lobban, D.E. Resasco, Catal. Lett. 130 (2009) 9.

25. Y. Liu, R. Sotelo-Boyás, K. Murata, T. Minowa, K. Sakanishi, Chem. Lett. 38 (2009) 552.

26. B. Donnis, R. G. Egeberg, P. Blom, K.G. Knudsen, Top Catal 52 (2009) 229.

27. J. Myllyoja, P. Aalto, E. Harlin, European Patent No. EP20050014426

28. R. Burch, A. Collins, Appl. Catal. 17 (1985) 373.

29. R. Burch, A. Collins, Appl. Catal. 18 (1985) 389.

Chapter 7

Summary and Overall Conclusions
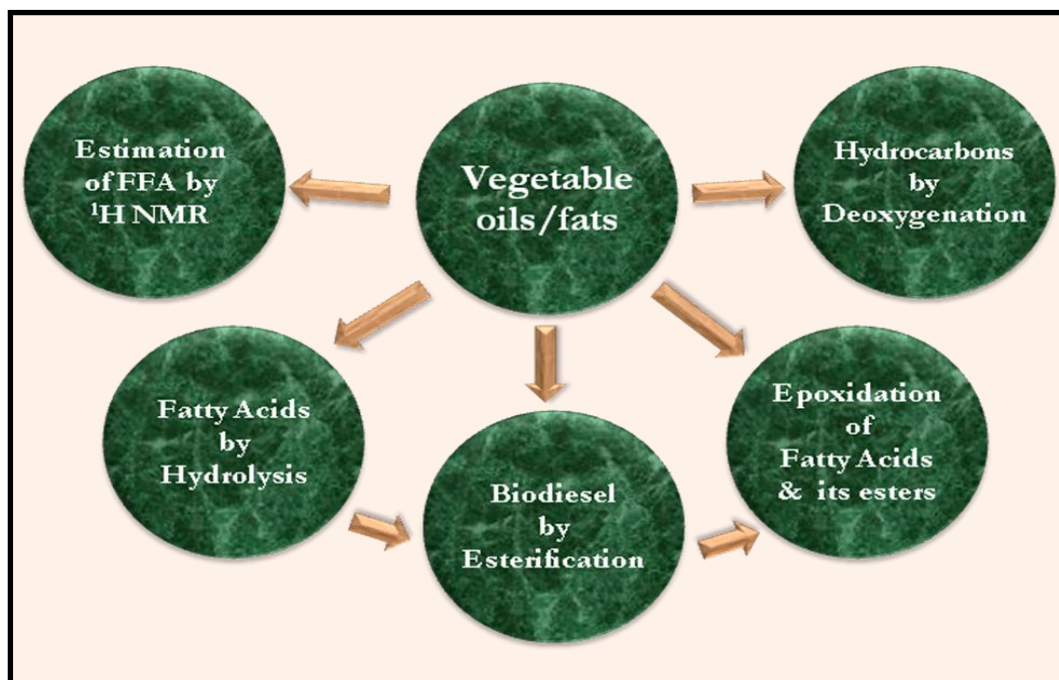
Depleting of fossil fuel resources, their escalating prices, environmental concerns about their emissions and increasing demand for fuels are the major drives for the research on alternative fuels. Biodiesel produced from vegetable oils is one of renewable fuel which fulfils most of the requirements necessary for application of a fuel in present diesel engines without any modifications. Conventionally, biodiesel (comprising of fatty acid methyl esters; FAME) is produced by transesterification of vegetable oil with methanol in the presence of alkali metal catalyst. Homogeneous base catalyst processes suffer from several drawbacks and disadvantages: soap production, low-quality glycerin and multiple unit operations are a few among several. Even in best processing units, about 1% feedstock is lost as soap and removal of soap from biodiesel creates a large amount of waste water. Soap (salts of fatty acids) formation is exacerbated by the presence of free fatty acids (FFA) and water in the feedstock. The alkali-process also requires high quality vegetable oil which amounts to 70 − 80% of the total production cost of biodiesel. Low-cost feedstock (e.g., non-edible oils, waste cooking oils and animal fats) containing high amount of FFA and moisture are not suitable for alkali process.

Acid catalysts are sometimes preferred to bases as they can convert low-grade feedstock into biodiesel. However, they work at a slower rate than bases and require a high amount of alcohol (around 40 times molar excess). It is used as a first stage in plants dealing with FFAs containing oils such as waste oil from food processing. Once the FFA has been esterified the oil is neutralized and then, passed to a second stage for base catalytic transesterification. Large doses of powerful acid, usually sulphuric acid, are needed (5-25%) so the plant has to be constructed from expensive acid-resistant materials. After processing, the acid remains in the glycerin which has to be neutralized and purified before it has any commercial value. As in the case of homogeneous base catalysts, a continuous supply of fresh catalyst is needed.

To overcome these disadvantages several solid acid catalyst processes have been introduced to convert vegetable oils into biodiesel. The ideal catalyst should be highly acidic (for faster reaction) and hydrophobic (to avoid deactivation from water produced in esterification and for better adsorption of hydrophobic vegetable oils and fatty acids). A more generic approach for biodiesel production from low-grade (high FFA and water

containing) feedstock has been explored in this thesis. In this approach, vegetable oils/fats are first hydrolyzed by reaction with water in the presence of a solid acid catalyst (Chapter 3) and then the fatty acids which are produced in the first step are esterified with an alcohol (Chapter 4). Design and development of hydrophobic catalysts and operation at moderate conditions are the major requirements. Several solid catalysts with different surface and acidic properties were studied for this process. Double-metal cyanide complexes of Fe and Zn were found to be highly efficient for this hydrolysis-*cum*-esterification process for conversion of low-grade oils and fats into biodiesel. Factors influencing the kinetics of reactions were investigated. It was concluded that *in addition to the acidic and textural properties, surface hydrophobicity and relative surface coverage by reactants/products also play an important role in reactions of vegetable oils with water and long-chain fatty acids with alcohols on solid acid catalysts*. This route can be competitive to base catalysis when used to process cheap, low-grade oils with high FFA content.

FFA content present in vegetable oils is one of the most important quality parameters. Therefore, estimation of FFA in oils/fats is an area of great importance and crucial to conversion of FFAs into biodiesel. A new ^{1}H NMR method is developed and reported in Chapter 2. Advantage of this method over conventional titration method is that *it estimates FFA content exclusively while titration gives total acid value that includes of FFA and other acid impurities*. Human error in observing end point especially in case of dark coloured non-edible oils can also be avoided. It is a fast method and avoids the use of large amount of solvent used in titration.

Besides the application of fatty acids and its esters (vegetable oils and biodiesel) as a fuel, these can also be converted to a number of intermediates and chemical derivatives. There has been increasing interest in using these substances as intermediates in the production of new bio-based industrial materials. Epoxidized fatty acid esters are one of these intermediates which are used as plasticizers that are compatible with polyvinyl chloride (PVC) and as stabilizers for PVC resins to improve flexibility, elasticity and toughness and to impart stability of polymer towards heat and UV radiation. The conventional manufacturing process via Prileshajev reaction using short-chain percarboxylic acids produces high amounts of waste and by-products. The other

known epoxidation methodologies are not up to the mark for application on industrial scale. A highly selective solid-catalyst-based process (beneficial from environmental and economic viewpoints) is highly desirable. Chapter 5 reports such a sustainable process and an efficient reusable catalyst for epoxidation of fatty acids and their esters with *tert.*-butyl hydrogen peroxide over alumina-supported group VI transition metal oxides catalysts (CrO_x/Al_2O_3, MoO_x/Al_2O_3 and WO_x/Al_2O_3). The effect of modification of alumina with phosphoric acid before loading the metal oxide on epoxidation activity was also investigated. The amount of metal oxide in the catalyst was varied from $0 - 15$ wt%. *A catalyst with 15 wt% MoO_x on Al_2O_3 was found superior to the rest of the catalysts investigated*. Kinetics of epoxidation was monitored by ^{1}H NMR spectroscopy and gas chromatography techniques.

The ester-based biodiesel has some limitations in cold climates due to its high pour point. Oxidation stability is another issue related to its long term storage. Hydrotreatment of vegetable oils yields hydrocarbon-like fuels (*2nd generation biodiesel or green diesel*) which have properties same as that of the petrodiesel. Moreover, low quality feedstock oils can be used. Catalytic application of γ-alumina-supported Ni-Mo catalyst in the production of 2nd generation biodiesel was investigated in Chapter 6. *Soybean oil was converted into diesel-like hydrocarbons selectively by deoxygenation in the presence of hydrogen over sulfided Ni-Mo supported on γ-alumina*. Vegetable oil was transformed into cetane booster hydrocarbons without the use of any solvent. *Their blending with commercial petrodiesel up to 20 wt% provides a blend with pour point less than 273 K.*

By and large, this thesis contributes to more sustainable catalytic processes for biodiesel production *via* hydrolysis–*cum*-esterification route and hydrodeoxygenation of vegetable oils over transition metal catalysts. It also enlightens the factors influencing the performance of the catalysts in the above reactions.

List of Publications

1. Regio- and stereoselective synthesis of β-amino alcohols over titanosilicate molecular sieves
   J. K. Satyarthi, L. Saikia, D. Srinivas, P. Ratnasamy
   Appl. Catal. A: General 330 (2007) 145 – 151.

2. Activation and reactivity of epoxides on solid acid catalysts
   L. Saikia, **J.K. Satyarthi**, D. Srinivas, P. Ratnasamy
   J. Catal. 252 (2007) 148 – 160.

3. Double metal cyanides as efficient solid acid catalysts for synthesis of β-amino alcohols under solvent-free conditions
   L. Saikia, **J.K. Satyarthi**, R. Gonnade, D. Srinivas, P. Ratnasamy
   Catal. Lett. 123 (2008) 24 - 31.

4. Estimation of free fatty acid content in oils, fats and biodiesel by ^{1}H NMR spectroscopy
   J.K. Satyarthi, D. Srinivas, P. Ratnasamy
   Energy & Fuels 23 (2009) 2273 - 2277.

5. Influence of surface hydrophobicity on esterification of fatty acids over solid catalysts
   J.K. Satyarthi, D. Srinivas , P. Ratnasamy
   Energy & Fuel 24 (2010) 2154 - 2161.

6. Hydrolysis of vegetable oils and fats to fatty acids over solid acid catalysts
   J.K. Satyarthi, D. Srinivas , P. Ratnasamy
   Appl. Catal. A: General 391 (2011) 427-435.

7. Biodiesel production from vegetable oils and animal fat over solid acid double metal cyanide catalysts
   D. Srinivas and **J.K. Satyarthi**
   Catal. Surveys Asia (2011) DOI 10.1007/s10563-010-9108-2.

8. Factors influencing the kinetics of esterification of fatty acids over solid acid catalysts
   J.K. Satyarthi, Sambhu R., D. Srinivas
   Energy & Fuels (2011) Communicated

9. Metal-incorporated hydrotalcites as solid base catalysts for biodiesel and biolubricant production,
   Rahul R., **J.K. Satyarthi**, D. Srinivas
   Proceedings of 20th National Symposium on Catalysis, Narosa Publications (2011) (Communicated).

10. Solid acid catalysts for biodiesel production from non-edible oils and fats
    J.K. Satyarthi, D. Srinivas
    Proceedings of 20th National Symposium on Catalysis, Narosa Publications (2011) (Communicated).

List of Patents

1. Process for producing fatty acids
   Darbha Srinivas, **Jitendra Kumar Satyarthi,** T. Raja, S. Deshpande
   India and PCT (INV-2009-17; 1690/DEL/2009; CSIR No. 0095NF2009) filed
   on July 2, 2009.
2. An improved process for production of epoxy functionalized fatty acids, their
   esters and mixtures thereof
   Darbha Srinivas, **Jitendra Kumar Satyarthi**
   India and PCT (INV-2010-16; 2270DEL2010; CSIR No. 141NF2010) filed on
   Sept 15, 2010.